Sharp Interface Models From Homogeneous Reaction Systems

Fernandez Fonseca, Andrea

Award date:
2013

Awarding institution:
University of Bath

Sharp Interface Models From Homogeneous Reaction Systems

submitted by

Andrea Fernández Fonseca

for the degree of Doctor of Philosophy

of the

University of Bath

Department of Mathematical Sciences

November 2013

ABSTRACT

This thesis investigates the fast-reaction limit for a one dimensional reaction-diffusion system describing the penetration of the carbonation reaction in concrete. Three conceptually different scaling regimes of the effective diffusivities of the driving chemical species are explored using matched asymptotics. The limiting models include one-phase and two-phase generalised Stefan moving boundary problems as well as a nonstandard two-scale (micro-macro) moving boundary problem. These sharp interface models are studied to uncover the mechanisms at the free boundary. A power law for the concentration of the chemical species at the interface is derived, as well as the large and small time asymptotic behaviour of the free boundary and the concentration profiles. Numerical results, supporting the analytical results, are presented throughout this thesis, including the application of the method of lines to solve the limiting Stefan problems. To conclude, numerical illustrations of different two-dimensional geometries are included.

ACKNOWLEDGEMENTS

I would like to express my gratitude to my supervisor, Jonathan Evans, for his patient guidance and support throughout. I would specially like to thank him for convincing me to pursue this Ph.D, and although I am sure there were moments when he had second thoughts, he still continued to encourage me. I would have never achieved this without him.

I would also like to thank Adrian Muntean for his input and advice on concrete carbonation. I thoroughly enjoyed my trips to Eindhoven filled with interesting conversations and lovely people. I am also grateful to the EPSRC for funding my studies.

Next, I would like to thank all the people in the Maths department and fellow Ph.D students from other departments who made my time here so enjoyable. I will not forget the Sunday coffees with the girls, the salsa nights with biology and the support group sessions with my fellow co-starters.

Last, but not least, I would like to thank my parents and my aunt for their continuous support and late night video sessions. I would not have managed without you.

Contents

List of Figures

List of Tables

Chapter 1

Introduction

Processes involving aggressive reactions such as carbonation, oxidation and sulfation are of great importance and understanding the underlying mechanisms has been a popular research topic [43, 26, 2]. In particular, having a good estimate on the life service of motorways, bridges, and sewage pipes systems (etc.) can save significant amounts of money and energy. The carbonation of concrete is vital towards determining the durability of concrete structures. A good theoretical multiscale understanding of the evolution of the carbonation reaction in such a complex multiphase material is vital towards obtaining accurate predictions of the durability of large concrete structures.

These chemical reactions are often modelled as reaction-diffusion and, where appropriate, convection systems [2, 20, 26, 27, 7]. This will be the approach taken here. We will study the problem of concrete carbonation, and investigate it in the limit of fast bulk reactions to obtain distinct sharp interface models.

1.1 Concrete Carbonation

The most common way in which reinforced concrete structures fail is by the corrosion of the reinforcing steel. Two examples of the damaged caused by corrosion are shown in figure 1.1. The products of corrosion occupy a larger volume than its constituent metal, increasing the internal pressure, such that spalling and cracks occur. Surrounding the steel bars, there is a protective oxide layer and it is the destruction of this layer that allows the steel to corrode. This is caused by either chloride penetration, a decreasing in the pH of the concrete or both, where the second mechanism accelerates the first. The latter is caused by concrete carbonation and is dominant in urban environments with a high concentration of carbon dioxide.

The process of concrete carbonation is a complex physiochemical process but it can be simplified to the single reaction of atmospheric carbon dioxide with calcium hydroxide found in the pore solution to form water and calcium carbonate. The pore solution

Figure 1.1: *Corrosion of the reinforced steel in concrete.*

is highly alkaline (pH $\approx$ 14) and as soon as the pH level decreases the microscopic oxide layer at the steel reinforcement disappears and the steel can corrode. This corrosion causes the durability of the structure to reduce dramatically. For more details on concrete carbonation and its relevance with respect to corrosion and durability issues, we refer the reader to [49, 32, 56] as well as to the references cited therein. Figure 1.2 shows a slice of partially carbonated concrete that has been sprayed with phenolphthalein, a colourless pH indicator that turns pink when the pH is above 9.5. Two very distinct regions, pink and colourless, depict the dramatic drop of the pH levels in the concrete block.

Figure 1.2: *Cross-section of partly carbonated concrete. Two distinct zones can be distinguished. The pink area corresponds to a high pH where the reaction has not yet taken place and the colourless region corresponds to a low pH.*

The reaction mechanism is as follows

$$\mathrm{CO_2}_{(\mathrm{g}\to\mathrm{aq})} + \mathrm{Ca(OH)_2}_{(\mathrm{s}\to\mathrm{aq})} \to \mathrm{CaCO_3}_{(\mathrm{aq}\to\mathrm{s})} + \mathrm{H_2O} \tag{1.1}$$

The atmospheric carbon dioxide diffuses through the unsaturated concrete matrix and dissolves into the pore water while the calcium hydroxide is available in the pore solution

by dissolution from the solid matrix. Free water and calcium carbonate are the main products of reaction (1.1). The latter one then quickly precipitates to the solid matrix [63]. In particular, calcium hydroxide is formed during hydration. The anhydrous calcium oxide of the cement CaO forms calcium silicate hydrate $mCaO{\cdot}SiO_2{\cdot}nH_2O$, denoted by C-S-H, and calcium hydroxide. However, C-S-H is insoluble and does not dissolve into the pore liquid as $Ca(OH)_2$ does. Despite this, C-S-H also reacts with CO_2 but the exact stoichiometric relations are unknown due to the many stages of C-S-H. As a consequence, the available macroscopic models capturing carbonation in concrete are complex and involve a large number of parameters. The challenge is to find minimal models that can accurately predict CO_2 penetration depths. In fact, C-S-H's reaction with CO_2 does not affect the alkalinity of the pore liquid [61]. For simplicity and with a minimal model in mind, C-S-H and its reactions will be neglected. Another interesting process taking place in the concrete carbonation procedure is called "curing". In practice, after mixing the concrete, the pores are maintained saturated with water for the hydration reactions to take place. During this period, this excess of water prevents any carbonation from happening. However, we will only concern ourselves with reaction (1.1).

The literature on the problem of concrete carbonation is vast due to the potentially devastating effects the corrosion of steel can cause. Further, the process is not only complex due to the amount of reactions taking place but there is also a large number of material/environment parameters involved. Material parameters include the composition of cement and concrete, porosity and pore size distribution. Further, environmental conditions such as the external carbon dioxide concentration, relative humidity and temperature all play a role. One of the first and leading articles is Papadakis et. al. [49] where a model for the carbonation of concrete in the limit of a CO_2 diffusion controlled environment is constructed. From a mathematical modelling perspective, the literature includes multi-scale carbonation, one or two moving reaction strips, as well as moving sharp interface models that investigate the above material and environmental parameters [43, 6, 46]. More rigorous analysis on the choice of models to determine the existence and uniqueness of solutions also exist such as [44, 45]. Numerical approaches allow a more detailed modelling to investigate the parameters. Examples include [38, 58] in one dimension and [59, 61] in two dimensions, where a finite element approach is considered in all of them. Other techniques and approaches include the unreacted core model [9] which considers a transitional zone rather than a sharp interface approach, mesoscale models [57, 67] and statistical models [64, 42]. All the above papers have one aim in common: to be able to predict the carbonation depth. Despite all this on-going research, the huge amount of parameters and complexity makes it difficult to propose a model that is able to obtain an accurate approximation for a general setting.

Our objective is no different here from the literature's common aim. We want to understand how fast the reaction (1.1) moves into the material, driven by CO_2 diffusion. We want to use a detailed reaction layer analysis to determine the speed of growth of the macroscopic carbonated phase (the colourless region in figure 1.2). In other words, we want to find the boundary conditions that need to be imposed at the reaction interface to describe its correct motion. Concrete carbonation is a complicated process, a snapshot of which is given in this thesis. However, instead of elaborating a more detailed and hence complex model with an increasing amount of parameters, we simplify the whole procedure to discover that the main interesting leading behaviours can be derived.

To this aim, we introduce a basic macroscopic reaction-diffusion model to describe the aqueous chemistry and transport involved in (1.1). However, before moving on, we note that this model will lead to one-phase and two-phase generalised Stefan problems. Again, the literature on Stefan problems is vast, as well as all the possible applications. Stefan problems were first introduced to model the melting of ice in 1890 and since then have been a constant area of research [19, 40, 33, 34, 22]. Several numerical methods have been implemented and many studies of all these different types can be found in [25, 8, 29]. However, the method of lines introduced by Meyer [41] is one of the most popular.

1.2 Model

We consider a sample of concrete occupying a region $\Omega \subset \mathbb{R}^d$, $d = 1, 2, 3$ with the vector $\mathbf{x}$ directed into the concrete. Denote Γ to be the boundary of Ω with outward unit normal $\mathbf{n}$. Further, let Γ^R be exposed to an external source of CO_2 and Γ^N is assumed impervious to all reaction species, $\Gamma = \Gamma^R \bigcup \Gamma^N$. Let $c = c(\mathbf{x}, t)$ and $h = h(\mathbf{x}, t)$ be the concentrations of $CO_{2_{(aq)}}$ and $Ca(OH)_{2(aq)}$ respectively, expressed as moles per unit volume (i.e. the intrinsic concentrations). We let the reactants CO_2 and $Ca(OH)_2$ diffuse and the product $CaCO_3$ is assumed to be static. We adopt the following set of reaction-diffusion equations,

$$\text{In } \Omega, \quad t > 0 : \quad \frac{\partial c}{\partial t} = \nabla \cdot (D_c \nabla c) - R(c, h)\,, \tag{1.2}$$

$$\frac{\partial h}{\partial t} = \nabla \cdot (D_h \nabla h) - R(c, h)\,, \tag{1.3}$$

with boundary conditions

$$\text{on } \Gamma^R \quad \mathbf{n} \cdot (-D_c \nabla c) = H^*(c^* - c), \quad \mathbf{n} \cdot (-D_h \nabla h) = 0, \tag{1.4}$$

$$\text{on } \Gamma^N \quad \mathbf{n} \cdot (-D_c \nabla c) = 0, \quad \mathbf{n} \cdot (-D_h \nabla h) = 0, \tag{1.5}$$

and initial conditions

$$\text{at } t = 0 \quad c = c^* c_i(\mathbf{x}), \quad h = h^0 h_i(\mathbf{x}). \tag{1.6}$$

Here R is the carbonization rate with reaction rate coefficient k. In particular, we will be considering reaction terms of the form

$$R(c, h) = k c^p h^q, \tag{1.7}$$

where p and q are positive constants. The initial hydroxide concentration has a representative value (taken as maximum) denoted by the constant h^0 and c^* is the average external atmospheric concentration of CO_2, the most common situation being $h_i(\mathbf{x}) = 1$, $c_i(\mathbf{x}) = 0$ for $\mathbf{x} \in \Omega$.

The diffusion coefficients $D_c \equiv D_c(c, h; k)$ and $D_h \equiv D_h(c, h; k)$ are those of CO_2 and $Ca(OH)_2$ respectively, which are not necessarily constant. Not only can the diffusion coefficients be concentration dependent but we also allow them to vary with the reaction rate coefficient. The modelling as well as the experimental literature, regard D_h as negligible compared to D_c [62, 51]. However, it is not possible to experimentally measure D_c in concrete since the results are falsified by carbonation occuring during the testing [61]. Hence, its choice has been widely studied [58, 38, 61, 35, 3] without a clear consensus on how to model its behaviour. The value of D_c has actually been computed from measurements for carbonated and uncarbonated concrete in [50], and although the results are not given, they report a decrease in its value. The two main factors, but not the only ones, that affect D_c are the porosity and relative humidity. The relative humidity is regarded as an environmental condition and will not be considered here. Experimental results show that as time increases and the reaction penetrates the concrete further, the porosity decreases [38, 50]. In this way, the diffusion coefficient of CO_2 may be expressed as $D_c = \hat{D}_c w \Phi(h)$ where w is a tortuosity factor and $\Phi(h)$ is the porosity which depends on the concentration of $Ca(OH)_2$. Justifying a possible $Ca(OH)_2$ dependence of the diffusivity. In [38], Φ_1 has been taken as an exponential law. Also, in [60] and [61] an exponential law for one of the many terms composing D_c has been adopted and in [35] the diffusion versus time plots show an exponential like decrease in D_c. This has motivated the consideration of the D_c, D_h dependence linked to $R(c, h)$ to be taken in Arrhenius forms

$$D_i = D_i^0 \left(1 - \exp\left(-\frac{\nu_i}{R_i}\right)\right), \quad i = c, h, \tag{1.8}$$

where ν_c, ν_h are suitable constants, R_c, R_h are based on partial reaction rates and D_c^0, D_h^0 are taken as the maximum values of the diffusion coefficients. This form of diffusion coefficients is the main modelling assumption and the idea is introduced by Evans [20]

for silicon oxidation. We now apply it to the case of concrete carbonation. Note that this model holds independently of the space dimension and so can be used for arbitrary geometries. Figure 1.3 shows a one- and a two-dimensional example.

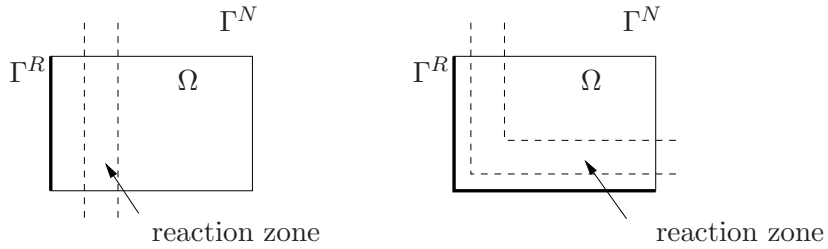

Figure 1.3: *Schematic view of a one- and two-dimensions carbonation scenario respectively.*

The transfer of CO_2 from the air to water phase (and vice versa) and the dissolution of $Ca(OH)_2$ from the solid matrix to water phase (and vice versa) are in local equilibrium i.e. all production terms by Henry's law vanish. As such, from a modelling perspective, we may justify the robin boundary condition for the aqueous carbon dioxide in (1.4) as follows. Denoting the concentration of gaseous carbon dioxide $CO_{2_{(g)}}$, in the concrete by c_g with diffusion coefficient D_{c_g}, its external atmospheric concentration c_g^* at the exposed concrete surface is given by

$$\text{on } \Gamma^{R^-} \quad \mathbf{n} \cdot (-D_{c_g} \nabla c_g) = H_g^*(c_g^* - c_g),$$

where H_g^* is the mass transfer constant. Considering a thin region at the surface, a mass flux balance gives

$$\mathbf{n} \cdot (-D_c \nabla c)|_{\Gamma^{R^+}} + \mathbf{n} \cdot (-D_{c_g} \nabla c_g)\big|_{\Gamma^{R^+}} = \mathbf{n} \cdot (-D_{c_g} \nabla c_g)\big|_{\Gamma^{R^-}},$$

on taking no flux for the aqueous carbon dioxide at the outer surface Γ^{R^-}. Assume the equilibrium balance $c = C^H c_g$ for the local exchange of gaseous and aqueous carbon dioxide, where C^H is the temperature dependent dimensionless Henry constant, a typical value being 0.82 at $20^0 C$ [38]. We may now combine these expressions to give (1.4), where

$$H^* = \frac{H_g^* D_c}{D_{c_g} + C^H D_c}, \quad c^* = C^H c_g^*.$$

We remark that the assumption of equilibrium balance between gaseous and aqueous carbon dioxide means that D_c should be taken as D_{c_g}, the governing equation (1.2) then being consistent with the models of [49, 51] when written in terms of c_g. More sophisticated models may relax this equilibrium assumption, allowing CO_2 in the gas and aqueous phases to be considered separately.

As mentioned earlier, we assume the product calcium carbonate to be static; however its formation may be modelled using a rate equation. Let $z = z(\mathbf{x}, t)$ be the

concentration of $CaCO_3$, then

$$\frac{\partial z}{\partial t} = R(c, h), \tag{1.9}$$

where its diffusivity is taken as being negligible. As such the amount of carbonate can be determined once (1.2)-(1.6) is solved, together with specifying a suitable initial condition e.g. $z = 0$ at $t = 0$.

It is worth mentioning that although we concentrate on concrete carbonation, the above model can be applied to many other settings. An example is the oxidation of binary alloys with surface poisons introduced by Hagan et.al. [26]. A small introduction for comparison purposes is given next.

1.2.1 Oxidation of binary alloys with surface poisons

Engineering alloys can form a protective layer of metal oxide at the surface so when exposed to high temperature corrosive environments, this external oxide layer separates the reactive metal from the environment. The formation of this outside layer is called external oxidation. However, in the absence of this protective layer, the metal oxide particles can be formed within the alloy causing its failure. This is known as internal oxidation. Surface poisons block the reversible reaction at the surface, in which oxygen atoms are formed. Hagan et. al. [26] investigate the effect of these surface poisons and discover how they can lead to the creation of external oxide layers in alloys that previously would have failed due to the occurrence of internal oxidation. The bulk oxidation reaction considered for metal A is

$$A + qO \rightarrow AO_q$$

where A denote metal atoms, O oxygen atoms and q is a positive integer. Let A, C and Z denote the concentration of metal A atoms, oxygen atoms and AO_q atoms respectively. Taking the alloy surface at $x = 0$, the governing equations are

$$\text{In } 0 < x < \infty : \quad \begin{aligned} \frac{\partial A}{\partial t} &= D_M \frac{\partial^2 A}{\partial x^2} - R(A, C), \\ \frac{\partial C}{\partial t} &= D_0 \frac{\partial^2 C}{\partial x^2} - qR(A, C), \\ \frac{\partial Z}{\partial t} &= R(A, C), \end{aligned}$$

with boundary conditions

$$\text{on } x = 0 \quad \frac{\partial A}{\partial x} = 0, \quad -D_0 \frac{\partial C}{\partial x} = k(C^* - C),$$

and initial conditions

$$\text{at } t = 0 \quad A = A_0, \quad C = 0, \quad Z = 0 \text{ for } 0 < x < \infty.$$

Here $R(A, C)$ is the rate of the oxidation reaction and D_M, D_0 are the diffusion coefficients of metal atoms in the alloy and of oxygen respectively. Both are taken to be constant and the diffusion of the oxide AO_q is assumed to be negligible. Further, A_0 is a constant representing the initial state of the alloy. It is assumed that all surface reactions providing oxygen to the alloy have first order reverse reactions in the concentration of oxygen at the surface. Therefore kC^* represents the production by the forward reactions and $kC(t, 0)$ represents the loss due to reverse reactions.

The addition of a convection term to (1.2)-(1.3) leads to models investigated for silicon oxidation [30, 31, 20, 22], marble sulfation [13] and internal oxidation of binary alloys [27] amongst others. Below, a brief introduction on the modifications needed for (1.2)-(1.6) are introduced for the particular case of silicon oxidation.

1.2.2 Silicon Oxidation

The oxidation of silicon is an important stage in the fabrication and process modelling of silicon device technologies. The process of the oxidation of silicon involves the reaction of an oxidant (either oxygen or steam) with silicon to form silicon oxide. The reaction equation is therefore

$$\mathrm{Si} + \mathrm{O_2} \rightarrow \mathrm{SiO_2},$$

for oxygen, and

$$\mathrm{Si} + 2\mathrm{H_2O} \rightarrow \mathrm{SiO_2} + 2\mathrm{H_2},$$

for steam. The silicon oxide formed during the reaction occupies a greater volume than the original silicon and is this associated volume expansion that makes the oxidation stage important. The volume expansions cause stresses and if these get too large then dislocation takes place and so the whole model breaks down. Therefore, special care is needed at this stage. Figure 1.4 shows a sketch of how the device evolves with time. The full oxidation problem is two-dimensional, but the behaviour far from the nitride cap is one-dimensional in nature.

The most widely accepted model for silicon oxidation is that of Deal and Grove [16] in which a number of assumptions for the process related to the chemistry are made. In the one-dimensional case the oxide, being incompressible, moves as a rigid body so that there is no need to consider its deformation. We define the oxide region to be $-f(t) < y < h(t)$, where $y = -f(t)$ is the Si/SiO_2 interface and $y = h(t)$ is the $\mathrm{SiO_2}$/oxidant interface (see figure 1.5). In this region the diffusion of oxidant, concentration $c = c(y, t)$, is governed by a linear diffusion equation with convection at

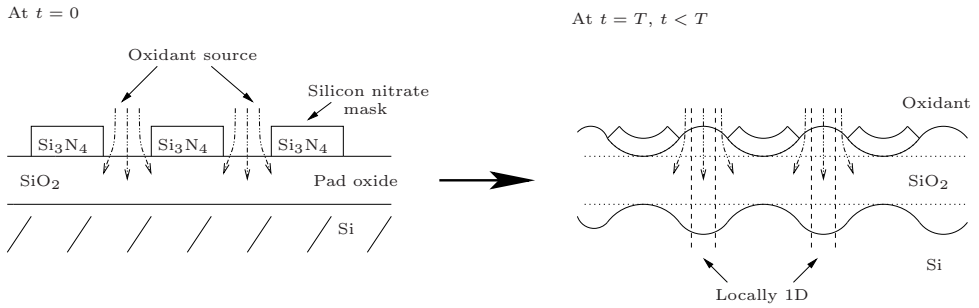

Figure 1.4: *Evolution of silicon oxidation device.*

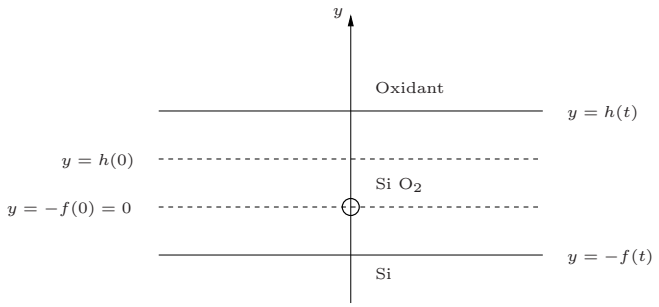

Figure 1.5: *Silicon oxidation domain.*

the oxide velocity dh/dt:

$$\frac{\partial c}{\partial t} + \frac{\mathrm{d}h}{\mathrm{d}t}\frac{\partial c}{\partial y} = D\frac{\partial^2 c}{\partial y^2}, \quad \text{in } -f(t) < y < h(t) \tag{1.10}$$

$$\text{on } y = h(t), \qquad D\frac{\partial c}{\partial y} = H(c^* - c)\ ; \tag{1.11}$$

$$\text{on } y = -f(t), \qquad D\frac{\partial c}{\partial y} - \left(\frac{\mathrm{d}h}{\mathrm{d}t} + \frac{\mathrm{d}f}{\mathrm{d}t}\right)c = kc\ ;, \tag{1.12}$$

$$\frac{1}{\beta}\left(D\frac{\partial c}{\partial y} - \left(\frac{\mathrm{d}h}{\mathrm{d}t} + \frac{\mathrm{d}f}{\mathrm{d}t}\right)c\right) = \frac{\mathrm{d}f}{\mathrm{d}t} = \frac{1}{\gamma}\left(\frac{\mathrm{d}h}{\mathrm{d}t} + \frac{\mathrm{d}f}{\mathrm{d}t}\right); \tag{1.13}$$

$$\text{at } t = 0, \qquad c = 0, \quad f = 0, \quad h = a\ . \tag{1.14}$$

Here, D is the diffusion coefficient, H is the gas-phase transport coefficient, c^* is the equilibrium concentration of oxidant in the oxide and k is the reaction coefficient. Equation (1.11) represents the absorption reaction which is taken to be first order, as is the silicon oxidation reaction in (1.12). Equation (1.13) represents conservation of silicon and here γ is the ratio of the specific volume of silicon to that of oxide and β is the number of oxidant molecules which react with a unit of volume of silicon to create a volume γ of oxide. For more details on this model we refer the reader to [31].

The Deal and Grove model above appears to give results in good agreement with experiment except for the growth of extremely thin oxides, when the physical mechanisms involved do not seem to be well understood. Below we summarise a system

of homogeneous reaction-convection-diffusion equations introduced by King [30] and further discussed in [20, 22].

Let n_1, n_2 and c be the concentration in moles per unit volume of Si, SiO_2 and oxidant respectively. Silicon oxidation is modelled as a homogeneous reaction with volume change as follows

$$\begin{aligned}
\text{In } -\infty < y \le h(t): \quad & \frac{\partial n_1}{\partial t} + \frac{\partial}{\partial y}(vn_1) = \frac{\partial}{\partial y}\left(D_m \frac{\partial n_1}{\partial y}\right) - R(c, n_1), \\
& \frac{\partial n_2}{\partial t} + \frac{\partial}{\partial y}(vn_2) = \frac{\partial}{\partial y}\left(D_m \frac{\partial n_2}{\partial y}\right) + R(c, n_1), \\
& \frac{\partial c}{\partial t} + \frac{\partial}{\partial y}(vc) = \frac{\partial}{\partial y}\left(D \frac{\partial c}{\partial y}\right) - \gamma R(c, n_1), \\
& \frac{\partial v}{\partial y} = \frac{\gamma - 1}{n} R(c, n_1), \\
& n_1 + \gamma n_2 = n,
\end{aligned}$$

with boundary conditions

$$\begin{aligned}
&\text{on } y = h(t) && D\frac{\partial c}{\partial y} = H(c^* - c), \quad \frac{\partial n_1}{\partial y} = \frac{\partial n_2}{\partial y} = 0, \quad v = h, \\
&\text{as } y \to -\infty && c \to 0, \quad n_1 \to 1, \quad n_2 \to 0,
\end{aligned}$$

and appropriate initial conditions. Here, n is the number of moles per unit volume of pure Si; $D = D(n_1)$ is the diffusion coeffcient of oxidant and $D = D_m(n_1)$ is the mutual diffusion coefficient of Si and SiO_2, both not necessarily constant; v is the local velocity; H is the gas-phase transport coefficient; c^* is the equilibrium concentration of oxidant in the oxide; γ is the ratio of the specific volume of silicon to that of oxide. Again, the Robin boundary condition on $y = h$ represents the absorption reaction which is taken to be first order.

This model is the analogous formulation to the set of reaction-diffusion equations (1.2)-(1.6) with added convection. Investigating two different regimes for the oxidant diffusivity in the fast reaction - slow diffusion limit leads to distinct sharp interface models for oxidation. The resulting models correspond to Stefan like problems that reproduce the Deal and Grove model (1.10)-(1.14). In this thesis, we derive the analogy of this for the concrete case.

Finally, for the internal oxidation of binary alloys, the convection term represents the bulk motion of the alloy away from the region to accommodate the extra volume caused by the oxidation reaction since the metal oxide occupies more volume than its constituent metal [27].

1.3 Approach and organisation of the thesis

We have introduced a basic reaction-diffusion model (1.2)-(1.6) to describe the aqueous chemistry and transport involved in (1.1). In it, our main assumption has been to let the diffusion coefficient be concentration and reaction rate dependent as shown in (1.8). From now on we will consider (1.2)-(1.6) in one-space dimension. In other words, we only have into account the situation depicted on the left of figure 1.3. We then use the technique of matched asymptotics [4] to perform a detailed analysis of the reaction layer for various physically relevant scaling regimes. These regimes will depend in the size of a relative transport parameter, which measures the characteristic ratio of diffusion and concentrations for CO_2 and $Ca(OH)_2$. Further, we investigate three different possible situations in regard to the diffusivities.

In chapter 2 we introduce the one-dimensional model and look at the first diffusion coefficient regime, where they remain order 1. We refer to this regime as slowly varying. This is the usual case which has received attention in the literature [26, 30, 43]. The other regimes, allow the diffusion coefficients to change their orders of magnitude in terms of a parameter ϵ. The diffusion coefficients are now termed rapidly varying. In chapter 3 we consider the second regime where we have only a rapidly varying CO_2 diffusivity, with the $Ca(OH)_2$ diffusivity slowly varying. Finally, as a third regime, looked at in chapter 4, we consider the effects of rapidly varying CO_2 and $Ca(OH)_2$ diffusivities simultaneously. All these cases lead to the derivation of conceptually different sharp interface models which are summarised in chapter 6. We see three main types; namely, one and two-phase Stefan like problems and two scale micro-macro free boundary problems. The latter is a completely new type of model in which the speed of the reaction interface is updated from a smaller length scale. Additionally, numerical results of the original system obtained using COMSOL Multiphysics are showed in sections 2.4, 3.2 and 4.2. These include a base case, in which the parameter values are chosen to match with the literature and a parameter variation section where the effects of changes to the parameter values are investigated. These corroborate the asymptotic results obtained for the various scaling cases. Moreover, using the information gathered from the numerical simulations, chapters 2, 3 and 4, are completed with a plot of the free boundary and, where applicable, of the boundary conditions needed at the reaction interface.

In chapters 5 and 6 we concentrate on analysing the resulting Stefan like problems from the previous three chapters. In the rapidly varying diffusion regimes, the Stefan problem is coupled to a micro problem, resulting in a one- or two-phase micro-macro Stefan like problem, depending on the scaling regime. These micro problems essentially determine the kinetic conditions necessary at the interface. For slowly varying diffusivities, these conditions are zero. The micro problems are composed of two second order ordinary differential equations and can be seen as stand-alone systems. Chapter

5 addresses whether these micro problems are set up correctly. An eigenmode analysis is carried out to determine the number of conditions imposed by the boundary conditions to ensure a well defined problem. We then solve these using MATLAB and compare the results to the ones obtained for the full reaction-diffusion system done in sections 2.4, 3.2 and 4.2. A power law for the kinetic conditions is also derived in the asymptotic limit of zero reaction speed, which is equivalent to the large time behaviour of the reaction. This is a novel result that builds on the new two scale micro-macro type of Stefan problem. Chapter 6 summarises the results from the previous chapters by stating all the different types of generalised Stefan problems coupled to their respective micro problems. One of the main aims is to determine the speed of growth of the macroscopic carbonated phase, denoted the interface. The boundary conditions necessary at the interface have already been determined and they have led to the consideration of the micro problems discussed in detail in chapter 5. To continue to investigate the behaviour of the interface, solutions to the generalised Stefan problems are required. Analytically, it is of interest to calculate the small and especially the large time behaviour of the interface and concentration profiles. We apply the approach seen in [26] as follows. Asymptotic approximations of the two limiting behaviours $t \ll 1$ and $t \gg 1$ are done in section 6.2, where the two and three term expansions obtained are also compared to the behaviours derived from the full reaction-diffusion system. Numerically, the full sharp interface Stefan problems can be solved. The method of lines [41] is applied and its results are recorded in section 6.3. To conclude this thesis, several two dimensional geometries are modelled in chapter 7 for the different types of diffusion coefficients considered in chapters 2, 3 and 4.

In essence, the main new contributions made by this thesis are the application of a reaction dependent diffusion coefficient leading to two scale micro-macro free boundary problems (chapters 3, 4), the power law for the kinetic conditions (chapter 5) and the asymptotic small and large time approximations of the free boundary (chapter 6). Numerically, it is also worth mentioning, the application of the method of lines (chapter 6), as well as the implementation of the carbonation model into COMSOL Multiphysics all throughout this thesis.

Chapter 2

Concrete Carbonation with Slowly Varying Diffusivity

In the present Chapter we formulate the one-space dimensional form of the reaction-diffusion model (1.2)-(1.6) and look at the fast reaction limit. The technique of matched asymptotics is used to derive the sharp interface models for the simplest diffusion case in which both D_c and D_h remain order 1 and have no explicit dependence on neither the concentration nor the reaction rate coefficient. This slowly varying regime will provide a useful base case against which to compare the effects of more rapidly varying diffusivities later in Chapters 3 and 4. Numerical results, supporting the asymptotics, illustrate the behaviour of the concentration profiles for several parameter regimes, as well as the behaviour of the free boundary.

2.1 The one-dimensional model equations

We consider the concrete occupying a one-dimensional slab geometry $\Omega = [0, L]$. The x-axis being directed into the concrete with surface $x = 0$ exposed to an external source of CO_2, whilst the surface $x = L$ is assumed impervious to all reaction species. Using the same notation as in section 1.2, we arrive at the one-dimensional case of (1.2)-(1.6)

$$\text{In}\, 0 < x < L,\ t > 0 : \quad \frac{\partial c}{\partial t} = \frac{\partial}{\partial x}\left(D_c \frac{\partial c}{\partial x}\right) - R(c, h)\,, \tag{2.1}$$

$$\frac{\partial h}{\partial t} = \frac{\partial}{\partial x}\left(D_h \frac{\partial h}{\partial x}\right) - R(c, h)\,, \tag{2.2}$$

with boundary conditions

$$\text{on}\, x = 0 \quad -D_c \frac{\partial c}{\partial x} = H^*(c^* - c),\ \frac{\partial h}{\partial x} = 0, \tag{2.3}$$

$$\text{on } x = L \quad \frac{\partial c}{\partial x} = 0,\ \frac{\partial h}{\partial x} = 0, \tag{2.4}$$

and initial conditions

$$\text{at } t = 0 \quad c = c^* c_i(x),\ h = h^0 h_i(x). \tag{2.5}$$

We nondimensionalise as follows

$$c = c^*\bar{c}, \quad h = h^0\bar{h}, \quad x = L\bar{x}, \quad t = \frac{L^2 h^0}{D_c^0 c^*}\bar{t},$$
$$D_c = D_c^0\bar{D}_c, \quad D_h = D_h^0\bar{D}_h, \quad R(c,h) = \theta r(\bar{c},\bar{h}),$$

where L is a characteristic length scale, θ a representative reaction rate scaling and we have taken D_c^0 and D_h^0 as the maximum values of the diffusion coefficients. Dropping $^-$'s, we obtain

$$\text{In } 0 < x < 1,\ t > 0 : \quad \epsilon^2\left(\mu\frac{\partial c}{\partial t} - \frac{\partial}{\partial x}\left(D_c\frac{\partial c}{\partial x}\right)\right) = -r(c,h), \tag{2.6}$$

$$\epsilon^2\left(\frac{\partial h}{\partial t} - \frac{\delta^2}{\epsilon^2}\frac{\partial}{\partial x}\left(D_h\frac{\partial h}{\partial x}\right)\right) = -r(c,h), \tag{2.7}$$

with boundary conditions

$$\text{on } x = 0 \quad -D_c\frac{\partial c}{\partial x} = H(1-c),\ \frac{\partial h}{\partial x} = 0, \tag{2.8}$$

$$\text{on } x = 1 \quad \frac{\partial c}{\partial x} = 0,\ \frac{\partial h}{\partial x} = 0, \tag{2.9}$$

initial conditions

$$\text{at } t = 0 \quad c = c_i(x),\ h = h_i(x), \tag{2.10}$$

and the nondimensional parameters being

$$\epsilon^2 = \frac{D_c^0 c^*}{L^2\theta}, \quad \delta^2 = \frac{D_h^0 h^0}{L^2\theta}, \quad \mu = \frac{c^*}{h^0}, \quad H = \frac{LH^*}{D_c^0}.$$

In the semi-infinite concrete case, L is at our disposal and can be taken to be D_c^0/H^* so that $H = 1$. Moreover, if H^* is infinite, then the Robin boundary condition in (2.3) simplifies to the Dirichlet boundary condition $c = c^*$ and so (2.8) becomes $c = 1$ if L is finite. In the semi-infinite regime, L will remain a free parameter with the lower bound $D_c^0 c^*/\theta < L^2$, since the parameter range of relevance is $\delta \le O(\epsilon)$ with $\epsilon \ll 1$ in order to evaluate the fast reaction limit $\epsilon \to 0$. The scaling θ is chosen so that $r(c,h) \le 1$ for $0 \le c \le 1$, $0 \le h \le 1$. To be more precise, for reaction terms of the form (1.7), we take

$$r(c,h) = c^p h^q, \tag{2.11}$$

by choosing $\theta = kc^{*^p} h^{0^q}$.

Typical values of the dimensional parameters are given in Table 2.1. It is worth mentioning that, experimentally, there are two types of settings, natural and accelerated. Parameter values for both are given in Table 2.1. Natural environments normally contain $0.03 - 0.05\%$ CO_2, with the evolution of the carbonation depth being slow and taking many years (typically 5-10 years). An accelerated carbonation chamber, exposes concrete to 50% CO_2 which dramatically reduces the time needed to perform experiments from years to a matter of days (typically upto 20 days). In [50] a time relationship between accelerated and normal environments for the carbonation depth is given such that $t_1/t_2 \sim 10^3$, where t_1 is the time required under normal exposure and t_2 under accelerated conditions. The reaction rate given corresponds to the common partial reaction orders $p = q = 1$. However, other values of these, $0.9 \leq p, q \leq 1.5$, also seem appropriate. A representative length L can be of the order of centimetres upto several metres i.e. $L = 0.1 - 10$m depending upon the situation and geometry considered. All these give the estimates for the non-dimensionalised parameters shown in Table 2.2. The parameter range of relevance is thus

$$\epsilon << 1, \quad \delta \leq O(\epsilon), \quad \mu << 1, \quad H = O(1), \tag{2.12}$$

where we note that the "relative transport parameter"

$$\frac{\delta^2}{\epsilon^2} = \frac{D_h^0 h^0}{D_c^0 c^*},$$

is typically small or at most order 1 [49]. The CO_2 interfacial exchange parameter H is estimated using the maximum values of the CO_2 diffusivities, which are expected to occur at the surface and for gas are denoted by $D_{c_g}^0$. Since $D_c^0 = D_{c_g}^0$ we have that $H = LH_g^*/D_{c_g}^0$, the larger values of this parameter suggesting that the interface exchanges are close to equilibrium.

Note that the diffusion coefficients now have dependencies on the parameter ϵ i.e. $D_c = D_c(c, h; \epsilon)$, $D_h = D_h(c, h; \epsilon)$ being the general form. As introduced in (1.8), we will focus on the simpler dependency cases $D_c(h; \epsilon)$, $D_h(c; \epsilon)$. In particular, three distinct cases will be discussed: the simplest of these (chapter 2) has $D_c = O(1)$ for $h = O(1)$ and $D_h = O(1)$ for $c = O(1)$, the second (chapter 3) has $D_c = O(\epsilon^2)$ for $h = O(1)$ with $h > 0$ and $D_h = O(1)$ for $c = O(1)$, while the final scenario (chapter 4) considers $D_c = O(\epsilon^2)$ for $h = O(1)$ with $h > 0$ and $D_h = O(\delta^2)$ for $c = O(1)$ with $c > 0$.

Parameter (units)	Value (accelerated)	Value (natural)
$D_c^0 = D_{cg}^0$ $(\mathrm{m^2 s^{-1}})$	$(0.5-5)\times 10^{-8}$	$(0.5-5)\times 10^{-8}$
D_h^0 $(\mathrm{m^2 s^{-1}})$	10^{-13}	10^{-13}
H_g^* $(\mathrm{m\ s^{-1}})$	1.16×10^{-2}	1.16×10^{-2}
c^* $(\mathrm{mol\ m^{-3}})$	4.38	2.71×10^{-3}
h^0 $(\mathrm{mol\ m^{-3}})$	1.04×10^{3}	1.04×10^{3}
k $(\mathrm{m^3 mol^{-1} s^{-1}})$	1.74×10^{-5}	4.6×10^{-5}

Table 2.1: *Typical parameter values for natural and accelerated carbonation obtained from [38], [60], [49], [51]. Concentrations are expressed in units of mol m^{-3} for consistency with the reaction rate (partial orders of the reaction being $p = q = 1$); the molar masses of 44.01 g for CO_2 and 74 g for $Ca(OH)_2$ may be used to convert to units of g m^{-3}.*

Nondimensional parameter	Value (accelerated)	Value (natural)
ϵ^2	$10^{-9}-10^{-4}$	$10^{-9}-10^{-4}$
δ^2	$10^{-11}-10^{-7}$	$10^{-10}-10^{-5}$
μ	10^{-3}	10^{-6}
H	$10^{4}-10^{7}$	$10^{4}-10^{7}$

Table 2.2: *Estimated nondimensional parameters using values in Table 2.1.*

2.2 The sharp interface model derivation

The limit $\epsilon \to 0$ will be considered; Ortoleva el.al. [47] refer to this as the fast-aqueous-reaction asymptotics. This corresponds to the bulk reaction being very rapid and the reaction is expected therefore to be essentially in equilibrium ($c = 0$ or $h = 0$ at leading order in ϵ) except in a thin boundary layer, the reaction zone, where virtually all the carbonation occurs.

The location of the reaction zone will be denoted by $x = s(t;\epsilon)$, which here is taken as a suitable point within its centre. Its specification is not unique and even experimentally there is no consensus on its definition [11]. Since our reaction species have monotonic concentration profiles, for definiteness we take $s(t;\epsilon)$ as the position where the concentrations of CO_2 and $Ca(OH)_2$ cross, i.e.

$$s(t;\epsilon) = \{x \in [0,L] | c(x,t) = h(x,t)\}. \tag{2.13}$$

As the reaction zone is very thin, $s(t;\epsilon)$ may be used to represent the position of the carbonation reaction front. In the literature there are alternative ways of defining

such a front (see the discussion in [38]). A common one is to use the degree of local carbonation as represented through a suitable high concentration isoline of the reaction product $CaCO_3$. Nevertheless, these alternative definitions should be equivalent to within the asymptotic thickness of the reaction zone.

The regions in which the reaction zone is in equilibrium are denoted as outer regions, where outer 1 has $h = o(1)$ and outer 2 has $c = o(1)$. Figure 2.1 illustrates schematically the set up just explained.

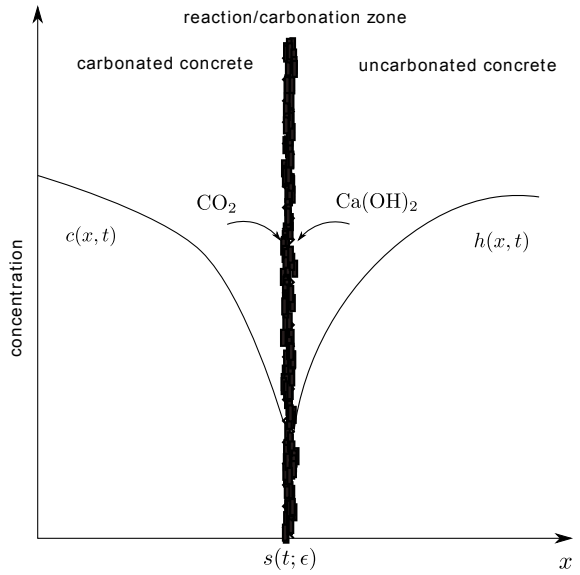

Figure 2.1: *A schematic illustration of the carbonation process in concrete. CO_2 enters the concrete and diffuses to the reaction (or carbonation) zone, where it rapidly reacts with $Ca(OH)_2$. Shown qualitatively are the concentration profiles $c(x,t)$, $h(x,t)$ and the reaction zone's position $s(t;\epsilon)$ at a fixed time t. The asymptotic structure of the reaction zone depends upon the properties of the diffusivities. It can be just a single region (as for the slowly varying diffusivities later on in this chapter) or have more than one region (as described in chapters 3 and 4 for rapidly varying diffusivities).*

The details of the reaction zone depend crucially on the behaviour of the diffusion coefficients, which we investigate in this and the next two chapters. For each regime we perform asymptotic expansions and consider the system's dependence on the size of the relative transport parameter. Further, for generality in derivation, we keep $\mu = O(1)$ and consider its vanishing limit later on in chapter 6 when seeking to solve the resulting sharp interface Stefan problems. However, before addressing all these different possible scenarios, we note general results which will apply for all cases.

2.2.1 Outer solutions

We take the limit $\epsilon \to 0$ and pose expansions of c and h to obtain two outer regions, in which the reaction is in equilibrium (i.e. $c \equiv 0$ or $h \equiv 0$), as described below. These expansions depend on the values of p and q. However, here we are only concerned

about the leading order behaviour which will be the same regardless of the values of p and q. Nevertheless, this dependence on p and q will appear when dealing with the correction terms (see Appendix A) and so for completeness we state the expansions in detail here. The location of the reaction zone also requires expansion. However, we denote the leading order term $s(t)$ and note that the higher order terms do not impact in the analysis to the orders of the calculations considered.

Outer1 $0 < x < s(t)$ (carbon dioxide region)

For $q \leq 1$ we pose the expansions

$$c = c_0 + \epsilon^2 c_1 + \ldots, \quad h = h_0 + \epsilon^2 h_1 + \ldots, \tag{2.14}$$

and for $q > 1$ we pose instead

$$c = c_0 + \epsilon^{\frac{2}{q-1}} c_1 + \ldots, \quad h = h_0 + \epsilon^{\frac{2}{q-1}} h_1 + \ldots. \tag{2.15}$$

Substituting (2.14) or (2.15) into (2.6), (2.7) gives

$$h_0 = 0$$

at leading order, and

$$\mu \frac{\partial c_0}{\partial t} - \frac{\partial}{\partial x}\left(D_{c_0} \frac{\partial c_0}{\partial x} \right) = 0, \tag{2.16}$$

where $D_{c_0}(c, h; \epsilon) = D_c(c_0, 0; 0)$, for any q. Note that the right hand side of (2.16) is 0. In fact, for $q \leq 1$, $h \equiv 0$ algebraically for all orders in ϵ and so it is exponentially small. For $q > 1$, the reaction term will appear for the first time at $O(\epsilon^{\frac{4}{q-1}})$. More details on the correction terms can be found in Appendix A.

Outer 2 $s(t) < x < 1$ (calcium hydroxide region)

For $p \leq 1$ we pose the expansions

$$c = c_0 + \epsilon^2 c_1 + \ldots, \quad h = h_0 + \epsilon^2 h_1 + \ldots, \tag{2.17}$$

and for $p > 1$ we pose instead

$$c = c_0 + \epsilon^{\frac{2}{p-1}} c_1 + \ldots, \quad h = h_0 + \epsilon^{\frac{2}{p-1}} h_1 + \ldots. \tag{2.18}$$

Substituting the expansions into (2.6), (2.7) we obtain

$$c_0 = 0$$

at leading order, and

$$\frac{\partial h_0}{\partial t} - \frac{\delta^2}{\epsilon^2} \frac{\partial}{\partial x}\left(D_{h_0} \frac{\partial h_0}{\partial x} \right) = 0, \tag{2.19}$$

where $D_{h_0}(c,h;\epsilon) = D_h(0,h_0;0)$, for any p. This equation may simplify further depending upon the relative sizes of δ and ϵ. Further, note that the reaction term does not play a roll in (2.19). For $p \leq 1$, $c \equiv 0$ algebraically to all orders in ϵ and so c is exponentially small. For $p > 1$, the reaction term will first appear in the hydroxide governing equation at $O(\epsilon^{\frac{4}{p-1}})$. More details on the correction terms can be found in Appendix A.

Outside the reaction zone, the reaction rate is negligible. In outer 1, $0 < x < s(t)$, h is negligible and so it is essentially calcium hydroxide free, having been used up in the reaction to form calcium carbonate. In outer 2, $s(t) < x < 1$, c is negligible, giving a region of almost pure calcium hydroxide.

2.2.2 Interface conditions

In practical terms it is the outer regions that are the ones of most significance; however, the interior layer must be analysed to obtain the continuity conditions linking both outers. Without appealing to such an inner analysis, we can use (2.6) and (2.7) to obtain the statement

$$\frac{\partial}{\partial t}(\mu c - h) = \frac{\partial}{\partial x}\left(D_c\frac{\partial c}{\partial x} - \frac{\delta^2}{\epsilon^2}D_h\frac{\partial h}{\partial x}\right).$$

This may now be used to obtain the jump condition at $x = s(t)$,

$$\left[D_c\frac{\partial c}{\partial x} - \frac{\delta^2}{\epsilon^2}D_h\frac{\partial h}{\partial x} + \dot{s}(\mu c - h)\right]_{s_-}^{s_+} = 0,$$

representing conservation of mass. Using the outer solutions this yields,

$$\text{at } x = s(t) \quad -D_{c_0}\frac{\partial c_0(s^-,t)}{\partial x} - \frac{\delta^2}{\epsilon^2}D_{h_0}\frac{\partial h_0(s^+,t)}{\partial x} = \dot{s}(\mu c_0(s^-,t) + h_0(s^+,t)). \quad (2.20)$$

This represents the Stefan type moving boundary condition on (2.16) and (2.19) for outers 1 and 2 respectively. However, we still remain two conditions short in terms of specifying the moving boundary problem for (2.16) and (2.19). These final conditions can only be found by undertaking an interior layer analysis of the reaction zone. They correspond to kinetic conditions and will take the general form

$$c_0(s^-,t) = \Phi_1(\dot{s}), \quad h_0(s^+,t) = \Phi_2(\dot{s}), \quad (2.21)$$

where the functions Φ_1 and Φ_2 are to be determined. To complete the sharp interface statement we require suitable initial conditions. These are parameter sensitive, the

most usual situation being

$$\begin{aligned} \text{at } t = 0 \quad & c_0 = c_i(x) \text{ for } 0 < x < s(0), \\ & h_0 = h_i(x) \text{ for } s(0) < x < 1, \\ & s(0) = s_0, \end{aligned} \tag{2.22}$$

with, more often than not, the initial position of the reaction zone being taken at the concrete surface $s_0 = 0$. In certain parameter regimes, there is an initial carbonation stage in which the reaction zone remains in its initial location for a finite time t_0. In this case we modify (2.22) to

$$\begin{aligned} \text{at } t = t_0 \quad & c_0 = C_i(x) \text{ for } 0 < x < s(t_0), \\ & h_0 = H_i(x) \text{ for } s(t_0) < x < 1, \\ & s(t_0) = s_0, \end{aligned} \tag{2.23}$$

where C_i and H_i are the resulting concentration profiles at the end of this initial carbonation stage.

The moving boundary problem (2.16), (2.19), (2.20), (2.21) with (2.22) or (2.23) is a two-phase problem in the regime $\delta = O(\epsilon)$. When $\delta \ll \epsilon$, it degenerates to a one-phase problem where Φ_2 is no longer needed.

2.3 Interior (reaction) layer analysis

We start by considering the simplest case in which neither D_c nor D_h have any explicit dependence upon ϵ. As such they remain order 1, which we refer to as slowly varying. To describe the interior layer we need to find a balance in (2.6) and (2.7) such that the reaction term $r \neq 0$ at leading order. In view of (2.16) we see that the flux of c must be $O(1)$ in the reaction layer. The reaction layer for slowly varying diffusivities comprises a single region whose behaviour is affected by the dependence of the parameter δ on ϵ. We describe this region for the parameter range $\delta \leq \epsilon$, larger values of δ not being physically relevant for the carbonation problem.

Before analysing the inner region in detail recall (2.19). For $\delta \ll \epsilon$ it will become

$$\frac{\partial h_0}{\partial t} = 0,$$

and so by (2.10) we will obtain

$$h_0 = h_i(x) \quad \text{in } s(t) < x < 1\,.$$

This suggests that h must be $O(1)$ in the reaction layer. Further, for $\delta = O(\epsilon)$ we

obtain

$$\frac{\partial h_0}{\partial t} - \frac{\partial}{\partial x}\left(D_{h_0}\frac{\partial h_0}{\partial x}\right) = 0,$$

which gives a different solution behaviour described in more detail in section 2.3.3.

The fullest balance in (2.6) and (2.7) is obtained for $\delta_{CR} = \epsilon^{\frac{p+2}{p+1}}$. Thus we obtain three possible asymptotic regimes for the parameter range $\delta \leq \epsilon$, namely $\delta \leq \delta_{CR}$, $\delta_{CR} \ll \delta \ll \epsilon$ and $\delta = O(\epsilon)$. For the remainder of this section we will consider these 3 cases separately and derive their corresponding sharp interface models.

2.3.1 Case $\delta \leq \delta_{CR}$

Here, $\delta_{CR} = \epsilon^{\frac{p+2}{p+1}}$ and it refers to the value of δ for which we obtain the fullest possible balance in the governing equations.
The required inner scalings are

$$x = s(t) + \epsilon^{\frac{2}{p+1}}\bar{x}, \quad c = \epsilon^{\frac{2}{p+1}}\bar{c}, \quad h = \bar{h}, \tag{2.24}$$

giving

$$\epsilon^{\frac{4}{p+1}}\mu\frac{\partial \bar{c}}{\partial t} - \epsilon^{\frac{2}{p+1}}\dot{s}\frac{\partial \bar{c}}{\partial \bar{x}} - \frac{\partial}{\partial \bar{x}}\left(D_c\frac{\partial \bar{c}}{\partial \bar{x}}\right) = -\bar{c}^p\bar{h}^q, \tag{2.25}$$

$$\epsilon^{\frac{2}{p+1}}\frac{\partial \bar{h}}{\partial t} - \dot{s}\frac{\partial \bar{h}}{\partial \bar{x}} - \frac{\delta^2}{\left(\epsilon^{\frac{p+2}{p+1}}\right)^2}\frac{\partial}{\partial \bar{x}}\left(D_h\frac{\partial \bar{h}}{\partial \bar{x}}\right) = -\bar{c}^p\bar{h}^q. \tag{2.26}$$

Posing the expansions

$$\bar{c} = \bar{c}_0 + o(1), \quad \bar{h} = \bar{h}_0 + o(1),$$

with

$$D_c(c,h) \sim D_c(0,\bar{h}_0), \quad D_h(c,h) \sim D_h(0,\bar{h}_0),$$

we obtain at leading order the following two possibilities:

- $\delta < \delta_{CR}$

$$D_c\frac{\partial \bar{c}_0}{\partial \bar{x}} = \dot{s}\bar{h}_0 + A_1(t), \tag{2.27}$$

$$\dot{s}\frac{\partial \bar{h}_0}{\partial \bar{x}} = \bar{c}_0^p\bar{h}_0^q, \tag{2.28}$$

where $A_1(t)$ arises from integrating and is a function of t to be determined. Matching into outer 2, the matching conditions

$$\text{as } \bar{x} \to +\infty \quad \bar{c}_0 \to 0, \quad D_c\frac{\partial \bar{c}_0}{\partial \bar{x}} \to 0, \quad \bar{h}_0 \to h_0(s^+,t), \tag{2.29}$$

give

$$A_1(t) = -\dot{s}h_0(s^+, t). \tag{2.30}$$

This system has an equilibrium point $(c^*, h^*) = (0, h_i)$. For $p = q = 1$ it has eigenvalues $\mu_{1,2} = \pm\sqrt{\frac{h_i}{D_c}}$ and Figure 2.1 shows the phase plane. For $p \neq 1$ the behaviour around the equilibrium point is nonlinear. The solution to the system (2.27)-(2.28) with (2.30) depends upon the values of p and q. Writing

$$\frac{\partial \bar{c}_0}{\partial \bar{h}_0} = \frac{\dot{s}^2(\bar{h}_0 - h_i)}{D_c \bar{c}_0^p \bar{h}_0^q},$$

we may integrate to obtain,

$$\begin{aligned}
&\frac{D_c}{\dot{s}^2}\frac{\bar{c}^{p+1}}{p+1} + \bar{h}_0^{1-q}\left(\frac{h_i}{1-q} - \frac{\bar{h}_0}{2-q}\right) = 0, && \text{for } 0 < q < 1\\
&\frac{D_c}{\dot{s}^2}\frac{\bar{c}^{p+1}}{p+1} - \bar{h}_0 + h_i(1 + \ln(\bar{h}_0) - \ln(h_i)) = 0, && \text{for } q = 1\\
&\frac{D_c}{\dot{s}^2}\frac{\bar{c}^{p+1}}{p+1} - \bar{h}_0^{-(q-1)}\left(\frac{h_i}{q-1} + \frac{\bar{h}_0}{2-q}\right) = 0, && \text{for } 1 < q < 2\\
&\frac{D_c}{\dot{s}^2}\frac{\bar{c}^{p+1}}{p+1} - \ln(\bar{h}_0) + h_i(h_i - \bar{h}_0) + \ln(h_i) = 0, && \text{for } q = 2\\
&\frac{D_c}{\dot{s}^2}\frac{\bar{c}^{p+1}}{p+1} + \bar{h}_0^{-(q-1)}\left(\frac{\bar{h}_0}{q-2} - \frac{h_i}{q-1}\right) - \frac{h_i^{-(q-2)}}{(q-2)(q-1)} = 0, && \text{for } q > 2.
\end{aligned}$$

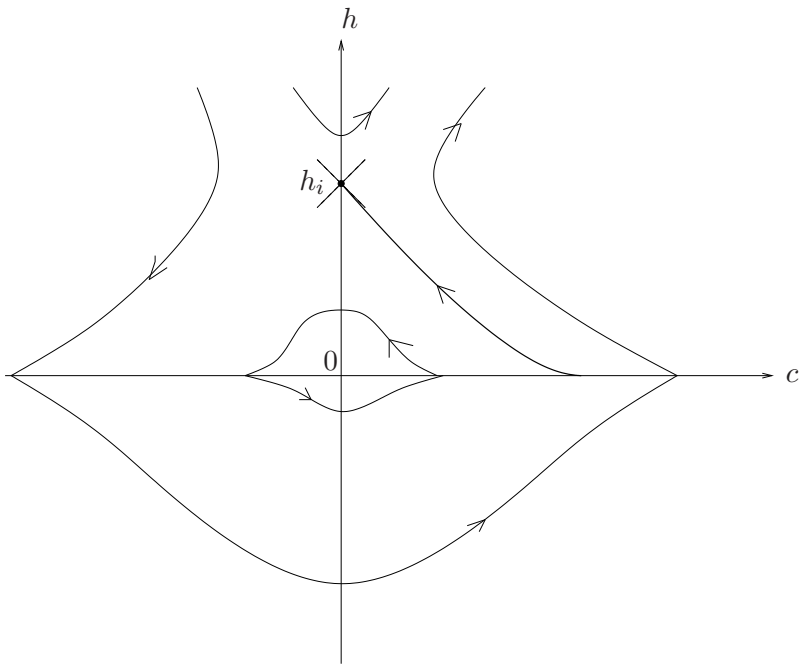

Figure 2.2: *The reaction zone phase plane for $p = q = 1$.*

- $\delta = \delta_{CR}$

$$D_c \frac{\partial \bar{c}_0}{\partial \bar{x}} = D_h \frac{\partial \bar{h}_0}{\partial \bar{x}} + \dot{s}\bar{h}_0 + A_2(t), \tag{2.31}$$

$$\dot{s}\frac{\partial \bar{h}_0}{\partial \bar{x}} + \frac{\partial}{\partial \bar{x}}\left(D_h \frac{\partial \bar{h}_0}{\partial \bar{x}}\right) = \bar{c}_0^p \bar{h}_0^q, \tag{2.32}$$

where $A_2(t)$ is a function of t to be determined. Matching into outer 2, the matching conditions (2.29) and

$$\text{as } \bar{x} \to +\infty \quad D_h \frac{\partial \bar{h}_0}{\partial \bar{x}} \to \frac{\delta^2}{\epsilon^2} D_{h_0} \frac{\partial h_0(s^+, t))}{\partial x}, \tag{2.33}$$

give

$$A_2(t) = -\frac{\delta^2}{\epsilon^2} D_{h_0} \frac{\partial h_0(s^+, t)}{\partial x} - \dot{s} h_0(s^+, t) = -\dot{s} h_0(s^+, t).$$

Hence, $A(t) := A_1(t) = A_2(t)$. The matching conditions for outer 1 are

$$\text{as } \bar{x} \to -\infty \quad D_c \frac{\partial \bar{c}_0}{\partial \bar{x}} \to D_{c_0} \frac{\partial c_0(s^-, t))}{\partial x}, \quad \bar{h}_0 \to 0, \tag{2.34}$$

which yield in both cases

$$A(t) = D_{c_0} \frac{\partial c_0(s^-, t)}{\partial x}.$$

Hence,

$$\text{at } x = s(t) \quad -D_{c_0} \frac{\partial c_0(s^-, t)}{\partial x} = \dot{s} h_0(s^+, t). \tag{2.35}$$

Further, by (2.24) we necessarily have

$$c_0(s^-, t) = 0, \tag{2.36}$$

as the"missing" second moving boundary condition for (2.16) i.e. $\Phi_1 = 0$ in (2.21), and so (2.35) with (2.36) correspond to (2.20) with (2.21). Finally, note that Φ_2 is not required here. Hence, for $\delta \leq \delta_{CR}$, we obtain the following one-phase problem

$$\text{in } 0 < x < s(t), t > 0 \qquad \mu \frac{\partial c_0}{\partial t} - \frac{\partial}{\partial x}\left(D_{c_0} \frac{\partial c_0}{\partial x}\right) = 0, \tag{2.37}$$

$$\text{on } x = 0 \qquad -D_{c_0} \frac{\partial c_0}{\partial x} = H(1 - c_0), \tag{2.38}$$

$$\text{on } x = s(t) \qquad c_0 = 0, \quad -D_{c_0} \frac{\partial c_0}{\partial x} = \dot{s} h_i(s), \tag{2.39}$$

$$\text{at } t = 0 \qquad c_0 = c_i(x) \text{ for } 0 \leq x \leq s_0, \quad s = s_0, \tag{2.40}$$

with $h_0 = h_i(x)$ for $s(t) \leq x \leq 1$.

2.3.2 Case $\delta_{CR} \ll \delta \ll \epsilon$

The scalings in this case are given by

$$x = s(t) + \delta \left(\frac{\epsilon}{\delta}\right)^p \bar{x}, \quad c = \left(\frac{\delta}{\epsilon}\right)^2 \bar{c}, \quad h = \bar{h}, \tag{2.41}$$

giving

$$\epsilon^2 \left(\frac{\epsilon}{\delta}\right)^{2(p-1)} \mu \frac{\partial \bar{c}}{\partial t} - \epsilon \left(\frac{\epsilon}{\delta}\right)^{p-1} \dot{s} \frac{\partial \bar{c}}{\partial \bar{x}} - \frac{\partial}{\partial \bar{x}} \left(D_c \frac{\partial \bar{c}}{\partial \bar{x}} \right) = -\bar{c}^p \bar{h}^q,$$
$$\epsilon^2 \left(\frac{\epsilon}{\delta}\right)^{2p} \frac{\partial \bar{h}}{\partial t} - \epsilon \left(\frac{\epsilon}{\delta}\right)^{p+1} \dot{s} \frac{\partial \bar{h}}{\partial \bar{x}} - \frac{\partial}{\partial \bar{x}} \left(D_h \frac{\partial \bar{h}}{\partial \bar{x}} \right) = -\bar{c}^p \bar{h}^q.$$

Posing the expansions

$$\bar{c} = \bar{c}_0 + \epsilon \left(\frac{\epsilon}{\delta}\right)^{p+1} \bar{c}_1 + \ldots, \quad \bar{h} = \bar{h}_0 + \epsilon \left(\frac{\epsilon}{\delta}\right)^{p+1} \bar{h}_1 + \ldots,$$

with

$$D_c(c,h) \sim D_c(0,\bar{h}_0), \quad D_h(c,h) \sim D_h(0,\bar{h}_0),$$

we obtain at leading order

$$\frac{\partial}{\partial \bar{x}} \left(D_c \frac{\partial \bar{c}_0}{\partial \bar{x}} \right) = \bar{c}_0^p \bar{h}_0^q, \quad \frac{\partial}{\partial \bar{x}} \left(D_h \frac{\partial \bar{h}_0}{\partial \bar{x}} \right) = \bar{c}_0^p \bar{h}_0^q.$$

At first order we have (for brevity we only record the case in which both diffusivities are constant, additional terms from the expansion of the diffusivities being present when they are concentration dependent)

$$\frac{\partial}{\partial \bar{x}} \left(D_c \frac{\partial \bar{c}_1}{\partial \bar{x}} \right) = p \bar{c}_0^{p-1} \bar{c}_1 \bar{h}_0^q + q \bar{c}_0^p \bar{h}_0^{q-1} \bar{h}_1,$$
$$\dot{s} \frac{\partial \bar{h}_0}{\partial \bar{x}} + \frac{\partial}{\partial \bar{x}} \left(D_h \frac{\partial \bar{h}_1}{\partial \bar{x}} \right) = p \bar{c}_0^{p-1} \bar{c}_1 \bar{h}_0^q + q \bar{c}_0^p \bar{h}_0^{q-1} \bar{h}_1.$$

Hence

$$D_c \frac{\partial \bar{c}_1}{\partial \bar{x}} = \dot{s} \bar{h}_0 + D_h \frac{\partial \bar{h}_1}{\partial \bar{x}} + A(t),$$

where $A(t)$ is a function of t to be determined. Matching into outer 1, the matching conditions

$$\text{as } \bar{x} \to -\infty \quad D_c \frac{\partial \bar{c}_0}{\partial \bar{x}} \to 0, \quad D_c \frac{\partial \bar{c}_1}{\partial \bar{x}} \to D_{c_0} \frac{\partial c_0(s^-,t)}{\partial x}, \quad \bar{h}_0 \to 0, \quad \bar{h}_1 \to 0,$$

give

$$A(t) = D_{c_0} \frac{\partial c_0(s^-,t)}{\partial x}.$$

The matching conditions for outer 2,

$$\begin{aligned}\text{as } \bar{x} \to +\infty \quad \bar{c}_0 \to 0, \quad \bar{c}_1 \to 0, \quad \bar{h}_0 \to h_0(s^+,t),\\ D_h \frac{\partial \bar{h}_0}{\partial \bar{x}} \to 0, \quad D_h \frac{\partial \bar{h}_1}{\partial \bar{x}} \to \frac{\delta^2}{\epsilon^2} D_{h_0} \frac{\partial h_0(s^+,t)}{\partial x},\end{aligned}$$

give

$$A(t) = -\frac{\delta^2}{\epsilon^2} D_{h_0} \frac{\partial h_0(s^+,t)}{\partial x} - \dot{s} h_0(s^+,t) = -\dot{s} h_0(s^+,t).$$

Hence, we obtain the interface condition

$$\text{at } x = s(t) \quad -D_{c_0} \frac{\partial c_0(s^-,t)}{\partial x} = \dot{s} h_0(s^+,t),$$

which corresponds to (2.20). Again, we necessarily have $c_0(s^-,t) = 0$ and thus $\Phi_1 = 0$ in (2.21) with Φ_2 not required. We then arrive at the same one phase Stefan problem as stated in (2.37)-(2.40). Note that here it is the first order terms which allow the fluxes to be matched with the outer regions. Figure 2.3 shows a schematic representation of the carbonation reaction for the case $\delta \ll \epsilon$.

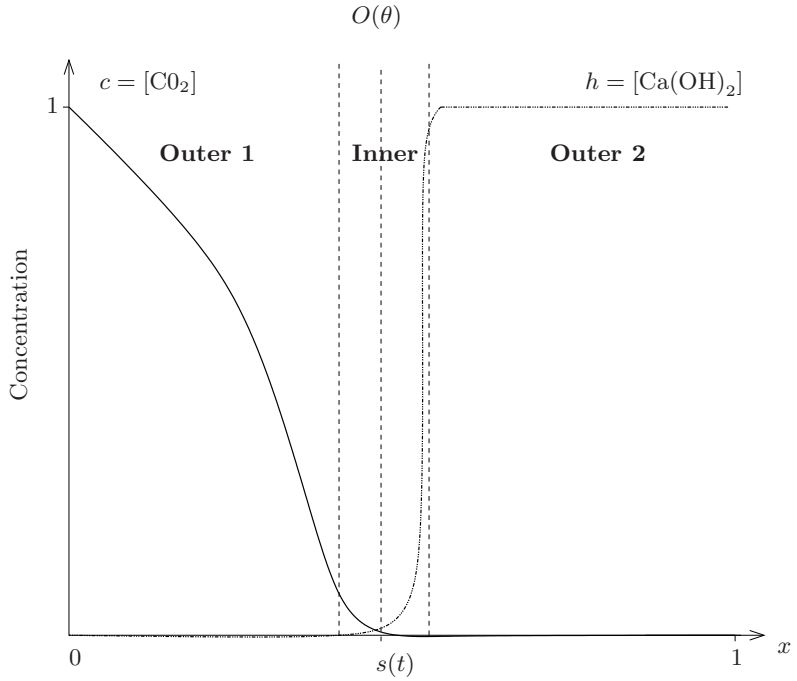

Figure 2.3: *A schematic illustration of the asymptotic regions for slowly varying diffusivitives ($D_c = O(1)$, $D_h = O(1)$) in the parameter case $\delta \ll \epsilon$. The regions outer 1 ($0 < x < s(t)$) and outer 2 ($s(t) < x < 1$) are the two outer regions surrounding a single interior reaction layer denoted inner. Its width of $O(\theta)$ is such that $\theta = \epsilon^{\frac{2}{p+1}}$ for $\delta \leq \delta_{CR}$ and $\theta = \delta \left(\frac{\delta}{\epsilon}\right)^p$ for $\delta_{CR} \ll \delta \ll \epsilon$.*

2.3.3 Case $\delta = O(\epsilon)$

In this parameter case, an altogether quite different scenario takes place. First there is an initial period in which the reaction zone remains at the surface. This period may be termed stage I carbonation, using the terminology introduced for metal oxidation [26] where a similar situation occurs. During this stage, the hydroxide at the surface is depleted, the details of which are described in Appendix B.1. This stage ends at a finite time t_0 when the surface hydroxide concentration becomes small (i.e. zero at leading order). After this, stage II carbonation takes place where the reaction zone moves into the concrete, which we describe here.

The required inner scalings are

$$x = s(t) + \epsilon^{\frac{2}{p+q+1}}\bar{x}, \quad c = \epsilon^{\frac{2}{p+q+1}}\bar{c}, \quad h = \epsilon^{\frac{2}{p+q+1}}\bar{h}, \tag{2.42}$$

giving

$$\epsilon^{\frac{4}{p+q+1}}\frac{\partial \bar{c}}{\partial t} - \epsilon^{\frac{2}{p+q+1}}\dot{s}\frac{\partial \bar{c}}{\partial \bar{x}} - \frac{\partial}{\partial \bar{x}}\left(D_c\frac{\partial \bar{c}}{\partial \bar{x}}\right) = -\bar{c}^p\bar{h}^q,$$
$$\epsilon^{\frac{4}{p+q+1}}\frac{\partial \bar{h}}{\partial t} - \epsilon^{\frac{2}{p+q+1}}\dot{s}\frac{\partial \bar{h}}{\partial \bar{x}} - \frac{\partial}{\partial \bar{x}}\left(D_h\frac{\partial \bar{h}}{\partial \bar{x}}\right) = -\bar{c}^p\bar{h}^q.$$

Posing the expansions

$$\bar{c} = \bar{c}_0 + \epsilon^2\bar{h}_1 + \ldots, \quad \bar{c} = \bar{c}_0 + \epsilon^2\bar{h}_1 + \ldots,$$

with

$$D_c(c,h) \sim D_c(0,0), \quad D_h(c,h) \sim D_h(0,0),$$

we obtain at leading order

$$D_c\frac{\partial \bar{c}_0}{\partial \bar{x}} = D_h\frac{\partial \bar{h}_0}{\partial \bar{x}} + A(t),$$
$$\frac{\partial}{\partial \bar{x}}\left(D_h\frac{\partial \bar{h}_0}{\partial \bar{x}}\right) = \bar{c}_0^p\bar{h}_0^q,$$

where $A(t)$ is a function of t to be determined. Matching into outer 1 and 2, the matching conditions

$$\text{as } \bar{x} \to -\infty \qquad D_c\frac{\partial \bar{c}_0}{\partial \bar{x}} \to D_{c_0}\frac{\partial c_0(s^-,t)}{\partial x}, \quad \bar{h}_0 \to 0,$$
$$\text{as } \bar{x} \to +\infty \qquad \bar{c}_0 \to 0, \quad D_h\frac{\partial \bar{h}_0}{\partial \bar{x}} \to D_{h_0}\frac{\partial h_0(s^+,t)}{\partial x},$$

give

$$\text{at } x = s(t) \quad c_0(s^-, t) = 0, \quad h_0(s^+, t) = 0, \tag{2.43}$$

$$D_{c_0}\frac{\partial c_0(s^-, t)}{\partial x} + D_{h_0}\frac{\partial h_0(s^+, t)}{\partial x} = 0, \tag{2.44}$$

corresponding to (2.20) and (2.21). Consequently, here we have $\Phi_1 = 0 = \Phi_2$ and we obtain the following two-phase boundary moving problem

$$\text{in } 0 < x < s(t),\, t > 0 \qquad \mu\frac{\partial c_0}{\partial t} - \frac{\partial}{\partial x}\left(D_{c_0}\frac{\partial c_0}{\partial x}\right) = 0, \tag{2.45}$$

$$\text{in } s(t) < x < 1,\, t > 0 \qquad \frac{\partial h_0}{\partial t} - \frac{\partial}{\partial x}\left(D_{h_0}\frac{\partial h_0}{\partial x}\right) = 0, \tag{2.46}$$

$$\text{on } x = 0 \qquad -D_{c_0}\frac{\partial c_0}{\partial x} = H(1 - c_0), \tag{2.47}$$

$$\text{on } x = s(t) \qquad c_0 = 0, \quad h_0 = 0, \quad D_{c_0}\frac{\partial c_0}{\partial x} + D_{h_0}\frac{\partial h_0}{\partial x} = 0, \tag{2.48}$$

$$\text{on } x = 1 \qquad D_{h_0}\frac{\partial h_0}{\partial x} = 0, \tag{2.49}$$

$$\text{at } t = t_0 \qquad c_0 = C_i \text{ for } 0 \le x \le s_0, \quad h_0 = H_i \text{ for } s_0 \le x \le 1, \quad s = s_0. \tag{2.50}$$

Here t_0 is the end of the time at which the reaction zone remains at the outer surface and after which it begins to ingress into the concrete. C_i, H_i denote the resulting concentration profiles at this time, which differ from their initial values c_i, h_i respectively. Figure 2.4 shows a schematic representation of the carbonation reaction in this regime.

2.4 Numerical Results

2.4.1 Scheme

It is of interest to see if the results derived above agree with numerical results. To do this comparison we implement equations (2.6)-(2.10) in the finite element package COMSOL Multiphysics. We define two reaction-diffusion equations with no flux boundary conditions except for at the boundary $x = 0$. A uniform mesh consisting of 400 quadratic Lagrange elements (1602 degrees of freedom) is used. It is worth mentioning that the mesh is chosen so that when refined, the computational time increases but the results remain the same. We choose to solve this time dependent problem using variable-order variable-step-size backward differentiation formulas i.e. BDF method, and set the error tolerances to be abs tol $= 10^{-6}$, rel tol $= 10^{-3}$. Due to the implicit nature of the time-stepping scheme used, a nonlinear system of equations must be solved at each step. For this, a nonlinear solver based on the damped Newton method is used.

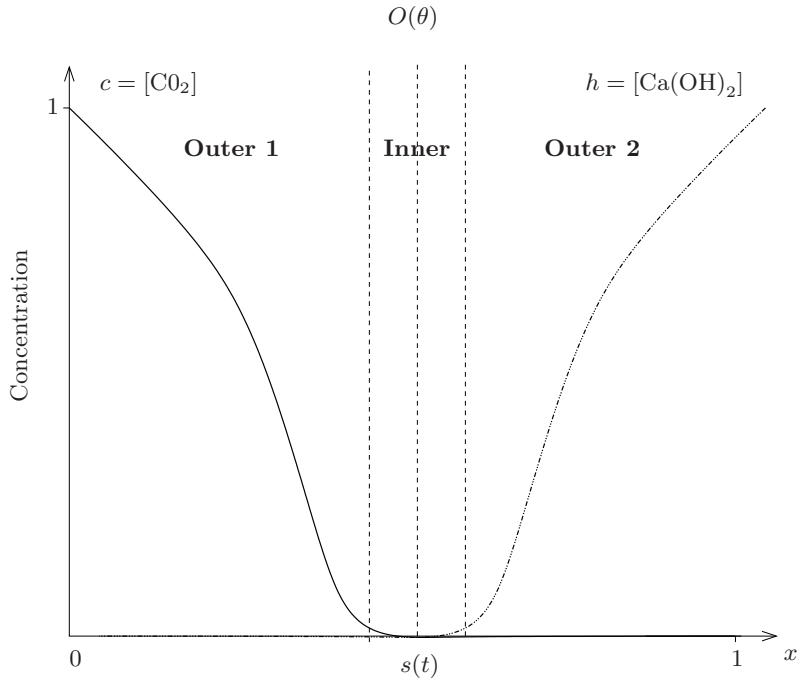

Figure 2.4: *A schematic illustration of the asymptotic regions for slowly varying diffusivitives* ($D_c = O(1)$, $D_h = O(1)$) *in the parameter case* $\delta = O(\epsilon)$. *The regions outer 1* ($0 < x < s(t)$) *and outer 2* ($s(t) < x < 1$) *are the two outer regions surrounding a single interior reaction layer denoted inner with* $\theta = \epsilon^{\frac{2}{p+q+1}}$.

For more details see [14]. The convergence criterion for this solver is as follows: let U be the current approximation to the true solution vector, and let E be the estimated error in this vector, then the software stops the iterations when the relative tolerance exceeds the relative error computed as the weighted Euclidean norm

$$err = \left(\frac{1}{N} \sum_{i=1}^{N} (|E_i|/W_i)^2 \right)^{1/2}.$$

Here N is the number of degrees of freedom and $W_i = \max(|U_i|, S_i)$, where S_i is a scale factor that the solver determines on the basis of the scaling method. Further, the nonlinear solver uses a linear system solver in each Newton step δU. The chosen linear solver is MUMPS (MUltifrontal Massively Parallel sparse direct Solver) and it works on systems of the form $Ax = b$. The convergence criterion here is $\rho|M^{-1}(b - Ax)| < \text{tol} \cdot |M^{-1}b|$. Here $M = LU$, where L and U are the LU factors computed by the solver, and ρ is the factor in error estimate which may be set by the user (default=400). When this criterion is satisfied the software returns a solution. The computational times vary drastically from a handfull of seconds to hours. As the values of ϵ and δ decrease, the problem becomes more singular and the computational time increases. In this chapter the longest time needed is of 40 seconds but in later chapters, the drastic changes in the diffusion coefficient, increases even further the time required and so the computations

may last hours.

2.4.2 Base Case

Figures 2.5-2.7 show the numerical solutions for the case $D_c = D_h = O(1)$ for different values of ϵ, namely $\epsilon = 10^{-1}$, 10^{-2} and 10^{-3} respectively. For each figure, the four conceptually different scaling regimes covering the asymptotic cases presented in section 2.3 are depicted. The initial data and parameter values taken are

$$h_i = 1, \quad c_i = 0 \ \text{ for } 0 \le x \le 1, \quad \mu = 10^{-3}, \quad H = 10^4, \quad p = q = 1, \tag{2.51}$$

and for simplicity, $D_c = D_h = 1$.

As the value of ϵ decreases, the numerical results resemble more the behaviours derived in section 2.3. As a general pattern, we see that the reaction zone moves further into the concrete as time passes and whilst c remains similar, h smooth's out as δ approaches ϵ.

We concentrate now on the parameter regime $\epsilon = 10^{-3}$ shown in figure 2.7. There is a clear marked change in behaviour between the case $\delta < \epsilon$ shown in (a)-(c) and $\delta = \epsilon$ shown in (d). The hydroxide profile falls to zero at the reaction front in (d) with noticeable diffusion ahead, in contrast to (a)-(c) where it is unity at the front and falls to zero within the reaction zone. Moreover, the rates at which the fronts move vary, with a time delay apparent in (d) compared to (a)-(c). This supports the stage I carbonation regime that is postulated to take place when $\delta = \epsilon$, in which the reaction zone remains at the surface for finite time as the hydroxide concentration falls. The reaction zone starts moving into the concrete once the hydroxide at the surface has been depleted. The speed at which the front ingresses into the concrete in (a)-(c) decreases. In (d) however, it increases drastically and although it starts later, due to stage I carbonation, by the time $t = 0.3$, the front has moved further into the concrete than for any of the other cases. This is due to the edge effects caused by the boundary condition at $x = 1$.

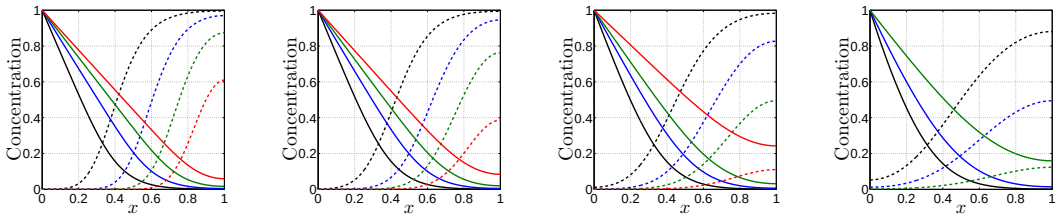

(a) $\delta = \epsilon^2$ (b) $\delta = \epsilon^{3/2}$ (c) $\delta = \epsilon^{1.25}$ (d) $\delta = \epsilon$

Figure 2.5: *Numerical results for slowly varying diffusivities and $\epsilon = 10^{-1}$. The initial data and parameter values are as stated in (2.51) and the selected δ values are stated in (a)-(d). The solid lines refer to the concentration of carbon dioxide while the dotted lines are the concentration of calcium hydroxide at times $t = 0.1$ (black), $t = 0.2$ (blue), $t = 0.3$ (green) and $t = 0.4$ (red).*

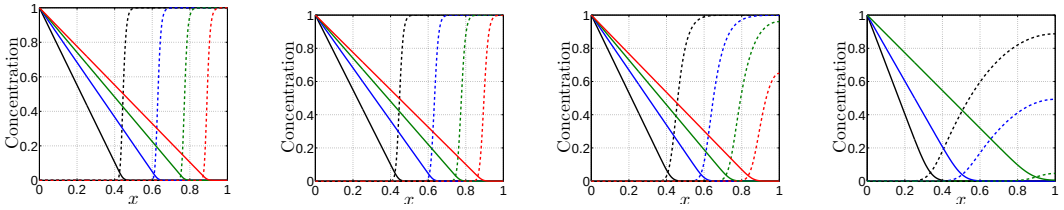

(a) $\delta = \epsilon^2$ (b) $\delta = \epsilon^{3/2}$ (c) $\delta = \epsilon^{1.25}$ (d) $\delta = \epsilon$

Figure 2.6: *Numerical results for slowly varying diffusivities and* $\epsilon = 10^{-2}$*. The initial data and parameter values are as stated in* (2.51) *and the selected* δ *values are stated in (a)-(d). The solid lines refer to the concentration of carbon dioxide while the dotted lines are the concentration of calcium hydroxide at times* $t = 0.1$ *(black),* $t = 0.2$ *(blue),* $t = 0.3$ *(green) and* $t = 0.4$ *(red).*

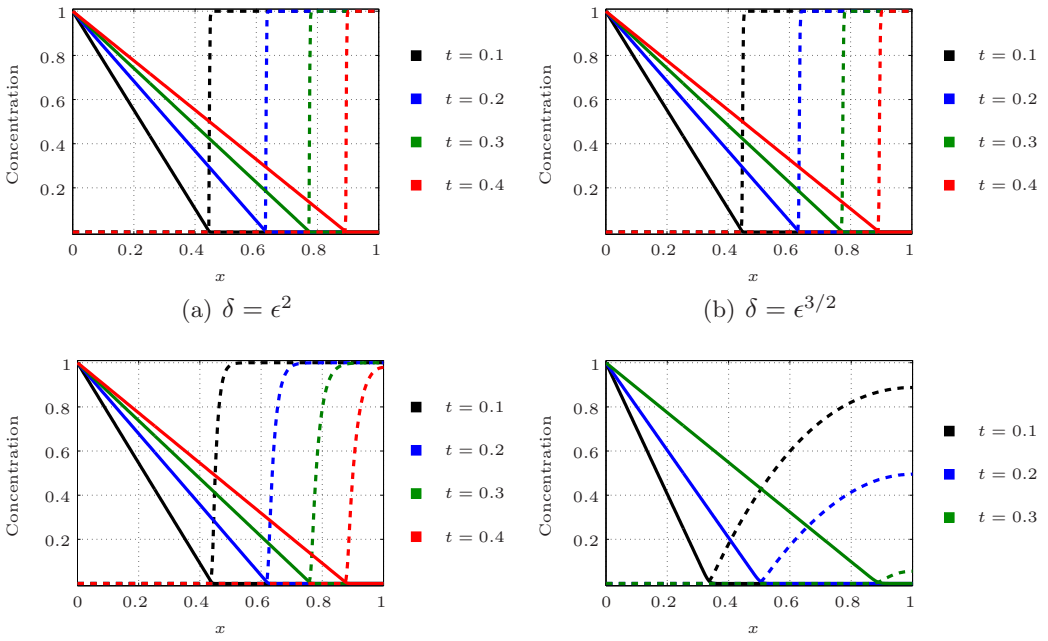

(a) $\delta = \epsilon^2$ (b) $\delta = \epsilon^{3/2}$

(c) $\delta = \epsilon^{1.25}$ (d) $\delta = \epsilon$

Figure 2.7: *Numerical results for slowly varying diffusivities and* $\epsilon = 10^{-3}$*. The initial data and parameter values are as stated in* (2.51) *and the selected* δ *values as stated in (a)–(d). The solid lines refer to the concentration of carbon dioxide while the dotted lines are the concentration of calcium hydroxide at the showed times.*

2.4.3 Parameter variation

It is now of interest to see how changing the values of the parameters may affect the behaviour of the system. Table 2.3 summarises the parameter cases considered, with the first three figures referring to the base case values.

In figures 2.8 and 2.9, where $\mu = 1$ and $H = 1$ respectively, we see that the reaction zone moves slower into the concrete block. However, the most significant observation in figure 2.9 is that c is no longer pinned at 1 at the surface. This agrees with the

	Parameter values				
Figure	ϵ	μ	H	p	q
2.5	10^{-1}	10^{-3}	10^4	1	1
2.6	10^{-2}	10^{-3}	10^4	1	1
2.7	10^{-3}	10^{-3}	10^4	1	1
2.8	10^{-3}	1	10^4	1	1
2.9	10^{-3}	10^{-3}	1	1	1
2.10	10^{-2}	10^{-3}	10^4	1.5	1
2.11	10^{-2}	10^{-3}	10^4	0.9	1
2.12	10^{-2}	10^{-3}	10^4	1	1.5
2.13	10^{-2}	10^{-3}	10^4	1	0.9

Table 2.3: *Base case and parameter values investigated.*

analysis done in appendix B for Stage I. There, we assume $H = O(1)$ and obtain a rescaling for c such that $c = \epsilon^{\frac{2}{p+1}}\bar{c}$. Hence, although there is also a Stage I for the parameter case $H = 10^4$, the analysis done in appendix B would have to be redone for the limit $H \to \infty$ in order to capture the details.

The remaining graphs (2.10-2.13) look at the effects caused by changing the powers p and q. In other words, we look at the effect of different reaction orders. Before analysing the graphs in detail, we state that in order to achieve these results, the following regularisation of the reaction term was necessary,

$$r = c(c^2 + \theta^2)^{\frac{p-1}{2}} * h(h^2 + \theta^2)^{\frac{q-1}{2}},$$

where $\theta = 10^{-3}$. Note that the value of ϵ is now 10^{-2} and so we will compare the remaining graphs with figure 2.6.

Figure 2.10 shows the concentrations of CO_2 and $Ca(OH)_2$ for $p = 1.5$. Recall $\delta_{CR} = \epsilon^{\frac{p+2}{p+1}}$ and so figures 2.10(a) and (b) relate to the regime $\delta \leq \delta_{CR}$ discussed in subsection 2.3.1, figure 2.10(c) to $\delta_{CR} \ll \delta \ll \epsilon$ in subsection 2.3.2 and figure 2.10(d) is covered in subsection 2.3.3. As a general trend in figure 2.10, we see that the curves are smoother and the value of c around the reaction zone increases. We look at the scalings taken for the different asymptotic regimes to identify the precise changes. Consider first figures 2.10(a) and (b) and recall (2.24). The rescaling of c for $p = 1$ is $c = \epsilon^1\bar{c}$ and for $p = 1.5$ is $c = \epsilon^{4/5}\bar{c}$, and so the concentration of CO_2 is bigger at the reaction zone. The thickness of the reaction zone also increases as p increases, explaining why the graphs are smoother. For figure 2.10(c), rescaling (2.41) shows that the value of c at the reaction zone is independent of p, but the thickness does depend on p and so we observe smoother curves. For $\delta = \epsilon$, figure 2.10(d), (2.42) implies that not only the value of c increases at the reaction zone but also the one for h. Note that here, h is no longer order 1 as in the previous two asymptotic regimes. Further, the thickness of the reaction zone also increases. In figure 2.11 we take $p = 0.9$ and it is clear that the

opposite changes to the ones observed for figure 2.10 happen.

The last two plots look at varying the value of q. In figure 2.12(a) and (b) the concentration of CO_2 at the reaction zone remains small and the acquired smoothness of the curves seen in figures 2.10(a) and (b) is gone since neither scalings (2.24) nor (2.41) depend on q. However, the scaling for $\delta = \epsilon$ does, see (2.42), and indeed, the concentration is bigger and the curves smoother when compared to figure 2.6. Following a similar argument for the plots in figure 2.13, the most significant change is in (d) where we obtain slightly sharper curves and smaller concentrations of CO_2 and $Ca(OH)_2$ around the reaction zone.

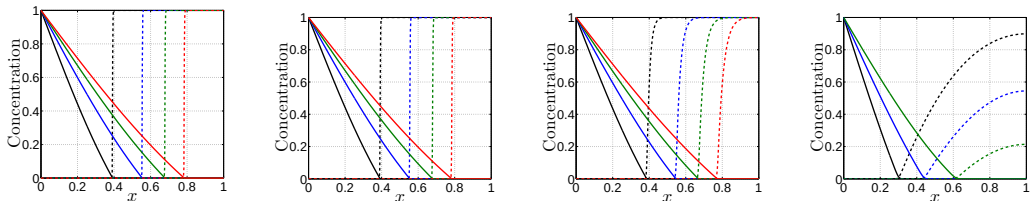

(a) $\delta = \epsilon^2$ (b) $\delta = \epsilon^{3/2}$ (c) $\delta = \epsilon^{1.25}$ (d) $\delta = \epsilon$

Figure 2.8: *Numerical results for slowly varying diffusivities. The parameter values are* $\epsilon = 10^{-3}$, $p = q = 1$, $\mu = 1$ *and* $H = 10^4$, *and selected* δ *as stated in (a)-(d). The solid lines refer to the concentration of carbon dioxide while the dotted lines are the concentration of calcium hydroxide at times* $t = 0.1$ *(black),* $t = 0.2$ *(blue),* $t = 0.3$ *(green) and* $t = 0.4$ *(red).*

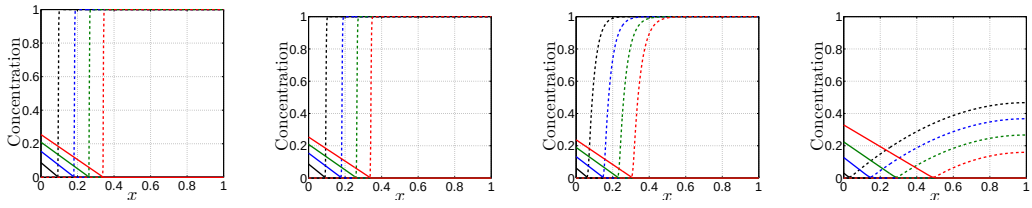

(a) $\delta = \epsilon^2$ (b) $\delta = \epsilon^{3/2}$ (c) $\delta = \epsilon^{1.25}$ (d) $\delta = \epsilon$

Figure 2.9: *Numerical results for slowly varying diffusivities. The parameter values are* $\epsilon = 10^{-3}$, $p = q = 1$, $\mu = 10^{-3}$ *and* $H = 1$, *and selected* δ *as stated in (a)-(d). The solid lines refer to the concentration of carbon dioxide while the dotted lines are the concentration of calcium hydroxide at times* $t = 0.1$ *(black),* $t = 0.2$ *(blue),* $t = 0.3$ *(green) and* $t = 0.4$ *(red), except for case (d) where* $t = 0.7, 0.8, 0.9, 1$ *respectively.*

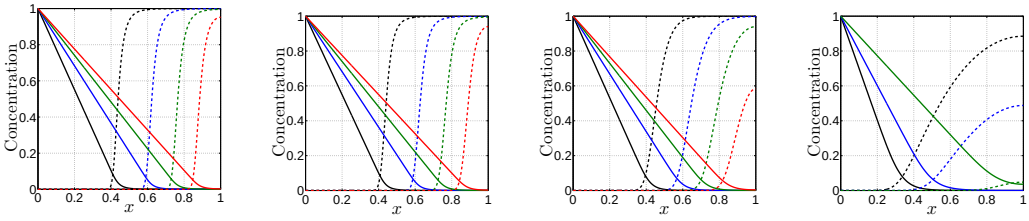

(a) $\delta = \epsilon^2$ (b) $\delta = \epsilon^{3/2}$ (c) $\delta = \epsilon^{1.25}$ (d) $\delta = \epsilon$

Figure 2.10: *Numerical results for slowly varying diffusivities. The parameter values are* $\epsilon = 10^{-2}$, $p = 1.5$, $q = 1$, $\mu = 10^{-3}$ *and* $H = 10^4$, *and selected* δ *as stated in (a)-(d). The solid lines refer to the concentration of carbon dioxide while the dotted lines are the concentration of calcium hydroxide at times* $t = 0.1$ *(black),* $t = 0.2$ *(blue),* $t = 0.3$ *(green) and* $t = 0.4$ *(red)*

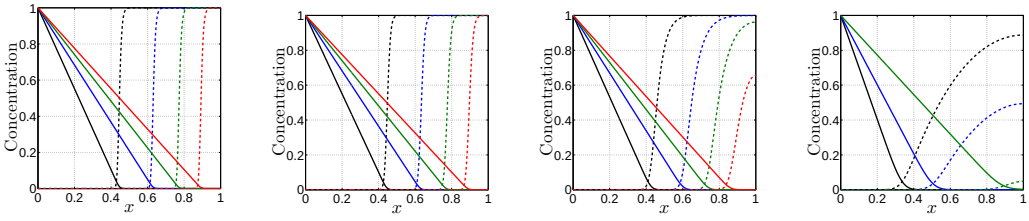

(a) $\delta = \epsilon^2$ (b) $\delta = \epsilon^{3/2}$ (c) $\delta = \epsilon^{1.25}$ (d) $\delta = \epsilon$

Figure 2.11: *Numerical results for slowly varying diffusivities. The parameter values are* $\epsilon = 10^{-2}$, $p = 0.9$, $q = 1$, $\mu = 10^{-3}$ *and* $H = 10^4$, *and selected* δ *as stated in (a)-(d). The solid lines refer to the concentration of carbon dioxide while the dotted lines are the concentration of calcium hydroxide at times* $t = 0.1$ *(black),* $t = 0.2$ *(blue),* $t = 0.3$ *(green) and* $t = 0.4$ *(red)*

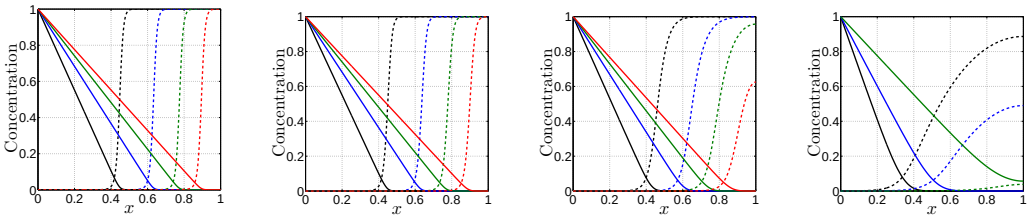

(a) $\delta = \epsilon^2$ (b) $\delta = \epsilon^{3/2}$ (c) $\delta = \epsilon^{1.25}$ (d) $\delta = \epsilon$

Figure 2.12: *Numerical results for slowly varying diffusivities. The parameter values are* $\epsilon = 10^{-2}$, $p = 1$, $q = 1.5$, $\mu = 10^{-3}$ *and* $H = 10^4$, *and selected* δ *as stated in (a)-(d). The solid lines refer to the concentration of carbon dioxide while the dotted lines are the concentration of calcium hydroxide at times* $t = 0.1$ *(black),* $t = 0.2$ *(blue),* $t = 0.3$ *(green) and* $t = 0.4$ *(red)*

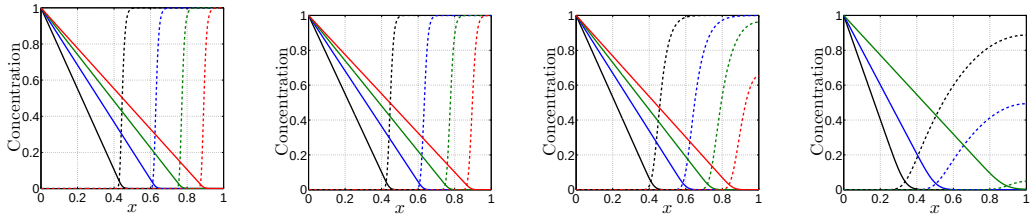

(a) $\delta = \epsilon^2$ (b) $\delta = \epsilon^{3/2}$ (c) $\delta = \epsilon^{1.25}$ (d) $\delta = \epsilon$

Figure 2.13: *Numerical results for slowly varying diffusivities. The parameter values are* $\epsilon = 10^{-2}$, $p = 1$, $q = 0.9$, $\mu = 10^{-3}$ *and* $H = 10^4$, *and selected* δ *as stated in (a)-(d). The solid lines refer to the concentration of carbon dioxide while the dotted lines are the concentration of calcium hydroxide at times* $t = 0.1$ *(black),* $t = 0.2$ *(blue),* $t = 0.3$ *(green) and* $t = 0.4$ *(red)*

2.4.4 Free boundary $s(t)$

One of the main unknowns is the localisation of the reaction zone $x = s(t;\epsilon)$. At this stage we may take the data obtained in COMSOL Multiphysics and equation (2.13) to find the position of the free boundary. Hence, $s(t)$ is calculated by finding the intersection of c and h for each time. Central differences is then used to obtain $\dot{s}(t)$.

Base case

We take parameter values (2.51), where in particular $p = q = 1$. Figures 2.14 and 2.15 show the behaviour of the carbonation front and its speed for all the different parameter regimes considered in section 2.3.

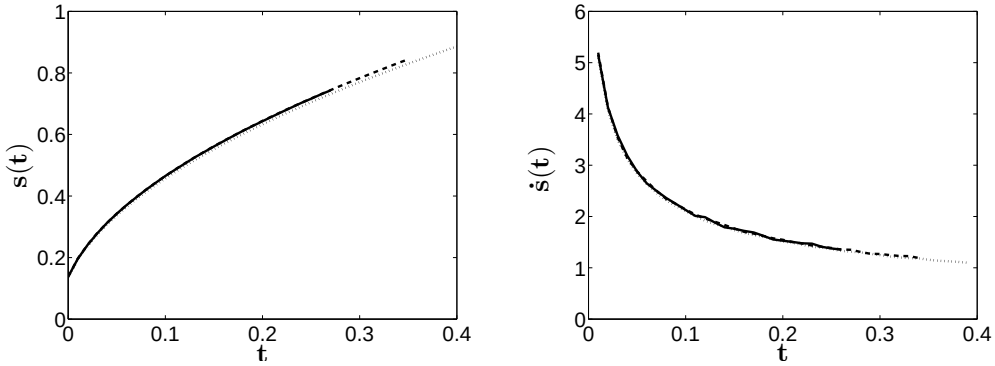

(a) Free boundary, $s(t)$. (b) Speed of free boundary, $\dot{s}(t)$.

Figure 2.14: *Free boundary results from* (2.6)-(2.10) *for slowly varying diffusivities and* $\delta \ll \epsilon$ *with* $\epsilon = 10^{-3}$. *Three values of* δ *are depicted:* $\delta = \epsilon^2$ *(dashed),* $\delta = \epsilon^{3/2}$ *(solid) and* $\delta = \epsilon^{1.25}$ *(dotted).*

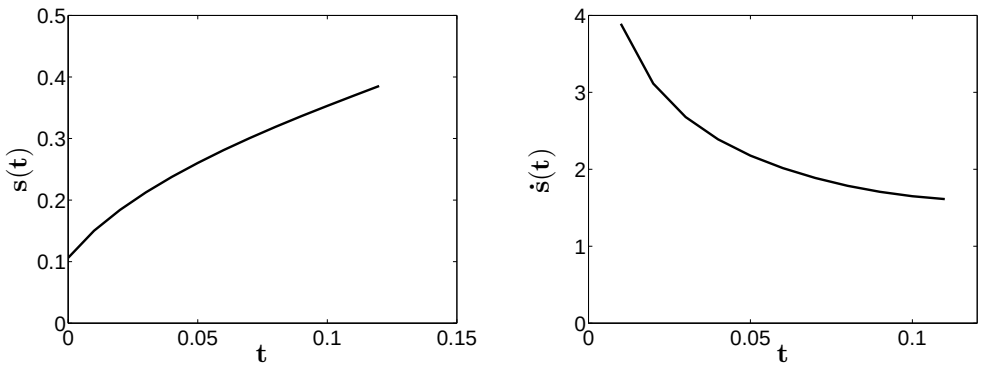

(a) Free boundary, $s(t)$. (b) Speed of free boundary, $\dot{s}(t)$.

Figure 2.15: *Free boundary results from* (2.6)-(2.10) *for slowly varying diffusivities and* $\delta = \epsilon$ *with* $\epsilon = 10^{-3}$.

It is worth mentioning that the above results have been truncated to eliminate the edge effects caused by the boundary condition at $x = 1$. From a practical point of view, it is the long-time behaviour that is more interesting to investigate, and so

the boundary effects are not considered here. In Chapter 6, the large and small time behaviour of the Stefan problems are derived and the behaviour of the free boundary obtained here is compared.

Different p and q

Here we take parameter values (2.51) but we now consider the following four combinations of p and q

$$p > 1,\, q = 1, \quad p = 1,\, q > 1, \quad p < 1,\, q = 1, \quad p = 1,\, q < 1.$$

As already mentioned, in chapter 6 we focus on the profile of the free boundary $s(t)$ but the analysis is restricted to the case $p = q = 1$. It is therefore of interest to obtain numerical results to see the effects of different reaction orders. Figure 2.16 shows how the resulting free boundary for all the above combinations of p and q are not very different from those of $p = q = 1$. This implies that the values of p and q have little effect on the behaviour of the interface.

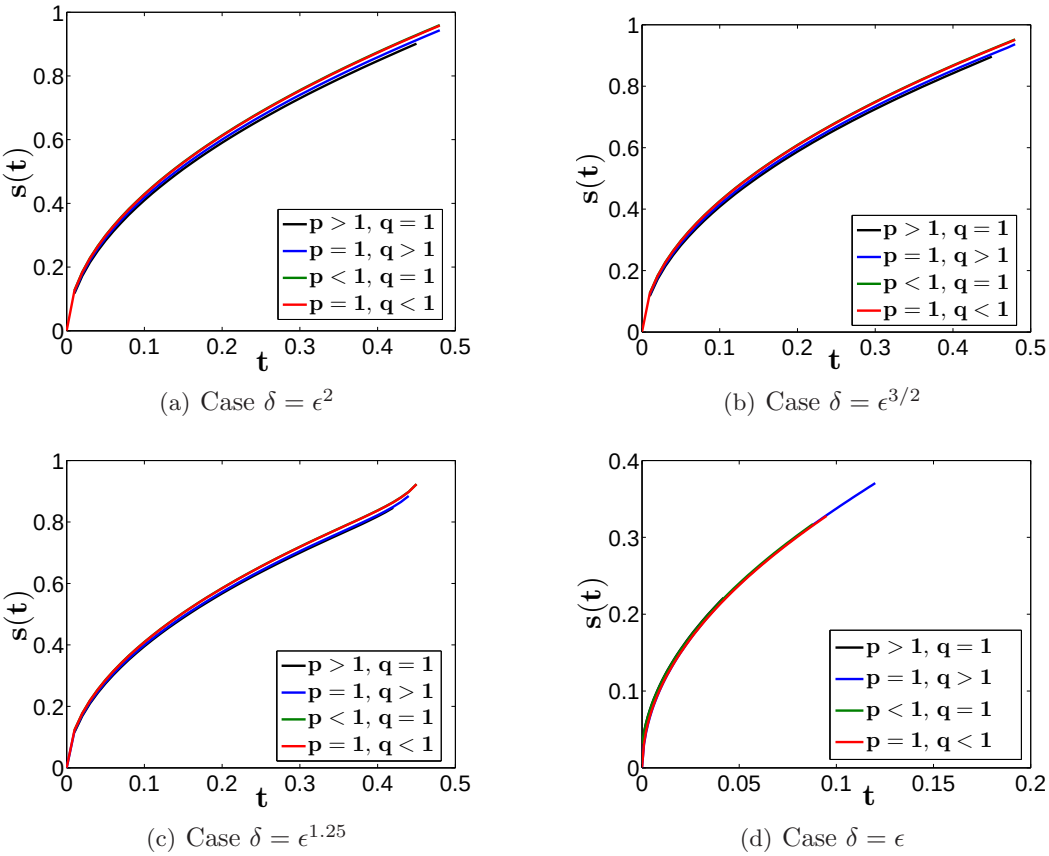

(a) Case $\delta = \epsilon^2$

(b) Case $\delta = \epsilon^{3/2}$

(c) Case $\delta = \epsilon^{1.25}$

(d) Case $\delta = \epsilon$

Figure 2.16: *Free boundary plots for slowly varying diffusivities with $\epsilon = 10^{-2}$ and different values of p, q as shown in table 2.3.*

This concludes the derivation of the sharp interface models in the fast reaction limit for slowly varying diffusivities. A one-phase Stefan model is obtained for $\delta \ll \epsilon$ and a two-phase one for $\delta = O(\epsilon)$. It is not until Chapter 6 that we will return to these models where they will be analysed further.

Note that the kinetic conditions (2.21) are zero. Although there exists several ways of determining the reaction front, the experimental evidence points towards $O(1)$ concentrations in the reaction zone. The CO_2 concentration plots in the experimental papers [65, 66] show that, at the measured reaction front, the concentration is roughly half or more than half of the initial one. Also, modelling papers, such as [61], suggest that the CO_2 kinetic condition is far from being zero. Regarding $Ca(OH)_2$, plots in [65, 11] suggest further that the concentration of $Ca(OH)_2$ is also $O(1)$ at the reaction front. From a modelling perspective, [62] uses the experimenta results in [52] to define the carbonation location in their model at the point where the concentration of $Ca(OH)_2$ has fallen to 50%. Therefore, it is realistic to look for order 1 values of CO_2 and $Ca(OH)_2$ at the interface. With this in mind, we move on to consider the next type of diffusion coefficients.

Chapter 3

Concrete Carbonation with One Rapidly Varying Diffusion Coefficient

In order to avoid obtaining $\Phi_1 = 0$ in (2.21) as a matching condition, it is clear that we need $c = O(1)$ in the reaction layer. We therefore consider the carbon dioxide diffusivity to depend on ϵ as well as the hydroxide concentration, i.e. $D_c = D_c(c, h; \epsilon)$. The hydroxide remains slowly varying i.e. $D_h = O(1)$. The insight obtained in the previous section has motivated us to consider the diffusivity with the properties[1]

$$D_c = \begin{cases} O(\epsilon^2) & \text{for } h = O(1),\ h > 0, \\ O(1) & \text{for } h = o(1),\ h > 0, \end{cases}$$

and $D_c(c, 0; \epsilon)$=1. Whilst the functional form is not important, for definiteness we may consider a hydroxide only dependent diffusivity $D_c(h; \epsilon)$ in the Arrhenius form

$$D_c = 1 - \exp\left(-\frac{\nu_1 \epsilon^2}{h^q}\right), \tag{3.1}$$

where ν_1 is a positive constant and q is the reaction order of the hydroxide as in (2.11). A schematic illustration of the behaviour of this diffusion coefficient is shown in figure 3.1. Here we take the power of h so that the diffusion coefficient is dependent on the reaction term. A more general power could be considered, with the below analysis only needing slight modifications as shown in detail in appendix C.

We consider the nondimensionalised problem (2.6)-(2.10) with D_c as in (3.1) and follow the same procedure as in Chapter 2. The outer solutions and jump conditions derived in section 2.2 hold here too and so we proceed to analyse the reaction zone.

[1] Consider (2.6) and (2.7) and substitute in the scalings $x = s(t) + \theta\bar{x}$ where $\theta \ll 1$ and c, h are $O(1)$. In order to obtain the fullest balance in (2.6) we required D_c to be scaled as $D_c = \epsilon^2 \bar{D}_c$.

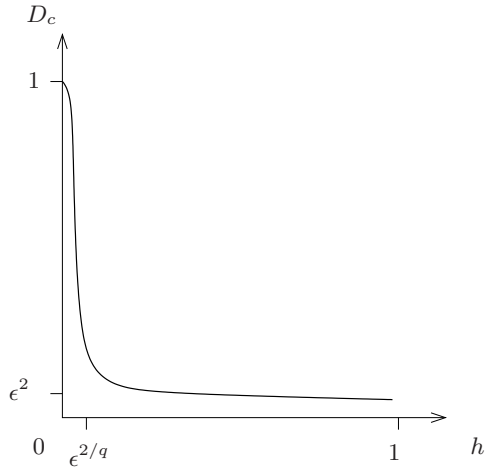

Figure 3.1: *A schematic illustration of the carbon dioxide diffusion coefficient D_c with the functional form* (3.1).

3.1 Interior (reaction) layer analysis: $D_c = O(\epsilon^2)$ and $D_h = O(1)$.

The behaviour of the reaction layer for a single rapidly varying diffusivity is also affected by the dependence of the parameter δ on ϵ as for slowly varying diffusivities. For the parameter range $\delta \leq \epsilon$, the fullest balance in (2.6) and (2.7) is now $\delta_{CR} = \epsilon^2$ and so we obtain three different asymptotic regimes, namely $\delta \leq \epsilon^2$, $\epsilon^2 \ll \delta \ll \epsilon$ and $\delta = O(\epsilon)$. For each of the following regimes, the inner region is now composed of at least 2 regions, denoted inner inner and inner 1. The inner inner is the equivalent region to the inner in Chapter 2 and inner 1 is an additional region required to facilitate the matching with outer 1. In particular, inner 1 accommodates the change in magnitude of the CO_2 diffusion coefficient, D_c.

3.1.1 The case $\delta \leq \epsilon^2$

This case is the simplest, where the reaction zone comprises two regions, inner inner and inner 1, which are looked at separately.

- **Inner Inner**

The required inner inner scalings are

$$x = s(t) + \epsilon^2 \bar{x}, \quad c = \bar{c}, \quad h = \bar{h}, \quad D_c = \epsilon^2 \bar{D}_c.$$

with $\bar{D}_c \sim \nu_1 / h^q$ for the functional form (3.1). Substituting these scalings into (2.6), (2.7) gives

$$\mu\epsilon^2 \frac{\partial \bar{c}}{\partial t} - \mu \dot{s} \frac{\partial \bar{c}}{\partial \bar{x}} - \frac{\partial}{\partial \bar{x}} \left(\bar{D}_c \frac{\partial \bar{c}}{\partial \bar{x}} \right) = -\bar{c}^p \bar{h}^q,$$

$$\epsilon^2\frac{\partial\bar{h}}{\partial t}-\dot{s}\frac{\partial\bar{h}}{\partial\bar{x}}-\frac{\delta^2}{\epsilon^4}\frac{\partial}{\partial\bar{x}}\left(D_h\frac{\partial\bar{h}}{\partial\bar{x}}\right)=-\bar{c}^p\bar{h}^q.$$

Posing the expansions

$$\bar{c}=\bar{c}_0+o(1),\quad \bar{h}=\bar{h}_0+o(1),$$

with

$$\bar{D}_c(c,h)\sim\bar{D}_c(\bar{c}_0,\bar{h}_0),\quad D_h(c,h)\sim D_h(\bar{c}_0,\bar{h}_0),$$

we obtain

$$\mu\dot{s}\frac{\partial\bar{c}_0}{\partial\bar{x}}+\frac{\partial}{\partial\bar{x}}\left(\bar{D}_c\frac{\partial\bar{c}_0}{\partial\bar{x}}\right)=\bar{c}_0^p\bar{h}_0^q,$$
$$\mu\dot{s}\bar{c}_0+\bar{D}_c\frac{\partial\bar{c}_0}{\partial\bar{x}}=\dot{s}\bar{h}_0+\frac{\delta^2}{\epsilon^4}D_h\frac{\partial\bar{h}_0}{\partial\bar{x}}+A(t),$$

where $A(t)$ is a function of t to be determined. Matching into outer 2, the matching conditions

$$\text{as }\bar{x}\to+\infty\quad \bar{c}_0\to 0,\quad \bar{h}_0\to h_0(s^+,t),\quad D_h\frac{\partial\bar{h}_0}{\partial\bar{x}}\to 0, \tag{3.2}$$

give

$$A(t)=-\dot{s}h_0(s^+,t). \tag{3.3}$$

Matching into outer 1, the matching conditions

$$\text{as }\bar{x}\to-\infty\quad \bar{c}_0\to c_0(s^-,t),\quad \bar{D}_c\frac{\partial\bar{c}_0}{\partial\bar{x}}\to D_{c_0}\frac{\partial c_0(s^-,t)}{\partial x},\quad \bar{h}_0\to 0, \tag{3.4}$$

yield

$$A(t)=\mu\dot{s}c_0(s^-,t)+D_{c_0}\frac{\partial c_0(s^-,t)}{\partial x}. \tag{3.5}$$

An additional region is required to facilitate the matching with outer 1 and explain (3.4), due to the change in the order of magnitude in the carbon dioxide diffusivity.

- **Inner1**

Here $h=O(\epsilon^{2/q})$, this being the scaling on which $D_c=O(1)$. The details depend on the value of $q\geq 0$ in the reaction term (2.11). There are three cases to consider separately.

(A) For $q>1$ the scalings are

$$x=s(t)+\epsilon^{\frac{2}{q}}\bar{X},\quad c=\bar{C},\quad h=\epsilon^{\frac{2}{q}}\bar{H},$$

with D_c as in (3.1), so that

$$\mu\epsilon^{\frac{4}{q}}\frac{\partial\bar{C}}{\partial t}-\mu\epsilon^{\frac{2}{q}}\dot{s}\frac{\partial\bar{C}}{\partial\bar{X}}-\frac{\partial}{\partial\bar{X}}\left(D_c\frac{\partial\bar{C}}{\partial\bar{X}}\right)=-\epsilon^{\frac{4}{q}}\bar{C}^p\bar{H}^q,$$

$$\epsilon^{\frac{2}{q}}\frac{\partial \bar{H}}{\partial t} - \dot{s}\frac{\partial \bar{H}}{\partial \bar{X}} - \left(\frac{\delta}{\epsilon^2}\right)^2 \epsilon^{\frac{2}{q}(q-1)}\frac{\partial}{\partial \bar{X}}\left(D_h\frac{\partial \bar{H}}{\partial \bar{X}}\right) = -\bar{C}^p\bar{H}^q.$$

Note that in this case the transition region is larger in size than the reaction layer, the inner inner region. Posing

$$\bar{C} \sim \bar{C}_0 + \epsilon^{\frac{2}{q}}\bar{C}_1, \quad \bar{H} \sim \bar{H}_0,$$

with

$$D_c(c,h) \sim D_c(\bar{C}_0, 0), \quad D_h(c,h) \sim D_h(\bar{C}_0, 0),$$

we obtain

$$\frac{\partial}{\partial \bar{X}}\left(D_c\frac{\partial \bar{C}_0}{\partial \bar{X}}\right) = 0, \quad \dot{s}\frac{\partial \bar{H}_0}{\partial \bar{X}} = \bar{C}_0^p\bar{H}_0^q,$$

at leading order, and

$$\mu\dot{s}\frac{\partial \bar{C}_0}{\partial \bar{X}} + \frac{\partial}{\partial \bar{X}}\left(D_c\frac{\partial \bar{C}_1}{\partial \bar{X}}\right) = 0,$$

at first order. After matching to outer 1 and the inner inner we have

$$\bar{C}_0 = c_0(s^-, t) = \Phi_1, \quad D_c\frac{\partial \bar{C}_1}{\partial \bar{X}} = D_{c_0}\frac{\partial c_0(s^-,t)}{\partial x}, \tag{3.6a}$$

$$\bar{H}_0 = \left(-\frac{q-1}{\dot{s}}c_0(s^-,t)^p\bar{X}\right)^{-\frac{1}{q-1}}. \tag{3.6b}$$

(B) For $q = 1$ the transition region is of the same size as the inner inner. We introduce the scalings

$$x = s(t) + \epsilon^2(S(t) + \bar{X}), \quad c = \bar{C}, \quad h = \epsilon^2\bar{H},$$

where $1 < S(t) < 1/\epsilon^2$. The governing equations become

$$\epsilon^4\mu\frac{\partial \bar{C}}{\partial t} - \epsilon^2\mu(\dot{s} + \epsilon^2\dot{S})\frac{\partial \bar{C}}{\partial \bar{X}} - \frac{\partial}{\partial \bar{X}}\left(D_c\frac{\partial \bar{C}}{\partial \bar{X}}\right) = -\epsilon^4\bar{C}^p\bar{H},$$
$$\epsilon^2\frac{\partial \bar{H}}{\partial t} - (\dot{s} + \epsilon^2\dot{S})\frac{\partial \bar{H}}{\partial \bar{X}} - \frac{\delta^2}{\epsilon^4}\frac{\partial}{\partial \bar{X}}\left(D_h\frac{\partial \bar{H}}{\partial \bar{X}}\right) = -\bar{C}^p\bar{H}.$$

Posing

$$\bar{C} \sim \bar{C}_0 + \epsilon^2\bar{C}_1, \quad \bar{H} \sim \bar{H}_0,$$

with

$$D_c(c,h) \sim D_c(\bar{C}_0, 0), \quad D_h(c,h) \sim D_h(\bar{C}_0, 0),$$

we obtain

$$\frac{\partial}{\partial \bar{X}}\left(D_c\frac{\partial \bar{C}_0}{\partial \bar{X}}\right) = 0, \quad \dot{s}\frac{\partial \bar{H}_0}{\partial \bar{X}} + \frac{\delta^2}{\epsilon^4}\frac{\partial}{\partial \bar{X}}\left(D_h\frac{\partial \bar{H}_0}{\partial \bar{X}}\right) = \bar{C}_0^p\bar{H}_0,$$

at leading order, and

$$\mu\dot{s}\frac{\partial \bar{C}_0}{\partial \bar{X}} + \frac{\partial}{\partial \bar{X}}\left(D_c\frac{\partial \bar{C}_1}{\partial \bar{X}}\right) = 0,$$

at first order. After matching to outer 1 and the inner inner we again obtain (3.6a), and taking D_h constant, $\bar{H}_0$ is given by

$$\bar{H}_0 = \exp\left(\frac{\epsilon^4}{\delta^2}\frac{\dot{s}}{2D_h}\left(-1+\sqrt{1+\frac{\delta^2}{\epsilon^4}\frac{4D_h c_0(s^-,t)^p}{\dot{s}^2}}\right)\right)\bar{X}.$$

Further,

$$S(t) \sim \frac{2\dot{s}}{c_0(s^-,t)^p}\ln(\epsilon).$$

(C) The third and final case to discuss is $0 < q < 1$. Here, the transition region is narrower than the inner inner. We introduce the scalings

$$x = s(t) + \epsilon^{\frac{1+q}{q}}\bar{X}, \quad c = \bar{C}, \quad h = \epsilon^{\frac{2}{q}}\bar{H},$$

to obtain

$$\mu\epsilon^{\frac{2}{q}(q+1)}\frac{\partial \bar{C}}{\partial t} - \mu\epsilon^{\frac{q+1}{q}}\dot{s}\frac{\partial \bar{C}}{\partial \bar{X}} - \frac{\partial}{\partial \bar{X}}\left(D_c\frac{\partial \bar{C}}{\partial \bar{X}}\right) = -\epsilon^{\frac{2}{q}(q+1)}\bar{C}^p\bar{H}^q,$$
$$\epsilon^{\frac{2}{q}}\frac{\partial \bar{H}}{\partial t} - \epsilon^{\frac{1-q}{q}}\dot{s}\frac{\partial \bar{H}}{\partial \bar{X}} - \frac{\delta^2}{\epsilon^4}\frac{\partial}{\partial \bar{X}}\left(D_h\frac{\partial \bar{H}}{\partial \bar{X}}\right) = -\bar{C}^p\bar{H}^q.$$

Posing

$$\bar{C} \sim \bar{C}_0 + \epsilon^{\frac{q+1}{q}}\bar{C}_1, \quad \bar{H} \sim \bar{H}_0,$$

with

$$D_c(c,h) \sim D_c(\bar{C}_0, 0), \quad D_h(c,h) \sim D_h(\bar{C}_0, 0),$$

we obtain

$$\frac{\partial}{\partial \bar{X}}\left(D_c\frac{\partial \bar{C}_0}{\partial \bar{X}}\right) = 0, \quad \frac{\delta^2}{\epsilon^4}\frac{\partial}{\partial \bar{X}}\left(D_h\frac{\partial \bar{H}_0}{\partial \bar{X}}\right) = \bar{C}_0^p\bar{H}_0^q,$$

at leading order, and

$$\mu\dot{s}\frac{\partial \bar{C}_0}{\partial \bar{X}} + \frac{\partial}{\partial \bar{X}}\left(D_c\frac{\partial \bar{C}_1}{\partial \bar{X}}\right) = 0,$$

at first order. After matching to outer 1 and the inner inner we obtain (3.6a), and taking D_h constant, $\bar{H}_0$ is given by

$$\bar{H}_0 = \begin{cases} \left(\frac{(1-q)^2 c_0(s^-,t)^p\epsilon^4}{2(1+q)D_h\delta^2}\bar{X}^2\right)^{\frac{1}{1-q}} & \text{for } \bar{X} > 0, \\ 0 & \text{for } \bar{X} < 0. \end{cases} \tag{3.7}$$

Further, the inner inner region is now restricted to $\bar{x} > 0$ with the inner 1 matching conditions occurring as $\bar{x} \to 0^+$.

Now, we are in a position to conclude and so (3.3) and (3.5) give

$$\text{at } x = s(t) \quad -D_{c_0}\frac{\partial c_0(s^-,t)}{\partial x} = \dot{s}(\mu c_0(s^-,t) + h_0(s^+,t)).$$

Further,

$$c_0(s^-,t) = \Phi_1,$$

and so we obtain the following one-phase problem

$$\text{in } 0 < x < s(t),\ t > 0 \qquad \mu\frac{\partial c_0}{\partial t} - \frac{\partial}{\partial x}\left(D_{c_0}\frac{\partial c_0}{\partial x}\right) = 0, \tag{3.8}$$

$$\text{on } x = 0 \qquad -D_{c_0}\frac{\partial c_0}{\partial x} = H(1-c_0), \tag{3.9}$$

$$\text{on } x = s(t) \qquad c_0 = \Phi_1(\dot{s}), \quad -D_{c_0}\frac{\partial c_0}{\partial x} = \dot{s}(\mu c_0 + h_i(s)), \tag{3.10}$$

$$\text{at } t = 0 \qquad c_0 = c_i(x) \text{ for } 0 \le x \le s_0, \quad s = s_0, \tag{3.11}$$

with $h_0 = h_i(x)$ for $s(t) \le x \le 1$. This is as in (2.37)-(2.40) but instead of (2.39) we now have a more general moving boundary (3.10). Moreover, Φ_1 is determined by the solution of the inner inner problem

$$\mu\dot{s}\frac{\partial \bar{c}_0}{\partial \bar{x}} + \frac{\partial}{\partial \bar{x}}\left(\bar{D}_c\frac{\partial \bar{c}_0}{\partial \bar{x}}\right) = \bar{c}_0^p\bar{h}_0^q, \tag{3.12}$$

$$\bar{D}_c\frac{\partial \bar{c}_0}{\partial \bar{x}} - \frac{\delta^2}{\epsilon^4}D_h\frac{\partial \bar{h}_0}{\partial \bar{x}} = \dot{s}(\bar{h}_0 - h_i(s) - \mu\bar{c}_0), \tag{3.13}$$

with

$$\text{as } \bar{x} \to +\infty \qquad \bar{c}_0 \to 0, \quad \bar{D}_c\frac{\partial \bar{c}_0}{\partial \bar{x}} \to 0 \quad \bar{h}_0 \to h_i(s), \tag{3.14}$$

$$\text{as } \bar{x} \to -\infty \qquad \bar{c}_0 \to \Phi_1(\dot{s}), \quad \bar{h}_0 \to 0, \tag{3.15}$$

where $\bar{D}_c = \frac{\nu_1}{h_0^q}$ and $D_h = O(1)$. Figure 3.2 shows a schematic summary of the carbonation reaction for this case.

3.1.2 The case $\epsilon^2 \ll \delta \ll \epsilon$

This case is the most involved one, where the reaction zone splits into three regions. In addition to the inner inner and inner 1 regions already discussed, we need an extra region, denoted as inner 2. Inner 2 is required to match the concentration of calcium hydroxide into outer 2. Hence, in progressing from outer 1 to outer 2, we label the regions as inner 1, inner inner and finally inner 2. This is summarised in figure 3.3 where the results derived below are included. We look at each region separately.

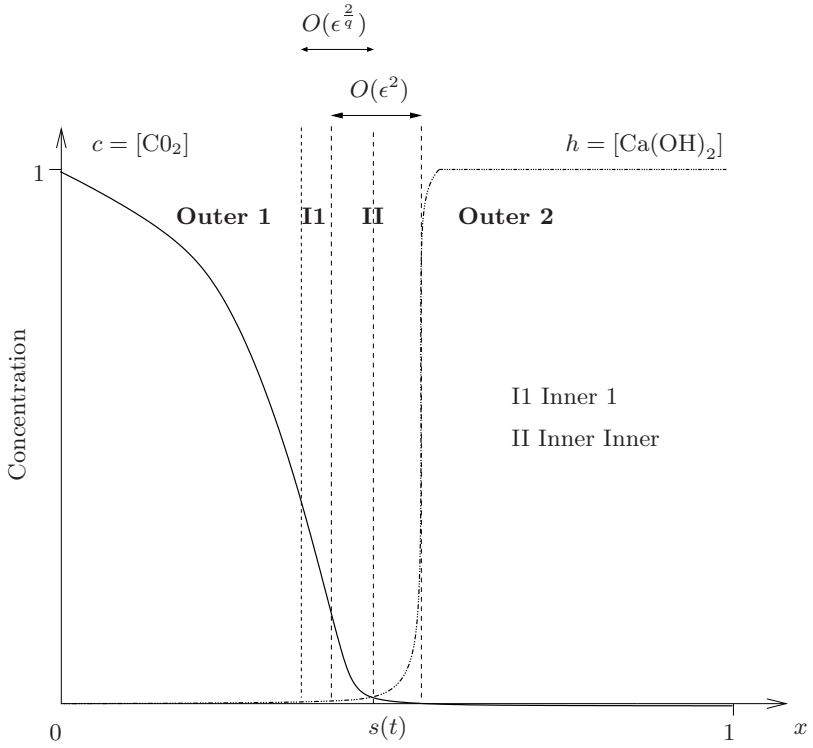

Figure 3.2: *A schematic illustration of the asymptotic regions for a rapidly varying CO_2 diffusivity ($D(c) = O(\epsilon^2)$, $D_h = O(1)$) in the parameter case $\delta \leq \epsilon^2$. The regions outer 1 ($0 < x < s(t)$) and outer 2 ($s(t) < x < 1$) are the two outer regions surrounding the reaction layer. It is composed of two regions: an inner inner region (II) and an inner 1 region (I1). Inner 1 acts as a transition region to facilitate the matching of the inner inner with outer 1. The case shown is for $q > 1$. Minor modifications are needed to inner 1 for $q \leq 1$.*

- **Inner Inner**

The required scalings are

$$x = s(t) + \left(\frac{\delta}{\epsilon}\right)^2 \bar{\epsilon}_2 \bar{x}, \quad c = \bar{c}, \quad h = \bar{\epsilon}_2 \bar{h}, \quad D_c = \frac{\epsilon^2}{\bar{\epsilon}_2^q} \bar{D}_c,$$

where

$$\bar{\epsilon}_2 = \left(\frac{\epsilon^2}{\delta}\right)^{\frac{2}{q+1}} < 1,$$

and $\bar{D}_c \sim \bar{\epsilon}_2^q \nu_1 / h^q$ for the functional form (3.1). The governing equations are now

$$\left(\frac{\delta}{\epsilon}\right)^2 \bar{\epsilon}_2 \mu \frac{\partial \bar{c}}{\partial t} - \mu \dot{s} \frac{\partial \bar{c}}{\partial \bar{x}} - \frac{\partial}{\partial \bar{x}} \left(\bar{D}_c \frac{\partial \bar{c}}{\partial \bar{x}}\right) = -\bar{c}^p \bar{h}^q,$$
$$\left(\frac{\delta}{\epsilon}\right)^2 \bar{\epsilon}_2^2 \frac{\partial \bar{h}}{\partial t} - \bar{\epsilon}_2 \dot{s} \frac{\partial \bar{h}}{\partial \bar{x}} - \frac{\partial}{\partial \bar{x}} \left(D_h \frac{\partial \bar{h}}{\partial \bar{x}}\right) = -\bar{c}^p \bar{h}^q.$$

We pose the expansions

$$\bar{c} = \bar{c}_0 + o(1), \quad \bar{h} = \bar{h}_0 + o(1),$$

with

$$\bar{D}_c(c,h) \sim \bar{D}_c(\bar{c}_0, 0), \quad D_h(c,h) \sim D_h(\bar{c}_0, 0).$$

At leading order we have

$$\mu \dot{s} \frac{\partial \bar{c}_0}{\partial \bar{x}} + \frac{\partial}{\partial \bar{x}} \left(\bar{D}_c \frac{\partial \bar{c}_0}{\partial \bar{x}} \right) = \bar{c}_0^p \bar{h}_0^q,$$
$$\mu \dot{s} \bar{c}_0 + \bar{D}_c \frac{\partial \bar{c}_0}{\partial \bar{x}} = D_h \frac{\partial \bar{h}_0}{\partial \bar{x}} + A(t).$$

where $A(t)$ is a function of t to be determined.

Matching into outer 2, the matching conditions

$$\text{as } \bar{x} \to +\infty \quad \bar{c} \to 0, \quad D_h \frac{\partial \bar{h}_0}{\partial \bar{x}} \to \dot{s} h_0(s^+, t) \tag{3.16}$$

give

$$A(t) = -\dot{s} h_0(s^+, t). \tag{3.17}$$

An additional region is required to facilitate the matching with outer 2 and explain (3.16) due to the change in the order of magnitude in the concentration of calcium hydroxide.

- **Inner 2**

Here, $h = O(1)$ since for the range $\epsilon^2 \ll \delta \ll \epsilon$ we have h order 1 in outer 2. This then forces the scaling for D_c to be $D_c = O(\epsilon^2)$.
The scaling is therefore

$$x = s(t) + \left(\frac{\delta}{\epsilon} \right)^2 \hat{X}, \quad c = 0, \quad h = \hat{H}, \quad D_c = \epsilon^2 \hat{D}_c,$$

where c is actually exponentially small in ϵ and $\hat{D}_c \sim \nu_1 / h^q$. The governing equation for the hydroxide at leading order in $\hat{X} > 0$ is

$$\dot{s} \frac{\partial \hat{H}_0}{\partial \hat{X}} + \frac{\partial}{\partial \hat{X}} \left(D_h \frac{\partial \hat{H}_0}{\partial \hat{X}} \right) = 0,$$

with $D_h(c,h) \sim D_h(0, \hat{H}_0)$. Matching into outer 2, the matching conditions

$$\text{as } \hat{X} \to +\infty \quad \hat{H}_0 \to h_0(s^+, t), \quad \frac{\partial \hat{H}_0}{\partial \hat{X}} \to 0$$

give

$$D_h \frac{\partial \hat{H}_0}{\partial \hat{X}} = \dot{s}(h_0(s^+, t) - \hat{H}_0).$$

Thus matching with inner inner we have the behaviour

$$\text{as } \hat{X} \to 0^+ \quad \hat{H}_0 \to 0, \quad D_h \frac{\partial \hat{H}_0}{\partial \hat{X}} \to \dot{s} h_0(s^+, t).$$

Further, in the case D_h a constant, we have the simple explicit solution

$$\hat{H}_0 = h_0(s^+, t)\left(1 - \exp\left(-\frac{\dot{s}}{D_h}\hat{X}\right)\right).$$

Consider the inner inner region now. Matching into outer 1, the matching conditions

$$\text{as } \bar{x} \to -\infty \quad \bar{c}_0 \to c_0(s^-, t), \quad \bar{D}_c \frac{\partial \bar{c}_0}{\partial \bar{x}} \to D_{c_0} \frac{\partial c_0(s^-, t)}{\partial x}, \tag{3.18}$$

give

$$A(t) = \mu \dot{s} \bar{c}_0(s^-, t) + D_{c_0} \frac{\partial c_0(s^-, t)}{\partial x}. \tag{3.19}$$

Inner 1 is now required to facilitate the matching with outer 1 and explain (3.18) as done in 3.1.1.

- **Inner 1**

The scalings are determined by the size of δ relative to a critical value $\delta_{CR} = \epsilon^{\frac{q+1}{q}}$ and the value of $q \geq 0$ in the reaction term (2.11).

(A) For the case $q > 1$, for which $\epsilon^2 < \delta_{CR} < \epsilon$, there are three cases to consider separately. Note that the transition region is larger in size than the inner inner.

1. For $\delta < \delta_{CR}$ the required scalings are

$$x = s(t) + \epsilon^{\frac{2}{q}} \bar{X}, \quad c = \bar{C}, \quad h = \epsilon^{\frac{2}{q}} \bar{H}, \tag{3.20}$$

with D_c as in (3.1), so that

$$\epsilon^{\frac{4}{q}} \mu \frac{\partial \bar{C}}{\partial t} - \epsilon^{\frac{2}{q}} \mu \dot{s} \frac{\partial \bar{C}}{\partial \bar{X}} - \frac{\partial}{\partial \bar{X}}\left(D_c \frac{\partial \bar{C}}{\partial \bar{X}}\right) = -\epsilon^{\frac{4}{q}} \bar{C}^p \bar{H}^q,$$
$$\epsilon^{\frac{2}{q}} \frac{\partial \bar{H}}{\partial t} - \dot{s} \frac{\partial \bar{H}}{\partial \bar{X}} - \frac{\delta^2}{\epsilon^{\frac{2(q+1)}{q}}} \frac{\partial}{\partial \bar{X}}\left(D_h \frac{\partial \bar{H}}{\partial \bar{X}}\right) = -\bar{C}^p \bar{H}^q.$$

Posing

$$\bar{C} \sim \bar{C}_0 + \epsilon^{\frac{2}{q}} \bar{C}_1, \quad \bar{H} \sim \bar{H}_0,$$

with

$$D_c(c, h) \sim D_c(\bar{C}_0, 0), \quad D_h(c, h) \sim D_h(\bar{C}_0, 0),$$

we obtain

$$\frac{\partial}{\partial \bar{X}}\left(D_c\frac{\partial \bar{C}_0}{\partial \bar{X}}\right)=0, \quad \dot{s}\frac{\partial \bar{H}_0}{\partial \bar{X}}=\bar{C}_0^p\bar{H}_0^q,$$

at leading order, and

$$\mu\dot{s}\frac{\partial \bar{C}_0}{\partial \bar{X}}-\frac{\partial}{\partial \bar{X}}\left(D_c\frac{\partial \bar{C}_1}{\partial \bar{X}}\right)=0$$

at first order. After matching to outer 1 and the inner inner we have

$$\bar{C}_0=c_0(s^-,t)=\Phi_1, \quad D_c\frac{\partial \bar{C}_1}{\partial \bar{X}}=D_{c_0}\frac{\partial c_0(s^-,t)}{\partial x}, \tag{3.21a}$$

$$\bar{H}_0=\left(-\frac{q-1}{\dot{s}}c_0(s^-,t)^p\bar{X}\right)^{-\frac{1}{q-1}}. \tag{3.21b}$$

2. For $\delta=\delta_{CR}$ the scalings (3.20) apply as does the subsequent analysis with the modification of the diffusion term entering the leading order hydroxide equation.

3. For $\delta>\delta_{CR}$ the required scalings are

$$x=s(t)+\left(\frac{\delta}{\epsilon}\right)\epsilon^{\frac{1}{q}}\bar{X}, \quad c=\bar{C}, \quad h=\epsilon^{\frac{2}{q}}\bar{H}, \tag{3.22}$$

so that

$$\left(\frac{\delta}{\epsilon}\right)^2\epsilon^{\frac{2}{q}}\mu\frac{\partial \bar{C}}{\partial t}-\left(\frac{\delta}{\epsilon}\right)\epsilon^{\frac{1}{q}}\mu\dot{s}\frac{\partial \bar{C}}{\partial \bar{X}}-\frac{\partial}{\partial \bar{X}}\left(D_c\frac{\partial \bar{C}}{\partial \bar{X}}\right)=-\left(\frac{\delta}{\epsilon}\right)^2\epsilon^{\frac{2}{q}}\bar{C}^p\bar{H}^q,$$
$$\epsilon^{\frac{2}{q}}\frac{\partial \bar{H}}{\partial t}-\left(\frac{\epsilon}{\delta}\right)\epsilon^{\frac{1}{q}}\dot{s}\frac{\partial \bar{H}}{\partial \bar{X}}-\frac{\partial}{\partial \bar{X}}\left(D_h\frac{\partial \bar{H}}{\partial \bar{X}}\right)=-\bar{C}^p\bar{H}^q.$$

Posing

$$\bar{C}\sim\bar{C}_0+\left(\frac{\delta}{\epsilon}\right)\epsilon^{\frac{1}{q}}\bar{C}_1, \quad \bar{H}\sim\bar{H}_0,$$

with

$$D_c(c,h)\sim D_c(\bar{C}_0,0), \quad D_h(c,h)\sim D_h(\bar{C}_0,0),$$

we obtain

$$\frac{\partial}{\partial \bar{X}}\left(D_c\frac{\partial \bar{C}_0}{\partial \bar{X}}\right)=0, \quad \frac{\partial}{\partial \bar{X}}\left(D_c\frac{\partial \bar{H}_0}{\partial \bar{X}}\right)=\bar{C}_0^p\bar{H}_0^q,$$

at leading order, and

$$\mu\dot{s}\frac{\partial \bar{C}_0}{\partial \bar{X}}+\frac{\partial}{\partial \bar{X}}\left(D_c\frac{\partial \bar{C}_1}{\partial \bar{X}}\right)=0,$$

at first order. After matching to outer 1 and inner inner we obtain (3.21a) and by taking D_h constant, we now have

$$\bar{H}_0=\left(\frac{(q-1)^2c_0(s^-,t)^p}{2(q+1)D_h}\bar{X}^2\right)^{-\frac{1}{q-1}}.$$

For the range $q \leq 1$, we note that $\delta_{CR} \leq \epsilon^2$ and so only the last regime in part (A) occurs here with slight modifications.

(B) For $q = 1$ the transition region is of the same size as the inner inner and so we introduce the scalings

$$x = s(t) + \delta(S(t) + \bar{X}), \quad c = \bar{C}, \quad h = \epsilon^{\frac{2}{q}}\bar{H},$$

where $1 < S(t) < 1/\delta$. The governing equations become

$$\delta^2\mu\frac{\partial \bar{C}}{\partial t} - \delta\mu(\dot{s} + \delta\dot{S})\frac{\partial \bar{C}}{\partial \bar{X}} - \frac{\partial}{\partial \bar{X}}\left(D_c\frac{\partial \bar{C}}{\partial \bar{X}}\right) = -\frac{\delta^2}{\epsilon}\bar{C}^p\bar{H},$$
$$\delta^2\frac{\partial \bar{H}}{\partial t} - \frac{\epsilon^2}{\delta}(\dot{s} + \delta\dot{S})\frac{\partial \bar{H}}{\partial \bar{X}} - \frac{\partial}{\partial \bar{X}}\left(D_h\frac{\partial \bar{H}}{\partial \bar{X}}\right) = -\bar{C}^p\bar{H}.$$

Posing

$$\bar{C} \sim \bar{C}_0 + \delta\bar{C}_1, \quad \bar{H} \sim \bar{H}_0,$$

with

$$D_c(c, h) \sim D_c(\bar{C}_0, 0), \quad D_h(c, h) \sim D_h(\bar{C}_0, 0),$$

we obtain

$$\frac{\partial}{\partial \bar{X}}\left(D_c\frac{\partial \bar{C}_0}{\partial \bar{X}}\right) = 0, \quad \frac{\partial}{\partial \bar{X}}\left(D_h\frac{\partial \bar{H}_0}{\partial \bar{X}}\right) = \bar{C}_0\bar{H}_0,$$

at leading order, and

$$\mu\dot{s}\frac{\partial \bar{C}_0}{\partial \bar{X}} + \frac{\partial}{\partial \bar{X}}\left(D_c\frac{\partial \bar{C}_1}{\partial \bar{X}}\right) = 0,$$

to first order.

After matching to outer 1 and the inner inner, we have (3.21a) and by taking D_h constant,

$$\bar{H}_0 = \exp(\sigma(t)\bar{X}) \quad \text{with} \quad S(t) \sim \frac{\ln(\delta)}{\sigma(t)},$$

where

$$\sigma(t) = \sqrt{\frac{c_0(s^-, t)^p}{D_h}}.$$

(C) For $0 < q < 1$ the inner 1 region is narrower than the inner inner region. The scalings are as in (3.22) and we obtain (3.21a) but $\bar{H}_0$ is now given by

$$\bar{H}_0 = \begin{cases} \left(\frac{(1-q)^2 c_0(s^-, t)^p}{2(q+1)D_h}\bar{X}^2\right)^{\frac{1}{1-q}} & \text{for } \bar{X} > 0, \\ 0 & \text{for } \bar{X} < 0. \end{cases} \tag{3.23}$$

Further, note that the inner inner region is now restricted to $\bar{x} > 0$ with the inner 1 matching conditions occurring as $\bar{x} \to 0^+$ instead.

Now we are in a position to conclude the analysis for the inner inner region. Collecting (3.17) and (3.19) give

$$\text{at } x = s(t) \quad -D_{c_0}\frac{\partial c_0(s^-,t)}{\partial x} = \dot{s}(\mu c_0(s^-,t) + h_0(s^+,t)).$$

Further,

$$c_0(s^-,t) = \Phi_1,$$

and so we obtain a one phase problem as in (3.8)-(3.11) with $h_0 = h_i(x)$ for $s(t) \le x \le 1$. Moreover, Φ_1 is determined by the solution to the inner inner problem described in (3.12)-(3.15) but with (3.13) replaced by

$$\bar{D}_c\frac{\partial \bar{c}_0}{\partial \bar{x}} - D_h\frac{\partial \bar{h}_0}{\partial \bar{x}} = -\dot{s}(\mu \bar{c}_0 + h_i(s)),$$

and the third condition in (3.14) replaced by

$$\text{as } \bar{x} \to +\infty \quad D_h\frac{\partial \bar{h}_0}{\partial \bar{x}} \to \dot{s}h_i(s).$$

3.1.3 The case $\delta = O(\epsilon)$

As in Section 2.3.3, there is a stage I carbonation where the reaction zone remains at the surface. At the end of stage I, stage II carbonation takes place in which the reaction zone moves into the concrete. Here we only consider stage II carbonation and the details for stage I can be found in appendix B.2.

The reaction zone comprises two regions, which we look at separately, as in section 3.1.1. The inner inner matches the order 1 flux of hydroxide from the outer 2 region as well as allowing the CO_2 concentrations to fall to o(1). Inner 1 is needed to accomodate the fall in CO_2 diffusivity, allowing matching between the inner inner and the outer 1 regions.

- **Inner inner**

The required scalings are

$$x = s(t) + \epsilon^{\frac{2}{q+1}}\bar{x}, \quad c = \bar{c}, \quad h = \epsilon^{\frac{2}{q+1}}\bar{h}, \quad D_c = \epsilon^{\frac{2}{q+1}}\bar{D}_c,$$

with $\bar{D}_c \sim \epsilon^{\frac{2}{q+1}}\nu_1/h^q$ for the functional form (3.1). These give

$$\epsilon^{\frac{2}{q+1}}\mu\frac{\partial \bar{c}}{\partial t} - \mu\dot{s}\frac{\partial \bar{c}}{\partial \bar{x}} - \frac{\partial}{\partial \bar{x}}\left(\bar{D}_c\frac{\partial \bar{c}}{\partial \bar{x}}\right) = -\bar{c}^p\bar{h}^q,$$
$$\epsilon^{\frac{2}{q+1}}\frac{\partial \bar{h}}{\partial t} - \epsilon^{\frac{2}{q+1}}\dot{s}\frac{\partial \bar{h}}{\partial \bar{x}} - \frac{\partial}{\partial \bar{x}}\left(D_h\frac{\partial \bar{h}}{\partial \bar{x}}\right) = -\bar{c}^p\bar{h}^q.$$

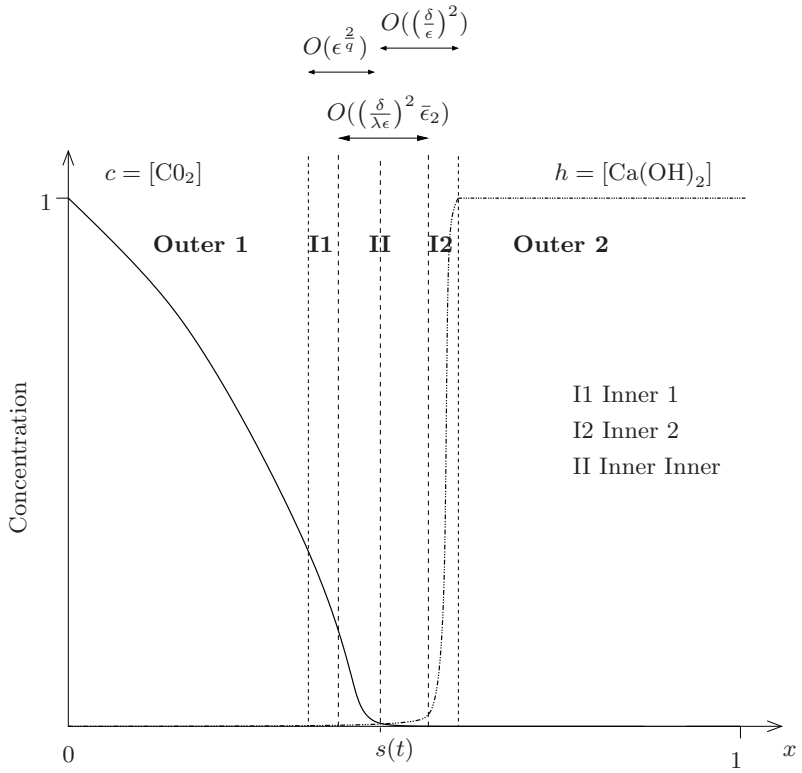

Figure 3.3: *A schematic illustration of the asymptotic regions for a rapidly varying CO_2 diffusivity ($D(c) = O(\epsilon^2)$, $D_h = O(1)$) in the parameter case $\epsilon^2 \ll \delta \ll \epsilon$. The reaction layer lies between outer regions outer 1 ($0 < x < s(t)$) and outer 2 ($s(t) < x < 1$). It is composed of three regions: an inner inner region (II) with $\bar{\epsilon}_2 = \left(\frac{\epsilon^2}{\delta}\right)^{\frac{2}{1+q}}$, together with inners 1 (I1) and 2 (I2). The inners 1 and 2 facilitate the matching of the inner inner region with the two outers. The case shown is for $q > 1$ and $\delta \leq \delta_{CR}$ with $\delta_{CR} = \epsilon^{\frac{1+q}{q}}$. Minor modifications are needed to inner 1 for the cases $q \leq 1$ and $\delta > \delta_{CR}$.*

Pose the expansions

$$\bar{c} = \bar{c}_0 + o(1), \quad \bar{h} = \bar{h}_0 + o(1),$$

with

$$\bar{D}_c(c, h) \sim \bar{D}_c(\bar{c}_0, 0), \quad D_h(c, h) \sim D_h(\bar{c}_0, 0).$$

At leading order we have

$$\mu \dot{s} \frac{\partial \bar{c}_0}{\partial \bar{x}} + \frac{\partial}{\partial \bar{x}} \left(\bar{D}_c \frac{\partial \bar{c}_0}{\partial \bar{x}} \right) = \bar{c}_0^p \bar{h}_0^q,$$
$$\mu \dot{s} \bar{c}_0 + \bar{D}_c \frac{\partial \bar{c}_0}{\partial \bar{x}} = D_h \frac{\partial \bar{h}_0}{\partial \bar{x}} + A(t)$$

where A(t) is a function of t to be determined. Matching into outer 1 as $\bar{x} \to -\infty$, the

matching conditions

$$\text{as } \bar{x} \to -\infty \quad \bar{c}_0 \to c_0(s^-,t), \quad \bar{D}_c \frac{\partial \bar{c}_0}{\partial \bar{x}} \to D_{c_0} \frac{\partial c_0(s^-,t)}{\partial x}, \quad \bar{h}_0 \to 0, \tag{3.24}$$

give

$$A(t) = \mu \dot{s} \bar{c}_0(s^-,t) + D_{c_0} \frac{\partial c_0(s^-,t)}{\partial x}. \tag{3.25}$$

Again, an additional region is necessary in order to facilitate the matching to outer 1 and understand (3.24).

- **Inner 1**

There are three cases to consider depending on the size of q.

(A) For $q > 1$ the scalings are

$$x = s(t) + \epsilon^{\frac{1}{q}} \bar{X}, \quad c = \bar{C}, \quad h = \epsilon^{\frac{2}{q}} \bar{H}, \tag{3.26}$$

and D_c as in (3.1), so that

$$\epsilon^{\frac{2}{q}} \mu \frac{\partial \bar{C}}{\partial t} - \epsilon^{\frac{1}{q}} \mu \dot{s} \frac{\partial \bar{C}}{\partial \bar{X}} - \frac{\partial}{\partial \bar{X}} \left(D_c \frac{\partial \bar{C}}{\partial \bar{X}} \right) = -\epsilon^{\frac{2}{q}} \bar{C}^p \bar{H}^q,$$
$$\epsilon^{\frac{2}{q}} \frac{\partial \bar{H}}{\partial t} - \epsilon^{\frac{1}{q}} \dot{s} \frac{\partial \bar{H}}{\partial \bar{X}} - \frac{\partial}{\partial \bar{X}} \left(D_h \frac{\partial \bar{H}}{\partial \bar{X}} \right) = -\bar{C}^p \bar{H}^q.$$

Note that in this case the transition region is larger in size than the inner inner. Posing

$$\bar{C} \sim \bar{C}_0 + \epsilon^{\frac{1}{q}} \bar{C}_1, \quad \bar{H} \sim \bar{H}_0,$$

with

$$D_c(c,h) \sim D_c(\bar{C}_0, 0), \quad D_h(c,h) \sim D_h(\bar{C}_0, 0),$$

we obtain

$$\frac{\partial}{\partial \bar{X}} \left(D_c \frac{\partial \bar{C}_0}{\partial \bar{X}} \right) = 0, \quad \frac{\partial}{\partial \bar{X}} \left(D_h \frac{\partial \bar{H}_0}{\partial \bar{X}} \right) = \bar{C}_0^p \bar{H}_0^q,$$

at leading order, and

$$\mu \dot{s} \frac{\partial \bar{C}_0}{\partial \bar{X}} + \frac{\partial}{\partial \bar{X}} \left(D_c \frac{\partial \bar{C}_1}{\partial \bar{X}} \right) = 0,$$

at first order. After matching to outer 1 and the inner inner and taking D_h constant, we have

$$\bar{C}_0 = c_0(s^-,t) = \Phi_1, \quad D_c \frac{\partial \bar{C}_1}{\partial \bar{X}} = D_{c_0} \frac{\partial c_0(s^-,t)}{\partial x}, \tag{3.27a}$$

$$\bar{H}_0 = \left(\frac{(1-q)^2 c_0(s^-,t)^p}{2(1+q) D_h} \bar{X}^2 \right)^{-\frac{1}{q-1}}. \tag{3.27b}$$

(B) For $q = 1$, the transition region is of the same size as the inner inner and so we

introduce the scalings

$$x = s(t) + \epsilon(S(t) + \bar{X}), \quad c = \bar{C}, \quad h = \epsilon^2 \bar{H},$$

where $1 < S(t) < 1/\epsilon$. The governing equations become

$$\epsilon^2 \mu \frac{\partial \bar{C}}{\partial t} - \mu\epsilon(\dot{s} + \epsilon\dot{S})\frac{\partial \bar{C}}{\partial \bar{X}} - \frac{\partial}{\partial \bar{X}}\left(D_c \frac{\partial \bar{C}}{\partial \bar{X}}\right) = -\epsilon^2 \bar{C}^p \bar{H},$$
$$\epsilon^2 \frac{\partial \bar{H}}{\partial t} - \epsilon(\dot{s} + \epsilon\dot{S})\frac{\partial \bar{H}}{\partial \bar{X}} - \frac{\partial}{\partial \bar{X}}\left(D_h \frac{\partial \bar{H}}{\partial \bar{X}}\right) = -\bar{C}^p \bar{H}.$$

Posing

$$\bar{C} \sim \bar{C}_0 + \epsilon \bar{C}_1, \quad \bar{H} \sim \bar{H}_0,$$

with

$$D_c(c, h) \sim D_c(\bar{C}_0, 0), \quad D_h(c, h) \sim D_h(\bar{C}_0, 0),$$

yields

$$\frac{\partial}{\partial \bar{X}}\left(D_c \frac{\partial \bar{C}_0}{\partial \bar{X}}\right) = 0, \quad \frac{\partial}{\partial \bar{X}}\left(D_h \frac{\partial \bar{H}_0}{\partial \bar{X}}\right) = \bar{C}_0^p \bar{H}_0,$$

at leading order, and

$$\mu \dot{s} \frac{\partial \bar{C}_0}{\partial \bar{X}} + \frac{\partial}{\partial \bar{X}}\left(D_c \frac{\partial \bar{C}_1}{\partial \bar{X}}\right) = 0,$$

at first order. After matching to outer 1 and the inner inner we again obtain (3.27a), taking D_h constant, (3.27b) becomes

$$\bar{H}_0 = \exp\left(\sqrt{\frac{c_0(s^-, t)^p}{D_h}}\bar{X}\right) \quad \text{with } S(t) \sim \sqrt{\frac{D_h}{c_0(s^-, t)^p}}\ln(\epsilon). \tag{3.28}$$

(C) For $0 < q < 1$, the inner 1 region is narrower than the inner inner. The scalings are as in (3.26). We obtain (3.27a) and taking D_h constant, $\bar{H}_0$ is given by

$$\bar{H}_0 = \begin{cases} \left(\frac{(1-q)^2 c_0(s^-, t)^p}{2(1+q)D_h}\bar{X}^2\right)^{-\frac{1}{q-1}} & \text{for } \bar{X} > 0, \\ 0 & \text{for } \bar{X} < 0. \end{cases} \tag{3.29}$$

Further, note that the inner inner region is now restricted to $\bar{x} > 0$ with the inner 1 matching conditions occurring as $\bar{x} \to 0^+$ instead.

Returning to the inner inner region, matching into outer 2, the matching conditions

$$\text{as } \bar{x} \to +\infty \quad \bar{c}_0 \to 0, \quad D_h \frac{\partial \bar{h}_0}{\partial \bar{x}} \to D_{h_0} \frac{\partial h_0(s^+, t)}{\partial x},$$

with necessarily

$$h_0(s^+, t) = 0, \tag{3.30}$$

give

$$A(t) = -D_{h_0}\frac{\partial h_0(s^+,t)}{\partial x}. \tag{3.31}$$

Hence, (3.25) and (3.31) give

$$\begin{aligned}\text{at } x = s(t) \qquad & c_0(s^-,t) = \Phi_1, \quad h_0(s^+,t) = 0,\\ & -D_{c_0}\frac{\partial c_0(s^-,t)}{\partial x} - D_{h_0}\frac{\partial h_0(s^+,t)}{\partial x} = \mu\dot{s}c_0(s^-,t)\end{aligned}$$

and so we obtain the following two-phase moving boundary problem

$$\text{in } 0 < x < s(t),\ t > 0 \qquad \mu\frac{\partial c_0}{\partial t} - \frac{\partial}{\partial x}\left(D_{c_0}\frac{\partial c_0}{\partial x}\right) = 0, \tag{3.32}$$

$$\text{in } s(t) < x < 1,\ t > 0 \qquad \frac{\partial h_0}{\partial t} - \frac{\partial}{\partial x}\left(D_{h_0}\frac{\partial h_0}{\partial x}\right) = 0, \tag{3.33}$$

$$\text{on } x = 0 \qquad -D_{c_0}\frac{\partial c_0}{\partial x} = H(1-c_0), \tag{3.34}$$

$$\text{on } x = s(t) \qquad c_0 = \Phi_1(\dot{s}), \quad h_0 = 0, \quad -D_{c_0}\frac{\partial c_0}{\partial x} - D_{h_0}\frac{\partial h_0}{\partial x} = \mu\dot{s}c_0, \tag{3.35}$$

$$\text{on } x = 1 \qquad D_{h_0}\frac{\partial h_0}{\partial x} = 0, \tag{3.36}$$

$$\text{at } t = t_0 \qquad c_0 = C_i \text{ for } 0 \le x \le s_0, \quad h_0 = H_i \text{ for } s_0 \le x \le 1, \quad s = s_0. \tag{3.37}$$

This is as in (2.45)-(2.50) but instead of (2.48) we now have a more general moving boundary condition (3.35). Moreover, Φ_1 is determined by the solution of the inner inner problem

$$\mu\dot{s}\frac{\partial \bar{c}_0}{\partial \bar{x}} + \frac{\partial}{\partial \bar{x}}\left(\bar{D}_c\frac{\partial \bar{c}_0}{\partial \bar{x}}\right) = \bar{c}_0^p\bar{h}_0^q, \tag{3.38}$$

$$\frac{\partial}{\partial \bar{x}}\left(D_h\frac{\partial \bar{h}_0}{\partial \bar{x}}\right) = \bar{c}_0^p\bar{h}_0^q, \tag{3.39}$$

with

$$\text{as } \bar{x} \to +\infty \quad \bar{c}_0 \to 0, \quad \bar{D}_c\frac{\partial \bar{c}_0}{\partial \bar{x}} \to 0, \quad D_h\frac{\partial \bar{h}_0}{\partial \bar{x}} \to D_{h_0}\frac{\partial h_0(s^+,t)}{\partial x}, \tag{3.40}$$

$$\text{as } \bar{x} \to -\infty \quad \bar{c}_0 \to \Phi_1(\dot{s}), \quad \bar{h}_0 \to 0 \tag{3.41}$$

where $\bar{D}_c = \frac{\nu_1}{\bar{h}_0^q}$ and $D_h = O(1)$. Finally, figure 3.4 shows a schematic representation of the carbonation reaction for this last parameter regime, $\delta = O(\epsilon)$.

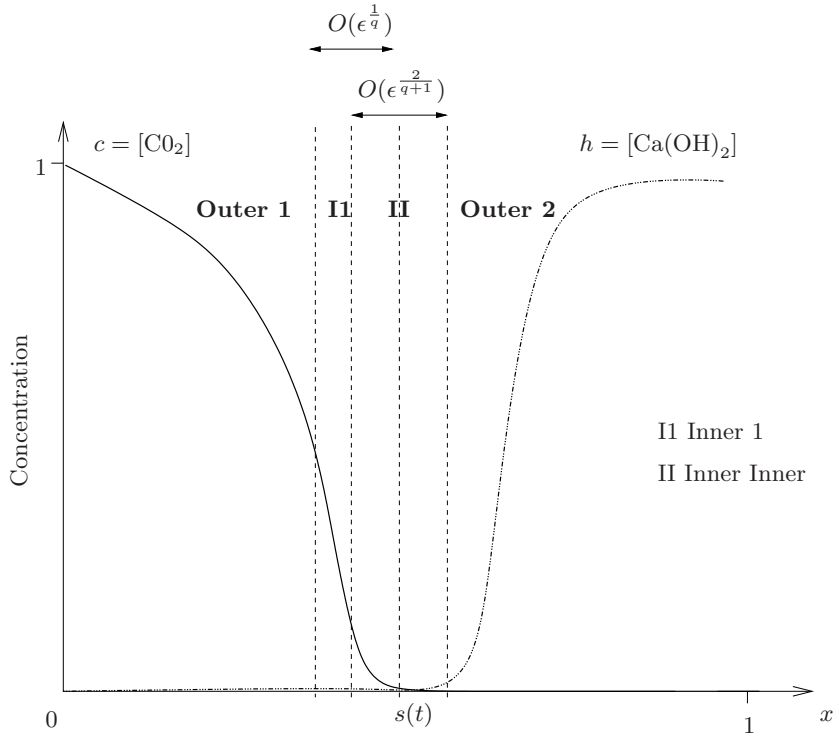

Figure 3.4: *A schematic illustration of the asymptotic regions for a rapidly varying CO_2 diffusivity ($D(c) = O(\epsilon^2)$, $D_h = O(1)$) in the parameter case $\delta = O(\epsilon)$. The regions outer 1 ($0 < x < s(t)$) and outer 2 ($s(t) < x < 1$) are the two outer regions surrounding the two layered reaction zone, comprised of an inner inner region and an inner 1 region. Inner 1 acts as a transition region to facilitate the matching of the inner inner region with outer 1 by accommodating the change in magnitude in the rapidly varying diffusivity. The case shown is for $q > 1$. Minor modifications are needed to inner 1 for $q \leq 1$.*

3.2 Numerical Results

3.2.1 Scheme

Here we present numerical simulations of the full model (2.6)-(2.10) for a rapidly varying CO_2 diffusivity and compare them to the asymptotics. The equations were implemented in COMSOL Multiphysics using the scheme and data/parameter values as specified in section 2.4. To avoid encountering singularities the following regularisations for the reaction term (2.11) and the diffusion coefficient (3.1) respectively were found necessary,

$$r = c(c^2 + \theta_1^2)^{\frac{p-1}{2}} * h(h^2 + \theta_1^2)^{\frac{q-1}{2}}, \quad D_c = 1 - \exp\left(-\frac{\nu_1 \epsilon^2}{(h^2 + \theta_2^2)^{\frac{q}{2}}}\right), \tag{3.42}$$

where $\theta_1 = 10^{-3}$ (only needed when $p \neq 1$, $q \neq 1$) and $\theta_2 \ll (\nu_1 \epsilon^2)^{1/q}$. The regularisation (3.42) for D_c avoids the singularity caused when $h = 0$. The value of θ_2 has to be chosen so that the $O(1)$ behaviour of D_c at this point is maintained. Further, we create a mesh consisting of 1600 quadratic Lagrangian elements (instead of 400) and

so the number of degrees of freedom solved for is 6402.

3.2.2 Base Case

Figure 3.5 shows the numerical results for $\epsilon = 10^{-2}$ with $\theta_2 = 10^{-5}$. Three selected cases of δ are shown covering the different asymptotic regimes noted in the previous section. Noteworthy features are the $O(1)$ concentrations of CO_2 at the reaction zone in all cases. Also the slower progress of the reaction zone compared to the corresponding situation in the slowly varying case. Again the case $\delta = \epsilon$ shown in figure 3.5(c) gives different behaviour to the case $\delta \ll \epsilon$, with the hydroxide concentration being small at the reaction zone front and stage I carbonation taking place initially.

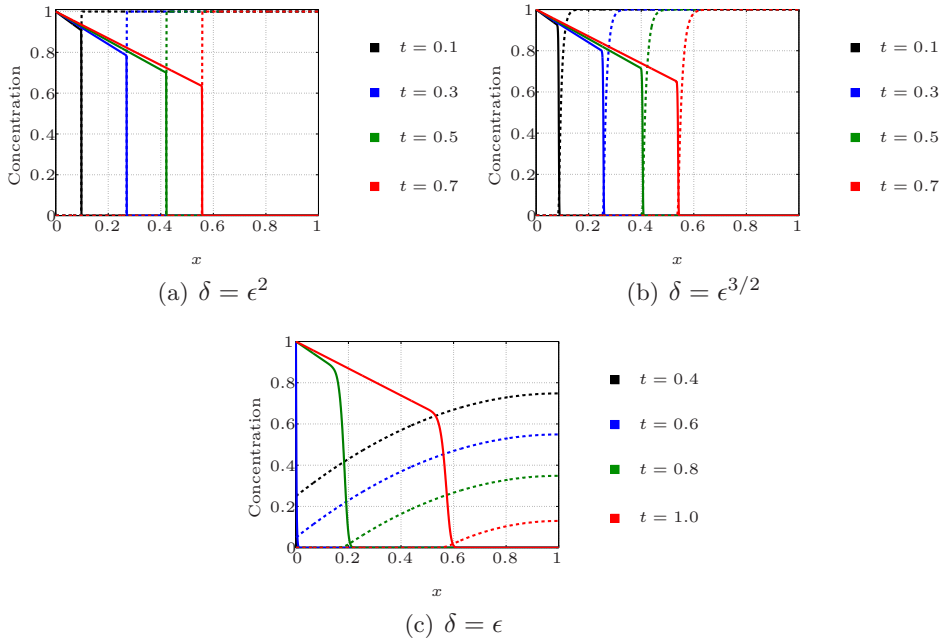

(a) $\delta = \epsilon^2$ (b) $\delta = \epsilon^{3/2}$

(c) $\delta = \epsilon$

Figure 3.5: *Numerical results for one rapidly varying diffusion coefficient D_c, as defined in* (3.1)*, for $\epsilon = 10^{-2}$, $\nu_1 = 1$. The initial data and parameter values are as stated in* (2.51) *and the selected δ values are as stated in (a)-(c). The solid lines refer to the concentration of carbon dioxide while the dotted lines are the concentration of calcium hydroxide.*

3.2.3 Parameter variation

As done in the previous chapter, it is of interest to see how a change in the parameters affects the behaviour of the system. In particular, we look at $\mu = 1$ (figure 3.6) and $H = 1$ (figure 3.7). The effects of changing p and q can be derived from the asymptotics. In this case, changing p will have little effect since neither of the scalings in the previous section depend on it. Further, as q increases, the thickness of the reaction zone and the concentration of hydroxide around such point will increase. From figure 3.6, we see

that the reaction zone moves slower into the concrete, indicating that if $h^0 \gg c^*$, the reaction occurs faster. Again, for $H = O(1)$, c is no longer pinned at 1.

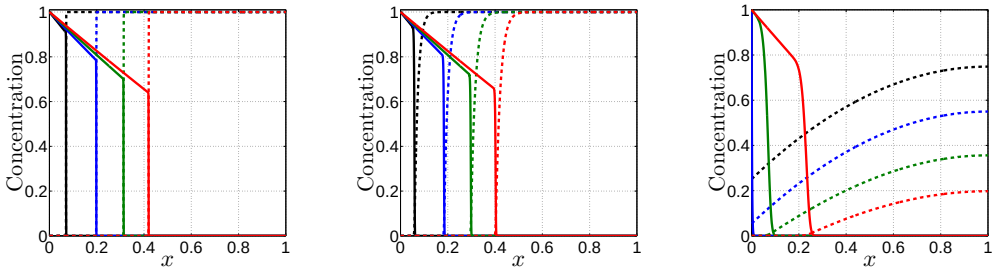

(a) $\delta = \epsilon^2$ (b) $\delta = \epsilon^{3/2}$ (c) $\delta = \epsilon$

Figure 3.6: *Numerical results for one rapidly varying diffusion coefficient D_c. The parameter values are $\epsilon = 10^{-2}$, $\nu_1 = 1$, $p = q = 1$, $\mu = 1$ and $H = 10^4$, and selected δ as stated in (a)-(c). The solid lines refer to the concentration of carbon dioxide while the dotted lines are the concentration of calcium hydroxide at times $t = 0.1$ (black), $t = 0.3$ (blue), $t = 0.5$ (green) and $t = 0.7$ (red) for (a) and (b), and $t = 0.4, 0.6, 0.8, 1.0$ respectively for (c).*

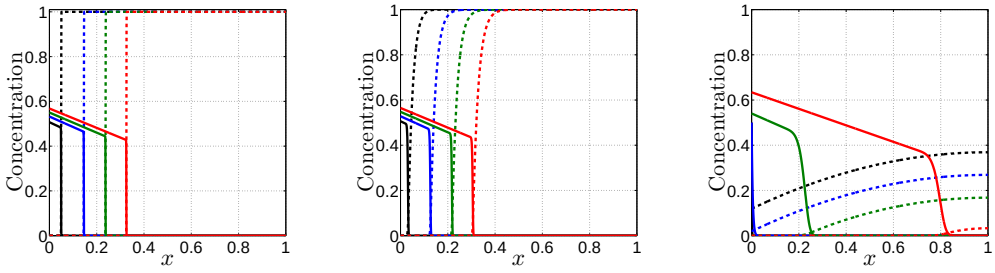

(a) $\delta = \epsilon^2$ (b) $\delta = \epsilon^{3/2}$ (c) $\delta = \epsilon$

Figure 3.7: *Numerical results for one rapidly varying diffusion coefficient D_c. The parameter values are $\epsilon = 10^{-2}$, $\nu_1 = 1$, $p = q = 1$, $\mu = 10^{-3}$ and $H = 1$, and selected δ as stated in (a)-(c). The solid lines refer to the concentration of carbon dioxide while the dotted lines are the concentration of calcium hydroxide at times $t = 0.1$ (black), $t = 0.3$ (blue), $t = 0.5$ (green) and $t = 0.7$ (red) for (a) and (b), and $t = 1.4, 1.6, 1.8, 2.0$ respectively for (c).*

3.2.4 Free boundary $s(t)$ and Kinetic condition $\Phi_1(\dot{s})$

As in subsection 2.4.4 we investigate the localisation of the reaction zone. However, $\Phi_1(\dot{s})$ is no longer zero. To be able to compute this quantity numerically a precise definition is required. Using the asymptotic analysis from section 3.1 as motivation, we define $\Phi_1(\dot{s})$ as follows

$$\Phi_1(\dot{s}) = \{c \in [0,1] | h(x,t) = \epsilon^{\frac{2}{q}}\}. \tag{3.43}$$

In other words, we take $\Phi_1(\dot{s})$ to be the concentration of CO_2 just before entering the reaction zone from the outer 1 region i.e. the concentration of CO_2 in inner 1.

Base case

We take parameter values (2.51) where in particular, $p = q = 1$. Figure 3.8 shows the plots of the interface $s(t)$, its speed $\dot{s}(t)$ and $\Phi_1(\dot{s})$ for the asymptotic regimes in the parameter range $\delta \ll \epsilon$. As already seen in subsection 2.4.4, the interface $s(t) \sim \sqrt{t}$. This result also hold for $\delta = \epsilon$ but the domain has been extended to see this. Figure

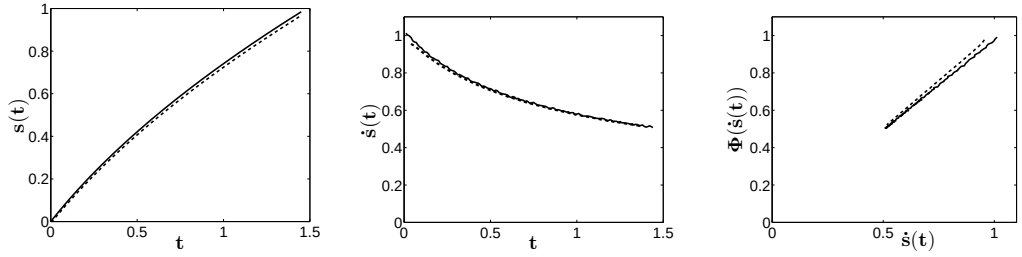

(a) Free boundary, $s(t)$. (b) Speed of free boundary, $\dot{s}(t)$. (c) Kinetic condition, $\Phi_1(\dot{s})$.

Figure 3.8: *Free boundary and kinetic condition results from* (2.6)-(2.10) *for a one rapidly varying diffusivity D_c and $\delta < \epsilon$ with $\epsilon = 10^{-2}$. Two values of δ are depicted, namely $\delta = \epsilon^2$ (solid line) and $\delta = \epsilon^{3/2}$ (dashed line).*

3.9 shows the asymptotic regime $\delta = \epsilon$ with domain $x = [0, 1]$. In particular, 3.9(a) and 3.9(b) have not been truncated and it can clearly be seen how the edge effects, first appearing in subsection 2.4.4, play a very important role. Figure 3.9(c) is the truncated version and with $\epsilon = 10^{-2}$, $\Phi_1(\dot{s})$ cannot be computed using (3.43). Extending the

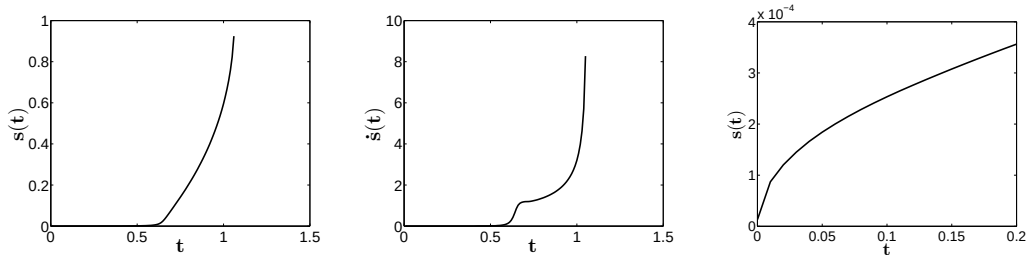

(a) Free boundary, $s(t)$. (b) Speed of free boundary, $\dot{s}(t)$. (c) Truncated free boundary.

Figure 3.9: *Free boundary results from* (2.6)-(2.10) *for a one rapidly varying diffusivity D_c and $\delta = \epsilon$ with $\epsilon = 10^{-2}$.*

domain to $x = [0, 50]$, figure 3.10 shows a more realistic plot of the long-time behaviour of the interface that we will revisit in more detail in chapter 6. The profile of $\Phi_1(\dot{s})$ appears to be linear in all regimes and table 3.1 corroborates this assumption. In it we include the curve fitting results given by the interactive toolbox cftool from MATLAB where the following equation was implemented

$$\Phi_{1,2}(\dot{s}) = a\dot{s}^b + c. \tag{3.44}$$

The key quantities determining the goodness of fit are the sum of squares due to error

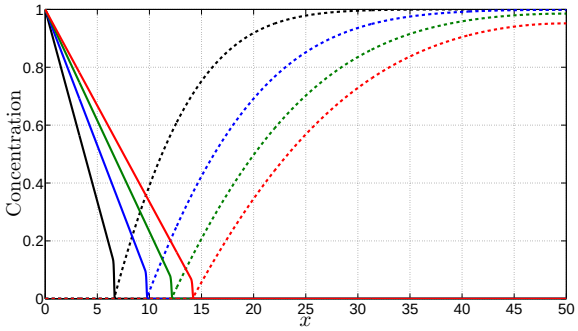

(a) Concentration of CO_2 (solid lines) and $Ca(OH)_2$ (dotted lines) for times $t = 50$ (black), $t = 100$ (blue), $t = 150$ (green) and $t = 200$ (red).

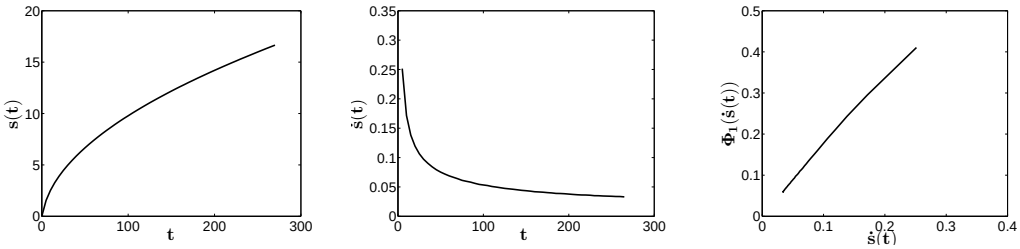

(b) Free boundary, $s(t)$. (c) Speed of free boundary, $\dot{s}(t)$. (d) Kinetic condition, $\Phi_1(\dot{s})$.

Figure 3.10: *Free boundary and kinetic condition results from* (2.6)-(2.10) *for a one rapidly varying diffusivity* D_c *and* $\delta = \epsilon$ *with* $\epsilon = 10^{-2}$ *and* $x = [0, 50]$.

(SSE), for which we seek for a value close to zero, and the adjusted R-square statistics in which a value close to one is ideal. The behaviour of $\Phi_1(\dot{s})$ will be revisited in chapter 5, where the micro problems are looked at in more detail.

	Cofficients (with 95% confident bounds)	Goodness of fit
$\delta \leq \epsilon^2$	a=0.972 (0.9439,1) b=0.9866 (0.9448,1.028) c=3.329×10^{-2} (-0.02598,0.03264)	SSE: 1.313×10^{-3} R-square: 0.9995 Adjusted R-square: 0.9995 RMSE: 3.052×10^{-3}
$\epsilon^2 < \delta < \epsilon$	a=0.9886 (0.9778,0.9994) b=1.043 (1.025,1.06) c=0.0269 (0.01534,0.03846)	SSE: 1.499×10^{-4} R-square: 0.9999 Adjusted R-square: 0.9999 RMSE: 1.066×10^{-3}
$\delta = \epsilon$	a=1.414 (1.39,1.437) b=0.8603(0.8466,0.8739) c=-0.0179 (-0.0206,-0.01521)	SSE: 5.578×10^{-5} R-square: 0.9997 Adjusted R-square: 0.9997 RMSE: 1.056×10^{-3}

Table 3.1: *Base case curve fitting results for all asymptotic regimes for* $\Phi_1(\dot{s}) = a\dot{s}^b + c$*, where* Φ_1 *is computed as in* (3.43) *after solving the full reaction-diffusion system with parameter values* (2.51) *and one rapidly varying diffusion coefficient.*

Different p and q

Here we take parameter values (2.51) but we now consider the following four combinations of p and q

$$p > 1,\, q = 1, \quad p = 1,\, q > 1, \quad p < 1,\, q = 1, \quad p = 1,\, q < 1.$$

In chapter 5 we focus on the micro problems and in particular, the profile of the kinetic conditions $\Phi_{1,2}$ for general values of p and q. In chapter 6, we focus on the profile of the free boundary $s(t)$ but the analysis is restricted to the case $p = q = 1$. For completion, figure 3.11 shows the resulting free boundary for all the above combinations of p and q. However, thinking ahead to chapter 5, we focus on Φ_1, figure 3.12. At first sight,

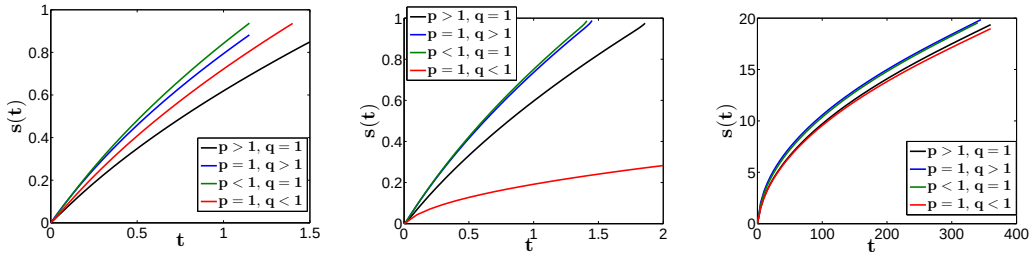

(a) Case $\delta \leq \epsilon^2$ with $\epsilon = 0.1$. (b) Case $\epsilon^2 < \delta < \epsilon$ with $\epsilon = 10^{-2}$. (c) Case $\delta = \epsilon$ with $\epsilon = 0.1$.

Figure 3.11: *Free boundary plots for one rapidly varying diffusivity and different values of p and q.*

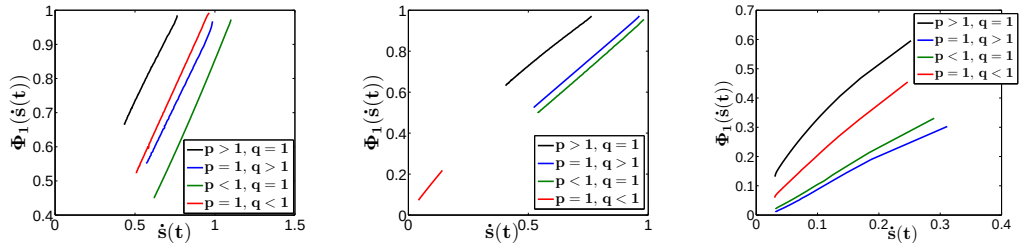

(a) Case $\delta \leq \epsilon^2$ with $\epsilon = 0.1$. (b) Case $\epsilon^2 < \delta < \epsilon$ with $\epsilon = 10^{-2}$. (c) Case $\delta = \epsilon$ with $\epsilon = 0.1$.

Figure 3.12: *Kinetic condition ($\Phi_1(\dot{s})$) plots for one rapidly varying diffusivity and different values of p and q.*

there does not seem to be much difference with the case $p = q = 1$ and it may be concluded that $\Phi_1(\dot{s})$ can be approximated by $\dot{s}(t)$ linearly. Table 3.2 shows the results of fitting the curve (3.44) with the plots in figure 3.12. The goodness of fit in all cases is very good. It is now clear that the relationship between $\Phi_1(\dot{s})$ and $\dot{s}$ in no longer linear everywhere, however the value of c can still be regarded as negligible. The most noteworthy feature is that the change of b seems to be more prominent when $p \neq 1$. The exact relationship and its dependence on the parameter p will be discussed further

		Cofficients (with 95% confident bounds)	Goodness of fit
$\delta \leq \epsilon^2$	$p > 1$	a=1.117 (1.091,1.142) b=0.7315 (0.7039,0.7592) c=0.06108 (0.03313,0.08902)	SSE: 1.635×10^{-4} Adjusted R-square: 0.9998 RMSE: 1.096×10^{-3}
	$q > 1$	a=0.8946 (0.8677,0.9215) b=1.126 (1.077,1.175) c=0.07441 (0.04629,0.1025)	SSE: 3.955×10^{-4} Adjusted R-square: 0.9997 RMSE: 2.009×10^{-3}
	$p < 1$	a=0.8557 (0.8537,0.8577) b=1.335 (1.331,1.339) c=-0.001232 (-0.003261,0.0007959)	SSE: 2.752×10^{-6} Adjusted R-square: 0.9999 RMSE: 2.352×10^{-4}
	$q < 1$	a=1.029 (1.018,1.039) b=1.004 (0.9886,1.02) c=3.431×10^{-3} (-7.702×10^{-3}, 0.01456)	SSE: 1.331×10^{-4} Adjusted R-square: 0.9999 RMSE: 1.004×10^{-3}
$\epsilon^2 < \delta < \epsilon$	$p > 1$	a=1.133 (1.121,1.145) b=0.6962 (0.6837,0.7086) c=0.029 (0.01566,0.04234)	SSE: 6.513×10^{-5} Adjusted R-square: 1 RMSE: 6.321×10^{-4}
	$q > 1$	a=1 (0.9961,1.004) b=1.01 (1.004),1.017) c=6.178×10^{-3} (1.805×10^{-3}, 0.01055)	SSE: 1.689×10^{-5} Adjusted R-square: 1 RMSE: 3.632×10^{-4}
	$p < 1$	a=0.9618 (0.9553,0.9683) b=1.096 (1.085,1.107) c=0.01008 (0.003227,0.01694)	SSE: 4.947×10^{-5} Adjusted R-square: 1 RMSE: 6.316×10^{-4}
	$q < 1$	a=1.295 (1.28,1.31) b=0.9141 (0.9063,0.9218) c=9.615×10^{-4} (-5.182×10^{-5},1.975×10^{-3})	SSE: 2.099×10^{-6} Adjusted R-square: 1 RMSE: 1.84×10^{-4}
$\delta = \epsilon$	$p > 1$	a=1.437 (1.42,1.454) b=0.5584(0.5436,0.5731) c=-0.06895 (-0.07784,-0.06007)	SSE: 2.206×10^{-4} Adjusted R-square: 0.9995 RMSE: 1.801×10^{-3}
	$q > 1$	a=1.003 (0.9702,1.036) b=0.9313 (0.9035,0.959) c=-0.03029 (-0.03344,-0.02714)	SSE: 2.796×10^{-4} Adjusted R-square: 0.998 RMSE: 2.074×10^{-4}
	$p < 1$	a=1.404 (1.32, 1.487) b=1.084 (1.055,1.118) c=-0.0112 (-0.01296,-0.00944)	SSE: 1.422×10^{-5} Adjusted R-square: 0.9995 RMSE: 4.867×10^{-4}
	$q < 1$	a=1.574 (4.5,1.648) b=0.8544 (0.8253,0.8835) c=-0.01579 (-0.0205,-0.01109)	SSE: 9.35×10^{-5} Adjusted R-square: 0.9993 RMSE: 1.191×10^{-3}

Table 3.2: *Different values of p and q curve fitting results for all asymptotic regimes for* $\Phi_1(\dot{s}) = a\dot{s}^b + c$*, where* Φ_1 *is computed as in* (3.43) *after solving the full reaction-diffusion system with parameter values* (2.51) *and one rapidly varying diffusion coefficient.*

in chapter 5.

In this chapter we have derived the sharp interface models in the fast reaction limit $\epsilon \to 0$, for a one rapidly varying diffusion coefficient. As for the slowly varying case, a one-phase Stefan model is obtained for the parameter regime $\delta \ll \epsilon$ and a two-phase one for $\delta = O(\epsilon)$. However, the reaction zone is no longer composed of a single layer and neither is $\Phi_1 = 0$ in (2.21), having to solve an inner problem to determine it. This leads to nonstandard two-scale (micro-macro) moving boundary problems. Nevertheless, Φ_2 is still zero in (2.21) and, with this in mind, we look at the third and final type of diffusion coefficients.

Chapter 4

Concrete Carbonation with Two Rapidly Varying Diffusion Coefficients

It still remains to obtain $\Phi_2 \neq 0$ for the kinetic boundary condition (2.21). To achieve this, we now consider the hydroxide diffusivity to depend on ϵ as well as the carbon dioxide concentration, i.e. $D_h = D_h(c;\epsilon)$. We arrive to a situation in which both diffusivities are rapidly varying, with D_c as defined in chapter 3 and D_h having the following behaviour

$$D_h = \begin{cases} O(\delta^2) & \text{for } c = O(1),\ c > 0, \\ O(1) & \text{for } c = o(1),\ c > 0, \end{cases}$$

and $D_h(0,h;\epsilon)$=1. This maintains an $O(1)$ flux of hydroxide in the reaction zone. For definiteness, a specific functional form could be the Arrhenius type,

$$D_h = 1 - \exp\left(-\frac{\nu_2 \delta^2}{c^p}\right), \tag{4.1}$$

where ν_2 is a positive constant and p is the reaction order of the carbon dioxide as in (2.11). A schematic illustration of the behaviour of this diffusion coefficient is shown in figure 4.1.

We consider the nondimensionalised problem (2.6)-(2.10) exposed in Chapter 2 but with D_c as in (3.1) and D_h as in (4.1). We follow the same procedure as in chapters 2 and 3. The outer solutions and jump conditions derived in Chapter 2 hold here too and so we proceed to analyse the reaction zone.

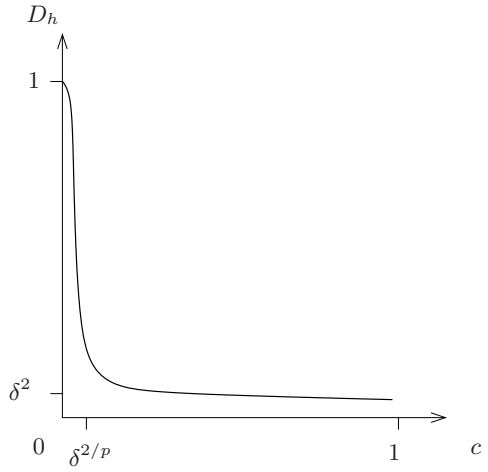

Figure 4.1: *A schematic illustration of the calcium hydroxide diffusion coefficient D_h with the functional form* (4.1).

4.1 Interior (reaction) layer analysis: $D_c = O(\epsilon^2)$ and $D_h = O(\delta^2)$

The behaviour of the reaction layer is still affected by the dependence of the parameter δ on ϵ and so we consider each asymptotic regime separately for the parameter range $\delta \leq \epsilon$. In this case, there are only two regimes to consider, namely $\delta \ll \epsilon$ and $\delta = O(\epsilon)$. For each of them, the reaction zone is now composed of three regions, denoted inner inner, inner 1 and inner 2. The inner inner region is where the reaction term is O(1) in both governing equations (2.6) and (2.7) and inners 1 and 2 are additional regions required to facilitate the matching of the inner inner with outers 1 and 2 respectively. Inner 1 accommodates the change in magnitude of the CO_2 diffusion coefficient D_c, as seen already in Chapter 3, and inner 2 is now introduced to match the change in magnitude happening in the hydroxide diffusion coefficient D_h.

4.1.1 The case $\delta \ll \epsilon$

As mentioned above, the reaction zone is comprised of the three regions inner inner, inner 1 and inner 2 and in this subsection we look at each of them separately for the parameter regime $\delta \ll \epsilon$.

- **Inner Inner**

The required inner inner scalings are

$$x = s(t) + \epsilon^2 \bar{x}, \quad c = \bar{c}, \quad h = \bar{h}, \quad D_c = \epsilon^2 \bar{D}_c, \quad D_h = \delta^2 \bar{D}_h,$$

with $\bar{D}_c \sim \nu_1/h^q$, $\bar{D}_h \sim \nu_2/c^p$ for the functional form (3.1) and (4.1) respectively.

Substituting these scalings in (2.6), (2.7) gives

$$\epsilon^2\mu\frac{\partial\bar{c}}{\partial t}-\mu\dot{s}\frac{\partial\bar{c}}{\partial\bar{x}}-\frac{\partial}{\partial\bar{x}}\left(\bar{D}_c\frac{\partial\bar{c}}{\partial\bar{x}}\right)=-\bar{c}^p\bar{h}^q,$$
$$\epsilon^2\frac{\partial\bar{h}}{\partial\bar{t}}-\dot{s}\frac{\partial\bar{h}}{\partial\bar{x}}-\left(\frac{\delta}{\epsilon}\right)^4\frac{\partial}{\partial\bar{x}}\left(\bar{D}_h\frac{\partial\bar{h}}{\partial\bar{x}}\right)=-\bar{c}^p\bar{h}^q.$$

Posing the expansions

$$\bar{c}=\bar{c}_0+o(1),\quad \bar{h}=\bar{h}_0+o(1),$$

with

$$\bar{D}_c(c,h)\sim\bar{D}_c(\bar{c}_0,\bar{h}_0),\quad \bar{D}_h(c,h)\sim\bar{D}_h(\bar{c}_0,\bar{h}_0),$$

we obtain

$$\mu\dot{s}\frac{\partial\bar{c}_0}{\partial\bar{x}}+\frac{\partial}{\partial\bar{x}}\left(\bar{D}_c\frac{\partial\bar{c}_0}{\partial\bar{x}}\right)=\bar{c}_0^p\bar{h}_0^q,$$
$$\mu\dot{s}\bar{c}_0+\bar{D}_c\frac{\partial\bar{c}_0}{\partial\bar{x}}=\dot{s}\bar{h}_0+A(t),$$

where $A(t)$ is a function of t to be determined. Matching into outer 1, the matching conditions

$$\text{as } \bar{x}\to-\infty\quad \bar{c}_0\to c_0(s^-,t),\quad \bar{D}_c\frac{\partial\bar{c}_0}{\partial\bar{x}}\to D_{c_0}\frac{\partial c_0(s^-,t)}{\partial x},\quad \bar{h}_0\to 0, \tag{4.2}$$

yield

$$A(t)=\mu\dot{s}c_0(s^-,t)+D_{c_0}\frac{\partial c_0(s^-,t)}{\partial x}. \tag{4.3}$$

Matching into outer 2, the matching conditions

$$\text{as } \bar{x}\to+\infty\quad \bar{c}_0\to 0,\quad \bar{h}_0\to h_0(s^+,t),\quad \bar{D}_h\frac{\partial\bar{h}_0}{\partial\bar{x}}\to D_{h_0}\frac{\partial h_0(s^+,t)}{\partial x}, \tag{4.4}$$

yield

$$A(t)=-\dot{s}h_0(s^+,t). \tag{4.5}$$

Two additional regions are required to facilitate the matching with outers 1 and 2, due to the order of magnitude change in the diffusivities, and to fully understand (4.2) and (4.4).

- **Inner 1**

Here $h=O(\epsilon^{2/q})$, this being the scaling on which $D_c=O(1)$. The scalings are determined by the size of δ relative to a critical value $\delta_{CR}=\epsilon^{\frac{q+1}{2q}}$ and the value of $q\geq 0$ in the reaction term (2.11). For the range $q\geq 1$, we note that $\delta_{CR}>\epsilon$ and so, it is not until $q<1$, case (C), that δ_{CR} will have an effect.

(A) For $q > 1$, the scalings are

$$x = s(t) + \epsilon^{\frac{2}{q}}\bar{X}, \quad c = \bar{C}, \quad h = \epsilon^{\frac{2}{q}}\bar{H}, \quad D_h = \delta^2\bar{D}_h, \tag{4.6}$$

with D_c as in (3.1) and $\bar{D}_h \sim \nu_2/c^p$, so that

$$\mu\epsilon^{\frac{4}{q}}\frac{\partial\bar{C}}{\partial t} - \mu\epsilon^{\frac{2}{q}}\dot{s}\frac{\partial\bar{C}}{\partial\bar{X}} - \frac{\partial}{\partial\bar{X}}\left(D_c\frac{\partial\bar{C}}{\partial\bar{X}}\right) = -\epsilon^{\frac{4}{q}}\bar{C}^p\bar{H}^q,$$
$$\epsilon^{\frac{2}{q}}\frac{\partial\bar{H}}{\partial t} - \dot{s}\frac{\partial\bar{H}}{\partial\bar{X}} - \left(\frac{\delta}{\epsilon}\right)^4\epsilon^{\frac{2}{q}(q-1)}\frac{\partial}{\partial\bar{X}}\left(\bar{D}_h\frac{\partial\bar{H}}{\partial\bar{X}}\right) = -\bar{C}^p\bar{H}^q.$$

Note that in this case the transition region, inner 1, is larger in size than the reaction layer, inner inner. Posing

$$\bar{C} \sim \bar{C}_0 + \epsilon^{\frac{2}{q}}\bar{C}_1, \quad \bar{H} \sim \bar{H}_0,$$

with

$$D_c(c,h) \sim D_c(\bar{C}_0, 0), \quad \bar{D}_h(c,h) \sim \bar{D}_h(\bar{C}_0, 0),$$

we obtain

$$\frac{\partial}{\partial\bar{X}}\left(D_c\frac{\partial\bar{C}_0}{\partial\bar{X}}\right) = 0, \quad \dot{s}\frac{\partial\bar{H}_0}{\partial\bar{X}} = \bar{C}_0^p\bar{H}_0^q,$$

at leading order, and

$$\mu\dot{s}\frac{\partial\bar{C}_0}{\partial\bar{X}} + \frac{\partial}{\partial\bar{X}}\left(D_c\frac{\partial\bar{C}_1}{\partial\bar{X}}\right) = 0,$$

at first order. After matching to outer 1 and the inner inner we have

$$\bar{C}_0 = c_0(s^-, t) = \Phi_1, \quad D_c\frac{\partial\bar{C}_1}{\partial\bar{X}} = D_{c_0}\frac{\partial c_0(s^-,t)}{\partial x}, \tag{4.7a}$$
$$\bar{H}_0 = \left(-\frac{q-1}{\dot{s}}c_0(s^-,t)^p\bar{X}\right)^{-\frac{1}{q-1}}. \tag{4.7b}$$

(B) For $q = 1$, the transition region is of the same size as the reaction layer. We introduce the scalings

$$x = s(t) + \epsilon^2(S(t) + \bar{X}), \quad c = \bar{C}, \quad h = \epsilon^2\bar{H}, \quad D_h = \delta^2\bar{D}_h,$$

where $1 < S(t) < 1/\epsilon^2$. The governing equations become

$$\epsilon^4\mu\frac{\partial\bar{C}}{\partial t} - \epsilon^2\mu(\dot{s} + \epsilon^2\dot{S})\frac{\partial\bar{C}}{\partial\bar{X}} - \frac{\partial}{\partial\bar{X}}\left(D_c\frac{\partial\bar{C}}{\partial\bar{X}}\right) = -\epsilon^4\bar{C}^p\bar{H},$$
$$\epsilon^2\frac{\partial\bar{H}}{\partial t} - (\dot{s} + \epsilon^2\dot{S})\frac{\partial\bar{H}}{\partial\bar{X}} - \left(\frac{\delta}{\epsilon}\right)^4\frac{\partial}{\partial\bar{X}}\left(\bar{D}_h\frac{\partial\bar{H}}{\partial\bar{X}}\right) = -\bar{C}^p\bar{H}.$$

Posing

$$\bar{C} \sim \bar{C}_0 + \epsilon^2 \bar{C}_1, \quad \bar{H} \sim \bar{H}_0,$$

with

$$D_c(c,h) \sim D_c(\bar{C}_0, 0), \quad \bar{D}_h(c,h) \sim \bar{D}_h(\bar{C}_0, 0),$$

we obtain

$$\frac{\partial}{\partial \bar{X}}\left(D_c \frac{\partial \bar{C}_0}{\partial \bar{X}}\right) = 0, \quad \dot{s}\frac{\partial \bar{H}_0}{\partial \bar{X}} = \bar{C}_0^p \bar{H}_0,$$

at leading order and

$$\mu \dot{s}\frac{\partial \bar{C}_0}{\partial \bar{X}} + \frac{\partial}{\partial \bar{X}}\left(D_c \frac{\partial \bar{C}_1}{\partial \bar{X}}\right) = 0,$$

at first order. After matching to outer 1 and the inner inner we again obtain (4.7a) and $\bar{H}_0$ is given by

$$\bar{H}_0 = \exp\left(\frac{c_0(s^-,t)^p}{\dot{s}}\bar{X}\right).$$

Further,

$$S(t) \sim \frac{2\dot{s}}{q c_0(s^-,t)^p}\ln(\epsilon).$$

(C) The third and final case to discuss is $0 < q < 1$. Recall that for this case the scalings are also determined by the size of δ relative to the critical value $\delta_{CR} = \epsilon^{\frac{q+1}{2q}}$, since for $q < 1$ we have that $\epsilon^2 < \delta_{CR} < \epsilon$. For this reason, we now have three cases to consider. Further, the inner 1 region now becomes narrower than the inner inner region.

1. For $\delta < \delta_{CR}$, the required scalings are as in (4.6) so that we obtain (4.7a) but $\bar{H}_0$ is now given by

$$\bar{H}_0 = \begin{cases} \left(\frac{(1-q)}{\dot{s}} c_0(s^-,t)^p \bar{X}\right)^{\frac{1}{1-q}} & \text{for } \bar{X} > 0, \\ 0 & \text{for } \bar{X} < 0. \end{cases}$$

2. For $\delta = \delta_{CR}$, the scalings (4.6) apply as does the subsequent analysis with the modification of the diffusion term entering the leading order hydroxide equation.

3. For $\delta > \delta_{CR}$, the required scalings are

$$x = s(t) + \delta^2 \epsilon^{\frac{1-q}{q}}\bar{X}, \quad c = \bar{C}, \quad h = \epsilon^{\frac{2}{q}}\bar{H}, \quad D_h = \delta^2 \bar{D}_h, \tag{4.8}$$

so that

$$\delta^4 \epsilon^{\frac{2(1-q)}{q}}\mu\frac{\partial \bar{C}}{\partial t} - \delta^2\epsilon^{\frac{1-q}{q}}\mu\dot{s}\frac{\partial \bar{C}}{\partial \bar{X}} - \frac{\partial}{\partial \bar{X}}\left(D_c\frac{\partial \bar{C}}{\partial \bar{X}}\right) = -\delta^4\epsilon^{\frac{2(1-q)}{q}}\bar{C}^p\bar{H}^q,$$

$$\epsilon^{\frac{2}{q}}\frac{\partial \bar{H}}{\partial t} - \frac{\epsilon^{\frac{q+1}{q}}}{\delta^2}\dot{s}\frac{\partial \bar{H}}{\partial \bar{X}} - \frac{\partial}{\partial \bar{X}}\left(\bar{D}_h\frac{\partial \bar{H}}{\partial \bar{X}}\right) = -\bar{C}^p\bar{H}^q.$$

Posing

$$\bar{C} \sim \bar{C}_0 + \delta^2 \epsilon^{\frac{1-q}{q}} \bar{C}_1, \quad \bar{H} \sim \bar{H}_0,$$

with

$$D_c(c,h) \sim D_c(\bar{C}_0, 0), \quad \bar{D}_h(c,h) \sim \bar{D}_h(\bar{C}_0, 0),$$

we obtain

$$\frac{\partial}{\partial \bar{X}} \left(D_c \frac{\partial \bar{C}_0}{\partial \bar{X}} \right) = 0, \quad \frac{\partial}{\partial \bar{X}} \left(\bar{D}_h \frac{\partial \bar{H}_0}{\partial \bar{X}} \right) = \bar{C}_0^p \bar{H}_0^q,$$

at leading order, and

$$\mu \dot{s} \frac{\partial \bar{C}_0}{\partial \bar{X}} + \frac{\partial}{\partial \bar{X}} \left(D_c \frac{\partial \bar{C}_1}{\partial \bar{X}} \right) = 0,$$

at first order. After matching to outer 1 and inner inner we obtain (4.7a) and

$$\bar{H}_0 = \begin{cases} \left(\frac{(1-q)^2 c_0(s^-,t)^p}{2(q+1)\bar{D}_h} \bar{X}^2 \right)^{\frac{1}{1-q}} & \text{for } \bar{X} > 0, \\ 0 & \text{for } \bar{X} < 0, \end{cases}$$

with $\bar{D}_h = \frac{\nu_2}{c_0(s^-,t)^p}$.

Further the inner inner region is now restricted to $\bar{x} > 0$ with the inner 1 matching conditions occurring as $\bar{x} \to 0^+$.

- **Inner 2**

Here $c = O(\delta^{2/p})$, this being the scaling in which $D_h = O(1)$. The scalings are determined by the size of δ relative to a critical value $\delta_{CR} = \epsilon^2$ and the value of $p \geq 0$ in the reaction term (2.11).

(A) For $p > 1$, the scalings are

$$x = s(t) + \epsilon^2 (S(t) + \hat{X}), \quad c = \delta^{\frac{2}{p}} \hat{C}, \quad h = \hat{H}, \quad D_c = \epsilon^2 \hat{D}_c, \tag{4.9}$$

with $\hat{D}_c \sim \nu_1 / h^q$ and D_h as in (4.1), so that

$$\epsilon^2 \mu \frac{\partial \hat{C}}{\partial t} - \mu(\dot{s} + \epsilon \dot{S}) \frac{\partial \hat{C}}{\partial \hat{X}} - \frac{\partial}{\partial \hat{X}} \left(\hat{D}_c \frac{\partial \hat{C}}{\partial \hat{X}} \right) = -\delta^{\frac{2(p-1)}{p}} \hat{C}^p \hat{H}^q,$$

$$\epsilon^2 \frac{\partial \hat{H}}{\partial t} - (\dot{s} + \epsilon^2 \dot{S}) \frac{\partial \hat{H}}{\partial \hat{X}} - \left(\frac{\delta}{\epsilon^2} \right)^2 \frac{\partial}{\partial \hat{X}} \left(D_h \frac{\partial \hat{H}}{\partial \hat{X}} \right) = -\delta^2 \hat{C}^p \hat{H}^q.$$

The critical value of δ here is $\delta_{CR} = \epsilon^2$ and there are three cases to consider separately.

1. For $\delta > \delta_{CR}$, we pose

$$\hat{C} \sim \hat{C}_0, \quad \hat{H} \sim \hat{H}_0 + \delta^2 \hat{H}_1,$$

with

$$\hat{D}_c(c,h) \sim \hat{D}_c(0,\hat{H}_0), \quad D_h(c,h) \sim D_h(0,\hat{H}_0),$$

to obtain

$$\mu\dot{s}\frac{\partial \hat{C}_0}{\partial \hat{X}} + \frac{\partial}{\partial \hat{X}}\left(\hat{D}_c\frac{\partial \hat{C}_0}{\partial \hat{X}}\right) = 0, \quad \frac{\partial}{\partial \hat{X}}\left(D_h\frac{\partial \hat{H}_0}{\partial \hat{X}}\right) = 0,$$

at leading order, and

$$\frac{\partial}{\partial \hat{X}}\left(D_h\frac{\partial \hat{H}_1}{\partial \hat{X}}\right) = 0,$$

at first order. After matching to outer 2 and inner inner we have

$$\hat{H}_0 = h_0(s^+,t), \quad D_h\frac{\partial \hat{H}_1}{\partial \hat{X}} = D_{h_0}\frac{\partial h_0(s^+,t)}{\partial x}, \tag{4.10a}$$

$$\hat{C}_0 = \exp\left(-\frac{\mu\dot{s}}{\hat{D}_c}\hat{X}\right). \tag{4.10b}$$

with $\hat{D}_c = \frac{\nu_1}{h_0(s^+,t)^q}$. Further,

$$S(t) = \frac{2}{p}\frac{\hat{D}_c}{\mu\dot{s}}\ln\left(\frac{1}{\delta}\right).$$

2. For $\delta = \delta_{CR} = \epsilon^2$, all the above analysis applies with the modification of the convection term entering the leading order hydroxide equation.

3. For $\delta < \delta_{CR}$, again all the above analysis applies, but now the hydroxide convection and diffusion terms balance in a thin region of size $\hat{X} = \left(\frac{\delta}{\epsilon^2}\right)^2$ centred at $S(t)$, which allows the required matching to outer 2.

(B) For $p = 1$, the scalings (4.9) apply as does the subsequent analysis and the different behaviours of the hydroxide equation regarding the value of δ. The only modification is that now the reaction term enters the leading order carbon dioxide equation.

(C) For $0 < p < 1$, the inner inner solution for $\bar{c}_0$ vanishes at $\bar{x} = S(t)$ and we modify the spatial scaling in (4.9) to

$$x = s(t) + \epsilon^2(S(t) + \delta^{\frac{1-p}{p}}\hat{X}),$$

so that

$$\epsilon^2\delta^{\frac{2(1-p)}{p}}\mu\frac{\partial \hat{C}}{\partial t} - \delta^{\frac{1-p}{p}}\mu(\dot{s}+\epsilon^2 S)\frac{\partial \hat{C}}{\partial \hat{X}} - \frac{\partial}{\partial \hat{X}}\left(\hat{D}_c\frac{\partial \hat{C}}{\partial \hat{X}}\right) = \hat{C}^p\hat{H}^q,$$

$$\epsilon^2\frac{\partial \hat{H}}{\partial t} - \delta^{-\frac{1-p}{p}}(\dot{s}+\epsilon^2 S)\frac{\partial \hat{H}}{\partial \hat{X}} - \left(\frac{\delta}{\epsilon^2}\right)^2\delta^{-\frac{2(1-p)}{p}}\frac{\partial}{\partial \hat{X}}\left(D_h\frac{\partial \hat{H}}{\partial \hat{X}}\right) = -\delta^2\hat{C}^p\hat{H}^q.$$

Again, the hydroxide equation depends upon the relative size of δ. The critical value here is $\delta_{CR} = \epsilon^{\frac{4p}{3p-1}}$. We look at each case separately. Note that this value of δ will only be valid for the range $1/3 < p < 1$. For $0 < p \leq 1/3$ we have the first case discussed below.

1. For $\delta > \delta_{CR}$ (or $0 < p \leq 1/3$), we pose

$$\hat{C} \sim \hat{C}_0, \quad \hat{H} \sim \hat{H}_0 + \delta^2 \delta^{\frac{1-p}{p}} \hat{H}_1,$$

with

$$\hat{D}_c(c,h) \sim \hat{D}_c(0,\hat{H}_0), \quad D_h(c,h) \sim D_h(0,\hat{H}_0),$$

to obtain

$$\frac{\partial}{\partial \hat{X}}\left(\hat{D}_c \frac{\partial \hat{C}_0}{\partial \hat{X}}\right) = \hat{C}_0^p \hat{H}_0^q, \quad \frac{\partial}{\partial \hat{X}}\left(D_h \frac{\partial \hat{H}_0}{\partial \hat{X}}\right) = 0,$$

at leading order, and

$$\frac{\partial}{\partial \hat{X}}\left(D_h \frac{\partial \hat{H}_1}{\partial \hat{X}}\right) = 0,$$

at first order. After matching to outer 2 and the inner inner we obtain (4.10a) and

$$\hat{C}_0 = \begin{cases} \left(\frac{(1-p)^2 h_0(s^+,t)^q}{2\hat{D}_c(p+1)} \hat{X}^2\right)^{\frac{1}{1-p}} & \text{for } \hat{X} < 0, \\ 0 & \text{for } \hat{X} > 0, \end{cases}$$

with $\hat{D}_c = \frac{\nu_1}{h_0(s^+,t)^q}$. Further the inner inner region is now restricted to $\bar{x} < 0$ with the inner 2 matching conditions occurring as $\bar{x} \to 0^-$.

2. For $\delta = \delta_{CR} = \epsilon^{\frac{4p}{3p-1}}$, all the above analysis applies with the modification of the convection term entering the leading order hydroxide equation.

3. For $\delta < \delta_{CR}$, again all the above analysis applies, but now the hydroxide convection and diffusion terms balance in a thin region of size $\hat{X} = \left(\frac{\delta}{\epsilon^2}\right)^2 \delta^{\frac{p-1}{p}}$ centred at $S(t)$, which allows the required matching to outer 2.

Now we understand (4.2) and (4.4) and so are in a position to conclude. Equations (4.3) and (4.5) give

$$\text{at } x = s(t) \quad -D_{c_0} \frac{\partial c_0(s^-,t)}{\partial x} = \dot{s}(\mu c_0(s^-,t) + h_0(s^+,t)).$$

Further

$$c_0(s^-,t) = \Phi_1,$$

and so we obtain the following one-phase problem

$$\text{in } 0 < x < s(t),\ t > 0 \qquad \mu \frac{\partial c_0}{\partial t} - \frac{\partial}{\partial x}\left(D_{c_0} \frac{\partial c_0}{\partial x}\right) = 0, \tag{4.11}$$

$$\text{on } x = 0 \qquad -D_{c_0}\frac{\partial c_0}{\partial x} = H(1 - c_0), \tag{4.12}$$

$$\text{on } x = s(t) \qquad c_0 = \Phi_1(\dot{s}), \quad -D_{c_0}\frac{\partial c_0}{\partial x} = \dot{s}(\mu c_0 + h_i(s)), \tag{4.13}$$

$$\text{at } t = 0 \qquad c_0 = c_i(x) \text{ for } 0 \le x \le s_0, \quad s = s_0, \tag{4.14}$$

with $h_0 = h_i(x)$ for $s(t) \le x \le 1$. This is as in (3.8)-(3.11) and Φ_1 is determined by the solution of the inner inner problem

$$\mu\dot{s}\frac{\partial \bar{c}_0}{\partial \bar{x}} + \frac{\partial}{\partial \bar{x}}\left(\bar{D}_c\frac{\partial \bar{c}_0}{\partial \bar{x}}\right) = \bar{c}_0^p\bar{h}_0^q, \tag{4.15}$$

$$\bar{D}_c\frac{\partial \bar{c}_0}{\partial \bar{x}} - \left(\frac{\delta}{\epsilon}\right)^4\bar{D}_h\frac{\partial \bar{h}_0}{\partial \bar{x}} = \dot{s}(\bar{h}_0 - h_i(s) - \mu\bar{c}_0), \tag{4.16}$$

with

$$\text{as } \bar{x} \to +\infty \qquad \bar{c}_0 \to 0, \quad \bar{D}_c\frac{\partial \bar{c}_0}{\partial \bar{x}} \to 0, \quad \bar{h}_0 \to h_i(s), \tag{4.17}$$

$$\text{as } \bar{x} \to -\infty \qquad \bar{c}_0 \to \Phi_1(\dot{s}), \quad \bar{h}_0 \to 0, \tag{4.18}$$

where $\hat{D}_c = \frac{\nu_1}{\bar{h}_0^q}$ and $\hat{D}_h = \frac{\nu_2}{\bar{c}_0^p}$. Figure 4.2 shows a schematic representation of the carbonation reaction for this parameter regime.

4.1.2 The case $\delta = O(\epsilon)$

The reaction zone is again composed of the three regions, inner inner, inner 1 and inner 2. However, the analysis of inners 1 and 2 is simplified since we no longer have different structures depending upon the relative size of the parameter δ. We look at each region separately.

- **Inner inner**

The required inner inner scalings are

$$x = s(t) + \epsilon^2\bar{x}, \quad c = \bar{c}, \quad h = \bar{h}, \quad D_c = \epsilon^2\bar{D}_c, \quad D_h = \delta^2\bar{D}_h,$$

with $\bar{D}_c \sim \nu_1/h^q$, $\hat{D}_h \sim \nu_2/c^p$ for the functional forms (3.1) and (4.1) respectively. These give

$$\epsilon^2\mu\frac{\partial \bar{c}}{\partial t} - \mu\dot{s}\frac{\partial \bar{c}}{\partial \bar{x}} - \frac{\partial}{\partial \bar{x}}\left(\bar{D}_c\frac{\partial \bar{c}}{\partial \bar{x}}\right) = -\bar{c}^p\bar{h}^q,$$

$$\epsilon^2\frac{\partial \bar{h}}{\partial \bar{t}} - \dot{s}\frac{\partial \bar{h}}{\partial \bar{x}} - \frac{\partial}{\partial \bar{x}}\left(\bar{D}_h\frac{\partial \bar{h}}{\partial \bar{x}}\right) = -\bar{c}^p\bar{h}^q.$$

Posing the expansions

$$\bar{c} = \bar{c}_0 + o(1), \quad \bar{h} = \bar{h}_0 + o(1),$$

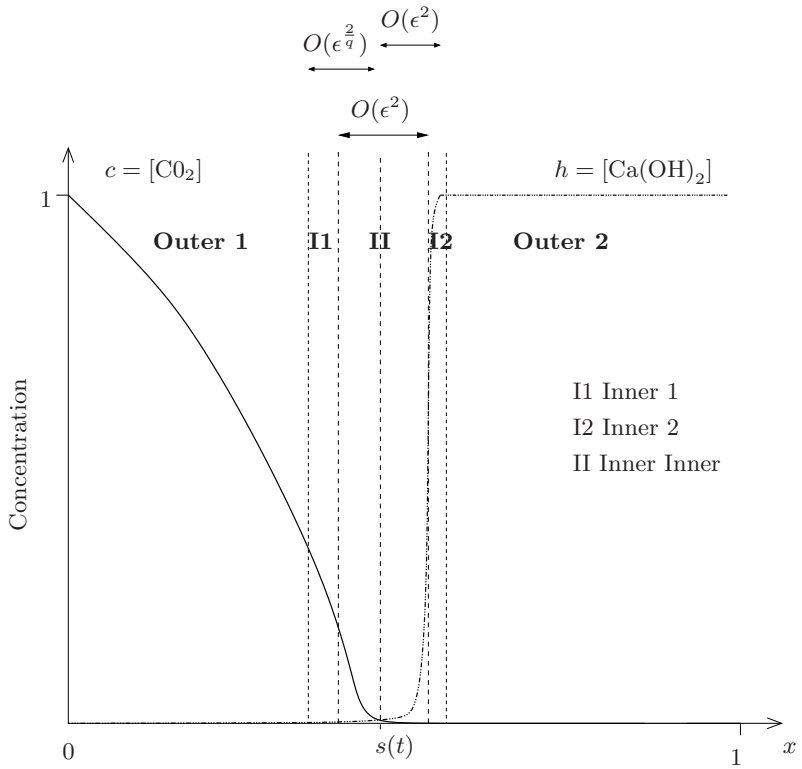

Figure 4.2: *A schematic illustration of the asymptotic regions for two rapidly varying diffusivities ($D(c) = O(\epsilon^2)$, $D_h = O(\delta^2)$) in the parameter case $\delta \ll \epsilon$. The reaction layer lies between outer regions outer 1 ($0 < x < s(t)$) and outer 2 ($s(t) < x < 1$). It is composed of three regions: an inner inner region (II), together with inners 1 (I1) and 2 (I2). The inners 1 and 2 facilitate the matching of the inner inner region with the two outers. The case shown is for $q > 1$ and $p \geq 1$. Minor modifications are needed to inner 1 and 2 for the cases $q \leq 1$ and $p < 1$ respectively.*

with

$$\bar{D}_c(c,h) \sim \bar{D}_c(\bar{c}_0, \bar{h}_0), \quad \bar{D}_h(c,h) \sim \bar{D}_h(\bar{c}_0, \bar{h}_0),$$

we obtain

$$\mu \dot{s} \frac{\partial \bar{c}_0}{\partial \bar{x}} + \frac{\partial}{\partial \bar{x}} \left(\bar{D}_c \frac{\partial \bar{c}_0}{\partial \bar{x}} \right) = \bar{c}_0^p \bar{h}_0^q,$$
$$\mu \dot{s} \bar{c}_0 + \bar{D}_c \frac{\partial \bar{c}_0}{\partial \bar{x}} = \dot{s} \bar{h}_0 + \bar{D}_h \frac{\partial \bar{h}_0}{\partial \bar{x}} + A(t),$$

where $A(t)$ is a function of t to be determined. Matching into outer 1, the matching conditions

$$\text{as } \bar{x} \to -\infty \quad \bar{c}_0 \to c_0(s^-, t), \quad \bar{D}_c \frac{\partial \bar{c}_0}{\partial \bar{x}} \to D_{c_0} \frac{\partial c_0(s^-, t)}{\partial x}, \quad \bar{h}_0 \to 0, \tag{4.19}$$

yield

$$A(t) = \mu \dot{s} c_0(s^-, t) + D_{c_0} \frac{\partial c_0(s^-, t)}{\partial x}. \tag{4.20}$$

Matching into outer 2, the matching conditions

$$\text{as } \bar{x} \to \infty \quad \bar{c}_0 \to 0, \quad \bar{h}_0 \to h_0(s^+, t), \quad \bar{D}_h \frac{\partial \bar{h}_0}{\partial \bar{x}} \to D_{h_0} \frac{\partial h_0(s^+, t)}{\partial x}, \tag{4.21}$$

yield

$$A(t) = -\dot{s} h_0(s^+, t) - D_{h_0} \frac{\partial h_0(s^+, t)}{\partial x}. \tag{4.22}$$

Two additional regions are required to facilitate the matching with outers 1 and 2, due to the order or magnitude change in the diffusivities, and to fully understand (4.19) and (4.21).

- **Inner 1**

The inner 1 region is required to account for the change in magnitude of the carbon dioxide diffusivity. There are three cases to consider depending on the size of $q > 0$.

(A) For $q > 1$, the scalings are

$$x = s(t) + \epsilon^{\frac{2}{q}} \bar{X}, \quad c = \bar{C}, \quad h = \epsilon^{\frac{2}{q}} \bar{H}, \quad D_h = \delta^2 \bar{D}_h, \tag{4.23}$$

with D_c as in (3.1) and $\bar{D}_h \sim \nu_2 / c^p$, so that

$$\begin{aligned} \mu \epsilon^{\frac{4}{q}} \frac{\partial \bar{C}}{\partial t} - \mu \epsilon^{\frac{2}{q}} \dot{s} \frac{\partial \bar{C}}{\partial \bar{X}} - \frac{\partial}{\partial \bar{X}} \left(D_c \frac{\partial \bar{C}}{\partial \bar{X}} \right) &= -\epsilon^{\frac{4}{q}} \bar{C}^p \bar{H}^q, \\ \epsilon^{\frac{2}{q}} \frac{\partial \bar{H}}{\partial t} - \dot{s} \frac{\partial \bar{H}}{\partial \bar{X}} - \frac{\epsilon^2}{\epsilon^{\frac{2}{q}}} \frac{\partial}{\partial \bar{X}} \left(\bar{D}_h \frac{\partial \bar{H}}{\partial \bar{X}} \right) &= -\bar{C}^p \bar{H}^q. \end{aligned}$$

Note that in this case inner 1 is larger in size than the inner inner. Posing

$$\bar{C} \sim \bar{C}_0 + \epsilon^{\frac{2}{q}} \bar{C}_1, \quad \bar{H} \sim \bar{H}_0,$$

with

$$D_c(c, h) \sim D_c(\bar{C}_0, 0), \quad \bar{D}_h(c, h) \sim \bar{D}_h(\bar{C}_0, 0),$$

we obtain

$$\frac{\partial}{\partial \bar{X}} \left(D_c \frac{\partial \bar{C}_0}{\partial \bar{X}} \right) = 0, \quad \dot{s} \frac{\partial \bar{H}_0}{\partial \bar{X}} = \bar{C}_0^p \bar{H}_0^q,$$

at leading order, and

$$\mu \dot{s} \frac{\partial \bar{C}_0}{\partial \bar{X}} + \frac{\partial}{\partial \bar{X}} \left(D_c \frac{\partial \bar{C}_1}{\partial \bar{X}} \right) = 0,$$

at first order. After matching to outer 1 and the inner inner we have

$$\bar{C}_0 = c_0(s^-, t) = \Phi_1, \quad D_c \frac{\partial \bar{C}_1}{\partial \bar{X}} = D_{c_0} \frac{\partial c_0(s^-, t)}{\partial x}, \tag{4.24a}$$

$$\bar{H}_0 = \left(-\frac{q-1}{\dot{s}} c_0(s^-,t)^p \bar{X} \right)^{-\frac{1}{q-1}}. \tag{4.24b}$$

(B) For $q = 1$, the transition region is of the same size as the reaction layer. We introduce the scalings

$$x = s(t) + \epsilon^2(S(t) + \bar{X}), \quad c = \bar{C}, \quad h = \epsilon^2 \bar{H}, \quad D_h = \delta^2 \bar{D}_h,$$

where $1 < S(t) < 1/\epsilon^2$. The governing equations become

$$\epsilon^4 \mu \frac{\partial \bar{C}}{\partial t} - \epsilon^2 \mu(\dot{s} + \epsilon^2 \dot{S}) \frac{\partial \bar{C}}{\partial \bar{X}} - \frac{\partial}{\partial \bar{X}} \left(D_c \frac{\partial \bar{C}}{\partial \bar{X}} \right) = -\epsilon^4 \bar{C}^p \bar{H},$$
$$\epsilon^2 \frac{\partial \bar{H}}{\partial t} - (\dot{s} + \epsilon^2 \dot{S}) \frac{\partial \bar{H}}{\partial \bar{X}} - \frac{\partial}{\partial \bar{X}} \left(\bar{D}_h \frac{\partial \bar{H}}{\partial \bar{X}} \right) = -\bar{C}^p \bar{H}.$$

Posing

$$\bar{C} \sim \bar{C}_0 + \epsilon^2 \bar{C}_1, \quad \bar{H} \sim \bar{H}_0,$$

with

$$D_c(c,h) \sim D_c(\bar{C}_0, 0), \quad \bar{D}_h(c,h) \sim \bar{D}_h(\bar{C}_0, 0),$$

we obtain

$$\frac{\partial}{\partial \bar{X}} \left(D_c \frac{\partial \bar{C}_0}{\partial \bar{X}} \right) = 0, \dot{s} \frac{\partial \bar{H}_0}{\partial \bar{X}} + \frac{\partial}{\partial \bar{X}} \left(\bar{D}_h \frac{\partial \bar{H}_0}{\partial \bar{X}} \right) = \bar{C}_0^p \bar{H}_0,$$

at leading order and

$$\mu \dot{s} \frac{\partial \bar{C}_0}{\partial \bar{X}} + \frac{\partial}{\partial \bar{X}} \left(D_c \frac{\partial \bar{C}_1}{\partial \bar{X}} \right) = 0,$$

at first order. After matching to outer 1 and the inner inner we again obtain (4.24a) and $\bar{H}_0$ is given by

$$\bar{H}_0 = \exp\left(\theta(t)\bar{X}\right) \quad \text{with} \quad S(t) \sim \frac{2}{q\theta(t)} \ln(\epsilon),$$

where

$$\theta(t) = \frac{\dot{s}}{2\bar{D}_h} \left(-1 + \sqrt{1 + \frac{4\bar{D}_h c_0(s^-,t)^p}{\dot{s}^2}} \right),$$

and $\bar{D}_h = \frac{\nu_2}{c_0(s^-,t)^p}$.

(C) For $q < 1$, the inner 1 region is narrower than the inner inner region. We introduce the scalings

$$x = s(t) + \epsilon^{\frac{q+1}{q}} \bar{X}, \quad c = \bar{C}, \quad h = \epsilon^{\frac{2}{q}} \bar{H}, \quad D_h = \epsilon^2 \bar{D}_h,$$

so that

$$\epsilon^{\frac{2(q+1)}{q}}\mu\frac{\partial\bar{C}}{\partial t}-\epsilon^{\frac{q+1}{q}}\mu\dot{s}\frac{\partial\bar{C}}{\partial\bar{X}}-\frac{\partial}{\partial\bar{X}}\left(D_c\frac{\partial\bar{C}}{\partial\bar{X}}\right)=-\epsilon^{\frac{2(q+1)}{q}}\bar{C}^p\bar{H}^q,$$
$$\epsilon^{\frac{2}{q}}\frac{\partial\bar{H}}{\partial t}-\epsilon^{\frac{1-q}{q}}\dot{s}\frac{\partial\bar{H}}{\partial\bar{X}}-\frac{\partial}{\partial\bar{X}}\left(\bar{D}_h\frac{\partial\bar{H}}{\partial\bar{X}}\right)=-\bar{C}^p\bar{H}^q.$$

Posing

$$\bar{C}\sim\bar{C}_0+\epsilon^{\frac{q+1}{q}}\bar{C}_1,\quad \bar{H}\sim\bar{H}_0,$$

with

$$D_c(c,h)\sim D_c(\bar{C}_0,0),\quad \bar{D}_h(c,h)\sim\bar{D}_h(\bar{C}_0,0),$$

we obtain

$$\frac{\partial}{\partial\bar{X}}\left(D_c\frac{\partial\bar{C}_0}{\partial\bar{X}}\right)=0,\quad \frac{\partial}{\partial\bar{X}}\left(\bar{D}_h\frac{\partial\bar{H}_0}{\partial\bar{X}}\right)=\bar{C}_0^p\bar{H}_0^q,$$

at leading order, and

$$\mu\dot{s}\frac{\partial\bar{C}_0}{\partial\bar{X}}+\frac{\partial}{\partial\bar{X}}\left(D_c\frac{\partial\bar{C}_1}{\partial\bar{X}}\right)=0,$$

at first order. After matching to outer 1 and the inner inner we obtain (4.24a) and

$$\bar{H}_0=\begin{cases}\left(\frac{(1-q)^2c_0(s^-,t)^p}{2(q+1)\bar{D}_h}\bar{X}^2\right)^{\frac{1}{1-q}} & \text{for } \bar{X}>0,\\ 0 & \text{for } \bar{X}<0,\end{cases}$$

with $\bar{D}_h=\frac{\nu_2}{c_0(s^-,t)^p}$. Further the inner inner region is now restricted to $\bar{x}>0$ with the inner 1 matching conditions occurring as $\bar{x}\to 0^+$.

- **Inner 2**

Inner 2 accounts for the change in magnitude of the calcium hydroxide diffusion coefficient. The details depend on the value of $p>0$ in the reaction term (2.11). There are three cases to be considered separately.

(A) For $p>1$, the required scalings are

$$x=s(t)+\epsilon^2(S(t)+\hat{X}),\quad c=\epsilon^{\frac{2}{p}}\hat{C},\quad h=\hat{H},\quad D_c=\epsilon^2\hat{D}_c,\tag{4.25}$$

with $\hat{D}_c\sim\nu_1/h^q$ and D_h as in (4.1), so that

$$\epsilon^2\mu\frac{\partial\hat{C}}{\partial t}-\mu(\dot{s}+\epsilon\dot{S})\frac{\partial\hat{C}}{\partial\hat{X}}-\frac{\partial}{\partial\hat{X}}\left(\hat{D}_c\frac{\partial\hat{C}}{\partial\hat{X}}\right)=-\epsilon^{\frac{2(p-1)}{p}}\hat{C}^p\hat{H}^q,$$
$$\epsilon^4\frac{\partial\hat{H}}{\partial t}-\epsilon^2(\dot{s}+\epsilon^2\dot{S})\frac{\partial\hat{H}}{\partial\hat{X}}-\frac{\partial}{\partial\hat{X}}\left(D_h\frac{\partial\hat{H}}{\partial\hat{X}}\right)=-\epsilon^4\hat{C}^p\hat{H}^q.$$

Posing

$$\hat{C} \sim \hat{C}_0, \quad \hat{H} \sim \hat{H}_0 + \epsilon^2 \hat{H}_1,$$

with

$$\hat{D}_c(c,h) \sim \hat{D}_c(0,\hat{H}_0), \quad D_h(c,h) \sim D_h(0,\hat{H}_0),$$

we obtain

$$\mu\dot{s}\frac{\partial \hat{C}_0}{\partial \hat{X}} + \frac{\partial}{\partial \hat{X}}\left(\hat{D}_c \frac{\partial \hat{C}_0}{\partial \hat{X}}\right) = 0, \quad \frac{\partial}{\partial \hat{X}}\left(D_h \frac{\partial \hat{H}_0}{\partial \hat{X}}\right) = 0,$$

at leading order, and

$$\dot{s}\frac{\partial \hat{H}_0}{\partial \hat{X}} + \frac{\partial}{\partial \hat{X}}\left(D_h \frac{\partial \hat{H}_1}{\partial \hat{X}}\right) = 0,$$

at first order. After matching to outer 2 and inner inner we have

$$\hat{H}_0 = h_0(s^+,t) = \Phi_2(\dot{s}), \quad D_h \frac{\partial \hat{H}_1}{\partial \hat{X}} = D_{h_0}\frac{\partial h_0(s^+,t)}{\partial x}, \tag{4.26a}$$

$$\hat{C}_0 = \exp\left(-\frac{\mu\dot{s}}{\hat{D}_c}\hat{X}\right), \tag{4.26b}$$

with $\hat{D}_c = \frac{\nu_1}{h_0(s^+,t)^q}$. Further,

$$S(t) = \frac{2}{p}\frac{\hat{D}_c}{\mu\dot{s}}\ln\left(\frac{1}{\epsilon}\right).$$

(B) For $p = 1$, the scalings (4.25) apply as does the subsequent analysis with the modification of the reaction term entering the leading order carbon dioxide equation. Hence (4.26a) remains unchanged and (4.26b) becomes

$$\hat{C}_0 = \exp\left(\sigma(t)\hat{X}\right) \quad \text{with} \quad S(t) \sim \frac{2}{p\sigma(t)}\ln(\epsilon),$$

where

$$\sigma(t) = \frac{\mu\dot{s}}{2\hat{D}_c}\left(-1 + \sqrt{1 + \frac{4\hat{D}_c h_0(s^+,t)^q}{\mu^2\dot{s}^2}}\right),$$

and $\hat{D}_c = \frac{\nu_1}{h_0(s^+,t)^q}$.

(C) For $0 < p < 1$, the inner inner solution for $\bar{c}_0$ vanishes at $\bar{x} = S(t)$ and we modify the spatial scaling in (4.25) to

$$x = s(t) + \epsilon^2(S(t) + \epsilon^{\frac{1-p}{p}}\hat{X}),$$

so that

$$\epsilon^{\frac{2}{p}}\mu\frac{\partial\hat{C}}{\partial t}-\epsilon^{\frac{1-p}{p}}\mu(\dot{s}+\epsilon^2\dot{S})\frac{\partial\hat{C}}{\partial\hat{X}}-\frac{\partial}{\partial\hat{X}}\left(\hat{D}_c\frac{\partial\hat{C}}{\partial\hat{X}}\right)=\hat{C}^p\hat{H}^q,$$
$$\epsilon^{\frac{2(p+1)}{p}}\frac{\partial\hat{H}}{\partial t}-\epsilon^{\frac{p+1}{p}}(\dot{s}+\epsilon^2\dot{S})\frac{\partial\hat{H}}{\partial\hat{X}}-\frac{\partial}{\partial\hat{X}}\left(D_h\frac{\partial\hat{H}}{\partial\hat{X}}\right)=-\epsilon^{\frac{2(p+1)}{p}}\hat{C}^p\hat{H}^q.$$

Posing

$$\hat{C}\sim\hat{C}_0,\quad \hat{H}\sim\hat{H}_0+\epsilon^2\epsilon^{\frac{1-p}{p}}\hat{H}_1,$$

with

$$\hat{D}_c(c,h)\sim\hat{D}_c(0,\hat{H}_0),\quad D_h(c,h)\sim D_h(0,\hat{H}_0),$$

we obtain

$$\frac{\partial}{\partial\hat{X}}\left(\hat{D}_c\frac{\partial\hat{C}_0}{\partial\hat{X}}\right)=\hat{C}_0^p\hat{H}_0^q,\quad \frac{\partial}{\partial\hat{X}}\left(D_h\frac{\partial\hat{H}_0}{\partial\hat{X}}\right)=0,$$

at leading order, and

$$\dot{s}\frac{\partial\hat{H}_0}{\partial\hat{X}}+\frac{\partial}{\partial\hat{X}}\left(D_h\frac{\partial\hat{H}_1}{\partial\hat{X}}\right)=0,$$

at first order. After matching to outer 2 and the inner inner we obtain (4.26a) and

$$\hat{C}_0=\begin{cases}\left(\frac{(1-p)^2h_0(s^+,t)^q}{2\hat{D}_c(p+1)}\hat{X}^2\right)^{\frac{1}{1-p}} & \text{for } \hat{X}<0,\\ 0 & \text{for } \hat{X}>0,\end{cases}$$

for $\hat{D}_c=\frac{\nu_1}{h_0(s^+,t)^q}$. Further the inner inner region is now restricted to $\bar{x}<0$ with the inner 2 matching conditions occurring as $\bar{x}\to 0^-$.

Now we are in a position to conclude and so (4.20) and (4.22) give

$$\text{at } x=s(t)\quad -D_{c_0}\frac{\partial c_0(s^-,t)}{\partial x}-D_{h_0}\frac{\partial h_0(s^+,t)}{\partial x}=\dot{s}(\mu c_0(s^-,t)+h_0(s^+,t)).$$

Further

$$c_0(s^-,t)=\Phi_1(\dot{s}),\quad h_0(s^+,t)=\Phi_2(\dot{s}),$$

and so we obtain the following two-phase problem

$$\text{in } 0<x<s(t),\ t>0\qquad \mu\frac{\partial c_0}{\partial t}-\frac{\partial}{\partial x}\left(D_{c_0}\frac{\partial c_0}{\partial x}\right)=0, \tag{4.27}$$
$$\text{in } s(t)<x<1,\ t>0\qquad \frac{\partial h_0}{\partial t}-\frac{\partial}{\partial x}\left(D_{h_0}\frac{\partial h_0}{\partial x}\right)=0, \tag{4.28}$$
$$\text{on } x=0\qquad -D_{c_0}\frac{\partial c_0}{\partial x}=H(1-c_0), \tag{4.29}$$

$$\text{on } x = s(t) \quad c_0 = \Phi_1(\dot{s}), \quad h_0 = \Phi_2(\dot{s}), \quad -D_{c_0}\frac{\partial c_0}{\partial x} - D_{h_0}\frac{\partial h_0}{\partial x} = \dot{s}(\mu c_0 + h_0), \tag{4.30}$$

$$\text{on } x = 1 \qquad D_{h_0}\frac{\partial h_0}{\partial x} = 0, \tag{4.31}$$

$$\text{at } t = 0 \qquad c_0 = c_i(x) \text{ for } 0 \le x \le s_0, \quad h_0 = h_i \text{ for } s_0 \le x \le 1, \quad s = s_0. \tag{4.32}$$

Figure 4.3 shows a schematic of this final scenario. This is as in (3.32)-(3.37) but instead of (3.35) we now have a more general moving boundary condition (4.30). Moreover, Φ_1 and Φ_2 are determined by the solution of the inner inner problem

$$\mu\dot{s}\frac{\partial \bar{c}_0}{\partial \bar{x}} + \frac{\partial}{\partial \bar{x}}\left(\bar{D}_c\frac{\partial \bar{c}_0}{\partial \bar{x}}\right) = \bar{c}_0^p \bar{h}_0^q, \tag{4.33}$$

$$\dot{s}\frac{\partial \bar{h}_0}{\partial \bar{x}} + \frac{\partial}{\partial \bar{x}}\left(\bar{D}_h\frac{\partial \bar{h}_0}{\partial \bar{x}}\right) = \bar{c}_0^p \bar{h}_0^q, \tag{4.34}$$

with

$$\text{as } \bar{x} \to +\infty \quad \bar{c}_0 \to 0, \quad \bar{D}_c\frac{\partial \bar{c}_0}{\partial \bar{x}} \to 0, \quad \bar{h}_0 \to \Phi_2(\dot{s}), \tag{4.35}$$

$$\text{as } \bar{x} \to -\infty \quad \bar{c}_0 \to \Phi_1(\dot{s}), \quad \bar{h}_0 \to 0, \quad \bar{D}_h\frac{\partial \bar{h}_0}{\partial \bar{x}} \to 0, \tag{4.36}$$

where $\bar{D}_c = \frac{\nu_1}{h_0^q}$ and $\bar{D}_h = \frac{\nu_2}{c_0^p}$.

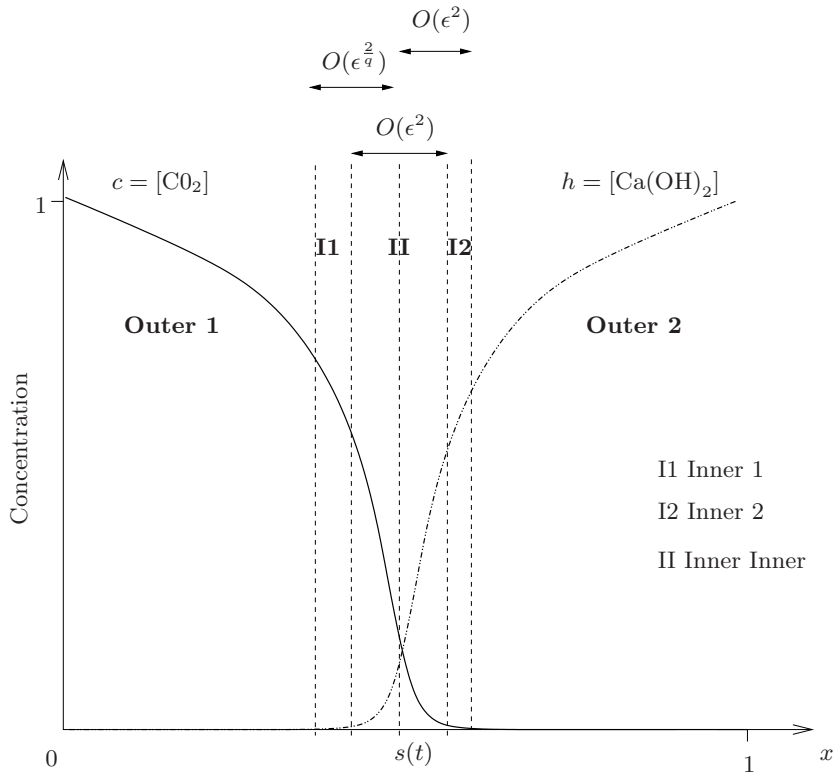

Figure 4.3: *A schematic illustration of the asymptotic regions for two rapidly varying diffusivities ($D(c) = O(\epsilon^2)$, $D_h = O(\delta^2)$) in the parameter case $\delta = O(\epsilon)$. The reaction layer lies between outer regions outer 1 ($0 < x < s(t)$) and outer 2 ($s(t) < x < 1$). It is composed of three regions: an inner inner region (II), together with inners 1 (I1) and 2 (I2). Inners 1 and 2 facilitate the matching of the inner inner region with the two outers. The case shown is for $q > 1$ and $p \geq 1$. Minor modifications are needed to inner 1 and 2 for the cases $q \leq 1$ and $p < 1$ respectively.*

4.2 Numerical Results

4.2.1 Scheme

We implement the scheme as in the previous numerical sections 2.4 and 3.2. To avoid encountering singularities, the regularisations (3.42) are implemented, but an analogous regularisation for the now rapidly varying $Ca(OH)_2$ diffusion coefficient is necessary. As such, we let

$$D_h = 1 - \exp\left(-\frac{\nu_2\delta^2}{(c^2+\theta_3^2)^{\frac{p}{2}}}\right),$$

where $\theta_3 \ll (\nu_2\delta^2)^{1/p}$. As for the regularisation performed in the previous chapter for the CO_2 diffusion coefficient (3.42), θ_3 has to be chosen with care so that the rapidly varying behaviour of D_h as exposed at the beginning of this chapter is not lost.

4.2.2 Base Case

Using the initial data and parameter values as in (2.51), figure 4.4 shows the numerical results for $\epsilon = 5 \times 10^{-2}$ and two selected values of δ. It is worth noting that the value for θ_2 in the CO_2 diffusion coefficient regularisation (3.42) has been kept as $\theta_2 = 10^{-5}$ and $\theta_3 = 10^{-5}$, which has been chosen such that the case $\delta = \epsilon^{1.5}$ satisfies the bound $\theta_2 \ll (\nu_2\delta^2)^{1/p}$ (with $\nu_2 = p = 1$). Compared to the single rapidly varying CO_2 diffusivity, the addition of a rapidly varying hydroxide diffusivity further slows down the progress of the reaction zone. The most significant change occurs in the $\delta = \epsilon$ regime, where now the hydroxide concentration is O(1) in the reaction zone and no longer small as for the slowly varying and single rapidly varying CO_2 cases in subsections 2.4.2 and 3.2.2. Also note that, Stage I carbonation no longer takes place in this case.

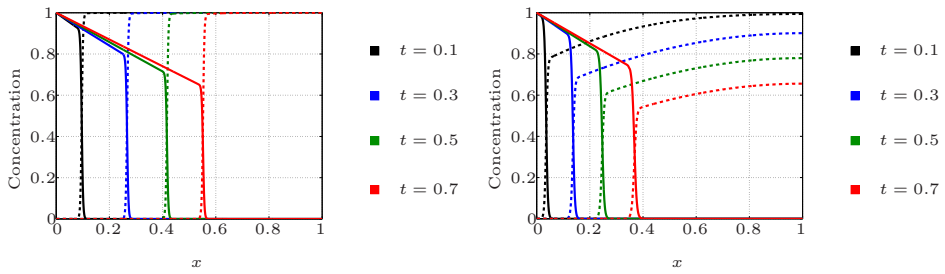

(a) $\delta = \epsilon^{1.5}$ (b) $\delta = \epsilon$

Figure 4.4: *Numerical results for two rapidly varying diffusivities. The parameter values are* $\epsilon = 5 \times 10^{-2}$, $\nu_1 = \nu_2 = 1$, $p = q = 1$, $\mu = 10^{-3}$ *and* $H = 10^4$. *The solid lines refer to the concentration of carbon dioxide while the dotted lines are the concentration of calcium hydroxide.*

4.2.3 Parameter Variation

As done in subsections 2.4.3 and 3.2.3 we investigate how changing the parameters affects the system. We consider $\mu = 1$ (figure 4.5) and $H = 1$ (figure 4.6). The same changes as experienced earlier reappear here. The reaction zone progresses at a slower rate into the concrete block in both scenarios and the concentration of CO_2 is no longer pinned at one when $H = 1$. Further, it is worth mentioning, that the reaction orders p and q will have little effect in this case, since in neither of the parameter regimes there is any dependence on them in the inner inner region.

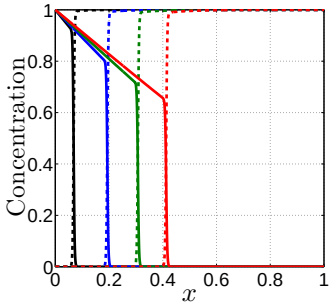

(a) Case $\delta = \epsilon^{1.5}$ and times $t = 0.1, 0.3, 0.5, 0.7$

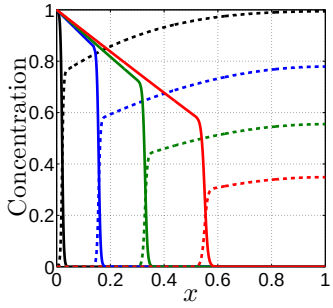

(b) Case $\delta = \epsilon$ and times $t = 0.1, 0.5, 0.9, 1.3$

Figure 4.5: *Numerical results for two rapidly varying diffusion coefficients. The parameter values are* $\epsilon = 5 \times 10^{-2}$, $\nu_1 = \nu_2 = 1$, $p = q = 1$, $\mu = 1$ *and* $H = 10^4$ *and selected times and* δ *as stated in (a) and (b).*

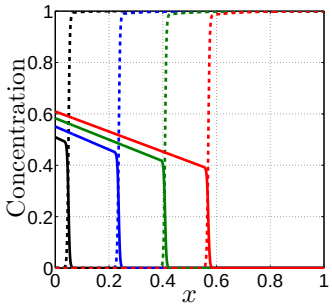

(a) Case $\delta = \epsilon^{1.5}$ and times $t = 0.1, 0.5, 0.9, 1.3$

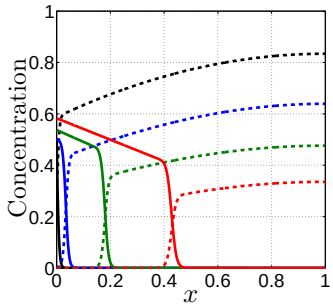

(b) Case $\delta = \epsilon$ and times $t = 0.5, 0.9, 1.3, 1.7$

Figure 4.6: *Numerical results for two rapidly varying diffusion coefficients. The parameter values are* $\epsilon = 5 \times 10^{-2}$, $\nu_1 = \nu_2 = 1$, $p = q = 1$, $\mu = 10^{-3}$ *and* $H = 1$ *and selected times and* δ *as stated in (a) and (b).*

4.2.4 Free boundary $s(t)$ and Kinetic conditions $\Phi_1(\dot{s})$, $\Phi_2(\dot{s})$

Here we investigate the localisation of the interface and the profiles of Φ_1 and Φ_2. The interface $s(t;\epsilon)$ is defined as in (2.13) and Φ_1 as in (3.43). As we have seen in

the analysis of this chapter and the numerical results above, for the $\delta = O(\epsilon)$ regime, $h = O(1)$ at the interface. This is the same as saying that Φ_2 is no longer zero and so we define it as

$$\Phi_2(\dot{s}) = \left\{ h \in [0,1] \mid c(x,t) = \delta^{\frac{2}{p}} \right\}. \tag{4.37}$$

Base Case

Figures 4.7 and 4.8 show the plots of the interface, its speed and the kinetic conditions for the parameter values (2.51) with $p = q = 1$. In figure 4.7 we consider the asymptotic regime $\delta \ll \epsilon$ and the same behaviours as seen in the previous equivalent subsections 2.4.4 and 3.2.4 are noted. For $\delta = \epsilon$, figure 4.8, the results have been truncated and the domain extended to $x \in [0, 25]$ to avoid the edge effects. The behaviour is again similar as seen previously but now note the addition of $\Phi_2(\dot{s})$ in figure 4.8(d), which appears to also have a linear profile.

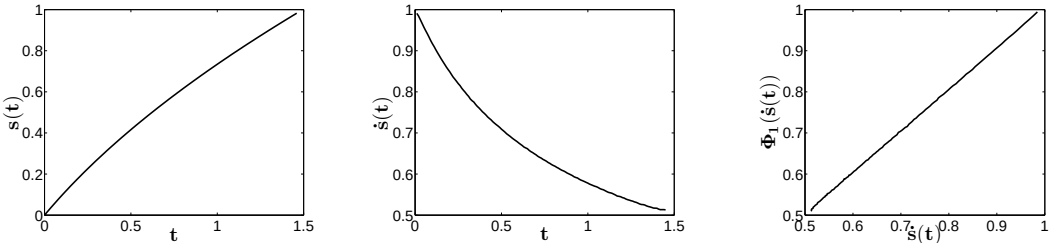

(a) Free boundary, $s(t)$ (b) Speed of free boundary, $\dot{s}(t)$ (c) Kinetic condition, $\Phi_1(\dot{s})$

Figure 4.7: *Numerical results of* (2.6)-(2.10) *for two rapidly varying diffusivities and* $\delta < \epsilon$*, namely* $\delta = \epsilon^{1.5}$*, with* $\epsilon = 5 \times 10^{-2}$*.*

The profiles of the kinetic conditions $\Phi_1(\dot{s})$ and $\Phi_2(\dot{s})$ shown in figures 4.7(c) and 4.8(d) are fitted to the curve (3.44) using the interactive curve fitting toolbox in MATLAB. Table 4.1 shows the best fit values of the coefficients and their goodness of fit statistics. For the regime $\delta \ll \epsilon$ we obtain a clear linear profile, but for $\delta = O(\epsilon)$ it is not as clear. It is not until chapter 5, where we derive the leading order behaviour of the kinetic conditions in the limit $\dot{s} \to 0$, that we may conclude a linear dependence.

Different p and q

We now investigate the effect of parameter values (2.51) but with the following changes in p and q

$$p > 1,\, q = 1, \quad p = 1,\, q > 1, \quad p < 1,\, q = 1, \quad p = 1,\, q < 1.$$

Figure 4.9 shows how the free boundary advances through the domain for the different asymptotic regimes $\delta \ll \epsilon$ and $\delta = O(\epsilon)$ respectively. The $\sqrt{t}$ behaviour seems to be maintained in all four combinations of p and q.

Figure 4.10 and table 4.2 concentrate on the kinetic conditions $\Phi_1(\dot{s})$ and $\Phi_2(\dot{s})$. Looking at figure 4.10, $\Phi_{1,2}(\dot{s})$ could still be approximated by $\dot{s}$. However, motivated

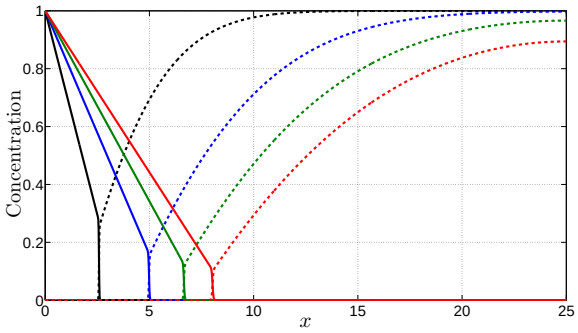

(a) Concentration of CO_2 (solid lines) and $Ca(OH)_2$ (dotted lines) for times $t = 10$ (black), $t = 30$ (blue), $t = 50$ (green) and $t = 70$ (red).

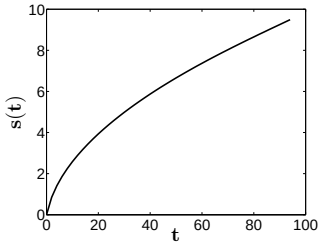

(b) Free boundary, $s(t)$

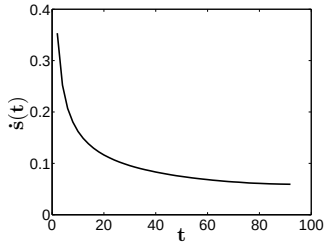

(c) Speed of free boundary, $\dot{s}(t)$

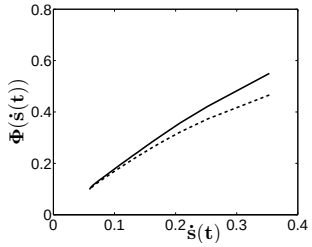

(d) Kinetic conditions, $\Phi_1(\dot{s})$ (solid) and $\Phi_2(\dot{s})$ (dashed)

Figure 4.8: *Numerical results of* (2.6)-(2.10) *for two rapidly varying diffusivities and* $\delta = \epsilon$ *with* $\epsilon = 5 \times 10^{-2}$ *and* $x = [0, 25]$.

		Cofficients (with 95% confident bounds)	Goodness of fit
$\delta \vee \epsilon$	$\Phi_1(\dot{s})$	a=1.02 (1.009,1.031) b=0.9879 (0.9718,1.004) c=-0.01184 (-0.02348,-1.998×10^{-4})	SSE: 1.752×10^{-4} Adjusted R-square: 0.9999 RMSE: 1.115×10^{-3}
$\delta = \epsilon$	$\Phi_1(\dot{s})$	a=1.453 (1.395,1.512) b=0.8404 (0.8048,0.8759) c=-0.03136 (-0.03992,-0.02281)	SSE: 1.598×10^{-5} Adjusted R-square: 0.9998 RMSE: 6.855×10^{-4}
	$\Phi_2\dot{s}$	a=1.166 (1.126,1.206) b=0.7285(0.6925,0.7644) c=-0.04816 (-0.05853,-0.03778)	SSE: 1.32×10^{-5} Adjusted R-square: 0.9998 RMSE: 6.234×10^{-4}

Table 4.1: *Base case curve fitting results for all asymptotic regimes for* $\Phi_{1,2}(\dot{s}) = a\dot{s}^b + c$. *The kinetic conditions* Φ_1 *and* Φ_2 *have been computed as in* (3.43) *and* (4.37) *respectively, after solving the full reaction-diffusion system with parameter values* (2.51) *and two rapidly varying diffusion coefficient.*

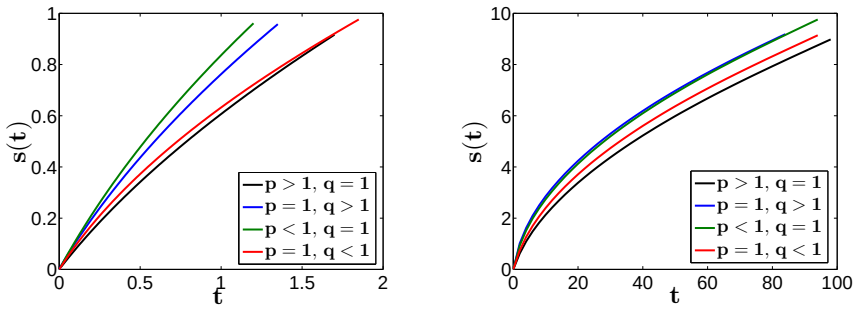

(a) Case $\delta < \epsilon$ with $\epsilon = 5 \times 10^{-2}$ (b) Case $\delta = \epsilon$ with $\epsilon = 0.1$

Figure 4.9: *Free boundary plots for two rapidly varying diffusivities and different values of p and q.*

by the results for the one rapidly varying case in section 3.2.4, note that in figure 4.10(a), the two cases in which $q \neq 1$ are very similar while for $p \neq 1$, there is a bigger difference between the profiles. For $\Phi_2(\dot{s})$ in figure 4.10(c), note that the opposite seems to happen. Noteworthy features of table 4.2 are the positive statistics results, indicating a good fit to (3.44), the negligible value of c in (3.44), indicating that $\Phi_{1,2}(\dot{s})$ cannot be approximated by a constant, and the previously pointed out features obtained from the corresponding graphs. In chapter 5, the relationship of the kinetic conditions with $\dot{s}(t)$ and its dependence on p and q will be derived analytically.

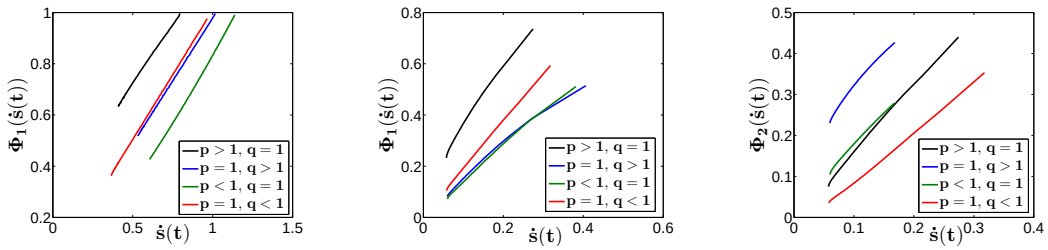

(a) Case $\delta < \epsilon$ with $\epsilon = 5 \times 10^{-2}$ (b) Case $\delta = \epsilon$ with $\epsilon = 0.1$ (c) Case $\delta = \epsilon$ with $\epsilon = 0.1$

Figure 4.10: *Kinetic conditions' plots, $\Phi_1(\dot{s})$ and $\Phi_2(\dot{s})$, for two rapidly varying diffusivities and different values of p and q.*

			Cofficients (with 95% confident bounds)	Goodness of fit
$\delta \leq \epsilon$	$\Phi_1(\dot{s})$	$p > 1$	a=1.157 (1.141,1.172) b=0.6666 (0.6514,0.6806) c=-0.003873 (-0.02088,0.01314)	SSE: 8.729×10^{-5} Adj. R-square: 0.9999 RMSE: 7.363×10^{-4}
		$q > 1$	a=0.9805 (0.9686,0.9924) b=1 (0.9827,1.017) c=-0.002205 (-0.01455,0.01014)	SSE: 1.544×10^{-4} Adj. R-square: 0.9999 RMSE: 1.103×10^{-3}
		$p \vee 1$	a=0.8294 (0.8273,0.8315) b=1.342 (1.337,1.346) c=3.751×10^{-3} (1.69×10^{-3}, 5.813×10^{-3})	SSE: 1.049×10^{-5} Adj. R-square: 1 RMSE: 3.021×10^{-4}
		$q < 1$	a=1.012 (1.003,1.021) b=1.009 (0.9911,1.026) c=-3.751×10^{-3} (-8.993×10^{-3},0.01111)	SSE: 1.21×10^{-3} Adj. R-square: 0.9997 RMSE: 2.488×10^{-3}
$\delta = \epsilon$	$\Phi_1(\dot{s})$	$p > 1$	a=1.742 (1.717,1.768) b=0.5745 (0.5426,0.6065) c=-0.09684 (-0.1245,-0.06923)	SSE: 3.63×10^{-4} Adj. R-square: 0.9993 RMSE: 2.84×10^{-3}
		$q > 1$	a=1.186 (1.153,1.218) b=0.7392 (0.7107,0.7677) c=-0.06379 (-0.07189,-0.05568)	SSE: 1.049×10^{-5} Adj. R-square: 0.9998 RMSE: 5.555×10^{-4}
		$p \vee 1$	a=1.295 (1.197,1.393) b=0.8567 (0.7912,0.922) c=-0.04106 (-0.05428,-0.02783)	SSE: 6.409×10^{-5} Adj. R-square: 0.9991 RMSE: 1.282×10^{-3}
		$q \vee 1$	a=1.748 (1.716,0.78) b=0.9194 (0.8991,0.9396) c=-0.01793 (-0.02365, -0.0122)	SSE: 8.862×10^{-5} Adj. R-square: 0.9989 RMSE: 1.774×10^{-3}
	$\Phi_2(\dot{s})$	$p > 1$	a=1.398 (1.368,1.427) b=0.784(0.759,0.809) c=-0.0691 (-0.07728,-0.06093)	SSE: 1.128×10^{-4} Adj. R-square: 0.9996 RMSE: 1.583×10^{-3}
		$q > 1$	a=1.277 (1.215,1.339) b=0.2705 (0.2345,0.3063) c=-0.3626 (-0.452,-0.2731)	SSE: 2.22×10^{-5} Adj. R-square: 0.9998 RMSE: 8.084×10^{-4}
		$p \vee 1$	a=1.062 (1.013,1.111) b=0.5809 (0.5073,0.6545) c=-0.09838 (-0.1325,-0.06424)	SSE: 8.862×10^{-5} Adj. R-square: 0.9989 RMSE: 1.507×10^{-3}
		$q \vee 1$	a=1.33 (1.308,1.352) b=1.109 (1.093,1.125) c=-0.01923 (-0.02119,-0.01727)	SSE: 3.347×10^{-5} Adj. R-square: 0.9998 RMSE: 8.822×10^{-4}

Table 4.2: *Different values of p and q curve fitting results for all asymptotic regimes for $\Phi_{1,2}(\dot{s}) = a\dot{s}^b + c$. The kinetic conditions Φ_1 and Φ_2 have been computed as in* (3.43) *and* (4.37) *respectively, after solving the full reaction-diffusion system with parameter values* (2.51) *and two rapidly varying diffusion coefficient.*

This chapter concludes the derivation of the sharp interface models in the fast reaction limit $\epsilon \to 0$ for concrete carbonation. Using the technique of matched asymptotics we have derived a one-phase Stefan model for the parameter regime $\delta \ll \epsilon$ and a two-phase Stefan model for $\delta = O(\epsilon)$. The choice of diffusion coefficients determines the structure of the kinetic boundary conditions (2.21). For slowly varying diffusivities (chapter 2), both $\Phi_1(\dot{s})$ and $\Phi_2(\dot{s})$ are zero. For a one rapidly varying CO_2 diffusivity, depending now on the reaction term (2.11), $\Phi_1(\dot{s})$ is no longer zero and its solution is determined by solving a micro problem obtained from the reaction layer (inner inner). Finally, in this chapter, we have looked at two rapidly varying diffusivities and for the two-phase Stefan model, where $\Phi_2(\dot{s})$ plays a role, we now obtain a non-zero $\Phi_2(\dot{s})$, which solution is also given by a micro problem. This leads to a non-standard, two-phase, micro-macro, moving boundary Stefan problem.

In the following chapters we analyse these derived Stefan problems further to achieve a better insight into the carbonation reaction. First we concentrate on the micro problems (chapter 5) to ultimately consider the full picture (chapter 6).

Chapter 5

The Derived Micro Problems

The results obtained in Chapters 2, 3 and 4 are either one- or two-phase generalised Stefan problems ($\delta \ll \epsilon$ or $\delta = O(\epsilon)$ respectively) with differing free boundary conditions (depending on the diffusion coefficients). In the following two chapters we collect and summarise these results and perform further analysis. We start by looking at the set of micro problems derived. These are used to update the concentrations of CO_2 and $Ca(OH)_2$ on the free boundary $x = s(t)$ of the macro problems, resulting in a coupled micro-macro system. The micro problems only arise when one or two diffusion coefficients are rapidly varying (Chapters 3 and 4 respectively). For slowly varying diffusivities (Chapter 2) both CO_2 and $Ca(OH)_2$ are zero at leading order on $x = s(t)$. Nevertheless, these micro problems can also be viewed as stand-alone problems and this is what this chapter will concentrate on. First, all the derived micro problems will be stated and then we proceed to do some analysis and numerical simulations on them.

5.1 The micro problems

Throughout chapters 3 and 4, five different micro problems are obtained. These are detailed and labelled as follows.

We denote as S-micro problems the micro problems obtained in chapter 3, where a single rapidly varying diffusion coefficient is considered:

- Let S1a be the micro problem from subsection 3.1.1 where $\delta \leq \epsilon^2$

$$\mu \dot{s} \frac{\partial \bar{c}_0}{\partial \bar{x}} + \frac{\partial}{\partial \bar{x}} \left(\bar{D}_c \frac{\partial \bar{c}_0}{\partial \bar{x}} \right) = \bar{c}_0^p \bar{h}_0^q, \tag{5.1}$$

$$\bar{D}_c \frac{\partial \bar{c}_0}{\partial \bar{x}} - \frac{\delta^2}{\epsilon^4} D_h \frac{\partial \bar{h}_0}{\partial \bar{x}} = \dot{s}(\bar{h}_0 - h_i(s) - \mu \bar{c}_0), \tag{5.2}$$

with

$$\text{as } \bar{x} \to +\infty \qquad \bar{c}_0 \to 0, \quad \bar{D}_c \frac{\partial \bar{c}_0}{\partial \bar{x}} \to 0 \quad \bar{h}_0 \to h_i(s), \tag{5.3}$$

$$\text{as } \bar{x} \to -\infty \qquad \bar{c}_0 \to \Phi_1(\dot{s}), \quad \bar{h}_0 \to 0, \tag{5.4}$$

where $\bar{D}_c = \frac{\nu_1}{\bar{h}_0^q}$ and $D_h = O(1)$.

- Let S1b be the micro problem from subsection 3.1.2 where $\epsilon^2 \ll \delta \ll \epsilon$

$$\mu \dot{s} \frac{\partial \bar{c}_0}{\partial \bar{x}} + \frac{\partial}{\partial \bar{x}} \left(\bar{D}_c \frac{\partial \bar{c}_0}{\partial \bar{x}} \right) = \bar{c}_0^p \bar{h}_0^q, \tag{5.5}$$

$$\bar{D}_c \frac{\partial \bar{c}_0}{\partial \bar{x}} - D_h \frac{\partial \bar{h}_0}{\partial \bar{x}} = -\dot{s}(\mu \bar{c}_0 + h_i(s)), \tag{5.6}$$

with

$$\text{as } \bar{x} \to +\infty \qquad \bar{c}_0 \to 0, \quad \bar{D}_c \frac{\partial \bar{c}_0}{\partial \bar{x}} \to 0 \quad D_h \frac{\partial \bar{h}_0}{\partial \bar{x}} \to \dot{s} h_i(s), \tag{5.7}$$

$$\text{as } \bar{x} \to -\infty \qquad \bar{c}_0 \to \Phi_1(\dot{s}), \quad \bar{h}_0 \to 0, \tag{5.8}$$

where $\bar{D}_c = \frac{\nu_1}{\bar{h}_0^q}$ and $D_h = O(1)$.

- Let S2 be the micro problem form subsection 3.1.3 where $\delta = O(\epsilon)$

$$\mu \dot{s} \frac{\partial \bar{c}_0}{\partial \bar{x}} + \frac{\partial}{\partial \bar{x}} \left(\bar{D}_c \frac{\partial \bar{c}_0}{\partial \bar{x}} \right) = \bar{c}_0^p \bar{h}_0^q, \tag{5.9}$$

$$\frac{\partial}{\partial \bar{x}} \left(D_h \frac{\partial \bar{h}_0}{\partial \bar{x}} \right) = \bar{c}_0^p \bar{h}_0^q. \tag{5.10}$$

with

$$\text{as } \bar{x} \to +\infty \quad \bar{c}_0 \to 0, \quad \bar{D}_c \frac{\partial \bar{c}_0}{\partial \bar{x}} \to 0, \quad D_h \frac{\partial \bar{h}_0}{\partial \bar{x}} \to D_{h_0} \frac{\partial h_0(s^+, t)}{\partial x}, \tag{5.11}$$

$$\text{as } \bar{x} \to -\infty \quad \bar{c}_0 \to \Phi_1(\dot{s}), \quad \bar{h}_0 \to 0, \quad D_h \frac{\partial \bar{h}_0}{\partial \bar{x}} \to 0, \tag{5.12}$$

where $\bar{D}_c = \frac{\nu_1}{\bar{h}_0^q}$ and $D_h = O(1)$.

We denote as D-micro problems the micro problems obtained in chapter 4, where two rapidly varying diffusivities are considered:

- Let D1 be the micro problem from subsection 4.1.1 where $\delta \ll \epsilon$

$$\mu\dot{s}\frac{\partial \bar{c}_0}{\partial \bar{x}} + \frac{\partial}{\partial \bar{x}}\left(\bar{D}_c \frac{\partial \bar{c}_0}{\partial \bar{x}}\right) = \bar{c}_0^p \bar{h}_0^q, \tag{5.13}$$

$$\bar{D}_c \frac{\partial \bar{c}_0}{\partial \bar{x}} = \dot{s}(\bar{h}_0 - h_i(s) - \mu \bar{c}_0), \tag{5.14}$$

with

$$\text{as } \bar{x} \to +\infty \qquad \bar{c}_0 \to 0, \quad \bar{D}_c \frac{\partial \bar{c}_0}{\partial \bar{x}} \to 0, \quad \bar{h}_0 \to h_i(s), \tag{5.15}$$

$$\text{as } \bar{x} \to -\infty \qquad \bar{c}_0 \to \Phi_1(\dot{s}), \quad \bar{h}_0 \to 0, \tag{5.16}$$

where $\bar{D}_c = \frac{\nu_1}{\bar{h}_0^q}$.

- Let D2 be the micro problem from subsection 4.1.2 where $\delta = O(\epsilon)$

$$\mu\dot{s}\frac{\partial \bar{c}_0}{\partial \bar{x}} + \frac{\partial}{\partial \bar{x}}\left(\bar{D}_c \frac{\partial \bar{c}_0}{\partial \bar{x}}\right) = \bar{c}_0^p \bar{h}_0^q, \tag{5.17}$$

$$\dot{s}\frac{\partial \bar{h}_0}{\partial \bar{x}} + \frac{\partial}{\partial \bar{x}}\left(\bar{D}_h \frac{\partial \bar{h}_0}{\partial \bar{x}}\right) = \bar{c}_0^p \bar{h}_0^q, \tag{5.18}$$

with

$$\text{as } \bar{x} \to +\infty \quad \bar{c}_0 \to 0, \quad \bar{D}_c \frac{\partial \bar{c}_0}{\partial \bar{x}} \to 0, \quad \bar{h}_0 \to \Phi_2(\dot{s}), \tag{5.19}$$

$$\text{as } \bar{x} \to -\infty \quad \bar{c}_0 \to \Phi_1(\dot{s}), \quad \bar{h}_0 \to 0, \quad \bar{D}_h \frac{\partial \bar{h}_0}{\partial \bar{x}} \to 0, \tag{5.20}$$

where $\bar{D}_c = \frac{\nu_1}{\bar{h}_0^q}$ and $\bar{D}_h = \frac{\nu_2}{\bar{c}_0^p}$.

5.2 Eigenmode analysis

To determine whether the micro problems are well defined we perform an eigenmode analysis on all five of them. This section is split into the S-Micro problems and the D-Micro problems. The case $p = q = 1$ will be explained in detail for all the problems. The conclusions obtained will then hold for $p, q > 1$, however more care is needed to determine the eigenmodes. As an example, the eigenmodes for the S1a micro problem will be derived.

The approach taken here is as in [55]. At each boundary we seek for perturbations of the form

$$\bar{c}_0 = \bar{C}_0 + \theta \bar{C}_1, \quad \bar{h}_0 = \bar{H}_0 + \theta \bar{H}_1, \tag{5.21}$$

where θ is an arbitrary small parameter and $\bar{C}_0$, $\bar{H}_0$ are the leading order behaviours of the dependent variables $\bar{c}_0$, $\bar{h}_0$ respectively as $\bar{x} \to -\infty$ or $\bar{x} \to +\infty$. Substituting the perturbation (5.21) into each micro problem, we linearise in $\bar{C}_1$ and $\bar{H}_1$ to obtain order θ terms, neglecting the forcing terms. For each limiting behaviour we identify the number of conditions imposed on the micro problem and check that we obtain the right amount for the system to be well defined. The eigenmodes that contradict the asymptotic expansions (5.21) are inconsistent and so we require them to be absent. To do this, the modes' multiplicative constant will be forced to be zero. Each eigenmode that requires this, imposes one condition.

5.2.1 S-Micro problems

The S-micro problems are those obtained for a single rapidly varying diffusivity. Recall that for the functional form (3.1) we have $\bar{D}_c = \nu_1/\bar{h}_0^q$ and so as $\bar{x} \to -\infty$, $\bar{D}_c$ becomes singular. To avoid this we introduce the following transformations,

$$\bar{c}_0 = y_1, \quad \bar{D}_c \bar{c}_0' = \frac{\nu_1 \bar{c}_0'}{\bar{h}_0^q} = y_2, \quad \bar{h}_0 = y_3 \tag{5.22}$$

where $' = \partial/\partial\bar{x}$ and perturb around y_1, y_2 and y_3, instead of using (5.21). Let $p = q = 1$ and consider each micro problem separately.

5.2.1.1 S1a micro problem

Consider S1a and let $\delta = \lambda\epsilon^2$. Making the transformation (5.22), (5.1)-(5.4) may be rewritten as

$$\mu\dot{s}y_1' + y_2' = y_1 y_3, \quad y_2 - \lambda^2 D_h y_3' = \dot{s}(y_3 - h_i - \mu y_1), \quad y_2 y_3 = \nu_1 y_1' \tag{5.23}$$

with

$$\text{as } \bar{x} \to +\infty \qquad y_1 \to 0, \quad y_2 \to 0, \quad y_3 \to h_i, \tag{5.24}$$

$$\text{as } \bar{x} \to -\infty \qquad y_1 \to \Phi_1, \quad y_2 \to -\dot{s}(h_i + \mu\Phi_1), \quad y_3 \to 0. \tag{5.25}$$

For $\bar{x} \to +\infty$, we substitute the perturbations

$$y_1 = \theta Y_1, \quad y_2 = \theta Y_2, \quad y_3 = h_i + \theta Y_3, \tag{5.26}$$

into (5.23) and equating the terms of order θ yields the following homogeneous system for Y_1, Y_2, and Y_3

$$\mu\dot{s}Y_1' + Y_2' = Y_1 h_i, \quad Y_2 - \lambda^2 D_h Y_3' = \dot{s}(Y_3 - \mu Y_1), \quad h_i Y_2 = \nu_1 Y_1'.$$

This third order linear system gives the eigenmodes

$$\left.\begin{array}{rcl} Y_1 &=& C_1\mathrm{e}^{A_+\bar{x}} \\ Y_2 &=& \frac{\nu_1}{h_i}A_+C_1\mathrm{e}^{A_+\bar{x}} \\ Y_3 &=& \frac{\nu_1A_++\mu h_1\dot{s}}{h_i(\lambda^2D_hA_++\dot{s})}C_1\mathrm{e}^{A_+\bar{x}} \end{array}\right\}, \quad \left.\begin{array}{rcl} Y_1 &=& C_2\mathrm{e}^{A_-\bar{x}} \\ Y_2 &=& \frac{\nu_1}{h_i}A_-C_2\mathrm{e}^{A_-\bar{x}} \\ Y_3 &=& \frac{\nu_1A_-+\mu h_1\dot{s}}{h_i(\lambda^2D_hA_-+\dot{s})}C_2\mathrm{e}^{A_-\bar{x}} \end{array}\right\}, \tag{5.27}$$

$$\left.\begin{array}{rcl} Y_1 &=& 0 \\ Y_2 &=& 0 \\ Y_3 &=& C_3\mathrm{e}^{-\frac{\dot{s}}{\lambda^2D_h}\bar{x}} \end{array}\right\}, \tag{5.28}$$

where $A_\pm = \frac{(-\mu\dot{s}\pm\sqrt{\mu^2\dot{s}^2+4\nu_1})h_i}{2\nu_1}$ and C_1, C_2, C_3 are all arbitrary constants. Note that the first set of eigenmodes contradicts the asymptotic expansions (5.26) forcing $C_1 = 0$. The boundary conditions as $\bar{x} \to +\infty$ therefore impose one condition.
For $\bar{x} \to -\infty$, we substitute the perturbations

$$y_1 = \Phi_1 + \theta Y_1, \quad y_2 = -\dot{s}(h_i + \mu\Phi_1) + \theta Y_2, \quad y_3 = \theta Y_3, \tag{5.29}$$

into (5.23) and the order θ terms yield

$$\mu\dot{s}Y_1' + Y_2' = \Phi_1 Y_3, \quad Y_2 - \lambda^2 D_h Y_3' = \dot{s}(Y_3 - \mu Y_1), \quad -\dot{s}(h_i + \mu\Phi_1)Y_3 = \nu_1 Y_1'. \tag{5.30}$$

This third order homogeneous system has the following possible eigenmodes

$$\left.\begin{array}{rcl} Y_1 &=& C_1\mathrm{e}^{A_+\bar{x}} \\ Y_2 &=& -\frac{\Phi_1\nu_1+\mu\dot{s}^2(h_i+\mu\Phi_1)}{\dot{s}(h_i+\mu\Phi_1)}C_1\mathrm{e}^{A_+\bar{x}} \\ Y_3 &=& -\frac{\nu_1}{\dot{s}(h_i+\mu\Phi_1)}A_+C_1\mathrm{e}^{A_+\bar{x}} \end{array}\right\}, \quad \left.\begin{array}{rcl} Y_1 &=& C_2\mathrm{e}^{A_-\bar{x}} \\ Y_2 &=& -\frac{\Phi_1\nu_1+\mu\dot{s}^2(h_i+\mu\Phi_1)}{\dot{s}(h_i+\mu\Phi_1)}C_2\mathrm{e}^{A_-\bar{x}} \\ Y_3 &=& -\frac{\nu_1}{\dot{s}(h_i+\mu\Phi_1)}A_-C_2\mathrm{e}^{A_-\bar{x}} \end{array}\right\}, \tag{5.31}$$

$$\left.\begin{array}{rcl} Y_1 &=& C_3 \\ Y_2 &=& -\mu\dot{s}C_3 \\ Y_3 &=& 0 \end{array}\right\}, \tag{5.32}$$

where $A_\pm = \frac{-\dot{s}\pm\sqrt{\dot{s}^2+4\lambda^2D_h\Phi_1}}{2\lambda^2D_h}$ and C_1, C_2, C_3 are arbitrary constants. As $\bar{x} \to -\infty$ the second condition is inconsistent with (5.29) giving a total of two conditions. In order for S1a to be well defined, three conditions are necessary. However, note that if Φ_1 is prescribed, the third set of eigenmodes above contradicts the asymptotic expansion too and hence we obtain our third missing condition.

Before continuing with S1b, consider $p > 1$, $q > 1$. The procedure for determining the eigenmodes requires greater care now. We focus on S1a and note that the remaining micro problems can be done in a similar way. We now perturb using the original variables as in (5.21). Further, when the concentrations tend to zero as $\bar{x} \to \pm\infty$ we seek for their leading order limiting behaviour and perturb around it.

As $\bar{x} \to +\infty$, $\bar{c}_0$ decays exponentially

$$\bar{c}_0 \sim A\exp\left(-\frac{\dot{s}\mu h_i^q}{\nu_1}\bar{x}\right), \tag{5.33}$$

for $\mu \neq 0$, where A is an arbitrary constant. The special case $\mu = 0$ is done below. We substitute the perturbations

$$\bar{c}_0 = \exp\left(-\frac{\dot{s}\mu h_i^q}{\nu_1}\bar{x}\right)(1+\theta\bar{C}_1), \quad \bar{h}_0 = h_i(1+\theta\bar{H}_1),$$

into (5.1)-(5.4). At $O(\theta)$ we obtain the homogeneous third order ordinary differential equation for $\bar{H}_1$

$$\frac{\lambda^2 D_h \nu_1}{\dot{s}h_i^q}\frac{\partial^3\bar{H}_1}{\partial\bar{x}^3} + (\mu\lambda^2 D_h p + \frac{\nu_1}{h_i^q})\frac{\partial^2\bar{H}_1}{\partial\bar{x}^2} + \mu\dot{s}p\frac{\partial\bar{H}_1}{\partial\bar{x}} - h_i^q p\exp\left(-\frac{(p-1)\mu\dot{s}h_i^q}{\nu_1}\bar{x}\right)\bar{H}_1,$$

and $\bar{C}_1$ can then be determined by

$$\bar{C}_1 = \left(\lambda^2 D_h\frac{\partial^2\bar{H}_1}{\partial\bar{x}^2} + \dot{s}\frac{\partial\bar{H}_1}{\partial\bar{x}}\right)\frac{h_i}{h_i^q p}\exp\left(\frac{\mu\dot{s}h_i^q p}{\nu_1}\bar{x}\right) - \frac{q}{p}\bar{H}_1.$$

Thus, as $\bar{x} \to +\infty$ the above equations give the eigenmodes

$$\left.\begin{array}{rcl} \bar{C}_1 &=& C_1\frac{h_i}{\mu}\exp\left(\frac{\mu\dot{s}h_i^q}{\nu_1}\bar{x} + A\exp(B\bar{x})\right) \\ \bar{H}_1 &=& C_1\exp\left(A\exp(B\bar{x})\right) \end{array}\right\},$$

where

$$A = \frac{p\nu_1^2}{\dot{s}^2\mu^2(p-1)(\lambda^2 D_h h_i^q\mu(p-1)-\nu_1)}, \quad B = -\frac{(p-1)\mu\dot{s}h_i^q}{\nu_1},$$

and

$$\left.\begin{array}{rcl} \bar{C}_1 &=& \frac{C_2\mu\dot{s}^2h_i}{\nu_1}(\mu\lambda^2 D_h h_i^q p - \nu_1) \\ \bar{H}_1 &=& C_2\exp\left(-\frac{\mu\dot{s}ph_i^q}{\nu_1}\bar{x}\right) \end{array}\right\}, \quad \left.\begin{array}{rcl} \bar{C}_1 &=& \frac{q}{p}C_3\exp\left(-\frac{\dot{s}}{\lambda^2 D_h}\bar{x}\right) \\ \bar{H}_1 &=& C_3\exp\left(-\frac{\dot{s}}{\lambda^2 D_h}\bar{x}\right) \end{array}\right\},$$

where C_1, C_2, C_3 are arbitrary constants. The first eigenmode is a constant with an exponential correction and so it is inconsistent. Note that the second eigenmode is consistent since it corresponds to the arbitrary constant for $\bar{c}_0$ in (5.33). Hence in total, as $\bar{x} \to +\infty$ we obtain one condition.

Before looking at the limit $\bar{x} \to -\infty$, we consider the case $\mu = 0$. The concentration $\bar{c}_0$ now decays algebraically as opposed to exponentially and so we introduce the perturbations

$$\bar{c}_0 = \left(\frac{A}{\bar{x}^2}\right)^{\frac{1}{p-1}}(1+\theta\bar{C}_1), \quad \bar{h}_0 = h_i(1+\theta\bar{H}_1),$$

where $A = \frac{2(p+1)\nu_1}{(p-1)^2 h_i^{2q}}$. This yields the eigenmodes

$$\left.\begin{array}{rcl} \bar{C}_1 &=& C_{1,2}\frac{\dot{s}h_i n_\pm}{h_i^q p}\left(\frac{A}{\bar{x}^2}\right)^{-\frac{p}{p-1}}\bar{x}^{n_\pm-1} \\ \bar{H}_1 &=& C_{1,2}\bar{x}^{n_\pm} \end{array}\right\},$$

where $n_\pm$ are the solutions to the quadratic equation $\nu_1 n^2 + \nu_1 n - A h_i^{2q} p$, and

$$\left.\begin{array}{rcl} \bar{C}_1 &=& -\frac{2C_3\dot{s}h_i}{h_i^q p}\bar{x}\left(\frac{A}{\bar{x}^2}\right)^{\frac{-p}{p+1}}\exp\left(-\frac{\dot{s}}{\lambda^2 D_h}\bar{x}\right) \\ \bar{H}_1 &=& C_3\bar{x}^2\exp\left(-\frac{\dot{s}}{\lambda^2 D_h}\bar{x}\right) \end{array}\right\}.$$

The condition $C_1 = 0$ is imposed since $\bar{x}^{n_+}$ blows up as $\bar{x} \to +\infty$. It is worth noticing that n_- is small enough so that $\bar{x}^{\frac{p+1}{p-1}+n_-} \to 0$ as $\bar{x} \to +\infty$ hence in total we obtain one condition as in the $\mu \neq 0$ case.
As $\bar{x} \to -\infty$, $\bar{h}_0$ decays to zero algebraically

$$\bar{h}_0 \sim \left(-\frac{(q-1)\Phi_1^p}{\dot{s}}\bar{x}\right)^{-\frac{1}{q-1}}.$$

We substitute the perturbations

$$\bar{c}_0 = \Phi_1(1+\theta\bar{C}_1), \quad \bar{h}_0 = (-A\bar{x})^{-\frac{1}{q-1}}(1+\theta\bar{H}_1),$$

where $A = \frac{(q-1)\Phi_1^p}{\dot{s}}$ into (5.1)-(5.4). As $\bar{x} \to -\infty$, $\bar{H}_1$ is determined by the solution to the homogeneous differential equation

$$\lambda^2 D_h \nu_1 \Phi_1 \frac{\partial^3 \bar{H}_1}{\partial \bar{x}^3} + \dot{s}\nu_1\Phi_1\frac{\partial^2\bar{H}_1}{\partial\bar{x}^2} + \frac{2\dot{s}\nu_1\Phi_1}{\bar{x}}\frac{\partial\bar{H}_1}{\partial\bar{x}} - \frac{\mu\dot{s}^2\Phi_1 b}{q-1}(-b\bar{x})^{\frac{1-2q}{q-1}}\bar{H}_1,$$

and consequently $\bar{C}_1$ can be calculated as

$$\bar{C}_1 = -\frac{q-1}{p}\left(\frac{\lambda^2 D_h}{\dot{s}}\frac{\partial^2\bar{H}_1}{\partial\bar{x}^2} + \frac{\partial\bar{H}_1}{\partial\bar{x}}\right)\bar{x} - \frac{q-1}{p}\bar{H}_1.$$

The eigenmodes are

$$\left.\begin{array}{rcl} \bar{C}_1 &=& \frac{2\lambda^2 D_h}{p\Phi_1^p}\frac{C_1}{\bar{x}^2} \\ \bar{H}_1 &=& C_1(-A\bar{x})^{-1} \end{array}\right\}, \quad \left.\begin{array}{rcl} \bar{C}_1 &=& -\frac{q-1}{p}C_2 \\ \bar{H}_1 &=& C_2 + A(-x)^{-\frac{1}{q-1}} \end{array}\right\},$$

$$\left.\begin{array}{rcl} \bar{C}_1 &=& \frac{q-1}{p}C_3\bar{x}^2\exp\left(-\frac{\dot{s}}{\lambda^2 D_h}\bar{x}\right) \\ \bar{H}_1 &=& C_3(-\bar{x})^2\exp\left(-\frac{\dot{s}}{\lambda^2 D_h}\bar{x}\right) \end{array}\right\},$$

where $C_2 = C_3 = 0$ so two conditions are imposed as long as Φ_1 is prescribed. It is worth mentioning that the second eigenmode is a constant with an infinitesimally

small correction. The micro problem S1a is therefore well defined for $p, q > 1$ with one condition imposed by the boundary condition $\bar{x} \to +\infty$ and two from $\bar{x} \to -\infty$. The remaining micro problems follow with the need to first find the limiting behaviours to perturb around.
We now go back to the case $p = q = 1$ and seek for the eigenmodes of the remaining micro problems.

5.2.1.2 S1b micro problem

We make the variable transformations (5.22) to obtain the problem

$$\mu\dot{s}y_1' + y_2' = y_1 y_3, \quad y_2 - D_h y_3' = -\dot{s}(h_i + \mu y_1), \quad y_2 y_3 = \nu_1 y_1', \tag{5.34}$$

with

$$\bar{x} \to +\infty \qquad y_1 \to 0, \quad y_2 \to 0, \quad D_h y_3' \to \dot{s}h_i, \tag{5.35}$$

$$\bar{x} \to -\infty \qquad y_1 \to \Phi_1, \quad y_2 \to -\dot{s}(h_i + \mu\Phi_1), \quad y_3 \to 0. \tag{5.36}$$

Comparing with S1a (5.23)-(5.25), note the disappearance of the y_3 variable in the second equation of (5.23) and the now Neumann boundary condition for y_3 as $\bar{x} \to +\infty$. For $\bar{x} \to +\infty$, we substitute the perturbations

$$y_1 = \theta Y_1, \quad y_2 = \theta Y_2, \quad y_3 = \frac{\dot{s}h_i}{D_h}\bar{x} + \theta Y_3, \tag{5.37}$$

into (5.34) and obtain the order θ homogeneous system

$$\mu\dot{s}Y_1' + Y_2' = \frac{\dot{s}h_i}{D_h}\bar{x}Y_1, \quad Y_2 - D_h Y_3' = -\dot{s}\mu Y_1, \quad \frac{\dot{s}h_i}{D_h}\bar{x}Y_2 = \nu_1 Y_1', \tag{5.38}$$

with eigenmodes

$$\left.\begin{array}{rcl} Y_1 &=& C_1 \mathrm{e}^{A_+\bar{x}^2} \\ Y_2 &=& \frac{2\nu_1 D_h A_+}{\dot{s}h_i} C_1 \mathrm{e}^{A_+\bar{x}^2} \\ Y_3 &=& \frac{C_1}{D_h}\left(\dot{s}\mu + \frac{2D_h\nu_1 A_+}{\dot{s}h_i}\right)\sqrt{-\frac{\pi}{4A_+}}\mathrm{erf}\left(\sqrt{-A_+}\bar{x}\right) \end{array}\right\}, \tag{5.39}$$

$$\left.\begin{array}{rcl} Y_1 &=& C_2 \mathrm{e}^{A_-\bar{x}^2} \\ Y_2 &=& \frac{2\nu_1 D_h A_-}{\dot{s}h_i} C_2 \mathrm{e}^{A_-\bar{x}^2} \\ Y_3 &=& \frac{C_2}{D_h}\left(\dot{s}\mu + \frac{2D_h\nu_1 A_-}{\dot{s}h_i}\right)\sqrt{-\frac{\pi}{4A_-}}\mathrm{erf}\left(\sqrt{-A_-}\bar{x}\right) \end{array}\right\}, \tag{5.40}$$

$$\left.\begin{array}{rcl} Y_1 &=& 0 \\ Y_2 &=& 0 \\ Y_3 &=& C_3 \end{array}\right\}, \tag{5.41}$$

where $A_\pm = \frac{\dot{s}h_i}{4\nu_1 D_h}\left(-\mu\dot{s} \pm \sqrt{\mu^2\dot{s}^2 + 4\nu_1}\right)$ and C_1, C_2 and C_3 are arbitrary constants. As $\bar{x} \to +\infty$ the first set of eigenmodes are inconsistent and so $C_1 = 0$, giving one condition.
For $\bar{x} \to -\infty$, we substitute the perturbations (5.29) into (5.34) and linearising in Y_1, Y_2 and Y_3 yields

$$\mu\dot{s}Y_1' + Y_2' = \Phi_1 Y_3, \quad Y_2 - D_h Y_3' = -\dot{s}\mu Y_1, \quad -\dot{s}(h_i + \mu\Phi_1)Y_3 = \nu_1 Y_1', \tag{5.42}$$

with eigenmodes as in (5.31) but with $A_\pm = \pm\sqrt{\frac{\Phi_1}{D_h}}$, and

$$\left.\begin{array}{rcl} Y_1 &=& C_3 \\ Y_2 &=& \left(\frac{\nu_1(1-\Phi_1)}{\dot{s}(h_i+\mu\Phi_1)} - \mu\dot{s}\right)C_3 \\ Y_3 &=& 0. \end{array}\right\},$$

as the third eigenmode. This yields two more conditions (as long as Φ_1 is prescribed), and with the condition imposed by the limit $\bar{x} \to +\infty$ we may conclude that S1b is well defined.

5.2.1.3 S2 micro problem

The micro problem S2 can be rewritten as

$$\mu\dot{s}y_1' + y_2' = y_1 y_3, \quad y_2 - D_h y_3' = -\mu\dot{s}y_1 - D_{h_0}\tilde{h}_0, \quad y_2 y_3 = \nu_1 y_1', \tag{5.43}$$

with

$$\bar{x} \to +\infty \qquad y_1 \to 0, \quad y_2 \to 0, \quad D_h y_3' \to D_{h_0}\tilde{h}_0, \tag{5.44}$$

$$\bar{x} \to -\infty \qquad y_1 \to \Phi_1, \quad y_2 \to -\dot{s}\mu\Phi_1 - D_{h_0}\tilde{h}_0, \quad y_3 \to 0, \tag{5.45}$$

where $D_{h_0}\tilde{h}_0 = D_{h_0}\frac{\partial h_0(s^+,t)}{\partial x}$ is the flux on outer 2 which is treated as a constant in the inner inner. This case is very similar to the S1b case. Note that (5.34) and (5.43) are essentially identical with the exception that the constant in the second equation is now $D_{h_0}\tilde{h}_0$.
For $\bar{x} \to +\infty$, we substitute the perturbations

$$y_1 = \theta Y_1, \quad y_2 = \theta Y_2, \quad y_3 = \frac{D_{h_0}}{D_h}\tilde{h}_0\bar{x} + \theta Y_3,$$

to obtain the homogeneous system (5.38) except for the coefficient of $\bar{x}$ in the first and third equations is now $\frac{D_{h_0}}{D_h}\tilde{h}_0$. Consequently, the eigenmodes are (5.39)-(5.41) but $\frac{\dot{s}h_i}{D_h}$ is now $\frac{D_{h_0}}{D_h}\tilde{h}_0$. Hence, we have one inconsistent eigenmode.
Looking at $\bar{x} \to -\infty$ we see that all the results are equivalent as to the S1b micro

problem with $\dot{s}(h_i+\mu\Phi_1)$ substituted with $\dot{s}\mu\Phi_1+D_{h_0}\tilde{h}_0$. In total, we have the necessary three conditions, as long as Φ_1 is prescribed.

5.2.2 D-Micro Problems

We consider now the micro problems obtained when both D_c and D_h are rapidly varying.

5.2.2.1 D1 micro problem

Consider D1 and note that (5.14) can be substituted into (5.13) to obtain two first order ordinary differential equations

$$\dot{s}\bar{h}_0' = \bar{c}_0\bar{h}_0, \quad \nu_1\bar{c}_0' = \dot{s}\bar{h}_0(\bar{h}_0 - h_i - \mu\bar{c}_0), \tag{5.46}$$

with

$$\bar{x} \to +\infty \quad \bar{c}_0 \to 0, \quad \bar{h}_0 \to h_i, \tag{5.47}$$

$$\bar{x} \to -\infty \quad \bar{c}_0 \to \Phi_1, \quad \bar{h}_0 \to 0, \tag{5.48}$$

where $' = \partial/\partial\bar{x}$. Note that the boundary condition for $\bar{D}_c\bar{c}_0'$ is no longer required. Consequently we are now looking for two inconsistent eigenmodes.
For $\bar{x} \to +\infty$ we substitute the perturbations

$$\bar{c}_0 = \theta\bar{C}_1, \quad \bar{h}_0 = h_i + \theta\bar{H}_1, \tag{5.49}$$

into (5.46), equate powers of θ and ignore forcing terms. We obtain the homogeneous system

$$\dot{s}\bar{H}_1' = h_i\bar{C}_1, \quad \nu_1\bar{C}_1' = \dot{s}h_i(\bar{H}_1 - \mu\bar{C}_1),$$

with eigenmodes

$$\left.\begin{array}{rcl} \bar{C}_1 & = & \frac{\dot{s}}{h_i}A_\pm C_{1,2}\mathrm{e}^{A_\pm\bar{x}} \\ \bar{H}_1 & = & C_{1,2}\mathrm{e}^{A_\pm\bar{x}} \end{array}\right\}, \tag{5.50}$$

where $A_\pm = \frac{-\mu\dot{s}\pm\sqrt{\mu^2\dot{s}^2+4\nu_1}}{2\nu_1}h_i$ and C_1, C_2 are arbitrary constants. As $\bar{x} \to +\infty$, the first set of eigenmodes contradict the perturbations (5.49), forcing $C_1 = 0$. Thus, this boundary condition imposes one condition.
For $\bar{x} \to -\infty$, we substitute the following perturbations

$$\bar{c}_0 = \Phi_1 + \theta\bar{C}_1, \quad \bar{h}_0 = \theta\bar{H}_1, \tag{5.51}$$

into (5.46) and ignoring the forcing terms, the order θ terms yield

$$\dot{s}\bar{H}_1^{'} = \Phi_1\bar{H}_1, \quad \nu_1\bar{C}_1^{'} = -\dot{s}(h_i + \mu\Phi_1)\bar{H}_1.$$

This second order homogeneous system has the eigenmodes

$$\left.\begin{array}{rcl}\bar{C}_1 &=& -\frac{\dot{s}^2(h_i+\mu\Phi_1)}{\nu_1\Phi_1}C_1\mathrm{e}^{\frac{\Phi_1}{\dot{s}}\bar{x}} \\ \bar{H}_1 &=& C_1\mathrm{e}^{\frac{\Phi_1}{\dot{s}}\bar{x}}\end{array}\right\}, \qquad \left.\begin{array}{rcl}\bar{C}_1 &=& C_2 \\ \bar{H}_1 &=& 0\end{array}\right\},$$

where C_1, C_2 are arbitrary constants. As $\bar{x} \to -\infty$ the constant eigenmode is inconsistent if Φ_1 is prescribed. Hence, the limiting behaviours impose two conditions as long as Φ_1 is prescribed.

5.2.2.2 D2 micro problem

Note that for D2 not only $\bar{D}_c$ becomes singular as $\bar{x} \to -\infty$ but from the functional form (4.1) we also have $\bar{D}_h = \nu_2/\bar{c}_0^p$, which becomes singular as $\bar{x} \to +\infty$. We introduce the three transformations in (5.22) and

$$\bar{D}_h\bar{h}_0' = \frac{\nu_2\bar{h}_0'}{\bar{c}_0} = y_4, \tag{5.52}$$

so that D2 becomes

$$\mu\dot{s}y_1' + y_2' = y_1y_3, \quad y_1y_2 - \dot{s}(y_3 - \mu y_1 - \Phi_2)y_1 + D_{h_0}\tilde{h}_0y_1 = \nu_2y_3', \quad y_2y_3 = \nu_1y_1' \tag{5.53}$$

with

$$\bar{x} \to +\infty \qquad y_1 \to 0, \quad y_2 \to 0, \quad y_3 \to \Phi_2, \tag{5.54}$$

$$\bar{x} \to -\infty \qquad y_1 \to \Phi_1, \quad y_2 \to -\dot{s}(\Phi_2 + \mu\Phi_1) - D_{h_0}\tilde{h}_0, \quad y_3 \to 0, \tag{5.55}$$

where $D_{h_0}\tilde{h}_0 = D_{h_0}\frac{\partial h_0(s^+,t)}{\partial x}$. For $\bar{x} \to +\infty$ we substitute the perturbations

$$y_1 = \theta Y_1, \quad y_2 = \theta Y_2, \quad y_3 = \Phi_2 + \theta Y_3,$$

into (5.53) to obtain

$$\mu\dot{s}Y_1' + Y_2' = \Phi_2Y_1, \quad D_{h_0}\tilde{h}_0Y_1 = \nu_2Y_3', \quad \Phi_2Y_2 = \nu_1Y_1'. \tag{5.56}$$

This third order homogeneous system has the eigenmodes

$$\left.\begin{array}{rcl} Y_1 &=& C_{1,2}\mathrm{e}^{A_\pm \bar{x}} \\ Y_2 &=& \frac{A_\pm \nu_1}{\Phi_2} C_{1,2}\mathrm{e}^{A_\pm \bar{x}} \\ Y_3 &=& \frac{D_{h_0}\tilde{h}_0}{\nu_2 A_\pm} C_{1,2}\mathrm{e}^{A_\pm \bar{x}} \end{array}\right\}, \quad \left.\begin{array}{rcl} Y_1 &=& 0 \\ Y_2 &=& 0 \\ Y_3 &=& C_3 \end{array}\right\},$$

where $A_\pm = \frac{-\mu\dot{s}\pm\sqrt{\mu^2\dot{s}^2+4\nu_1}}{2\nu_1}\Phi_2$ and C_1, C_2, C_3 are all arbitrary constants. Thus, the boundary conditions as $\bar{x} \to +\infty$ impose one condition. Note that if Φ_2 is defined then $C_3 = 0$, and so we have another inconsistent eigenmode.
For $\bar{x} \to -\infty$, we perturb (5.53) as follows

$$y_1 = \Phi_1 + \theta Y_1, \quad y_2 = -\dot{s}(\Phi_2 + \mu\Phi_1) - D_{h_0}\tilde{h}_0 + \theta Y_2, \quad y_3 = \theta Y_3,$$

and the eigenmodes of the resulting homogeneous system are

$$\left.\begin{array}{rcl} Y_1 &=& C_{1,2}\mathrm{e}^{A_\pm \bar{x}} \\ Y_2 &=& -\left(\mu\dot{s} + \frac{\nu_1\Phi_1}{\dot{s}(\Phi_2+\mu\Phi_1)+D_{h_0}\tilde{h}_0}\right) C_{1,2}\mathrm{e}^{A_\pm \bar{x}} \\ Y_3 &=& -\frac{\nu_1 A_\pm}{\dot{s}(\Phi_2+\mu\Phi_1)+D_{h_0}\tilde{h}_0} C_{1,2}\mathrm{e}^{A_\pm \bar{x}} \end{array}\right\}, \quad \left.\begin{array}{rcl} Y_1 &=& C_3 \\ Y_2 &=& -\mu\dot{s}C_3 \\ Y_3 &=& 0 \end{array}\right\},$$

where $A_\pm = \frac{-\dot{s}\pm\sqrt{\dot{s}^2+4\nu_2}}{2\nu_2}\Phi_1$ and C_1, C_2, C_3 are arbitrary constants. Hence this boundary condition imposes one condition unless Φ_1 is defined, in which case we obtain two. Thus, as long as either Φ_1 or Φ_2 are prescribed we obtain three inconsistent modes for the micro problem to be well-posed.

Summarising, in all cases, the boundary condition as $\bar{x} \to +\infty$ imposes one condition and as $\bar{x} \to -\infty$, two further conditions are imposed (except for D2, where there is only one). Computing the eigenmodes has determined that all the micro problems have a consistent number of boundary conditions.

5.3 Numerical results

Since all micro problems are well defined, it is now possible to evaluate them numerically and solve for $\Phi_{1,2}$. Note that the eigenmode analysis above states that Φ_1 has to be prescribed. With this in mind, we view the problems stated in section 5.1 as initial value problems with the initial condition being the boundary condition as $\bar{x} \to -\infty$. The ordinary differential equations are then solved backwards in space. The value of Φ_1 can range between zero and one and so we systematically go through each one until the conditions as $\bar{x} \to +\infty$ are satisfied. Due to the sensitivity of the value of Φ_1 on the systems, great care is needed. The idea is to improve the value of Φ_1 gradually by increasing the range of the domain slowly using the previous approximation for Φ_1 as

the new initial guess.

Graphs 5.1 to 5.3 show the plots of Φ_1 vs $\dot{s}(t)$ given by the micro problems S1a to D1 respectively for $p = q = 1$. We see a roughly linear relation which coincides with the results obtained in sections 3.2.4 and 4.2.4. For S2, the flux is treated as an extra parameter. Figure 5.2 shows a three dimensional plot of the possible behaviours depending on the values of $\dot{s}$, Φ_1 and the flux. An analogous procedure can be used to obtain a result for Φ_1 and Φ_2 in D2. However, checking the boundary conditions as $\bar{x} \to +\infty$ is no longer as straight forward since $\bar{h}_0 \to \Phi_2$, an unknown, there.

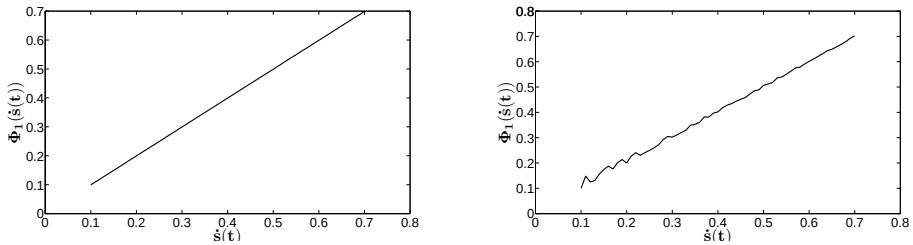

(a) S1a, (5.1)-(5.4). (b) S1b, (5.5)-(5.8).

Figure 5.1: *Profile of $\Phi_1(\dot{s})$ obtained for each S1-Micro problem. The micro problems are treated as initial value problems with initial condition as $\bar{x} \to -\infty$ and solved for values of Φ_1 for which the conditions as $\bar{x} \to +\infty$ are satisfied. The parameter values are $\lambda = \mu = \bar{D}_c = D_h = h_i = 1$ and tspan=[-26,26].*

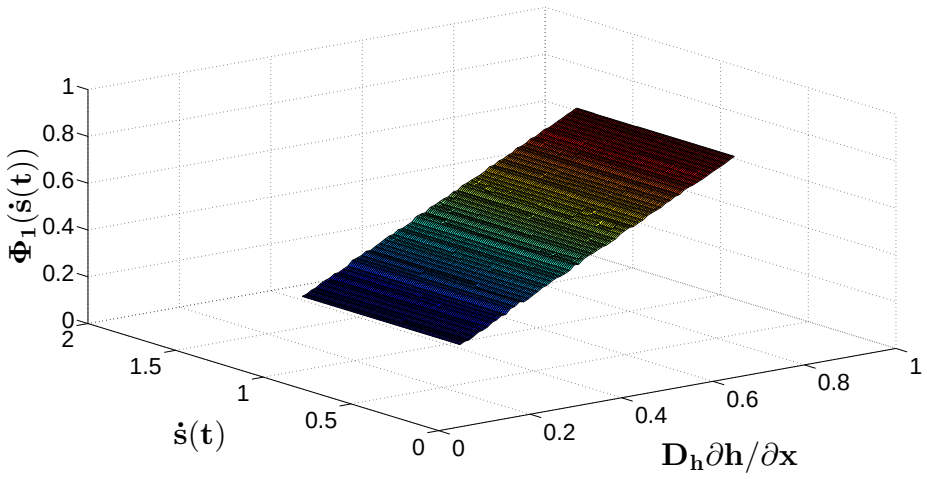

Figure 5.2: *S2-Micro problem,* (5.9)-(5.12). *The outer 2 flux of h is now an extra parameter.*

5.4 Asymptotic limit $\dot{s}(t) \to 0$

From the previous numerical sections 2.4.4, 3.2.4 and 4.2.4, taking the limit $\dot{s}(t) \to 0$ is equivalent to investigating the large time behaviour. It is of interest to investigate

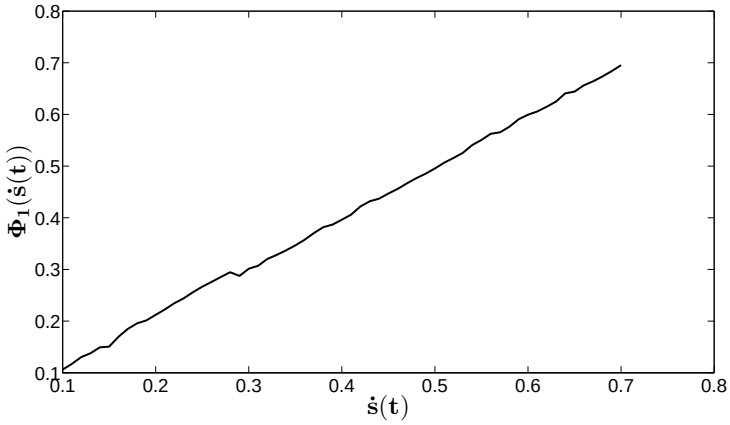

Figure 5.3: *D1-Micro problem,* (5.13)-(5.16).

analytically the structure of the kinetic conditions $\Phi_1(\dot{s})$ and $\Phi_2(\dot{s})$ given by the micro problems. To do this, we look at each problem separately.

5.4.1 S-Micro Problems

Let $\dot{s}(t) = 0$ in S1a and S1b, then $\Phi_1 = 0$ at leading order. This suggests considering the next order terms.

Concentrating on S1a with $\delta = \lambda\epsilon^2$, we rescale as follows

$$\bar{c_0} = 0, \quad \bar{h}_0 = \bar{H}, \quad \bar{x} = \dot{s}^{-1}\bar{X},$$

so that the boundary condition (5.3) is satisfied. We denote this region as the outer. The governing equation (5.2) gives

$$\bar{H} = h_i - A\exp\left(-\frac{1}{\lambda^2 D_h}\bar{X}\right),$$

where A is an arbitrary constant. As $\bar{X} \to -\infty$, $\bar{H} \to 0$ and so we truncate the above solution at

$$X_0 = \lambda^2 D_h \ln\left(\frac{A}{h_i}\right).$$

A boundary layer is now required to smooth $\bar{h}_0$ as $\bar{x} \to -\infty$. The scalings are

$$\bar{c_0} \to \dot{s}^{\frac{2}{p+1}} C, \quad \bar{h}_0 = \dot{s}^{\frac{2}{(p+1)(q+1)}} H, \quad \bar{x} = X_0 + \dot{s}^{\frac{1-q-p-pq}{(p+1)(q+1)}} X, \tag{5.57}$$

such that

$$\mu\dot{s}^{\frac{q+2}{(p+1)(q+1)}} C_X + \left(\nu_1 \frac{C_X}{H^q}\right)_X = C^p H^q, \quad \nu_1 \frac{C_X}{H^q} - \lambda^2 D_h H_X = -h_i + \dot{s}^{\frac{2}{(p+1)(q+1)}} H - \mu\dot{s}^{\frac{2p}{p+1}},$$

where $(*)_X$ denotes differentiation with respect to X. Hence

$$\nu_1 \left(\left(\lambda^2 D_h \frac{H_{XX}}{H^q} \right)^{\frac{1}{p}} \right)_X = H^q (\lambda^2 D_h H_X - h_i), \tag{5.58}$$

with

$$\text{as } X \to -\infty \quad H \to 0, \quad \lambda^2 D_h \frac{H_{XX}}{H^q} \to a^p, \tag{5.59}$$

$$\text{as } X \to +\infty \quad \lambda^2 D_h H \to h_i X, \tag{5.60}$$

where the latter boundary condition is obtained by matching to the outer and a is a constant. Figure 5.4 shows a sketch of the solution of $\bar{h}_0$ where, without loss of generality, we choose $A = h_i$ and so $X_0 = 0$. Furthermore,

$$C = \left(\lambda^2 D_h \frac{H_{XX}}{H^q} \right)^{\frac{1}{p}}. \tag{5.61}$$

The structure of the kinetic condition is thus given by the power law

$$\Phi_1 \sim a * \dot{s}^{\frac{2}{p+1}}, \tag{5.62}$$

where $a = \left(\lambda^2 D_h \frac{H_{XX}}{H^q} \right)^{\frac{1}{p}}$. Hence, Φ_1 depends on the value of p but is independent of the value of q in (2.11).

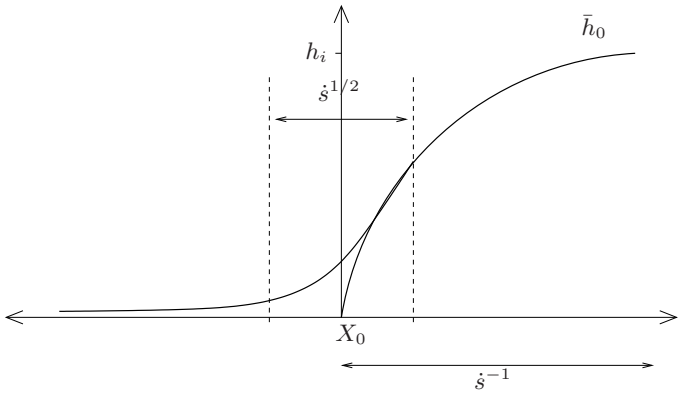

Figure 5.4: *Sketch of the behaviour of $\bar{h}_0$ for micro problem S1a with $p = q = 1$.*

For S1b, the now Neumann condition for $\bar{h}_0$ in (5.7) simplifies the whole analysis. Substituting the scalings (5.57) in (5.5)-(5.8), yields at leading order (5.58) with (5.59), (5.60) and (5.61) where $\lambda = 1$. The structure of the kinetic condition is as in (5.62). These results are in good agreement with the ones given by solving the full reaction-diffusion system (2.6)-(2.10). The cases for $\delta \ll \epsilon$ in tables 3.1 and 3.2 coincide with the relationship (5.62).

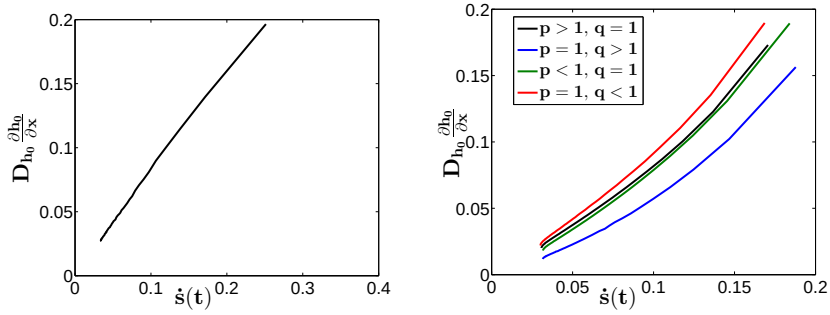

(a) $p = q = 1$ (b) Different p, q

Figure 5.5: *Dependence of* $D_{h_0}\frac{\partial h_0(s^+,t)}{\partial x}$ *on* $\dot{s}$ *for the regime* $\delta = O(\epsilon)$ *extracted from solving the full reaction-diffusion system with one rapidly varying diffusion coefficient* D_c*. The derivative was calculated using central difference around the point* $x = s(t) + \epsilon^{\frac{2}{q+1}}$ *which is where the outer 2 region starts.*

Consider S2, equating (5.9) and (5.10) and integrating yields

$$\bar{D}_c \frac{\partial \bar{c}_0}{\partial \bar{x}} - D_h \frac{\partial \bar{h}_0}{\partial \bar{x}} = -\dot{s}\mu\bar{c}_0 - D_{h_0}\frac{\partial h_0(s^+,t)}{\partial x}. \tag{5.63}$$

Setting $\dot{s} = 0$ in (5.9) and (5.63) yields a regular problem, in which S2 has no dependence on $\dot{s}$. This gives that Φ_1 is a constant. However, figure 3.10(d) in chapter 3 implies that Φ_1 does depend in $\dot{s}$. For this reason, and to be able to conclude how Φ_1 depends on $\dot{s}$, we argue that the outer 2 flux is of $O(\dot{s})$. Figure 5.5 shows that this assumption is reasonable. Specifically, we set

$$D_{h_0}\frac{\partial h_0(s^+,t)}{\partial x} \sim A\dot{s}, \tag{5.64}$$

where A is an arbitrary constant, and so the results obtained for S1b above follow with h_i replaced by A. The comparison to the case $\delta = O(\epsilon)$ in tables 3.1 and 3.2 is not ideal. The right behaviour in the coefficient of b of (3.44) is observed, however its value is not as accurate as for the regime $\delta \ll \epsilon$. This could be due to the now relatively large value of ϵ taken to solve the full reaction-diffusion system.

5.4.2 D-Micro Problems

Letting $\dot{s} = 0$ in D1 gives $\Phi_1 = 0$ and so we introduce the scalings

$$\bar{c}_0 = \dot{s}^{\frac{2}{1+p}}C, \quad \bar{h}_0 = H, \quad \bar{x} = \dot{s}^{\frac{1-p}{1+p}}X,$$

into (5.13)-(5.16). Analogous calculations as done for the S-Micro problems yield at leading order

$$\nu_1 \left(\left(\frac{H_X}{H^q} \right)^{\frac{1}{p}} \right)_X = H^q(H - h_i),$$

with

$$\text{as } X \to -\infty \quad H \to 0, \qquad \text{as } X \to +\infty \quad H \to h_i,$$

and

$$C = \left(\frac{H_X}{H^q} \right)^{\frac{1}{p}}.$$

Further Φ_1 behaves as in (5.62) with $a = \left(\frac{H_X}{H^q} \right)^{\frac{1}{p}}$.

For D2 we rewrite (5.18) as

$$\bar{D}_c \frac{\partial \bar{c}_0}{\partial \bar{x}} - \bar{D}_h \frac{\partial \bar{h}_0}{\partial \bar{x}} = \dot{s}(\bar{h}_0 - \Phi_2 - \mu \bar{c}_0) - D_{h_0} \frac{\partial h_0(s^+, t)}{\partial x}, \tag{5.65}$$

which has been obtained by equating (5.17) and (5.18) and integrating. As for the S2 micro problem, we argue that the flux of h_0 in outer 2 can be approximated by (5.64). Figures 4.8(d), 4.10(c) and table 4.2 suggest that the kinetic conditions are not a constant. The flux of h_0 in outer 2 is plotted in figure 5.6, suggesting that the assumption (5.64) is reasonable for D2.

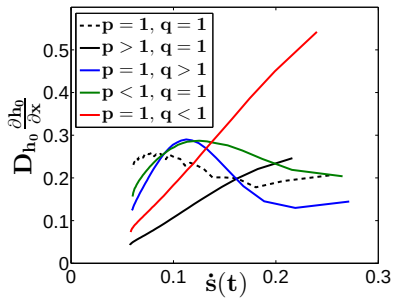

Figure 5.6: *Dependance of $D_{h_0} \frac{\partial h_0(s^+,t)}{\partial x}$ on $\dot{s}$ for the regime $\delta = O(\epsilon)$ extracted from solving the full reaction-diffusion system with two rapidly varying diffusion coefficients. The derivative was calculated using central difference around the point $x = s(t) + \epsilon^2$ which is where the outer 2 region starts.*

Rescaling as follows

$$\bar{c}_0 = \dot{s}^{\frac{2}{p+1}} C, \quad \bar{h}_0 = \dot{s}^{\frac{2}{q+1}} H, \quad \bar{x} = \dot{s}^{\frac{(1-p)(q+1)-2q(p+1)}{(q+1)(p+1)}} X,$$

yields

$$\left(\nu_1 \frac{C_X}{H^q} \right)_X = C^p H^q, \quad \nu_1 \frac{C_X}{H^q} - \nu_2 \frac{H_X}{C^p} = -A,$$

with

$$\text{as } X \to +\infty \quad C \to 0, \quad H \to b, \quad \text{as } X \to -\infty \quad C \to a.$$

Thus, the kinetic conditions can be approximated by the power laws

$$\Phi_1 \sim a * \dot{s}^{\frac{2}{p+1}} \quad \text{and} \quad \Phi_2 \sim b * \dot{s}^{\frac{2}{q+1}}, \tag{5.66}$$

where a, b are constants. These results can be compared with the ones extracted from the full reaction-diffusion system (2.6)-(2.10) displayed in tables 4.1 and 4.2. For D1, the agreement is excellent. For D2, similar behaviours are seen but the large ϵ value and the consideration of all the computed $\dot{s}(t)$ in tables 4.1 and 4.2 instead of just $\dot{s} \ll 1$ make the values of the coefficients in (3.44) differ slightly.

This chapter shows that all the micro problems are well defined and that they can be solved numerically. Further, the main result here is the analytical approximation of the kinetic conditions for large time. The concentration of CO_2 on the free boundary, $\Phi_1(\dot{s})$, given by the micro problems, has the general profile $\Phi_1 \sim \dot{s}^{\frac{2}{p+1}}$, independent of q. Similarly, for the $Ca(OH)_2$ we obtain $\Phi_2 \sim \dot{s}^{\frac{2}{q+1}}$. We are now in a position to consider the generalised Stefan problems. Returning to the role of the micro problems in the broader picture, these are necessary to obtain the concentrations of CO_2 and $Ca(OH)_2$ at the reaction zone. It is worth mentioning that these concentrations can also be obtained from the solution to the full reaction-diffusion system (2.6) to (2.10) as shown in sections 3.2.4 and 4.2.4. When solving the macro problems later, both approaches will be taken and compared.

Chapter 6

The Generalised Stefan Problems

We are now in a position to recap the full scope of all the results obtained in chapters 2, 3 and 4, with the assurance, from chapter 5, that the micro problems in the latter two chapters are well defined. First, the derived one- and two-phase micro-macro problems are summarised. Large and small time asymptotics are performed and finally we apply the method of lines to solve the Stefan problems numerically.

6.1 The derived micro-macro problems

There are two distinct asymptotic regimes, namely $\delta \ll \epsilon$ and $\delta = O(\epsilon)$. For $\delta \ll \epsilon$, we obtain one-phase problems, while for $\delta = O(\epsilon)$, we have two-phase problems. The type of diffusion coefficients chosen will impact on the interface conditions. This section considers these two different types of Stefan problems separately.

The one-phase problem

In the case $\delta \ll \epsilon$ we obtain the one-phase problem:

$$\text{in } 0 < x < s(t),\ t > 0 \qquad \mu \frac{\partial c_0}{\partial t} = \frac{\partial}{\partial x}\left(D_{c_0} \frac{\partial c_0}{\partial x} \right), \tag{6.1}$$

$$\text{on } x = 0 \qquad -D_{c_0} \frac{\partial c_0}{\partial x} = H(1 - c_0), \tag{6.2}$$

$$\text{on } x = s(t) \qquad c_0 = \Phi_1(\dot{s}), \quad -D_{c_0} \frac{\partial c_0}{\partial x} = \dot{s}(\mu c_0 + h_i(s)), \tag{6.3}$$

$$\text{at } t = 0 \qquad c = c_i \text{ for } 0 \le x \le s_0, \quad s = s_0, \tag{6.4}$$

with $h_0 = h_i$ for $s(t) \le x \le 1$.

The value of Φ_1 depends on the behaviour of the diffusion coefficients as follows:

- For slowly varying CO_2 and $Ca(OH)_2$ diffusivities, chapter 2 gives $\Phi_1 = 0$.
- For a rapidly varying CO_2 diffusivity only, chapter 3 shows that Φ_1 is given as the solution to a micro problem which depends upon the size of δ relative to ϵ^2.

In particular, for $\delta \leq \epsilon^2$, Φ_1 is determined by S1a, (5.1)-(5.4), and for $\epsilon^2 \ll \delta \ll \epsilon$ its solution is given by S1b, (5.5)-(5.8).

- When both diffusivities vary rapidly, chapter 4, Φ_1 is now determined by the solution of the micro problem denoted as D1, (5.13)-(5.16).

The two-phase problem

In the case $\delta = O(\epsilon)$, we obtain the two-phase problem:

$$\text{in } 0 < x < s(t),\ t > 0 \qquad \mu \frac{\partial c_0}{\partial t} = \frac{\partial}{\partial x}\left(D_{c_0} \frac{\partial c_0}{\partial x} \right), \tag{6.5}$$

$$\text{in } s(t) < x < 1,\ t > 0 \qquad \frac{\partial h_0}{\partial t} = \frac{\partial}{\partial x}\left(D_{h_0} \frac{\partial h_0}{\partial x} \right), \tag{6.6}$$

$$\text{on } x = 0 \qquad -D_{c_0} \frac{\partial c_0}{\partial x} = H(1 - c_0), \tag{6.7}$$

$$\text{on } x = s(t) \qquad c_0 = \Phi_1(\dot{s}), \quad h_0 = \Phi_2(\dot{s}), \tag{6.8}$$

$$-D_{c_0} \frac{\partial c_0}{\partial x} - D_{h_0} \frac{\partial h_0}{\partial x} = \dot{s}(\mu c_0 + h_0), \tag{6.9}$$

$$\text{on } x = 1 \qquad D_{h_0} \frac{\partial h_0}{\partial x} = 0, \tag{6.10}$$

$$\text{at } t = t_0 \qquad c_0 = C_i \text{ for } 0 \leq x \leq s_0, \quad h_0 = H_i \text{ for } s_0 \leq x \leq 1, \tag{6.11}$$

$$s = s_0. \tag{6.12}$$

We recall that t_0 is the time for which the reaction zone remains at the surface (stage I carbonation) and begins to ingress into the concrete. C_i and H_i denote the resulting concentration profiles at this time, which differ from their initial values c_i, h_i respectively, except for when both diffusivities are rapidly varying. In the latter case there is no stage I carbonation and so $t_0 = 0$, $C_i = c_i$ and $H_i = h_i$.

The values of Φ_1 and Φ_2 depend upon the behaviour of the diffusion coefficients as follows:

- For slowly varying CO_2 and $Ca(OH)_2$ diffusivities, chapter 2 implies that $\Phi_1 = 0 = \Phi_2$.
- For a single rapidly varying CO_2 diffusivity, chapter 3, $\Phi_2 = 0$ and Φ_1 is determined by the micro problem S2, (5.9)-(5.12).
- For two rapidly varying diffusivities, chapter 4 gives that Φ_1 and Φ_2 are determined by the micro problem D2, (5.17)-(5.20).

6.2 Large and small time behaviour

For the one-phase problem (6.1)-(6.4) and the two-phase problem (6.5)-(6.12), the parameter $1/\mu$ represents the Stefan number. Relevant to the concrete situation is the

large Stefan number limit $\mu \to 0$. In this limit, the problems become quasi-steady due to the now disparate time-scales of diffusion and reaction. In this section we solve these quasi steady problems in the two asymptotic regimes $t \gg 1$, large time behaviour, and $t \ll 1$, small time behaviour, for $p = q = 1$. A comparison of their solutions to the numerical results of the reaction-diffusion system (2.6)-(2.10) is also given.

6.2.1 One-phase problem

The asymptotics of this problem for power law forms of $\Phi_1 = \dot{s}^n$ are described in [21, 23]. Taking the limit $\mu \to 0$, after an initial transient regime $t = O(\mu)$ in which the interface is stationary at leading order, an explicit solution for the quasi-steady problem $t > O(\mu)$ when $D_{c_0} \equiv 1$ is

$$c_0 = \Phi_1 + \frac{(1-\Phi_1)(s-x)}{\left(\frac{1}{H}+s\right)}, \tag{6.13}$$

with the interface $s(t)$ determined by the solution of

$$h_i(s)\left(\frac{1}{H}+s\right)\dot{s} + \Phi_1(\dot{s}) = 1, \qquad s(0) = s_0. \tag{6.14}$$

We now investigate all the possible forms of Φ_1.

Slowly varying diffusivities ($D_c = O(1)$, $D_h = O(1)$)

Take $\Phi_1 = 0$ and so the interface (6.14) becomes

$$s(t) = \frac{1}{H}\left(-1 + \sqrt{1 + \frac{2H^2}{h_i}t}\right). \tag{6.15}$$

For $t \to \infty$, the large time behaviour of the interface is

$$s \sim \sqrt{\frac{2t}{h_i}} - \frac{1}{H}, \tag{6.16}$$

and for completion

$$c_0 \sim 1 - \left(\frac{1}{H} - x\right)\sqrt{\frac{h_i}{2t}}.$$

Figure 6.1(a) shows the plot of the interface for this asymptotic regime $t \gg 1$ (6.16) along with the numerically calculated interface obtained by solving (2.6)-(2.10) in COMSOL Multiphysics. The initial data and parameter values taken for all the simulations in this chapter are

$$h_i = 1, \quad c_i = 0 \quad \text{for } 0 \le x \le X, \quad \mu = 10^{-3}, \quad H = 1, \quad p = q = 1. \tag{6.17}$$

The agreement in figure 6.1(a) is excellent but in order to get a more in depth com-

parison we use the interactive curve fitting toolbox in MATLAB. First, we note that substituting the parameter values used in the numerical simulations i.e. $H = h_i = 1$, into (6.16) yields $s(t) \sim \sqrt{2t} - 1$. We now plot the numerical simulation results and fit the custom equation

$$f(t) = a\sqrt{t} + b. \tag{6.18}$$

The coefficients calculated with 95% confident bounds are

$$a = 1.412\ (1.412, 1.412), \quad b = -0.9869\ (-0.99, -0.9839).$$

This fit has a sum of squares due to error (SSE) value of 1.55×10^{-4} and an adjusted R-square statistics of 1. Recall that, for the SSE fit, a value closer to zero indicates a better fit, while for the adjusted R-square statistics, we look for a value close to 1.

For $t \to 0$, we Taylor expand (6.15) to obtain the small time behaviour

$$s \sim \frac{H}{h_i}t - \frac{H^3}{2h_i^2}t^2 \quad \text{and} \quad c_0 \sim \frac{H^2}{h_i}t - x.$$

More care is needed now for the comparison of the small time behaviour. The numerical simulations of the full reaction-diffusion system and the above analytical results with the parameter values (6.17) are shown in figure 6.2(a). The analytical approximation displays the same qualitative behaviour but the quantitative comparison is not ideal. Fitting a curve of the form $f(t) = t + at^2$, where the coefficient of t has been imposed, in the curve fitting toolbox for the COMSOL simulations gives $a = -0.5206$ with SSE$= 1.78 \times 10^{-2}$ and adjusted R-square=0.9747.

One and two rapidly varying diffusivities ($D_c = O(\epsilon^2)$, $D_h = O(1)$ and $D_c = O(\epsilon^2)$, $D_h = O(\delta^2)$ respectively)

From the simulations in chapters 3 and 4 (figures 3.8(c) and 4.7(c)) or the results of the micro problems S1a, S1b and D1 in chapter 5 (figures 5.1 and 5.3) we see that

$$\Phi_1 \sim \dot{s}.$$

In this case (6.14) gives

$$s(t) = \frac{(H + h_i)}{Hh_i}\left(-1 + \sqrt{(}1 + \frac{2H^2h_i}{(H + h_i)^2}t)\right). \tag{6.19}$$

The large time behaviour $t \to \infty$ of the interface and the concentration of CO_2 is

$$s \sim \sqrt{\frac{2t}{h_i}} - \frac{H + h_i}{Hh_i}, \quad \text{and} \quad c_0 \sim 1 + \frac{1}{\sqrt{2h_it}} - \frac{h_i}{2\sqrt{t} - 1}x. \tag{6.20}$$

The comparisons between the numerical simulations and the approximation of the interface $s(t) \sim \sqrt{2t} - 2$, i.e. (6.20) with $H = h_i = 1$, for one and two rapidly vary-

ing diffusion coefficients are shown in figures 6.1(b) and 6.1(c) respectively. For one rapidly varying diffusion coefficient, the custom equation fit (6.18) gives coefficients with 95% confident bounds of $a = 1.401$ $(1.4, 1.401)$ and $b = -1.788$ $(-1.792, -1.783)$, $SSE = 4.197 \times 10^{-4}$ and adjusted R-square= 1. For two rapidly varying diffusivities the coefficients with 95% confident bounds are $a = 1.408$ $(1.408, 1.408)$ and $b = -1.814$ $(-1.817, -1.812)$, $SSE = 9.513 \times 10^{-5}$ and adjusted R-square= 1.

The small time behaviour $t \to 0$ is

$$s \sim \frac{H}{h_i + H} t - \frac{H^3 h_i}{2(h_i + H)^3} t^2 \quad \text{and} \quad c_0 \sim \frac{H}{h_i + H} + \frac{H^2 h_i}{(h_i + H)^3} t - \frac{H h_i}{h_i + H} x.$$

Figure 6.2(b) and 6.2(c) shows the comparison of the analytical approximation $s(t) \sim \frac{1}{2}t - \frac{1}{16}t^2$ with the numerical results for one and two rapidly varying diffusion coefficients respectively.

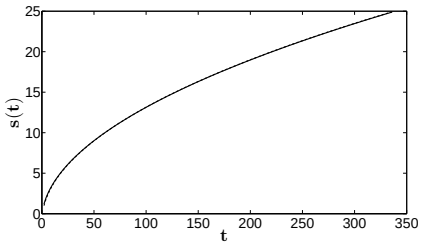

(a) Slowly varying - Here $\epsilon = 10^{-2}$ and the large time approximation of the interface is $s(t) \sim \sqrt{2t} - 1$.

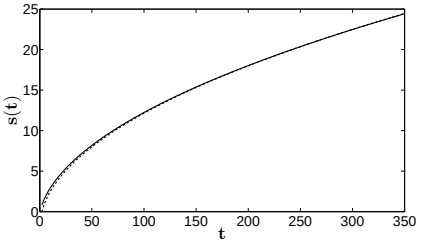

(b) One rapidly varying - Here $\epsilon = 10^{-1}$ and the large time approximation of the interface is $s(t) \sim \sqrt{2t} - 2$.

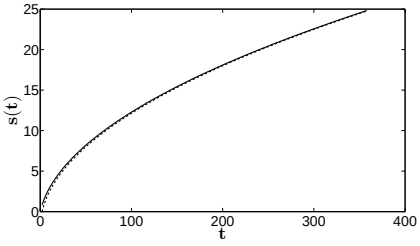

(c) Two rapidly varying - Here $\epsilon = 10^{-1}$ and the large time approximation of the interface is $s(t) \sim \sqrt{2t} - 2$.

Figure 6.1: *Large time behaviour: Comparison of the COMSOL Multiphysics simulations for the full reaction-diffusion system* (2.6)-(2.10) *on the domain* $0 \leq x \leq 25$ *with* $\delta = \epsilon^2$, ϵ *as stated in each subfigure and* $h_i = H = 1$, $\mu = 10^{-3}$, $\nu_1 = \nu_2 = 1$ *(solid line) and the analytical large time behaviour for the one-phase Stefan problems (dotted line).*

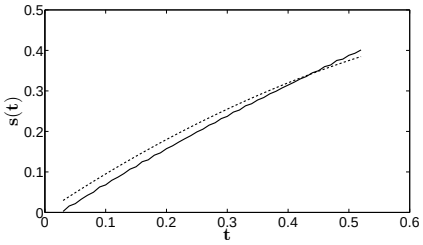

(a) Slowly varying - Here $\epsilon = 10^{-2}$ and the small time approximation of the interface is $s(t) \sim t - \frac{1}{2}t^2$.

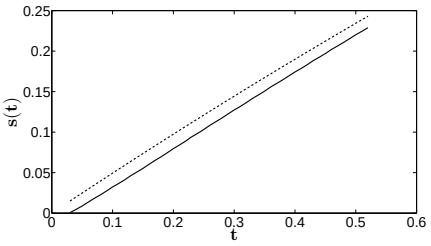

(b) One rapidly varying - Here $\epsilon = 10^{-1}$ and the small time approximation of the interface is $s(t) \sim \frac{1}{2}t - \frac{1}{16}t^2$.

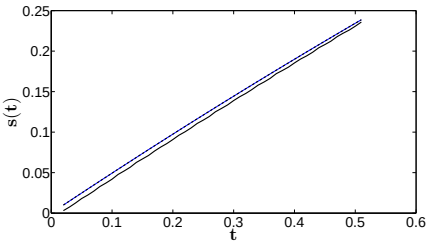

(c) Two rapidly varying - Here $\epsilon = 10^{-1}$ and the small time approximation of the interface is $s(t) \sim \frac{1}{2}t - \frac{1}{16}t^2$.

Figure 6.2: *Small time behaviour: Comparison of the COMSOL Multiphysics simulations for the full reaction-diffusion system* (2.6)-(2.10) *on the domain* $0 \leq x \leq 25$ *with* $\delta = \epsilon^2$, ϵ *as stated in each subfigure and* $h_i = H = 1$, $\mu = 10^{-3}$, $\nu_1 = \nu_2 = 1$ *(solid line) and the analytical small time behaviour for the one-phase Stefan problems (dotted line).*

6.2.2 Two-phase problem

In the quasi-steady CO_2 limit $\mu \to 0$, we again have solution (6.13) in the case $D_{c_0} \equiv 1$. This gives the non-standard Stefan problem for the $Ca(OH)_2$ as

$$\text{in } s(t) < x < 1, t > 0 \qquad \frac{\partial h_0}{\partial t} = \frac{\partial}{\partial x}\left(D_{h_0}\frac{\partial h_0}{\partial x}\right), \tag{6.21}$$

$$\text{on } x = 1 \qquad D_{h_0}\frac{\partial h_0}{\partial x} = 0, \tag{6.22}$$

$$\text{on } x = s(t) \qquad \begin{cases} h_0 &= \Phi_2(\dot{s}), \\ D_{h_0}\frac{\partial h_0}{\partial x} &= \frac{1}{\left(\frac{1}{H}+s\right)} - \frac{\Phi_1(\dot{s})}{\left(\frac{1}{H}+s\right)} - \dot{s}\Phi_2(\dot{s}), \end{cases} \tag{6.23}$$

$$\text{at } t = t_0 \qquad h_0 = H_i \text{ for } s_0 \le x \le 1, \quad s = s_0. \tag{6.24}$$

This problem in the slowly varying diffusivity case when $\Phi_1 = 0 = \Phi_2$ has been considered by [26] in the context of binary alloy oxidation. However, the more general statement has not received attention. Here we will consider $\Phi_1 = 0 = \Phi_2$, $\Phi_1 \neq 0$, $\Phi_2 = 0$ and $\Phi_1 \neq 0$, $\Phi_2 \neq 0$. These three cases correspond to the slowly, one rapidly varying and two rapidly varying scenarios respectively. The actual forms taken for Φ_1 and Φ_2 will be introduced and justified later on. The ideas, steps and methods are quite similar in all three cases. Therefore, we treat only the slowly varying case in detail.

As in the previous section we will also compare the derived approximations with numerical simulations of (2.6)-(2.10). However, for the small time behaviour, the appearance of a stage I carbonation makes it even more difficult to compare the asymptotic behaviour with the numerical one. In order to do this comparison, much more care is needed between the transition from Stage I and Stage II. For example, further investigation on the definition of the interface taken (2.13) is needed. Actually, the small time behaviour is of small practical sense. It is the large time behaviour that has most significance. However, the mathematics involved in obtaining the small time approximations are interesting. For this reasons, we perform the analysis for small and large time behaviour but only compare the results to numerical data in the large time scenario.

6.2.2.1 Slowly varying diffusivity

We start with the simplest of all the cases. This has been considered in [26], where the large and small time and parameter behaviour is derived using Laplace/Fourier transforms. Here, we only look at the large and small time behaviour and use asymptotic expansions instead to determine the structure of the interface as well as the concentration of calcium hydroxide.

Consider the semi-infinite version of (6.21)-(6.24) with $\Phi_1 = 0 = \Phi_2$. Recall that

there is now a stage I carbonation and so $t_0 \neq 0$ in (6.4). To simplify the analysis we perform transformations such that the problem starts at zero and fix the domain. With this in mind we introduce the new variables

$$\tau = \frac{1}{D_{h_0}}(t - t_0), \quad y = \frac{1}{D_{h_0}}(x - s(t)). \tag{6.25}$$

The problem we will be working on is now,

$$\text{In } 0 < y < \infty,\ \tau > 0 \qquad \frac{\partial h_0}{\partial \tau} = \frac{\partial^2 h_0}{\partial y^2} + \frac{\dot{s}}{D_{h_0}}\frac{\partial h_0}{\partial y}, \tag{6.26}$$

$$\text{on } y = 0, \qquad h_0 = 0 \quad \frac{\partial h_0}{\partial y} = \frac{1}{\frac{1}{H} + s}, \tag{6.27}$$

$$\text{as } y \to \infty \qquad h_0 \to h_i \tag{6.28}$$

$$\text{at } \tau = 0, \qquad h_0 = H_i \text{ for } 0 \leq y \leq \infty, \quad s = 0. \tag{6.29}$$

Large time asymptotics

To analyse the large time behaviour $\tau \to \infty$, introduce the artificial parameter $\tau = \frac{T}{\theta}$, $\theta \ll 1$, $T = O(1)$. Further, use the nontrivial balance $y = \frac{Y}{\theta^{1/2}}$ and $s = \frac{L}{\theta^{1/2}}$ and consider the asymptotic expansions

$$h_0 = h^0(Y,T) + \theta^{1/2}h^1(Y,T) + \theta h^2(Y,T), \quad L = L^0(T) + \theta^{1/2}L^1(T) + \theta L^2(T). \tag{6.30}$$

We substitute the expansions (6.30) into the transformed problem (6.26)-(6.29) and equate the powers of θ. The $O(1)$ terms yield the leading order problem

$$\frac{\partial h^0}{\partial T} = \frac{\partial^2 h^0}{\partial Y^2} + \frac{1}{D_{h_0}}\frac{\mathrm{d}L^0}{\mathrm{d}T}\frac{\partial h^0}{\partial Y}, \tag{6.31}$$

$$\text{on } Y = 0 \qquad h^0 = 0, \quad \frac{\partial h^0}{\partial Y} = \frac{1}{L^0}, \tag{6.32}$$

$$\text{as } Y \to \infty \qquad h^0 = h_i. \tag{6.33}$$

The above problem is invariant under the transformations

$$Y = \alpha\bar{Y}, \quad T = \alpha^2\bar{T}, \quad L^0 = \alpha\bar{L}^0, \quad h^0 = \bar{h}^0.$$

This suggests the similarity solution

$$h^0 = f_0(\eta) \quad \eta = YT^{-1/2}, \quad L^0 = \alpha_0 T^{1/2},$$

for some α_0 to be determined. Hence, solving the leading order problem has been

reduced to solving the ordinary differential equation

$$f_0'' + \frac{1}{2}\left(\eta + \frac{\alpha_0}{D_{h_0}}\right) f_0' = 0, \tag{6.34}$$

where $' = \frac{\mathrm{d}}{\mathrm{d}\eta}$ and subject to the boundary conditions

$$f_0(0) = 0, \quad f_0'(0) = \frac{1}{\alpha_0}, \quad f_0(\infty) = h_i. \tag{6.35}$$

Integrating (6.34) and using the boundary conditions (6.35) we obtain the similarity solution

$$f_0 = \frac{1}{\alpha_0}\int_0^\eta \exp\left(-\frac{1}{2}\left(\frac{t^2}{2} + \frac{\alpha_0 t}{D_{h_0}}\right)\right)\mathrm{d}t, \tag{6.36}$$

where α_0 is given by the transcendental equation

$$\alpha_0 = \frac{1}{h_i}\int_0^\infty \exp\left(-\frac{1}{2}\left(\frac{t^2}{2} + \frac{\alpha_0 t}{D_{h_0}}\right)\right)\mathrm{d}t. \tag{6.37}$$

Equating the $O(\theta^{1/2})$ terms in (6.26)-(6.29) after substituting (6.30) gives

$$\frac{\partial h^1}{\partial T} = \frac{\partial^2 h^1}{\partial Y^2} + \frac{1}{D_{h_0}}\frac{\mathrm{d}L^0}{\mathrm{d}T}\frac{\partial h^1}{\partial Y}, \tag{6.38}$$

$$\text{on } Y = 0 \qquad h^1 = 0, \quad \frac{\partial h^1}{\partial Y} = -\frac{(L^1 + \frac{1}{H})}{L^0}\frac{\partial h^0}{\partial Y}, \tag{6.39}$$

$$\text{as } Y \to \infty \qquad h^1 = 0. \tag{6.40}$$

This problem has the similarity solution

$$h^1 = T^{-1/2} f_1(\eta) \quad \eta = YT^{-1/2}, \quad L^1 = \alpha_1,$$

for some constant α_1 to be determined. The ordinary differential equation obtained now is

$$f_1'' + \frac{1}{2}\left(\eta + \frac{\alpha_0}{D_{h_0}}\right) f_1' + \frac{1}{2} f_1 = 0, \tag{6.41}$$

with the boundary conditions

$$f_1(0) = 0, \quad f_1'(0) = -\frac{\alpha_1 + \frac{1}{H}}{\alpha_0^2}, \quad f_1(\infty) = 0. \tag{6.42}$$

Solving (6.41) gives

$$f_1(\eta) = \left(C_1 + C_2 \mathrm{erf}\left(\frac{1}{2}\left(\eta + \frac{\alpha_0}{D_{h_0}}\right) i\right)\right) \exp\left(-\frac{1}{2}\left(\frac{\eta^2}{2} + \frac{\alpha_0 \eta}{D_{h_0}}\right)\right),$$

where C_1 and C_2 are constants of integration to be determined using the boundary

conditions (6.42). In particular, the boundary conditions on $\eta = 0$ give

$$C_1 = -C_2 \text{erf}\left(\frac{\alpha_0 i}{2D_{h_0}}\right) \text{ with } C_2 = -\frac{\sqrt{\pi}(\alpha_1 + \frac{1}{H})}{\alpha_0^2 i} \exp\left(-\left(\frac{\alpha_0}{2D_{h_0}}\right)^2\right).$$

It remains to determine α_1. For this, we consider the asymptotic expansion of f_1 as $\eta \to \infty$

$$f_1(\eta) \sim \frac{2iC_2}{\sqrt{\pi}} \exp\left(\frac{\alpha_0^2}{4D_{h_0}^2}\right) \frac{1}{\eta}.$$

Hence, $f_1 \to 0$ algebraically as $\eta \to \infty$. The third condition in (6.42) is not sufficient to conclude the value of α_1. We need to know the rate at which the solution tends to zero. To this aim we consider the $\tau = O(1)$ problem (6.26)-(6.29) in the $y \to \infty$ limit and seek a WKBJ expansion. Doing this and putting back into (Y, T) variables, we see that

$$h_0 \sim h_i - h_i \exp\left(-\frac{Y^2}{4T}\right), \tag{6.43}$$

i.e. h_0 tends to h_i with and exponential corrector and not an algebraic one. Hence $C_1 = 0 = C_2$. Further,

$$f_1 = 0 \quad \text{and} \quad \alpha_1 = -\frac{1}{H}. \tag{6.44}$$

Before moving on it is worth mentioning that to obtain (6.43) we make use of the initial condition of $Ca(OH)_2$. Recall that this is the leading order concentration of $Ca(OH)_2$ at the end of stage I carbonation and we derive this in Appendix B.1. For the semi-infinite case, we use Laplace transforms to obtain (B.10). From there we can extract the concentration profile H_i for h_0 by denoting $t = t_0$ to be the time at which the leading order concentration of $Ca(OH)_2$ falls to zero at the reaction zone in stage I leaving $H_i = h_0(x, t_0)$. However, this expression is difficult to work with and so instead, an equivalent but new format for the initial condition is derived, directly from the outer 2 region for Stage I (B.5)-(B.8). The solution to this problem has the form $h_0 = h_i - A$ and so substituting this ansatz into (B.5)-(B.8) leaves a problem for A that has a similarity solution. The initial condition of $Ca(OH)_2$ is now

$$h_0(0, y) = h_{ic}(y) = h_i + Hy\text{erfc}\left(\frac{Hy}{h_i\sqrt{\pi}}\right) - h_i \exp\left(-\frac{H^2y^2}{h_i^2\pi}\right). \tag{6.45}$$

This is the initial condition used in the workout for (6.43) and the one that will be used for the remainder of this section. This initial condition is much easier to work with and for future reference we state the derivatives with respect to y

$$\frac{\mathrm{d}h_{ic}}{\mathrm{d}y} = H\text{erfc}\left(\frac{Hy}{\sqrt{\pi}h_i}\right), \quad \frac{\mathrm{d}^2h_{ic}}{\mathrm{d}y^2} = -\frac{2H^2}{\pi h_i} \exp\left(-\frac{H^2y^2}{\pi h_i^2}\right),$$

$$\frac{\mathrm{d}^3 h_{ic}}{\mathrm{d}y^3} = \frac{4H^4 y}{\pi^2 h_i^3}\exp\left(-\frac{H^2 y^2}{\pi h_i^2}\right).$$

The results (6.44) obtained for the $O(\theta^{1/2})$ motivates going a step further and looking for the next order term $h^2(Y,T)$. Hence, consider the $O(\theta)$ terms from (6.26)-(6.29) when expansions (6.30) are substituted in

$$\frac{\partial h^2}{\partial T} = \frac{\partial^2 h^2}{\partial Y^2} + \frac{1}{D_{h_0}}\left(\frac{\mathrm{d}L^0}{\mathrm{d}t}\frac{\partial h^2}{\partial Y} + \frac{\mathrm{d}L^2}{\mathrm{d}t}\frac{\partial h^0}{\partial Y}\right), \tag{6.46}$$

$$\text{on } Y = 0 \qquad h^2 = 0, \quad \frac{\partial h^2}{\partial Y} = -\frac{L^2}{L^0}\frac{\partial h^0}{\partial Y}, \tag{6.47}$$

$$\text{as } Y \to \infty \qquad h^2 = 0. \tag{6.48}$$

This problem is invariant under the transformations

$$Y = \alpha\bar{Y}, \quad T = \alpha^2\bar{T}, \quad L^2 = \alpha^{\sigma+1}\bar{L}^2, \quad h^2 = \alpha^\sigma \bar{h}^2.$$

To determine the value of σ, consider either the initial condition in the limit $y \to \infty$ or the expansion for L. Either of these methods give that $\sigma = -2$ and hence (6.46)-(6.48) has the similarity solution

$$h_2 = T^{-1} f_2(\eta) \quad \eta = YT^{-1/2}, \quad L^2 = \alpha_2 T^{-1/2},$$

for some constant α_2. This results in the following ordinary differential equation

$$f_2'' + \frac{1}{2}\left(\eta + \frac{\alpha_0}{D_{h_0}}\right) f_2' + f_2 = -\frac{\alpha_2}{2\alpha_0 D_{h_0}}\exp\left(-\frac{1}{2}\left(\frac{\eta^2}{2} + \frac{\alpha_0\eta}{D_{h_0}}\right)\right), \tag{6.49}$$

with boundary conditions

$$f_2(0) = 0, \quad f_2'(0) = -\frac{\alpha_2}{\alpha_0}, \quad f_2(\infty) = 0. \tag{6.50}$$

Integrating (6.49) we obtain

$$\begin{aligned} f_2(\eta) =& C_1(D_{h_0}\eta + \alpha_0)\exp\left(-\frac{1}{2}\left(\frac{\eta^2}{2} + \frac{\alpha_0\eta}{D_{h_0}}\right)\right) \\ &+ C_2\left(2D_{h_0} + \sqrt{\pi}\,(D_{h_0}\eta + \alpha_0)\,i\mathrm{erf}\left(\frac{1}{2}\left(\eta + \frac{\alpha_0}{D_{h_0}}\right)i\right)\exp\left(-\frac{1}{4}\left(\eta + \frac{\alpha_0}{D_{h_0}}\right)^2\right)\right) \\ &- \frac{\alpha_2}{\alpha_0^2}\exp\left(-\frac{1}{2}\left(\frac{\eta^2}{2} + \frac{\alpha_0\eta}{D_{h_0}}\right)\right)\eta. \end{aligned}$$

The boundary conditions (6.50) at $\eta = 0$ imply that $C_1 = 0 = C_2$ and so

$$f_2(\eta) = -\frac{\alpha_2}{\alpha_0^2}\exp\left(-\frac{1}{2}\left(\frac{\eta^2}{2} + \frac{\alpha_0\eta}{D_{h_0}}\right)\right)\eta. \tag{6.51}$$

It still remains to determine α_2. Note that adding a constant to the leading order problem (6.31)-(6.33) does not change it but produces an extra term of $O(T^{-1/2})$. Hence, it is not possible to find the value of α_2 since there is an influence from the leading order problem. In other words, L^2 can only be determined up to a constant, which in this case we denote as α_2. A possibility is to numerically solve the full transformed problem (6.26)-(6.29) and pick up this constant for large time.

Collecting all the results we have that for $\tau \to \infty$

$$s(\tau) \sim \alpha_0\sqrt{\tau} - \frac{1}{H} + \alpha_2\tau^{-1/2}, \tag{6.52}$$

and

$$h_0(y,\tau) = \frac{1}{\alpha_0}\int_0^{\frac{y}{\sqrt{\tau}}} \exp\left(-\frac{1}{2}\left(\frac{t^2}{2} + \frac{\alpha_0 t}{D_{h_0}}\right)\right)\mathrm{d}t - \frac{\alpha_2}{\alpha_0^2}\exp\left(-\frac{1}{2}\left(\frac{y^2}{2\tau} + \frac{\alpha_0 y}{D_{h_0}\sqrt{\tau}}\right)\right)\frac{y}{\tau^{3/2}},$$

where α_0 is as in (6.37) and α_2 remains undetermined.

It is now of interest to compare (6.52) with the numerical results achieved in COMSOL, as done for the one-phase Stefan problem, and to obtain a numerical approximation to the value of α_2. The initial and parameter values chosen are as in (6.17). First we evaluate α_0, completing the square in (6.37) yields

$$\alpha_0\exp\left(-\frac{\alpha_0^2}{4}\right) = \frac{1}{h_i}\int_0^{\infty}\exp\left(-\frac{(t+\alpha_0)^2}{4}\right)\mathrm{d}t.$$

Performing the change of variables $z = \frac{t+\alpha_0}{2}$ we obtain

$$\alpha_0\exp\left(-\frac{\alpha_0^2}{4}\right) = \frac{\sqrt{\pi}}{h_i}\mathrm{erfc}\left(\frac{\alpha_0}{2}\right).$$

From [1], we may approximate the error function to obtain

$$\alpha_0 = \frac{\sqrt{\pi}}{h_i}\left(\frac{a_1}{1+p\alpha_0/2} + \frac{a_2}{(1+p\alpha_0/2)^2} + \frac{a_3}{(1+p\alpha_0/2)^3} + \frac{a_4}{(1+p\alpha_0/2)^4} + \frac{a_5}{(1+p\alpha_0/2)^5}\right).$$

Solving for α_0 yields $\alpha_0 = 1.063193548$ and so (6.52) gives

$$s(\tau) \sim 1.0632\sqrt{\tau} - 1 + \alpha_2\tau^{-1/2}. \tag{6.53}$$

Consider the first two terms only. Implementing the custom equation

$$f(t) = a\sqrt{t - \frac{\pi}{4}} + b, \tag{6.54}$$

into the interactive curve fitting toolbox in MATLAB with the COMSOL Multiphysics simulation gives $a = 1.073$ $(1.069, 1.077)$, $b = -0.9633$ $(-1.024, -0.9022)$, SSE= 1.688×10^{-2} and adjusted R-square= 0.9999. To achieve a value for α_2 we plug in the whole approximation (6.53) in the curve fitting toolbox and we obtain

$$\alpha_2 = 2.998\ (2.806, 3.189).$$

Figure 6.3(a) shows the plots for the numerical simulation, and the two and three term expansions of the interface (6.53). Although the two term expansion shows a good qualitative agreement we see that the three term expansion approximates the numerical solution better.

Small time asymptotics

Let $\tau = \theta T$, $\theta \ll 1$ in (6.26)-(6.29). Consider the $T = O(1)$ and substitute the nontrivial balance $s = \theta L$, then

$$\frac{\partial h_0}{\partial T} = \theta \frac{\partial^2 h_0}{\partial y^2} + \frac{\theta}{D_{h_0}} \frac{\mathrm{d}L}{\mathrm{d}T} \frac{\partial h_0}{\partial y}, \tag{6.55}$$

$$\text{on } y = 0 \qquad h_0 = 0, \quad \left(\frac{1}{H} + \theta L\right) \frac{\partial h_0}{\partial y} = 1, \tag{6.56}$$

$$\text{as } y \to \infty \qquad h_0 \to h_i, \tag{6.57}$$

$$\text{at } T = 0 \qquad h_0 = h_{ic}(y), \quad L = 0. \tag{6.58}$$

This problem has a boundary layer around $y = 0$. Consider first the outer expansions

$$h_0 \sim h^0 + \theta^{1/2} h^{1/2} + \theta h^1 + \theta^{3/2} h^{3/2}, \quad L \sim L^0 + \theta^{1/2} L^{1/2}. \tag{6.59}$$

Substituting into (6.55) and equating powers of θ we obtain,

$$\theta^0 : \qquad h^0 = h_{ic}(y), \tag{6.60}$$

$$\theta^{1/2} : \qquad h^{1/2} = 0, \tag{6.61}$$

$$\theta : \qquad \frac{\partial h^1}{\partial T} = \frac{\partial^2 h^0}{\partial y^2} + \frac{1}{D_{h_0}} \frac{\mathrm{d}L^0}{\mathrm{d}T} \frac{\partial h^0}{\partial y}, \tag{6.62}$$

$$\theta^{3/2} : \qquad \frac{\partial h^{3/2}}{\partial T} = \frac{1}{D_{h_0}} \frac{\mathrm{d}L^{1/2}}{\mathrm{d}T} \frac{\partial h^0}{\partial y}. \tag{6.63}$$

We now consider the boundary layer $y = \theta^{1/2} Y$ and rescale $h_0 = \theta^{1/2} A$. We

substitute the inner expansions

$$A \sim A_0 + \theta^{1/2} A_{1/2} + \theta A_1 \tag{6.64}$$

into (6.55)-(6.58) and equate powers of θ.

At $O(\theta^0)$:

$$\frac{\partial A_0}{\partial T} = \frac{\partial^2 A_0}{\partial Y^2}, \tag{6.65}$$

$$\text{on } Y = 0 \quad A_0 = 0, \quad \frac{\partial A_0}{\partial Y} = H. \tag{6.66}$$

This problem has the similarity solution

$$A_0(Y,T) = HY. \tag{6.67}$$

At $O(\theta^{1/2})$:

$$\frac{\partial A_{1/2}}{\partial T} = \frac{\partial^2 A_{1/2}}{\partial Y^2} + \frac{H}{D_{h_0}} \frac{\mathrm{d}L^0}{\mathrm{d}T}, \tag{6.68}$$

$$\text{on } Y = 0 \quad A_{1/2} = 0, \quad \frac{\partial A_{1/2}}{\partial Y} = 0, \tag{6.69}$$

has the similarity solution

$$A_{1/2}(Y,T) = -\frac{H\alpha_0}{2D_{h_0}} Y^2 \quad \text{and} \quad L^0 = \alpha_0 T, \tag{6.70}$$

where α_0 is a constant to be determined via matching. It is worth noting that in order to fully determine the transformations under which this problem is invariant we need to consider the initial condition as stated in (6.45).

At $O(\theta)$:

$$\frac{\partial A_1}{\partial T} = \frac{\partial^2 A_1}{\partial Y^2} + \frac{1}{D_{h_0}} \left(H \frac{\mathrm{d}L^{1/2}}{\mathrm{d}T} - \frac{H\alpha_0^2}{D_{h_0}} Y \right), \tag{6.71}$$

$$\text{on } Y = 0 \quad A_1 = 0, \quad \frac{\partial A_1}{\partial Y} = \alpha_0 H^2 T, \tag{6.72}$$

has the similarity solution

$$\begin{aligned} A_1(Y,T) =& \frac{H\alpha_0}{6} \left(\frac{\alpha_0}{D_{h_0}^2} - H \right) Y^3 - H^2 \alpha_0 Y T \\ &+ H\alpha_{1/2} \left(\frac{1}{D_{h_0}} - \mathrm{e}^{-\frac{Y^2}{4T}} \mathrm{hypergeom}\left([2], [\frac{1}{2}], \frac{Y^2}{4T} \right) \right) T^{3/2}, \end{aligned} \tag{6.73}$$

and

$$L^{1/2} = \alpha_{1/2} T^{3/2}, \tag{6.74}$$

where $\alpha_{1/2}$ is a constant to be determined via matching.

We revisit the outer region. Recall the $O(\theta)$ equation (6.62) and substitute in $L^0 = \alpha_0 T$ and the initial condition (6.45). We obtain

$$h^1(y,T) = \left(\frac{\alpha_0 H}{D_{h_0}} \text{erfc}\left(\frac{Hy}{h_i\sqrt{\pi}} \right) - \frac{2H^2}{h_i \pi} \exp\left(-\frac{H^2 y^2}{h_i^2 \pi} \right) \right) T + C, \tag{6.75}$$

where C is a constant of integration. Using the boundary condition as $y \to \infty$ we obtain $C = 0$.

For the $O(\theta^{3/2})$ problem (6.63), we substitute $L^{1/2} = \alpha_{1/2} T^{3/2}$ and the initial condition (6.45) to give

$$h^{3/2}(y,T) = \frac{\alpha_{1/2} H}{D_{h_0}} \text{erfc}\left(\frac{Hy}{h_i\sqrt{\pi}} \right) T^{3/2}. \tag{6.76}$$

We are now in a position to match the outer region and the inner region. Using a Taylor expansion around $y = 0$ we obtain from the outer region

$$\begin{aligned}
h_0 &= h_{ic}(y) + \theta h^1(y,T) + \theta^{3/2} h^{3/2}(y,t) + \dots \\
&= h_{ic}(\theta^{1/2} Y) + \theta h^1(\theta^{1/2} Y, T) + \theta^{3/2} h^{3/2}(\theta^{1/2} Y, t) + \dots \\
&= h_{ic}(0) + \theta^{1/2} h_{ic}^{'}(0) Y + \frac{\theta Y^2}{2} h_{ic}^{''}(0) + \frac{\theta^{3/2} Y^3}{6} h_{ic}^{'''}(0) + \dots \\
&\quad + \theta h^1(0,T) + \theta^{3/2} Y h^{1'}(0,T) + \dots \\
&\quad + \theta^{3/2} h^{3/2}(0,T) + \dots,
\end{aligned}$$

where h_{ic}' denotes its derivative with respect to y. Equating powers of θ once more

$$\begin{aligned}
O(\theta^0): &\quad h_{ic}(0) = 0, \\
O(\theta^{1/2}): &\quad h_{ic}^{'}(0) Y = HY \Rightarrow h_{ic}^{'}(0) = H, \\
O(\theta): &\quad \frac{h_{ic}^{''}(0)}{2} Y^2 + h^1(0,T) = -\frac{H\alpha_0}{2D_{h_0}} Y^2 \Rightarrow \alpha_0 = \frac{2HD_{h_0}}{h_i \pi}, \\
O(\theta^{3/2}): &\quad \frac{h_{ic}^{'''}(0)}{6} Y^3 + h^{1'}(0,T) Y + h^{3/2}(0,T) = A_1 \\
&\Rightarrow -\frac{4H^3}{h_i^2 \pi^2} YT + \frac{\alpha_{1/2} H}{D_{h_0}} T^{3/2} = \left(\frac{H\alpha_0}{6} \left(\frac{\alpha_0}{D_{h_0}} + H \right) - \frac{H\alpha_{1/2}\sqrt{\pi}}{8} \right) Y^3 \\
&\qquad + \left(H^2 \alpha_0 - \frac{3H\alpha_{1/2}}{4} \right) YT + H\alpha_{1/2} T^{3/2} \\
&\Rightarrow \alpha_{1/2} = \frac{16H^4}{3\pi h_i^2} \left(1 + \frac{D_{h_0} \pi h_i}{2H^2} \right) \frac{1}{\pi^{3/2}}.
\end{aligned}$$

Hence, the small time behaviour is

$$s(\tau) = \frac{2HD_{h_0}}{\pi h_i}\tau + \frac{16H^4}{3\pi h_i^2}\left(1 + \frac{D_{h_0}\pi h_i}{2H^2}\right)\left(\frac{\tau}{\pi}\right)^{3/2}, \tag{6.77}$$

and

$$\begin{aligned} h_0(y,\tau) =& h_i + \frac{H\alpha_{1/2}}{D_{h_0}}\tau^{3/2} + \ldots - \exp\left(-\frac{H^2y^2}{\pi h_i^2}\right)\left(h_i + \frac{2H^2}{\pi h_i} + \ldots\right) \\ &+ H\mathrm{erf}\left(\frac{Hy}{\sqrt{\pi}h_i}\right)\left(y + \frac{\alpha_0}{D_{h_0}}\tau - \frac{\alpha_{1/2}}{D_{h_0}}\tau 3/2 + \ldots\right). \end{aligned} \tag{6.78}$$

6.2.2.2 One rapidly varying diffusion coefficient

For large time we use the one-phase case as motivation and we consider $\Phi_1 = A\dot{s} + B$, where A, B are arbitrary constants. The concentration of c at Stage I in B.2 causes $B = 0$ for small time and so we take the simpler form $\Phi_1 = \dot{s}$ for this case. The results in sections 3.2.4 and 4.2.4 further suggest that $B = 0$ for large time too, however, to keep it as general as possible, we consider $B \neq 0$.

Consider (6.21)-(6.24) with $\Phi_1 = A\dot{s} + B$ and $\Phi_2 = 0$. Performing the transformations (6.25) we obtain

$$\text{In } 0 < y < \infty,\ \tau > 0 \qquad \frac{\partial h_0}{\partial \tau} = \frac{\partial h_0}{\partial y^2} + \frac{1}{D_{h_0}}\frac{\mathrm{d}s}{\mathrm{d}\tau}\frac{\partial h_0}{\partial y}, \tag{6.79}$$

$$\text{on } y = 0 \qquad h_0 = 0, \quad \frac{\partial h_0}{\partial y} = \frac{1-B}{\frac{1}{H}+s} - \frac{A}{D_{h_0}(\frac{1}{H}+s)}\frac{\mathrm{d}s}{\mathrm{d}\tau}, \tag{6.80}$$

$$\text{as } y \to \infty \qquad h_0 \to h_i, \tag{6.81}$$

$$\text{at } \tau = 0 \qquad h_0 = h_{ic}, \quad s = 0. \tag{6.82}$$

Large time asymptotics

We introduce the artificial parameter $\tau = \frac{T}{\theta}$, $\theta \ll 1$ and $T = O(1)$ and use the nontrivial balances $y = \frac{Y}{\theta^{1/2}}$ and $s = \frac{L}{\theta^{1/2}}$. Further, we substitute the asymptotic expansions (6.30) in (6.79)-(6.82) and start to equate powers of θ.

At leading order we obtain (6.31)-(6.33) but the second condition in (6.32) is now $\frac{\partial h^0}{\partial y} = \frac{1-B}{L^0}$. This problem has the similarity solution

$$h^0 = \frac{1-B}{\alpha_0}\int_0^{YT^{-1/2}} \exp\left(-\frac{1}{2}\left(\frac{t^2}{2} + \frac{\alpha_0 t}{D_{h_0}}\right)\right)\mathrm{d}t \quad \text{and} \quad L^0 = \alpha_0 T^{1/2}, \tag{6.83}$$

where

$$\alpha_0 = \frac{1-B}{h_i}\int_0^{\infty} \exp\left(-\frac{1}{2}\left(\frac{t^2}{2} + \frac{\alpha_0 t}{D_{h_0}}\right)\right)\mathrm{d}t. \tag{6.84}$$

At the next order we obtain (6.38)-(6.40) but the second condition in (6.39) has the extra term $\frac{A}{D_{h_0}L^0}\frac{\mathrm{d}L^0}{\mathrm{d}T}$. The similarity solution obtained now is

$$h^1 = 0 \quad \text{and} \quad L^1 = -\frac{1}{H} + \frac{A\alpha_0^2}{2D_{h_0}(1-B)}, \tag{6.85}$$

where we have resorted to the $\tau = O(1)$ problem, taken the limit $y \to \infty$ and used the initial condition (6.45) to determine how the solution tends to h_i. Finally, the $O(\theta)$ terms yield (6.46)-(6.48) but due to the slight difference in h^0 here compared to the slowly varying case, the similarity solution obtained is

$$h^2 = \frac{\alpha_2(B-1)}{\alpha_0^2}\exp\left(-\frac{1}{2}\left(\frac{Y^2}{2T} + \frac{\alpha_0 Y}{D_{h_0}\sqrt{T}}\right)\right)\frac{Y}{T^{3/2}} \quad \text{and} \quad L^2 = \alpha_2 T^{-1/2}, \tag{6.86}$$

where α_2 may not be determined analytically. Hence as $\tau \to \infty$

$$s(\tau) \sim \alpha_0\sqrt{\tau} - \frac{1}{H} + \frac{A\alpha_0^2}{2(1-B)D_{h_0}} + \alpha_2\tau^{-1/2}, \tag{6.87}$$

and

$$h_0(y,\tau) \sim \frac{1-B}{\alpha_0}\left(\int_0^{\frac{y}{\sqrt{\tau}}} \exp\left(-\frac{1}{2}\left(\frac{t^2}{2} + \frac{\alpha_0 t}{D_{h_0}}\right)\right)\mathrm{d}t \right.$$
$$\left. -\frac{\alpha_2}{\alpha_0}\exp\left(-\frac{1}{2}\left(\frac{y^2}{2\tau} + \frac{\alpha_0 y}{D_{h_0}\sqrt{\tau}}\right)\right)\frac{y}{\tau^{3/2}}\right),$$

where α_0 is as in (6.84) and α_2 remains undetermined.

To be able to compare the large time behaviour of the interface for one rapidly varying diffusion coefficient, we not only need to evaluate α_0 but also approximate the values of A and B. We solve (2.6)-(2.10) with COMSOL Multiphysics using the parameter and initial data as in (6.17). Recall the definition for Φ_1 as stated in (3.43), we fit a polynomial of degree 1 in the interactive curve fitting toolbox to obtain $A = 2.095$ and $B = -0.03262$. Following the same method as in the slowly varying case, (6.84) can be evaluated to obtain $\alpha_0 = 1.087189559$. Further, $\alpha_1 = 0.199013423346$. Fitting the custom equation (6.54) we obtain $a = 1.079$ $(1.075, 1.083)$, $b = -1.344$ $(-1.41, -1.277)$. A two term expansion is not sufficient. Referring to figure 6.3(b) we see how the behaviour is captured but the third term is needed to improve the quantitative match. Implementing

$$s(\tau) \sim 1.08719\sqrt{\tau} - 0.19901 + \alpha_2\tau^{-1/2},$$

yields $\alpha_2 = -26.35$ $(-27.37, -25.33)$.

Small time asymptotics

Consider (6.79)-(6.82) with $A = 1$ and $B = 0$. To analyse the small time behaviour we let $\tau = \theta T$, $\theta \ll 1$ and consider the $T = O(1)$ problem with the nontrivial balance $s = \theta L$. This yields (6.55)-(6.58) but, due to the nonzero Φ_1, the right hand side of the second equation in (6.56) changes to $1 - \frac{\mathrm{d}L}{\mathrm{d}T}$. As in the slowly varying case, this

is still a problem with a boundary layer at $y = 0$ since for $\theta \ll 1$ we lose the highest derivative in the governing equation (6.55). Posing the outer expansions (6.59), we obtain (6.60)-(6.63).

At the boundary layer we rescale $y = \theta^{1/2}Y$ and $h_0 = \theta^{1/2}A$. Substituting in the inner expansion (6.64) we proceed systematically to solve for increasing powers of θ.

At $O(\theta^0)$ we obtain (6.65)-(6.66) with the right hand side of the second condition in (6.66) as $H(1 - \frac{\mathrm{d}L^0}{\mathrm{d}T})$. This problem has the similarity solution

$$A_0(Y,T) = H(1-\alpha_0)Y, \quad L^0 = \alpha_0 T,$$

where α_0 is a constant to be determined via matching. In the slowly varying case, L^0 was only found at the next order. Knowing L^0 at $O(\theta^0)$ instead, implies that we will have a three term expansion for the free boundary $s(t)$ instead of a two term one. However, matching will impose that $\alpha_0 = 0$.

At $O(\theta^{1/2})$ we obtain (6.68)-(6.69) with the exception that the Neumann boundary condition is no longer zero. Instead, at $Y = 0$ we have $\frac{\partial A_{1/2}}{\partial Y} = -H\frac{\mathrm{d}L^{1/2}}{\mathrm{d}T}$. This problem has the similarity solution

$$\begin{aligned} A_{1/2}(Y,T) = &-\left(\frac{H\alpha_0(1-\alpha_0)}{2D_{h_0}} + \frac{3\sqrt{\pi}}{8}H\alpha_{1/2}\mathrm{erf}\left(\frac{Y}{2\sqrt{T}}\right)\right)Y^2 \\ &- \frac{3}{4}H\alpha_{1/2}\exp\left(-\frac{Y^2}{4T}\right)YT^{1/2} - \frac{3\sqrt{\pi}}{4}H\alpha_{1/2}\mathrm{erf}\left(\frac{Y}{2\sqrt{T}}\right)T, \end{aligned} \tag{6.88}$$

and

$$L^{1/2}(T) = \alpha_{1/2}T^{3/2},$$

where $\alpha_{1/2}$ is a constant to be determined via matching.

At $O(\theta)$ we obtain

$$\begin{aligned} \frac{\partial A_1}{\partial T} &= \frac{\partial^2 A_1}{\partial Y^2} + \frac{1}{D_{h_0}}\left(\frac{\mathrm{d}L^0}{\mathrm{d}T}\frac{\partial A_{1/2}}{\partial Y} + \frac{\mathrm{d}L^{1/2}}{\mathrm{d}T}\frac{\partial A_0}{\partial Y}\right), \\ \text{on } Y = 0 \quad A_1 = 0, &\quad \frac{\partial A_1}{\partial Y} = -H\left(H\alpha_0(1-\alpha_0)T + \frac{\mathrm{d}L^1}{\mathrm{d}T}\right). \end{aligned}$$

Due to the increased complexity of $A_{1/2}(Y,T)$ in (6.88) we simplify the above problem by substituting in the fact that $\alpha_0 = 0$. This will be justified later on when matching to the outer. We therefore solve

$$\begin{aligned} \frac{\partial A_1}{\partial T} &= \frac{\partial^2 A_1}{\partial Y^2} + \frac{3H\alpha_{1/2}}{2D_{h_0}}T^{1/2}, \\ \text{on } Y = 0 \quad A_1 = 0, &\quad \frac{\partial A_1}{\partial Y} = -H\frac{\mathrm{d}L^1}{\mathrm{d}T}, \end{aligned}$$

to give the similarity solution

$$A_1(Y,T) = -\frac{1}{3}H\alpha_1 Y^3 - 2H\alpha_1 YT + H\alpha_{1/2}\left(\frac{1}{D_{h_0}} - \exp\left(-\frac{Y^2}{4T}\right)\text{hypergeom}\left([2],[\frac{1}{2}],\frac{Y^2}{4T}\right)\right)T^{3/2}.$$

and

$$L^1(T) = \alpha_1 T^2$$

Revisiting the outer region and substituting the now known structures of L^0 and $L^{1/2}$ we obtain (6.75) and (6.76). Using a Taylor expansion around $y = 0$ we match the outer region with the inner region and in this case we obtain

$$\begin{aligned}
&O(\theta^0): && h_{ic}(0) = 0,\\
&O(\theta^{1/2}): && h_{ic}'(0)Y = H(1-\alpha_0)Y \Rightarrow \alpha_0 = 0,\\
&O(\theta): && \frac{1}{2}h_{ic}''(0)Y^2 + h^1(0,T) = A_{1/2}(Y,T)\\
& && \Rightarrow -\frac{H^2}{\pi h_i}Y^2 - \frac{2H^2}{\pi h_i}T = -\frac{3\sqrt{\pi}}{8}H\alpha_{1/2}Y^2 - \frac{3\sqrt{\pi}}{4}H\alpha_{1/2}T\\
& && \Rightarrow \alpha_{1/2} = \frac{8H}{3\pi^{3/2}h_i},\\
&O(\theta^{3/2}): && h_{ic}'''(0)Y^3 + h^{1'}(0,T)Y + h^{3/2}(0,T) = A_1(Y,T)\\
& && \Rightarrow \frac{8H^2}{3\pi^{3/2}D_{h_0}h_i}T^{3/2} = -H\left(\frac{\alpha_1}{3} + \frac{\sqrt{\pi}\alpha_{1/2}}{8}\right)Y^3\\
& && \quad - H\left(2\alpha_1 + \frac{3\sqrt{\pi}}{4}\alpha_{1/2}\right)YT + \frac{H\alpha_{1/2}}{D_{h_0}}T^{3/2}\\
& && \Rightarrow \alpha_1 = -\frac{H}{\pi h_i}.
\end{aligned}$$

Hence, for one rapidly varying diffusion coefficient, taking $\Phi_1 = \dot{s}$, the small time behaviour of the interface is

$$s(\tau) \sim \frac{8H}{3h_i}\left(\frac{\tau}{\pi}\right)^{3/2} - \frac{H}{\pi h_i}\tau^2, \tag{6.89}$$

and

$$h_0(y,\tau) \sim h_i + \frac{H\alpha_{1/2}}{D_{h_0}}\tau^{3/2} - \left(h_i + \frac{2H^2}{\pi h_i}\tau\right)\exp\left(-\frac{H^2y^2}{\pi h_i^2}\right) + H\left(y - \frac{\alpha_{1/2}}{D_{h_0}}\tau^{3/2}\right)\text{erf}\left(\frac{Hy}{\sqrt{\pi}h_i}\right).$$

6.2.2.3 Two rapidly varying diffusion coefficients

We now consider the last case where both Φ_1 and Φ_2 are non-zero. Although this might seem like the most involved case, recall that now we no longer have a Stage I carbonation and so the initial condition (6.24) becomes

$$\text{at } t = 0 \quad h_0 = h_i \text{ for } s_0 \leq x \leq 1, \quad s = s_0.$$

Figure 4.8 as well as table 4.2 and the analysis in section 5.4 suggest that $\Phi_1 \sim \dot{s}$ and $\Phi_2 \sim \dot{s}$. We therefore consider $\Phi_1 = A_1\dot{s}$ and $\Phi_2 = A_2\dot{s}$ where A_1, A_2 are arbitrary constants for small time. To keep the analysis as general as possible, for large time, we take $\Phi_1 = A_1\dot{s} + B_1$ and $\Phi_2 = A_2\dot{s} + B_2$ where B_1, B_2 are arbitrary constants such that $B_1 \neq 0$ and $B_2 \neq 0$.

Performing the transformations

$$\tau = \frac{1}{D_{h_0}}t, \quad y = \frac{1}{D_{h_0}}(x - s(t)),$$

in (6.21)-(6.24), we obtain

$$\text{In } 0 < y < \infty,\ \tau > 0 \qquad \frac{\partial h_0}{\partial \tau} = \frac{\partial^2 h_0}{\partial y^2} + \frac{1}{D_{h_0}}\frac{\mathrm{d}s}{\mathrm{d}\tau}\frac{\partial h_0}{\partial y}, \tag{6.90}$$

$$\text{on } y = 0 \qquad h_0 = \frac{A_2}{D_{h_0}}\frac{\mathrm{d}s}{\mathrm{d}\tau} + B_2, \tag{6.91}$$

$$\frac{\partial h_0}{\partial y} = \frac{1 - B_1}{\frac{1}{H} + s} - \frac{1}{D_{h_0}}\left(\frac{A_1}{(\frac{1}{H} + s)} + B_2\right)\frac{\mathrm{d}s}{\mathrm{d}\tau} - \frac{A_2}{(D_{h_0})^2}\left(\frac{\mathrm{d}s}{\mathrm{d}\tau}\right)^2, \tag{6.92}$$

$$\text{as } y \to \infty \qquad h_0 \to h_i, \tag{6.93}$$

$$\text{at } \tau = 0 \qquad h_0 = h_i, \quad s = 0. \tag{6.94}$$

Large time asymptotics

Let $\tau = \frac{T}{\theta}$, $\theta \ll 1$ and consider the $T = O(1)$. We may now investigate the large time behaviour $\tau \to \infty$ of (6.90)-(6.94). We introduce the nontrivial balances $y = \frac{Y}{\theta^{1/2}}$, $s = \frac{L}{\theta^{1/2}}$ and substitute the asymptotic expansions (6.30). Then, the leading order problem gives

$$h^0 = h_i - C\text{erfc}\left(\frac{Y}{2\sqrt{T}} + \frac{\alpha_0}{2D_{h_0}}\right) \quad \text{and} \quad L^0 = \alpha_0 T^{1/2}, \tag{6.95}$$

where

$$h_i - C\text{erfc}\left(\frac{\alpha_0}{2D_{h_0}}\right) = B_2, \tag{6.96}$$

is a transcendental equation for α_0 and

$$C = \sqrt{\pi}\left(\frac{1-B_1}{\alpha_0} - \frac{B_2\alpha_0}{2D_{h_0}}\right)\exp\left(\left(\frac{\alpha_0}{2D_{h_0}}\right)^2\right).$$

At the next order we obtain

$$h^1 = \frac{A_2\alpha_0}{2D_{h_0}}\exp\left(-\frac{1}{2}\left(\frac{Y}{2T} + \frac{\alpha_0 Y}{D_{h_0}\sqrt{T}}\right)\right)T^{-1/2}, \tag{6.97}$$

and

$$L^1 = -\frac{1}{H} + \frac{A_1\alpha_0^2}{2(1-B_1)D_{h_0}}. \tag{6.98}$$

Note that h^1 is no longer zero. This is due to the fact that $\Phi_2 \neq 0$ and so the first condition in (6.23) will no longer be zero. For completion we go one step further and obtain

$$h^2 = \left(\frac{(B_1-1)\alpha_2}{\alpha_0^2} + \frac{B_2\alpha_2}{2D_{h_0}}\right)\exp\left(-\frac{1}{2}\left(\frac{Y^2}{2T} + \frac{\alpha_0 Y}{D_{h_0}\sqrt{T}}\right)\right)\frac{Y}{T^{3/2}}, \tag{6.99}$$

and

$$L^2 = \alpha_2 T^{-1/2}, \tag{6.100}$$

where α_2 may not be determined analytically. Hence, as $\tau \to \infty$

$$s(\tau) \sim \alpha_0\sqrt{\tau} - \frac{1}{H} + \frac{A_1\alpha_0^2}{2(1-B_1)D_{h_0}} + \alpha_2\tau^{-1/2}, \tag{6.101}$$

and

$$\begin{aligned} h_0(y,\tau) =& h_i - C\mathrm{erfc}\left(\frac{y}{2\sqrt{\tau}} + \frac{\alpha_0}{2D_{h_0}}\right) \\ &+ \frac{A_2\alpha_0}{2D_{h_0}}\exp\left(-\frac{1}{2}\left(\frac{y^2}{2\tau} + \frac{\alpha_0 y}{D_{h_0}\sqrt{\tau}}\right)\right)\tau^{-1/2} \\ &+ \left(\frac{(B_1-1)\alpha_2}{\alpha_0^2} + \frac{B_2\alpha_2}{2D_{h_0}}\right)\exp\left(-\frac{1}{2}\left(\frac{y^2}{2\tau} + \frac{\alpha_0 y}{D_{h_0}\sqrt{\tau}}\right)\right)\frac{y}{\tau^{3/2}}, \end{aligned} \tag{6.102}$$

where α_0 is as in (6.96) and α_2 is arbitrary.

Solving (2.6)-(2.10) with COMSOL Multiphysics and using the definition for Φ_1 and Φ_2 as stated in (3.43) and (4.37) respectively, we obtain $A_1 = 2.192$, $B_1 = -0.02047$ and $A_2 = 1.992$, $B_2 = -0.01379$. This yields $\alpha_0 = 1.08095$ and $\alpha_1 = 0.25493$. Fitting

$$f(\tau) = a\sqrt{\tau} + b$$

in the curve fitting tool box gives the coefficient $a = 1.079$ $(1.075, 1.083)$ with 95% confident bounds, indicating a good agreement with the analytical value of α_0. However,

$b = -1.852$ $(-1.916, -1.788)$ indicating that and extra term is necessary to obtain an accurate result. Plugging in

$$s(\tau) = 1.08095\sqrt{\tau} + 0.25493 + \alpha_2 \tau^{-1/2}$$

gives the approximate value of $\alpha_2 = -34.69$ $(-35.78, -33.61)$. Finally, figure 6.3(c) corroborates the improvement achieved by the addition of the third term in the expansion for the interface.

Small time asymptotics

Recall (6.90)-(6.94) and let $B_1 = 0 = B_2$. Introduce the artificial parameter $\tau = \theta T$, $\theta \ll 1$ and consider the $T = O(1)$ problem. Substitute in the nontrivial balance $y = \theta^{1/2} Y$, $s = \theta L$ and so

$$\frac{\partial h_0}{\partial T} = \frac{\partial^2 h_0}{\partial Y^2} + \frac{\theta^{1/2}}{D_{h_0}} \frac{\mathrm{d}L}{\mathrm{d}T} \frac{\partial h_0}{\partial Y}, \tag{6.103}$$

$$\text{on } Y = 0 \qquad h_0 = \frac{A_2}{D_{h_0}} \frac{\mathrm{d}L}{\mathrm{d}T}, \tag{6.104}$$

$$\left(\frac{1}{H} + \theta L\right) \frac{\partial h_0}{\partial Y} = \theta^{1/2} \left(1 - \frac{A_1}{D_{h_0}} \frac{\mathrm{d}L}{\mathrm{T}} - \left(\frac{1}{H} + \theta L\right) \frac{A_2}{(D_{h_0})^2} \left(\frac{\mathrm{d}L}{\mathrm{d}T}\right)^2\right),$$

$$\text{as } Y \to \infty \qquad h_0 \to h_i, \tag{6.105}$$

$$\text{at } T = 0 \qquad h_0 = h_i, \quad L = 0. \tag{6.106}$$

Note that we no longer have a boundary layer. Pose the expansions

$$h_0 = h^0 + \theta^{1/2} h^{1/2} + \theta h^1 + \ldots, \quad L = L^0 + \theta^{1/2} L^{1/2} + \theta L^1 + \ldots,$$

and equate powers of θ in (6.103)-(6.106). At leading order we obtain

$$\frac{\partial h^0}{\partial T} = \frac{\partial^2 h^0}{\partial Y^2},$$

$$\text{on } Y = 0 \qquad h^0 = \frac{A_2}{D_{h_0}} \frac{\mathrm{d}L^0}{\mathrm{d}T}, \quad \frac{\partial h^0}{\partial Y} = 0,$$

$$\text{as } Y \to \infty \qquad h^0 \to h_i,$$

$$\text{at } T = 0 \qquad h^0 = h_i, \quad L^0 = 0.$$

This has the similarity solution

$$h^0(Y, T) = h_i \quad \text{and} \quad L^0(T) = \alpha_0 T,$$

with

$$\alpha_0 = \frac{D_{h_0} h_i}{A_2}. \tag{6.107}$$

At the next order, we obtain

$$\begin{aligned}
&&\frac{\partial h^{1/2}}{\partial T} &= \frac{\partial^2 h^{1/2}}{\partial Y^2},\\
\text{at } Y=0 \qquad && h^{1/2} &= \frac{A_2}{D_{h_0}}\frac{\mathrm{d}L^{1/2}}{\mathrm{d}T}, \quad \frac{\partial h^{1/2}}{\partial Y} = H - \frac{HA_1}{D_{h_0}}\frac{\mathrm{d}L^0}{\mathrm{d}T} - \frac{A_2}{(D_{h_0})^2}\left(\frac{\mathrm{d}L^0}{\mathrm{d}T}\right)^2,\\
\text{as } Y\to\infty \qquad && h^{1/2} &\to 0,\\
\text{at } T=0 \qquad && h^{1/2} &= 0, \quad L^{1/2}=0,
\end{aligned}$$

which has a similarity solution

$$h^{1/2}(Y,T) = \frac{\sqrt{\pi}}{2}C\mathrm{erfc}\left(\frac{Y}{2\sqrt{T}}\right)Y - C\exp\left(-\frac{Y^2}{4T}\right)T^{1/2}$$

and

$$L^{1/2}(T) = \alpha_{1/2}T^{3/2},$$

with

$$\alpha_{1/2} = -\frac{2D_{h_0}C}{3A_2}, \tag{6.108}$$

where

$$C = \frac{2}{\sqrt{\pi}}\left(H - \frac{HA_1h_i}{A_2} - \frac{h_i^2}{A_2}\right). \tag{6.109}$$

Finally, we may go one step further, the $O(\theta)$ terms give

$$\begin{aligned}
&&\frac{\partial h^1}{\partial T} &= \frac{\partial^2 h^1}{\partial Y^2} + \frac{1}{D_{h_0}}\frac{\mathrm{d}L^0}{\mathrm{d}T}\frac{\partial h^{1/2}}{\partial Y},\\
\text{on } Y=0 \qquad && h^1 &= \frac{A_2}{D_{h_0}}\frac{\mathrm{d}L^1}{\mathrm{d}T},\\
&& \frac{\partial h^1}{\partial Y} &= -\frac{HA_1}{D_{h_0}}\frac{\mathrm{d}L^{1/2}}{\mathrm{d}T} - \frac{2A_2}{(D_{h_0})^2}\frac{\mathrm{d}L^0}{\mathrm{d}T}\frac{\mathrm{d}L_{1/2}}{\mathrm{d}T},\\
\text{as } Y\to\infty \qquad && h^1 &\to 0,\\
\text{at } T=0 \qquad && h^1 &= 0, \quad L^1=0.
\end{aligned}$$

which has the similarity solution

$$\begin{aligned}
h^1(Y,T) = \frac{C}{A_2}\Bigg(&\frac{5}{4}h_i\exp\left(-\frac{Y^2}{4T}\right)\frac{Y}{T^{1/2}} - \frac{\sqrt{\pi}}{8}h_i\mathrm{erfc}\left(\frac{Y}{2\sqrt{T}}\right)\left(6+5\frac{Y^2}{T}\right) +\\
&\frac{HA_1}{2}\exp\left(-\frac{Y^2}{4T}\right)\frac{Y}{T^{1/2}} + \frac{\sqrt{\pi}HA_1}{4}\mathrm{erfc}\left(\frac{Y}{2\sqrt{T}}\right)\left(2+\frac{Y^2}{T}\right)\Bigg)T,
\end{aligned}$$

and

$$L^1(T) = \alpha_1 T^2,$$

with

$$\alpha_1 = -\frac{\sqrt{\pi} D_{h_0} C}{4A_2^2}\left(\frac{3}{2}h_i + HA_1\right), \tag{6.110}$$

where C is as in (6.109). Recollecting all the information, for two rapidly varying diffusion coefficients, the small time behaviour $\tau \to 0$ of the interface is

$$s(\tau) \sim \alpha_0 \tau + \alpha_{1/2}\tau^{3/2} + \alpha_1 \tau^2 \tag{6.111}$$

where α_0, $\alpha_{1/2}$, α_1 are as in (6.107), (6.108), (6.110) respectively, and

$$\begin{aligned} h_0(y,\tau) \sim & h_i + \frac{\sqrt{\pi}}{2} C\left(y - \frac{h_i}{4A_2}(6\tau + 5y^2) + \frac{HA_1}{2A_2}(2\tau + y^2)\right)\operatorname{erfc}\left(\frac{y}{2\sqrt{\tau}}\right) \\ & - C\left(\tau^{1/2} - \frac{5h_i}{4A_2}y\tau^{1/2} - \frac{HA_1}{2A_2}y\tau^{1/2}\right)\exp\left(-\frac{y^2}{4\tau}\right) \end{aligned}$$

where C is as in (6.109).

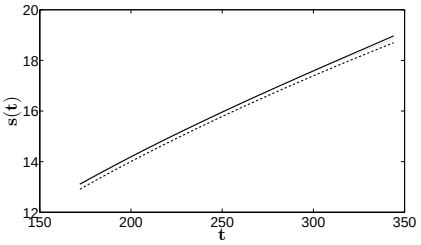

(a) Slowly varying - Here $\epsilon = 10^{-2}$ and the analytical approximation of the interface is $s(t) \sim 1.0632\sqrt{t-\frac{\pi}{4}} - 1 + 2.998(t-\frac{\pi}{4})^{-1/2}$

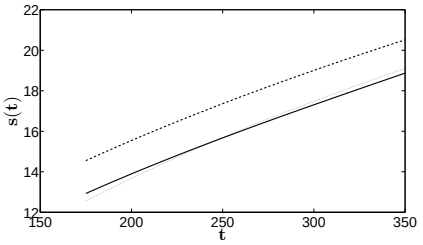

(b) One rapidly varying - Here $\epsilon = 10^{-1}$, the analytical approximation of the interface is $s(t) \sim 1.08719\sqrt{t-\frac{\pi}{4}} + 0.19901 - 26.35(t-\frac{\pi}{4})^{-1/2}$ and $\Phi_1 \sim 2.095\dot{s} - 0.03262$.

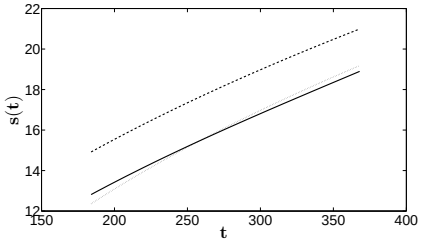

(c) Two rapidly varying - Here $\epsilon = 10^{-1}$, the analytical approximation of the interface is $s(t) \sim 1.08095\sqrt{t} + 0.25493 - 2.143$, $\Phi_1 \sim 2.192\dot{s} - 0.02047$ and $\Phi_2 \sim 1.992\dot{s} - 0.01379$

Figure 6.3: *Large time behaviour: Comparison of COMSOL results for the full reaction-diffusion system* (2.6)-(2.10) *on the domain* $0 \leq x \leq 50$ *with* $\delta = \epsilon$, ϵ *as stated in each subfigure and* $h_i = H = 1$, $\mu = 10^{-3}$, $p = q = 1$ *and* $\nu_1 = \nu_2 = 1$ *(solid line) and the analytical large time behaviour for the two-phase Stefan problem taking two terms in the expansion (dashed line) and three terms (dotted line).*

6.3 Numerical results

We are now interested in numerically solving the problems arising for the quasi-steady CO_2 limit $\mu \to 0$ for the one-phase (6.14) and two-phase (6.21)-(6.24) problems. In each case, the numerical solution will be compared to the COMSOL Multiphysics simulations as done in the previous section. However, to obtain a better understanding of this comparison, we consider also the relative percentage error

$$R.E. = \frac{N - C}{C} \times 100,$$

where N corresponds to the numerical results obtained here and C to the COMSOL simulation results.

6.3.1 One-Phase Problem

For slowly varying diffusivities ($\Phi_1 = 0$) the comparison of the free boundary (6.15) is shown in figure 6.4.

For one and two rapidly varying diffusivities, Φ_1 is no longer zero. In order to determine the value of Φ_1 two approaches can be taken.

1. Approximate Φ_1 as done for the analytical results in section 6.2.

Let $\Phi_1 \sim A * \dot{s}$ where A is a constant obtained from the COMSOL results. In this case, the free boundary is given by (6.19) with $A = 1$.

2. Approximate Φ_1 using the respective micro problems from Chapter 5.

For a one rapidly varying diffusion coefficient, we couple micro problems S1a ($\delta \leq \epsilon^2$) and S1b ($\epsilon^2 \ll \delta \ll \epsilon$) with (6.14) and for two rapidly varying diffusion coefficients we use micro problem D1. Each micro problem calculates the value of Φ_1 for a particular chosen $\dot{s}(t)$. To this aim we define a partition $\{0 = t_0 < t_1 < \ldots < t_N = T\}$ of $[0, T]$ with $\Delta t = t_i - t_{i-1}$, $i = 1, \ldots, N$ and use the substitution

$$\dot{s}(t_n) = \frac{s(t_n) - s(t_{n-1})}{\Delta t}.$$

Hence, $s(t_n)$ is a root of the scalar equation

$$\sigma(x) = h_i \left(\frac{1}{H} + x \right) \left(\frac{x - s_{n-1}}{\Delta t} \right) + \Phi_1 \left(\frac{x - s_{n-1}}{\Delta t} \right) - 1. \tag{6.112}$$

The function $\sigma_n(x)$ is evaluated at successive mesh points of the grid beyond $s(t_{n-1})$ until it changes sign, say between x_l and x_{l+1}. The free boundary $s(t_n)$ is now determined as the root of the quadratic interpolant through $\sigma(x_{l-1})$, $\sigma(x_l)$ and $\sigma(x_{l+1})$. Figures 6.5 and 6.6 show the results for one and two rapidly varying diffusion coefficients respectively.

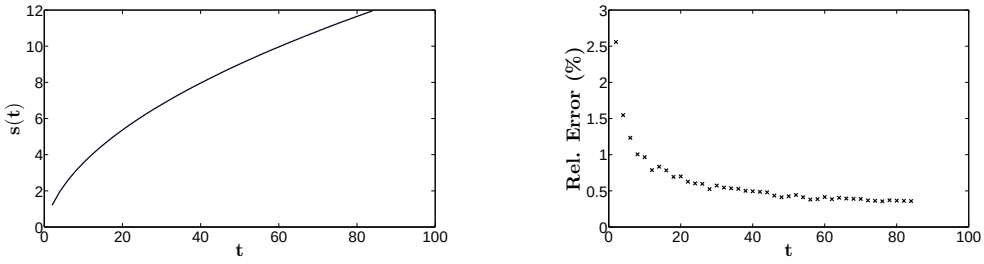

(a) Free boundary (b) Relative Error

Figure 6.4: *Comparison of the COMSOL simulations (solid line) with the numerical results of* (6.14) *(blue dashed line) for the one phase case and slowly varying diffusion coefficients.*

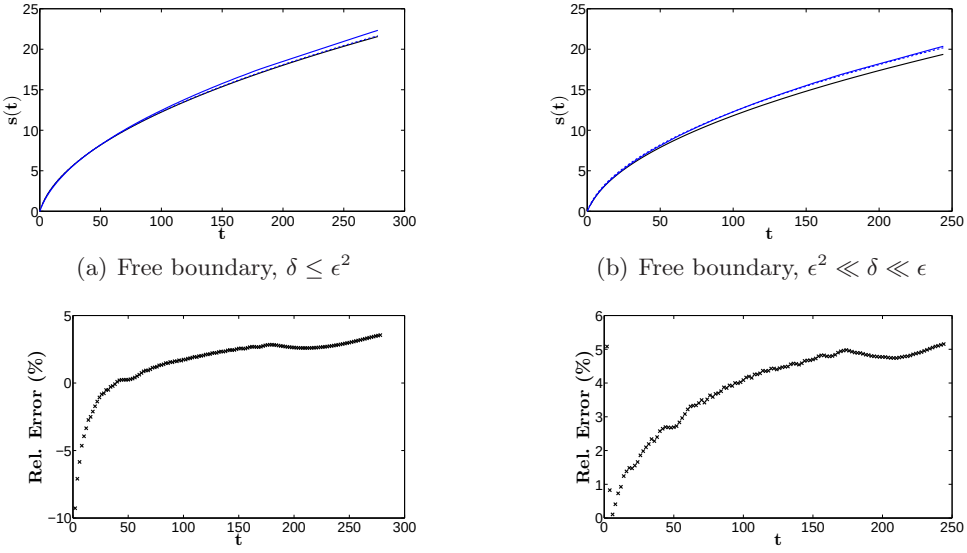

(a) Free boundary, $\delta \leq \epsilon^2$

(b) Free boundary, $\epsilon^2 \ll \delta \ll \epsilon$

(c) Relative Error of COMSOL simulations and (6.14) with Φ_1 approximated using the micro problem S1a.

(d) Relative Error of COMSOL simulations and (6.14) with Φ_1 approximated using the micro problem S1b.

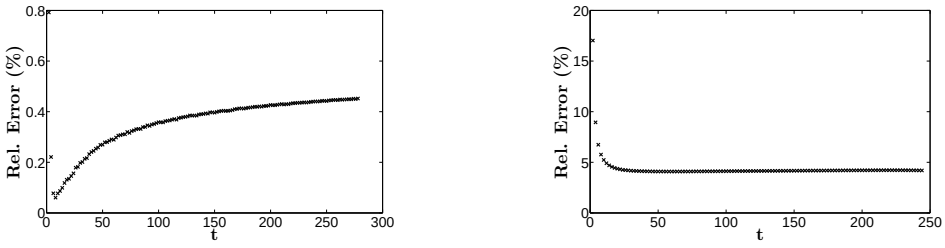

(e) Relative Error of COMSOL simulations and (6.14) with Φ_1 approximated by $\Phi_1 \sim \dot{s}$.

(f) Relative Error of COMSOL simulations and (6.14) with Φ_1 approximated by $\Phi_1 \sim \dot{s}$.

Figure 6.5: *Comparison of the COMSOL simulations with the numerical results of* (6.14) *for one rapidly diffusion coefficient and the parameter regime $\delta \ll \epsilon$. The first column corresponds to the parameter regime $\delta \leq \epsilon^2$ and the second column considers $\epsilon^2 \ll \delta \ll \epsilon$. In 6.5(a),6.5(b) the black solid line represents the free boundary obtained from COMSOL and the blue lines refer to the numerical results of* (6.14)*, where Φ_1 has been approximated using the micro problems (solid line) and as $\Phi_1 \sim \dot{s}$ (dashed line).*

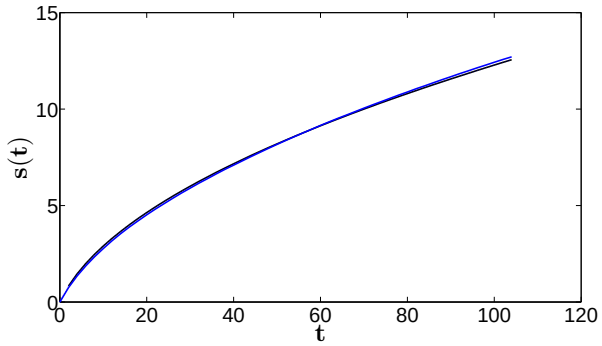

(a) Free boundary

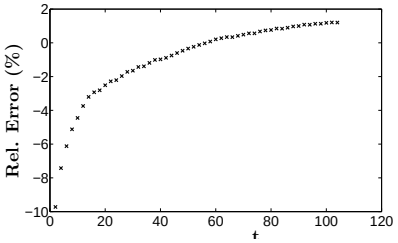

(b) Relative Error of COMSOL simulations and (6.14) with Φ_1 approximated using the micro problem D1 ($\Phi_2 = 0$).

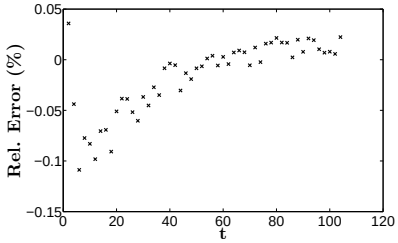

(c) Relative Error of COMSOL simulations and (6.14) with Φ_1 approximated by $\Phi_1 \sim \dot{s}$ ($\Phi_2 = 0$).

Figure 6.6: *Comparison of the COMSOL simulations with the numerical results of* (6.14) *for two rapidly varying diffusion coefficients. In 6.6(a) the black solid line represents the free boundary obtained from COMSOL and the blue lines refer to the numerical results of* (6.14)*, where* Φ_1 *has been approximated using the micro problem D1 (solid line) and as* $\Phi_1 \sim \dot{s}$ *(dashed line).*

6.3.2 Two-Phase Problem

The method of lines will be used to solve the problem (6.21)-(6.24) numerically. This method was introduced by Meyer [41] and the main idea is to replace partial differential equations by a sequence of free boundary problems for ordinary differential equations at discrete time levels.

To this aim we discretise the continuous time problem (6.21)-(6.24). We define a partition $\{t_0 < t_1 < \ldots < t_N = T\}$ of $[t_0, T]$ with equal subintervals $\Delta t = t_i - t_{i-1}$, $i = 1, \ldots, N$ and substitute the simplest time discretisation

$$\frac{\partial h_0}{\partial t}(x, t_n) \sim \frac{h_0(x, t_n) - h_0(x, t_{n-1})}{\Delta t}, \quad \dot{s}(t_n) \sim \frac{s(t_n) - s(t_{n-1})}{\Delta t}.$$

Hence, at time level $t = t_n$ the solution $\{h_n(x), s_n\}$ is computed as the solution of the following second order differential equation

$$\text{in } s_n < x < 1 \quad D_{h_0} h_n^{''} - \frac{1}{\Delta t}(h_n - h_{n-1}) = 0, \tag{6.113}$$

$$D_{h_0} h_n^{'}(1) = 0, \tag{6.114}$$

$$h_n(s_n) = \Phi_2\left(\frac{s_n - s_{n-1}}{\Delta t}\right), \quad s_0 = s(t_0) = 0, \tag{6.115}$$

$$D_{h_0} h_n^{'}(s_n) = \frac{1}{\frac{1}{H} + s_n} - \frac{\Phi_1}{\frac{1}{H} + s_n} - \frac{s_n - s_{n-1}}{\Delta t}\Phi_2, \tag{6.116}$$

where $h_n = h_0(x, t_n)$, $h_n^{'} = \mathrm{d}h_n/\mathrm{d}x$. It is assumed that the function h_{n-1} (defined over $[s_{n-1}, 1]$) and s_{n-1} are both known. The method of invariant imbedding (or sweep method) is now used to solve (6.113)-(6.116) and to determine the position of the moving boundaries at successive times $t = t_n$. Full details of this technique can be found in [41, 24]. Writing (6.113)-(6.116) as a first order system over $(s_n, 1)$

$$h_n^{'} = \frac{v_n}{D_{h_0}}, \quad v_n^{'} = \frac{1}{\Delta t}(h_n - h_{n-1}).$$

We exploit the observation that h_n and v_n are related through the Riccati transformation

$$v_n(x) = R(x) h_n(x) + W_n(x), \tag{6.117}$$

where R and W are obtained by solving the final value problems, also known as the invariant imbedding equations

$$R^{'} = \frac{1}{\Delta t} - \frac{1}{D_{h_0}} R^2, \quad R(1) = 0, \tag{6.118}$$

$$W_n^{'} = -\frac{R(x)}{D_{h_0}} W_n - \frac{h_{n-1}(x)}{\Delta t}, \quad W_n(1) = 0. \tag{6.119}$$

The Riccati equation (6.118) has the closed form solution

$$R(x) = \sqrt{\frac{D_{h_0}}{\Delta t}} \tanh\left(\frac{x-1}{\sqrt{D_{h_0}\Delta t}}\right), \tag{6.120}$$

and the linear equation (6.119) is integrated to give

$$W_n(x)\cosh\left(\frac{x-1}{\sqrt{D_{h_0}\Delta t}}\right) = \frac{1}{\Delta t}\int_x^1 h_{n-1}(\tau)\cosh\left(\frac{\tau-1}{\sqrt{D_{h_0}\Delta t}}\right)\mathrm{d}\tau. \tag{6.121}$$

The Riccati relation (6.117) has to hold for all x, hence also at the free boundary s_n. Thus substituting (6.117) into the discretized boundary condition (6.116) shows that s_n is a root of the scalar equation

$$\begin{aligned}\sigma_n(x) =& R(x)\Phi_2\left(\frac{x-s_{n-1}}{\Delta t}\right) + W_n(x) + \frac{1}{\frac{1}{H}+x}\left(\Phi_1\left(\frac{x-s_{n-1}}{\Delta t}\right) - 1\right)\\ &+ \frac{x-s_{n-1}}{\Delta t}\Phi_2\left(\frac{x-s_{n-1}}{\Delta t}\right) = 0.\end{aligned} \tag{6.122}$$

Note that $\sigma_n(x)$ may have a root smaller than s_{n-1} and so we choose the smallest root of $\sigma_n(x) = 0$ such that $x > s_{n-1}$. The function $\sigma_n(x)$ is then evaluated at successive mesh points of the grid beyond s_{n-1} until it changes sign between say, x_{l-1} and x_l. The free boundary s_n is now determined as the root of the quadratic interpolant through $\sigma(x_{l-1})$, $\sigma(x_l)$ and $\sigma(x_{l+1})$, i.e. Find $x \in [x_{l-1}, x_{l+1}]$ such that

$$\tilde{\sigma}(x) = l_{l-1}(x)\sigma(x_{l-1}) + l_l(x)\sigma(x_l) + l_{l+1}(x)\sigma(x_{l+1}), \tag{6.123}$$

where

$$\begin{aligned} l_{l-1}(x) &= \frac{(x-x_l)(x-x_{l+1})}{(x_{l+1}-x_l)(x_{l-1}-x_{l+1})},\\ l_l(x) &= \frac{(x-x_{l-1})(x-x_{l+1})}{(x_l-x_{l-1})(x_l-x_{l+1})},\\ l_{l+1}(x) &= \frac{(x-x_{l-1})(x-x_l)}{(x_{l+1}-x_{l-1})(x_{l+1}-x_l)}. \end{aligned}$$

Given s_n, we have

$$h_n(s_n) = \Phi_2(\dot{s}_n), \tag{6.124}$$

where

$$\dot{s}_n = \frac{s_n - s_{n-1}}{\Delta t},$$

and

$$D_{h_0}h_n^{'} = v_n(s_n) = -\left(\frac{\Phi_1 - 1}{\frac{1}{H} - s_n} + \dot{s}\Phi_2\right).$$

Thus, the triple $\{h_n(s_n), v_n(s_n), s_n\}$ is an exact solution of (6.115), (6.116) and (6.117). Once s_n is determined, h_n can be found by integrating forwards over $(s_n, 1]$ the Riccati transformation

$$D_{h_0} h_n^{'} = v_n = R(x)h_n + W_n(x),$$

with $h_n(s_n)$ as in (6.124). Finally, h_n is extended over $[0, s_n]$ as a C^1 linear function.

To determine Φ_1 and/or Φ_2 we restrict ourselves to the first approach mentioned in the one phase case. Taking $D_{h_0} = 1$, the above algorithm is implemented as follows:

1. For a given interval $[0, X]$ a variable but time independent mesh with grid points $\{x_k\}_{k=0}^{K}$ is imposed with $x_{K-i} = X - (i/K)^2 X$ so that the mesh points cluster near the boundary at X.

2. We take the following initial conditions

$$s_0 = 0,\ t_0 = \begin{cases} \pi/4 & \text{if } \Phi_1 = 0 \text{ and/or } \Phi_2 = 0 \\ 0 & \text{if } \Phi_2 \neq 0, \end{cases} \qquad h_0(s) = \begin{cases} 0 & \text{if } t_0 \neq 0 \\ 1 & \text{if } t_0 = 0, \end{cases}$$

$$h_0(x_k) = \begin{cases} 1 + \operatorname{erfc}\left(\frac{x_k}{\sqrt{\pi}}\right) x_k - \exp\left(-\frac{x_k^2}{\pi}\right) & \text{if } t_0 \neq 0 \\ 1 & \text{if } t_0 = 0. \end{cases}$$

3. Define the vectors $\tilde{T} = [t_0]$ and $S = [0]$ to store the time iterations and the location of the free boundary at each time iteration respectively. Further, set $m_0 = 1$.

4. Time iteration n: $t = \tilde{T}(\text{end}) + \Delta t$, where $\Delta t = 10^{-2}$.
   Update the time vector: $\tilde{T} = [\tilde{T}, t]$.

5. Set previous time loop values s_{n-1}=s_n, $h_{n-1}(x_k) = h_n(x_k)$, $h_{n-1}(s_{n-1}) = h_n(s_n)$, $m_{n-1} = m_n$.

6. Solve for $R(x_k)$ as in (6.120).

7. Evaluate $W_n(x_k)$ in (6.121) backwards on the fixed mesh choosing the trapezoidal rule as our quadrature rule

$$W_n(x_k) = aW_n(x_{k+1}) + \frac{x_{k+1} - x_k}{2\Delta t}(ah_{n-1}(x_{k+1}) + h_{n-1}(x_k)), \tag{6.125}$$

   where

$$a = \frac{\cosh\left(\frac{x_{k+1} - X}{\sqrt{\Delta t}}\right)}{\cosh\left(\frac{x_k - X}{\sqrt{\Delta t}}\right)}.$$

8. For $x \in [x_{m_{n-1}} - 2, X]$, evaluate $\sigma(x)$ at each grid point as in (6.122) until $\sigma(x)$ changes sign between x_{l-1} and x_l.

Set $m_n = l$ and calculate $\sigma(x_{l+1})$.
Note: If $m_{n-1} < 3$, set $m_{n-1} = 3$.

9. Determine s_n: Evaluate (6.123), the root of the quadratic interpolant through $\sigma(x_{l-1})$, $\sigma(x_l)$ and $\sigma_{x_{l+1}}$.
Update the free boundary vector: $S = [S, s_n]$.

10. Evaluate $h_{n-1}(s_n)$: Linear interpolation between two known grid points

$$h_{n-1}(s_n) = h_{n-1}(x_{l-1}) + \frac{s_n - x_{l-1}}{x_l - x_{l-1}}(h_{n-1}(x_l) - h_{n-1}(x_{l-1})).$$

11. Evaluate $W_n(s_n)$: Substitute $x_k = s_n$ and $x_{k+1} = x_l$ into (6.125) and use h_{n-1} as in step 10.

12. Evaluate $h_n(s_n)$ as in (6.124).

13. Evaluate $h_n(x)$, $x \in [0, X]$:

    - At $x = x_l$: Integrate from s_n to x_l using the trapezoidal rule

    $$h_n(x_l) = a h_n(s_n) + \frac{x_l - s_n}{2}\left(a W_n(s_n) + W_n(x_l)\right)$$

    where $a = \cosh\left(\frac{x_l - X}{\sqrt{\Delta t}}\right) / \cosh\left(\frac{s_n - X}{\sqrt{\Delta t}}\right)$, $W_n(s_n)$as in step 11 and $h_n(s_n)$ as in step 12.
    - For $x \in [x_{l+1}, X]$: Integrate forwards over the fixed mesh using the trapezoidal rule

    $$h_n(x_{k+1}) = a h_n(x_k) + \frac{x_{k+1} - x_k}{2}\left(a W_n(x_k) + W_n(x_{k+1})\right)$$

    where $a = \cosh\left(\frac{x_{k+1} - X}{\sqrt{\Delta t}}\right) / \cosh\left(\frac{x_k - X}{\sqrt{\Delta t}}\right)$.
    - For $x \in [0, x_{l-1}]$: Extend h_n over as a C^1 linear function

    $$h_n(x_k) = l_{k+1}(x_k)h_n(x_{k+1}) + l_{k+2}(x_k)h_n(x_{k+2}) + l_{k+3}(x_k)h_n(x_{k+3}),$$

    where

    $$\begin{aligned} l_{k+1}(x_k) &= \frac{(x_k - x_{k+2})(x_k - x_{k+3})}{(x_{k+1} - x_{k+2})(x_{k+1} - x_{k+3})}, \\ l_{k+2}(x_k) &= \frac{(x_k - x_{k+1})(x_k - x_{k+3})}{(x_{k+2} - x_{k+1})(x_{k+2} - x_{k+3})}, \\ l_{k+3}(x_k) &= \frac{(x_k - x_{k+1})(x_k - x_{k+2})}{(x_{k+3} - x_{k+1})(x_{k+3} - x_{k+2})}. \end{aligned}$$

14. Repeat steps 4 - 13 until $t = T$.

Figures 6.7(a) and 6.7(b) show the comparison of the above algorithm with the COMSOL Multiphysics simulations for slowly and one rapidly varying diffusivities. For two rapidly varying diffusivities, the numerical solution of (6.21)-(6.24) with $\Phi_1 \neq 0$, $\Phi_2 \neq 0$ remains an open problem. Neither the sweep method explained here nor the use of inbuilt MATLAB ODE solvers to obtain a solution to (6.118), (6.119) directly, yield satisfactory results. There are many papers concerning the solution via the method of lines approach of two phase Stefan problems starting with [39]. The boundary condition at the free interface has the form

$$\gamma_1(s(t),t)\frac{\partial c}{\partial x}(s(t),t) - \gamma_2(s(t),t)\frac{\partial h}{\partial x}(s(t),t) + \lambda(s(t),t)\frac{\mathrm{d}s}{\mathrm{d}t} = \mu(s(t),t),$$

and it is the appearance of the nonlinear term $\dot{s}\Phi_2(\dot{s})$ in (6.23) that requires more investigation.

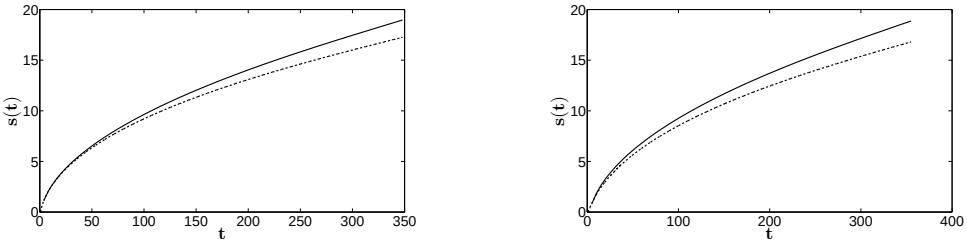

(a) Slowly varying diffusivitives (b) One rapidly varying diffusivity

Figure 6.7: *Comparison of the COMSOL simulations (solid line) with the numerical results of* (6.21)-(6.24) *(dashed line) calculated using the method of lines.*

In this chapter, the derived one- and two-phase micro-macro problems from chapters 2, 3 and 4 have been considered in detail for the quasi-steady CO_2 limit $\mu \to 0$. The large and small time behaviours have been computed as well as the numerical solutions using the method of lines.

Chapter 7

Simulations in Two Dimensions

All the modelling, analysis and numerical simulations have been done in one dimension only. However, in reality, concrete carbonation can not only occur in one dimension. Figure 7.1 shows several different shapes of concrete that have been sprayed with phenolphthalein to detect the change in pH. These pictures motivate this last chapter in which we look at the full reaction-diffusion system (1.2)-(1.6) in two dimensions and generalise to higher dimensions the one and two-phase Stefan problems. The results in this chapter are only meant to be a sneak peek into the large amount of further research possibilities that there is in higher dimensions.

(a) Square (b) Circle (c) Crack

Figure 7.1: *Examples of partly carbonated concrete segments sprayed with phenolphthalein. The pink areas correspond to high pH, where the carbonation has not yet taken place, and the colourless regions correspond to low pH, where carbonation has occurred. These pictures have been obtained from [48], [5] and [15] respectively.*

Figure 7.2 shows a schematic of a two-phase region with moving boundary $f(\mathbf{x}, t) = 0$ with outward unit normal $\mathbf{n}$ and velocity along the normal $v_n = -\frac{\partial f}{\partial t}/|\nabla f|$. For the fixed boundaries, let $\mathbf{n}$ denote their corresponding outward normal. Using the notation in figure 7.2, the higher dimensional version of the one-phase Stefan problem (6.1)-(6.4) is

$$\text{In } \Omega_1,\ t > 0: \qquad \mu \frac{\partial c_0}{\partial t} = \nabla \cdot (D_{c_0} \nabla c_0),$$

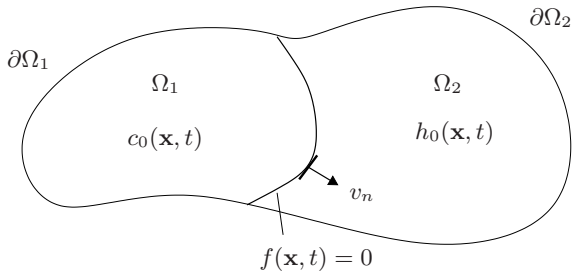

Figure 7.2: *Two-phase region with a moving boundary* $f(\mathbf{x},t)=0$.

$$
\begin{aligned}
&\text{on } \partial\Omega_1 && \mathbf{n}\cdot(-D_{c_0}\nabla c_0) = H(1-c_0),\\
&\text{on } f(\mathbf{x},t)=0 && c_0 = \Phi_1(v_n,\kappa), \quad \mathbf{n}\cdot(-D_{c_0}\nabla c_0) = v_n(\mu c_0 + h_0),\\
&\text{at } t=0 && c_0(\mathbf{x},0) = c_i(\mathbf{x}), \quad f(\mathbf{x},t) = f_0(\mathbf{x}).
\end{aligned}
$$

The two-phase Stefan problem (6.5)-(6.12) becomes

$$
\begin{aligned}
&\text{In } \Omega_1,\ t>0: && \mu\frac{\partial c_0}{\partial t} = \nabla\cdot(D_{c_0}\nabla c_0),\\
&\text{In } \Omega_2,\ t>0: && \frac{\partial h_0}{\partial t} = \nabla\cdot(D_{h_0}\nabla h_0),\\
&\text{on } \partial\Omega_1 && \mathbf{n}\cdot(-D_{c_0}\nabla c_0) = H(1-c_0),\\
&\text{on } f(\mathbf{x},t)=0 && c_0 = \Phi_1(v_n,\kappa), \quad h_0 = \Phi_2(v_n,\kappa),\\
& && \mathbf{n}\cdot(-D_{c_0}\nabla c_0) - \mathbf{n}\cdot(-D_{h_0}\nabla h_0) = v_n(\mu c_0 + h_0),\\
&\text{on } \partial\Omega_2 && \mathbf{n}\cdot(D_{h_0}\nabla h_0) = 0,\\
&\text{at } t=0 && c_0(\mathbf{x},0) = C_i(\mathbf{x}), \quad h_0(\mathbf{x},0) = H_i(\mathbf{x}), \quad f(\mathbf{x},t) = f_0(\mathbf{x}).
\end{aligned}
$$

Note that $\Phi_{1,2}$ will now also depend on the mean curvature κ. In the 1D scenario, the free boundary was computed as the point where the concentrations of CO_2 and $Ca(OH)_2$ meet. However, in order to extract this level set from the simulations we would have to determine κ. Many different forms for κ can be found in the literature [10, 68, 18]. In [12] a linear combination of v_n and κ is used, and based on the work of Chapter 5, a power law in v_n and a power law in κ would be expected. The analysis nevertheless gets much more intricate. Looking at the simulations depicted here, the interface looks symmetric and so taking the curvature as constant might be a reasonable assumption. The problem could therefore seen as the 1D case one, simplifying the work.

To finish, we implement in COMSOL Multiphysics three different two-dimensional scenarios depicted in figure 7.3. Figures 7.4-7.7 depict the scenario in figure 7.3(a), figures 7.8-7.10 refer to figure 7.3(b) and the rest show the geometry in figure 7.3(c). We implement the reaction-diffusion equations (2.6)-(2.10) in 2D with a free triangular mesh of 36992 elements (148930 degrees of freedom), 17536 elements (70786 degrees of freedom) and 19840 elements (80194 degrees of freedom) for geometries depicted in

figure 7.3 (a), (b) and (c) respectively. Refining the mesh does not affect the results and the parameter values used are

$$h_i = 1, \quad c_i = 0 \text{ for } 0 \leq x \leq 1, \quad \mu = 10^{-3}, \quad H = 10^4, \quad p = q = 1.$$

The computational times are in the range of hours. It is here where an adaptive mesh that tracks the free boundary and is finer around it, would be most useful.

For each geometry, the three different diffusion coefficient cases are shown for the parameter regime $\delta = O(\epsilon)$, with $\epsilon = 10^{-2}$ for slowly and one rapidly varying diffusion coefficients and $\epsilon = 10^{-1}$ for two rapidly varying diffusion coefficients. In addition, figure 7.4 includes the case $\delta = \epsilon^2$. This allows a comparison between the two parameter regimes, $\delta \ll \epsilon$ and $\delta = O(\epsilon)$, that gave different behaviours in the one dimensional case. It is worth mentioning that simulations for any other two dimensional geometries and three dimensional settings can be obtained in COMSOL in the exact same way.

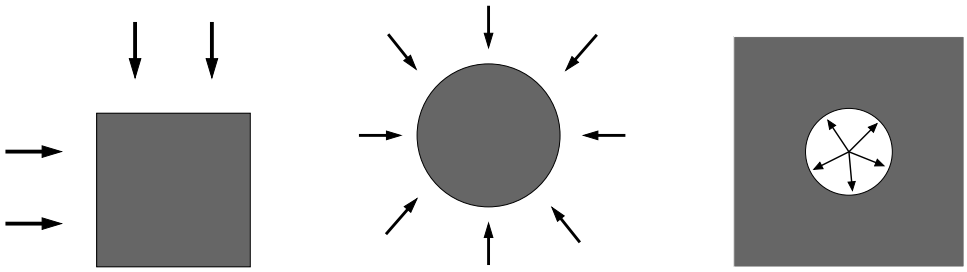

(a) Square (b) Circle (c) Hole

Figure 7.3: *The three 2D geometries considered in this section. The arrows denote the entrance of external CO_2.*

Similar behaviours as the ones observed in the one dimensional case can be seen. The reaction still seems to occur as a sharp front. Figures 7.4 and 7.5 show that for $\delta \ll \epsilon$, the concentration of $Ca(OH)_2$ is unity and falls to zero at the reaction front while, for $\delta = O(\epsilon)$ there is noticeable diffusion. In both geometries, the reaction slows down as we progress though the different diffusion coefficient cases.

To obtain more details, further analysis is needed. Nevertheless, these simulations provide a very good initial idea on the reaction's behaviour for any kind of geometry.

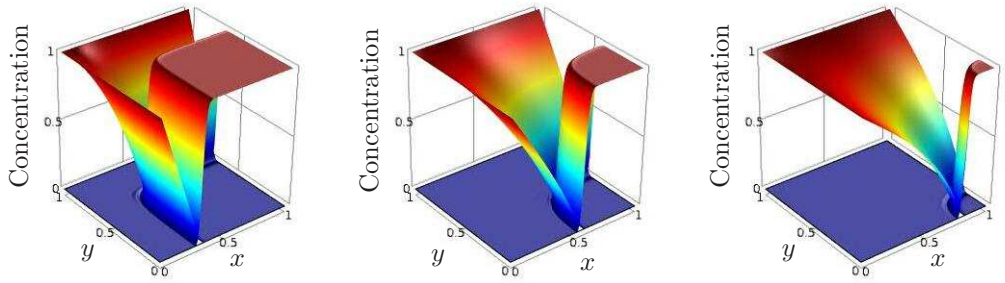

(a) $t = 0.05$ (b) $t = 0.15$ (c) $t = 0.25$

Figure 7.4: *Concentration profiles of CO_2 and $Ca(OH)_2$ for the scenario depicted in figure 7.3(a) with slowly varying diffusion coefficients and $\delta = \epsilon^2$, $\epsilon = 10^{-2}$. The times are as stated in (a) - (c).*

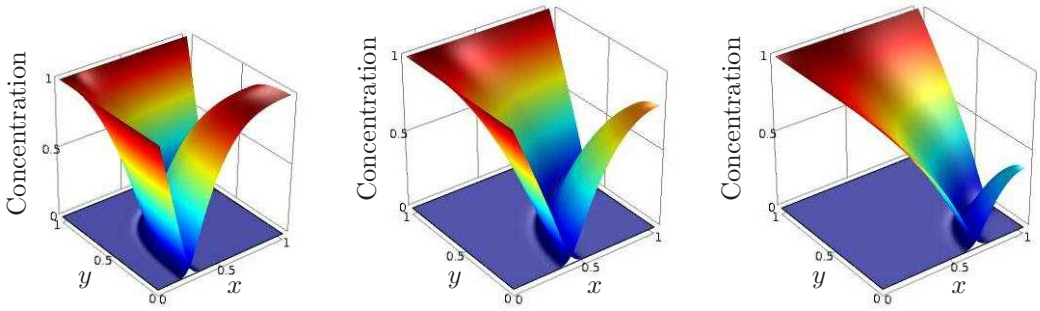

(a) $t = 0.05$ (b) $t = 0.10$ (c) $t = 0.15$

Figure 7.5: *Concentration profiles of CO_2 and $Ca(OH)_2$ for the scenario depicted in figure 7.3(a) with slowly varying diffusion coefficients and $\delta = \epsilon$, $\epsilon = 10^{-2}$. The times are as stated in (a) - (c).*

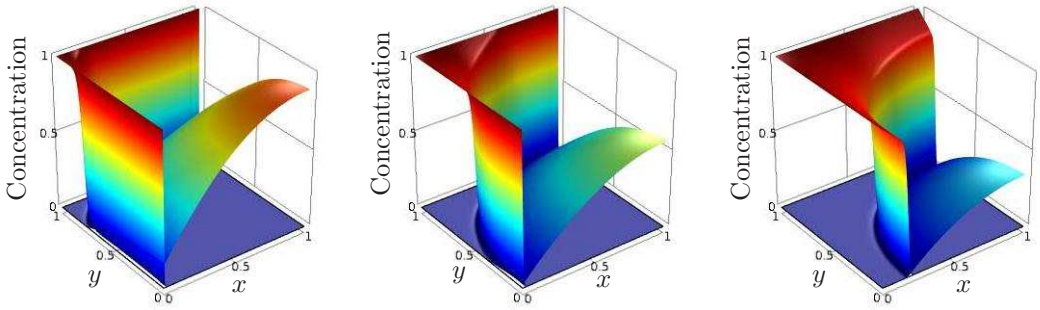

(a) $t = 0.15$ (b) $t = 0.25$ (c) $t = 0.35$

Figure 7.6: *Concentration profiles of CO_2 and $Ca(OH)_2$ for the scenario depicted in figure 7.3(a) with one rapidly varying diffusion coefficient and $\delta = \epsilon$, $\epsilon = 10^{-2}$. The times are as stated in (a) - (c).*

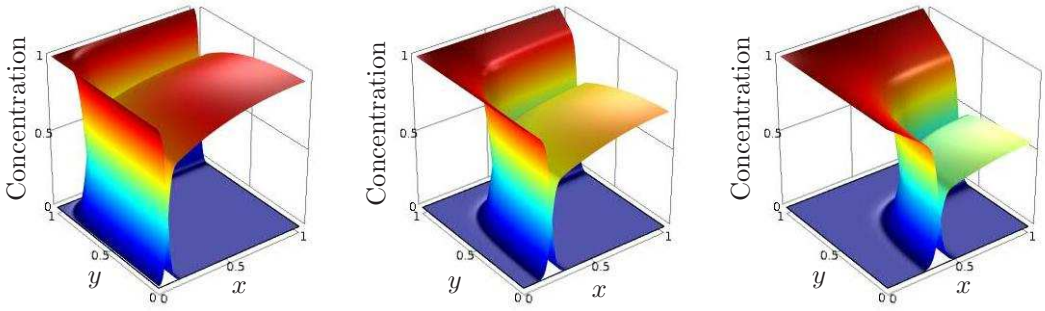

(a) $t = 0.15$ (b) $t = 0.35$ (c) $t = 0.55$

Figure 7.7: *Concentration profiles of CO_2 and $Ca(OH)_2$ for the scenario depicted in figure 7.3(a) with two rapidly varying diffusion coefficients and $\delta = \epsilon$, $\epsilon = 10^{-1}$. The times are as stated in (a) - (c).*

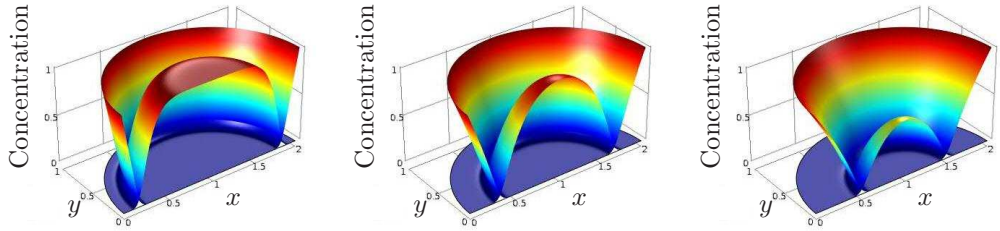

(a) $t = 0.02$ (b) $t = 0.06$ (c) $t = 0.10$

Figure 7.8: *Concentration profiles of CO_2 and $Ca(OH)_2$ for the scenario depicted in figure 7.3(b) with slowly varying diffusion coefficients and $\delta = \epsilon$, $\epsilon = 10^{-2}$. The times are as stated in (a) - (c).*

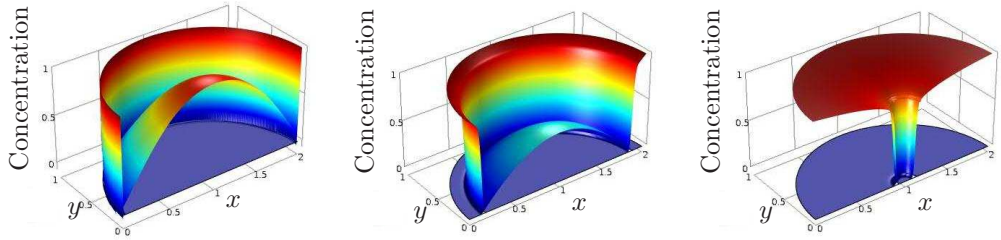

(a) $t = 0.10$ (b) $t = 0.25$ (c) $t = 0.40$

Figure 7.9: *Concentration profiles of CO_2 and $Ca(OH)_2$ for the scenario depicted in figure 7.3(b) with one rapidly varying diffusion coefficient and $\delta = \epsilon$, $\epsilon = 10^{-2}$. The times are as stated in (a) - (c).*

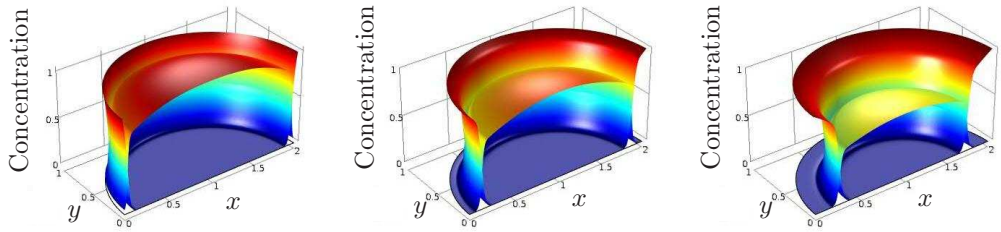

(a) $t = 0.10$ (b) $t = 0.25$ (c) $t = 0.40$

Figure 7.10: *Concentration profiles of CO_2 and $Ca(OH)_2$ for the scenario depicted in figure 7.3(b) with two rapidly varying diffusion coefficients and $\delta = \epsilon$, $\epsilon = 10^{-1}$. The times are as stated in (a) - (c).*

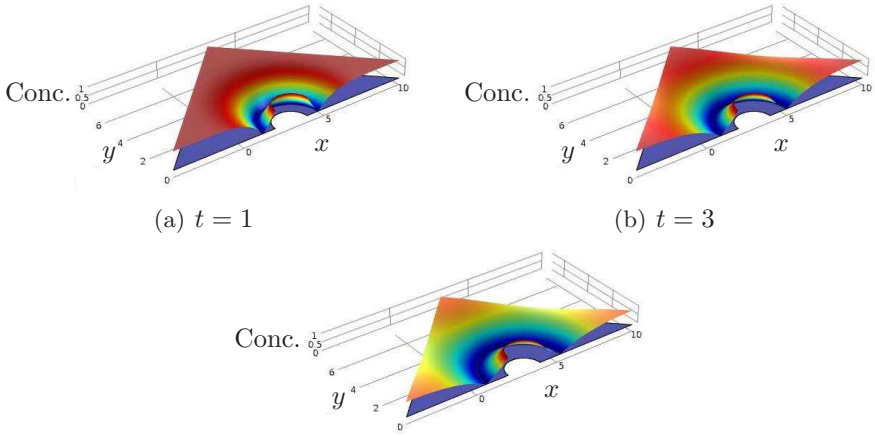

(a) $t = 1$ (b) $t = 3$

(c) $t = 5$

Figure 7.11: *Concentration profiles of CO_2 and $Ca(OH)_2$ for the scenario depicted in figure 7.3(c) with slowly varying diffusion coefficients and $\delta = \epsilon$, $\epsilon = 10^{-2}$. The times are as stated in (a) - (c).*

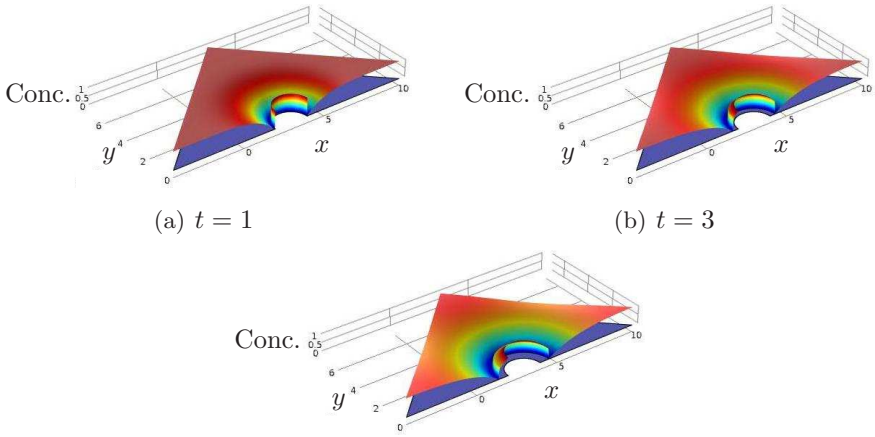

(a) $t = 1$ (b) $t = 3$

(c) $t = 5$

Figure 7.12: *Concentration profiles of CO_2 and $Ca(OH)_2$ for the scenario depicted in figure 7.3(c) with one rapidly varying diffusion coefficient and $\delta = \epsilon$, $\epsilon = 10^{-2}$. The times are as stated in (a) - (c).*

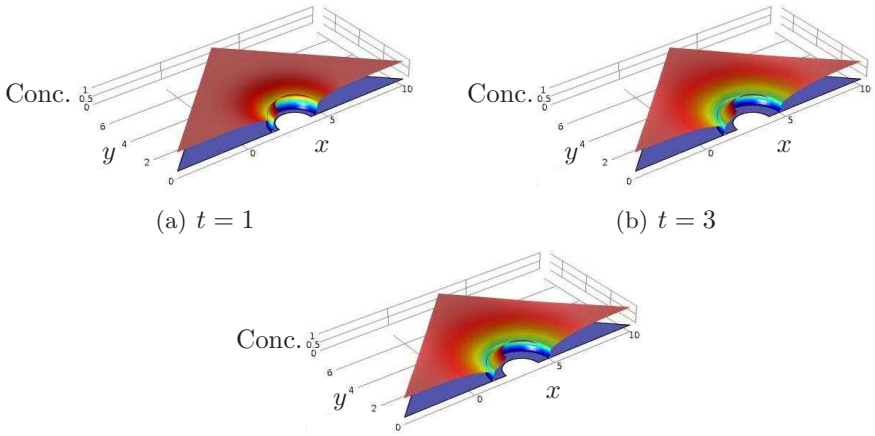

(a) $t = 1$ (b) $t = 3$

(c) $t = 5$

Figure 7.13: *Concentration profiles of CO_2 and $Ca(OH)_2$ for the scenario depicted in figure 7.3(c) with two rapidly varying diffusion coefficient and $\delta = \epsilon$, $\epsilon = 10^{-1}$. The times are as stated in (a) - (c).*

Chapter 8

Conclusions

8.1 Summary

A set of reaction-diffusion equations representing the concrete carbonation process has been analysed in the limit $\epsilon \to 0$, which represents the fast reaction - slow diffusion limit. Three conceptually different scaling regimes (in terms of ϵ) of the diffusivities of the two main species CO_2 and $Ca(OH)_2$ are explored. Using the technique of matched asymptotics, different sharp interface models in the form of generalised Stefan problems are derived, depending upon the properties of the diffusivities as well as the size of the relative transport parameter $\delta^2/\epsilon^2 = D_h^0 h^0 / D_c^0 C^* \leq O(1)$. These two considerations determine the type of sharp interface Stefan problem and the kinetic conditions at the interface.

For $\delta \ll \epsilon$, the following one-phase Stefan problem results

$$
\begin{aligned}
&\text{in } 0 < x < s(t),\ t > 0 && \mu \frac{\partial c_0}{\partial t} = \frac{\partial}{\partial x}\left(D_{c_0} \frac{\partial c_0}{\partial x} \right), \\
&\text{on } x = 0 && -D_{c_0} \frac{\partial c_0}{\partial x} = H(1 - c_0), \\
&\text{on } x = s(t) && c_0 = \Phi_1(\dot{s}), \quad -D_{c_0} \frac{\partial c_0}{\partial x} = \dot{s}(\mu c_0 + h_i(s)), \\
&\text{at } t = 0 && c = c_i \text{ for } 0 \leq x \leq s_0, \quad s = s_0,
\end{aligned}
$$

with $h_0 = h_i$ for $s(t) \leq x \leq 1$.

For $\delta = O(\epsilon)$, we obtain the two-phase Stefan problem

$$
\begin{aligned}
&\text{in } 0 < x < s(t),\ t > 0 && \mu \frac{\partial c_0}{\partial t} = \frac{\partial}{\partial x}\left(D_{c_0} \frac{\partial c_0}{\partial x} \right), \\
&\text{in } s(t) < x < 1,\ t > 0 && \frac{\partial h_0}{\partial t} = \frac{\partial}{\partial x}\left(D_{h_0} \frac{\partial h_0}{\partial x} \right), \\
&\text{on } x = 0 && -D_{c_0} \frac{\partial c_0}{\partial x} = H(1 - c_0),
\end{aligned}
$$

$$
\begin{aligned}
&\text{on } x = s(t) && c_0 = \Phi_1(\dot{s}), \quad h_0 = \Phi_2(\dot{s}),\\
& && -D_{c_0}\frac{\partial c_0}{\partial x} - D_{h_0}\frac{\partial h_0}{\partial x} = \dot{s}(\mu c_0 + h_0),\\
&\text{on } x = 1 && D_{h_0}\frac{\partial h_0}{\partial x} = 0,\\
&\text{at } t = t_0 && c_0 = C_i \text{ for } 0 \le x \le s_0, \quad h_0 = H_i \text{ for } s_0 \le x \le 1,\\
& && s = s_0.
\end{aligned}
$$

The sharp interface kinetic conditions for large time are derived to be

$$\Phi_1 = a\dot{s}^{\frac{2}{p+1}}, \quad \Phi_2 = b\dot{s}^{\frac{2}{q+1}},$$

where appropriate, noting that a and b are determined by solving a micro problem. This derivation of the derivation of the behaviour of the kinetic conditions is one of the main results of this thesis. A similar power law has been derived in the case of silicon oxidation [22]. These micro problems describe the reaction zone, thus capturing features of the model on smaller length scales. Further, an eigenmode analysis has been carried out on the systems that yield the micro scale information to conclude that they have a consistent amount of boundary conditions. Therefore, the resulting sharp interface model, considered as a macroscale model, is one of the main results since it contains microscale information, which we argue is more appropriate than simply stating an empirical kinetic condition as previously done in the literature [43].

The macro problems are investigated for the small and large time behaviour of the free boundary as well as the profiles of the main reaction species. The interface has a $\sqrt{t}$ leading order behaviour for $t \gg 1$, agreeing with the carbonation literature [49, 38, 52, 58] amongst others, as well as the metal oxidation [26] and the silicon oxidation [16]. In particular, the dimensional large time behaviour for the interface is

$$s(t) \sim k\sqrt{\frac{D_c^0 c^*}{h^0}t} \quad \text{as} \quad t \to \infty \tag{8.1}$$

where k is a problem dependent dimensionless constant. For the one-phase scenario $k = \sqrt{2}$ and for the two-phase case $k \sim 1$. Although a direct comparison to experimental results of the reaction front obtained here is not given, a rough comparison is possible since (8.1) is equivalent to the behaviour derived in [50] and [43] with $k = \sqrt{2}$. Comparisons to experimental results in both papers yield satisfactory results, suggesting that $\delta \ll \epsilon$ is the most appropriate regime. For $t \ll 1$, the interface appears to be linear. This is a novel result for carbonation but has been previously derived for metal oxidation [26]. An estimate for the leading order coefficients and the next order terms are formulated and used to compare these limiting behaviours with the initial set of reaction-diffusion equations. Numerical schemes modelling carbonation are usually

based on finite element approaches [61]. Here, the method of lines is implemented to obtain numerical solutions of the generalised Stefan problems. These are then compared to the simulations of the set of reaction-diffusion equations obtained in the finite element based program COMSOL Multiphysics. To finalise, numerical results of the full reaction-diffusion equations in two dimensions give an initial insight into the behaviour of more complex geometries.

8.2 Future Directions

The following are a set of points specific to the work done in this thesis that have remained unsolved.

- All the COMSOL Multiphysics simulations have been done using a static uniform mesh. To avoid singularities, due to the small value of ϵ, regularisations for the reaction and diffusion terms were used. It would be of interest to implement a non-uniform adaptive mesh that tracks the moving interface such that a finer mesh is created around it. This would decrease the computational speed and resolve the rapid concentration changes possibly without the need for regularising.

- From the results in chapter 7, the radially symmetric problem is a potential problem for future study.

- In Chapter 5, we numerically solve the micro problems using a shooting method approach. For the purpose of the work presented here, the results were satisfactory, although not all micro problems were solved. However, to conclude more detailed results, an alternative more reliable, efficient and less computationally expensive numerical algorithm would be necessary.

- In Chapter 6, it remains to numerically solve for the two-phase problem with $\Phi_2 \neq 0$. Neither the sweep method applied to all other Stefan problems nor the use of inbuilt MATLAB ODE solvers yielded satisfactory results. The appearance of the nonlinear term $\dot{s}\Phi_2(\dot{s})$ at the interface, requires more investigation

To conclude, a list of open problems that either build on the work done to enhance it further or suggest new approaches motivated by this work is given.

- It is of interest to validate the two-scale models using for example the experimental data as reported in [46] or [49]. It is unclear for the moment whether the leading order two-scale sharp interface model or the reaction-diffusion model, is the best option.

- The choice of the most appropriate diffusion situation i.e. one or both rapidly varying, is a modelling aspect. It will ultimately depend on the best fit with experimental observations for the carbonation zone.

- For the practical corrosion problem, the geometry of the concrete structure plays an important role. It is of interest to extend the asymptotics to two and three dimensional cases and explore the effect of corners on the speed of the moving reaction interface.

- In [28] (section 1.5 and chapter 9), one derived a class of distributed-microstructure models. Roughly speaking, it is about two-scale systems of PDEs which are coupled via micro-macro boundary conditions. In [37] the authors report on such two-scale problems where, at the micro level, a sharp interface model is responsible for the evolution of micro-free reaction boundaries. It would therefore be of interest to derive via homogenization techniques the two scale model exposed here. Examples on homogenization techniques applied to reaction-diffusion problems can be found in [53, 54, 36, 67].

- Are there any connections between this two-scale result and the Localized Model-Upscaling (LMU) method by Pierre Degond et al. [17]? LMU is typically used in the context of Boltzmann-like equations. Essentially, it consists in coupling a perturbation model and its asymptotic limit model via a transition zone. In the transition zone, the solution is decomposed into a microscopic fraction (described by the perturbation problem) and a macroscopic one (described by the limit problem).

- The well-posedness of the single scale Stefan-like problem can be investigated by means of standard methods for free boundary problems like for example in [24]. However, for the two scale free boundary problems this is an open problem. We expect that methods developed in [44, 45] can be adapted to cope with the two-scale structure of this problem.

- Once the limit problems are shown to be well-posed, the next step is to prove rigorously the passing to the limit $\epsilon \to 0$ by getting an upper bound on the convergence rate (corrector estimate). This issue is open even for the derivation (as fast-reaction limit) of the standard Stefan problem.

Appendix A

Correction Terms

Here we look for the correction terms of h and c in outers 1 and 2 respectively since from section 2.2.1 we see that in Outer 1 $h_0 = 0$ and in Outer 2 $c_0 = 0$. These correction terms will depend on the value of p and q. A schematic of this dependence is as follows:

$$\text{Outer 1} \begin{cases} q > 1 \Rightarrow & \text{algebraic,} \\ q \leq 1 \Rightarrow & \text{exponentially small,} \end{cases}$$

$$\text{Outer 2} \begin{cases} p > 1 \Rightarrow & \text{algebraic,} \\ p \leq 1 \Rightarrow & \text{exponentially small.} \end{cases}$$

We will now consider the algebraic and exponential terms separately.

Algebraic Terms

Outer 1 Recall that for $q > 1$ we pose the expansion (2.15) and so (2.6), (2.7) yield

$$\frac{\partial h_1}{\partial t} - \frac{\delta^2}{\epsilon^2}\frac{\partial}{\partial x}\left(D_h \frac{\partial h_1}{\partial x}\right) = -c_0^p h_1^q.$$

Outer 2 Recall that for $p > 1$ we pose the expansion (2.18) and so (2.6), (2.7) yield

$$\mu\frac{\partial c_1}{\partial t} - \frac{\partial}{\partial x}\left(D_c \frac{\partial c_1}{\partial x}\right) = -c_1^p h_0^q.$$

Exponentially Small terms

For $q \leq 1$ and $p \leq 1$ we pose the expansions (2.14) in outer 1 and (2.17) in outer 2 respectively. We then have that algebraically, to all powers of ϵ, $h \equiv 0$ and $c \equiv 0$ respectively. We therefore seek for exponentially small terms.

For simplicity we will only consider the case where $p = q = 1$ and the limit $\mu \to 0$ (recall (2.12)). The most complicated balance in (2.6)-(2.7) is $\delta^2 = \lambda\epsilon^3$, $\lambda = O(1)$ and so this section will be divided into three separate cases: $\lambda = 0$, $\lambda = O(1)$ and $\lambda \to \infty$.

Before going any further, it is worth noticing that in the limit $\mu \to 0$, outer 1 simplifies to

$$\frac{\partial}{\partial x}\left(D_{c_0}\frac{\partial c_0}{\partial x}\right) = 0,$$

and so using the boundary condition (2.8) and taking D_c to be constant we obtain

$$c_0 = a_0 x + b_0 \quad \text{with } a_0 = H(1 - b_0).$$

- **Case** $\lambda = 0$

Here we consider the nondimensionalised problem,

$$\epsilon^2\left(\mu\frac{\partial c}{\partial t} - \frac{\partial}{\partial x}\left(D_c\frac{\partial c}{\partial x}\right)\right) = -ch, \quad \epsilon^2\frac{\partial h}{\partial t} = -ch,$$

with boundary conditions

$$\text{on } x = 0 \quad -D_c\frac{\partial c}{\partial x} = H(1-c), \qquad \text{on } x = 1 \quad \frac{\partial c}{\partial x} = 0,$$

and initial condition as in (2.10). We then obtain three separate regions.
Outer 1 We pose the WKBJ expansions

$$c = \sum_{i=0}^{\infty}\epsilon^{2i}c_{2i} + \epsilon^2 A_c \exp\left(-\frac{\alpha_0(x,t)}{\epsilon^2}\right), \quad h = A_h \exp\left(-\frac{\alpha_0(x,t)}{\epsilon^2}\right),$$

where

$$\begin{aligned} A_c &= A_c(x,t;\epsilon) = A_c^0(x,t) + \epsilon^2 A_c^2(x,t) + O(\epsilon^4), \\ A_h &= A_h(x,t;\epsilon) = A_h^0(x,t) + \epsilon^2 A_h^2(x,t) + O(\epsilon^4). \end{aligned}$$

A_c and A_h contain the non-singular terms with respect to ϵ of the WKBJ expansions. We then obtain

$$\frac{\partial \alpha_0}{\partial t} = c_0, \quad A_h^{2n} = \frac{\partial A_h^{2(n-1)}}{\partial t} + c_{2n} \quad \text{for } n \geq 1, \quad A_c^0 = \frac{c_0}{D_{c_0}}\left(\frac{\partial \alpha_0}{\partial x}\right)^{-2} A_h^0.$$

Outer 2 Posing the WKBJ expansions

$$c = \epsilon^{1+n} A_c \exp\left(-\frac{\alpha_0(x,t)}{\epsilon}\right), \quad h = h_1 - \epsilon^n A_h \exp\left(-\frac{\alpha_0(x,t)}{\epsilon}\right),$$

where

$$A_c = A_c(x,t;\epsilon) = A_c^0(x,t) + \epsilon A_c^1(x,t) + O(\epsilon^2), \tag{A.1}$$
$$A_h = A_h(x,t;\epsilon) = A_h^0(x,t) + \epsilon A_h^1(x,t) + O(\epsilon^2), \tag{A.2}$$

we obtain

$$\alpha_0 = \sqrt{\frac{h_i}{D_c}}x + \bar{\alpha_0}(t), \quad A_c^0 = A_c^0(t), \quad A_h^0 = h_i\left(\frac{\mathrm{d}\bar{\alpha}_0}{\mathrm{d}t}\right)^{-1} A_c^0,$$

where $\bar{\alpha}_0$ will be determined via matching.

Inner The required inner scalings are

$$x = s(t) + \epsilon\bar{x}, \quad c = \epsilon\bar{c}, \quad h = \bar{h}, \tag{A.3}$$

to obtain

$$\epsilon^2\mu\frac{\partial\bar{c}}{\partial t} - \epsilon\dot{s}\frac{\partial\bar{c}}{\partial\bar{x}} - \frac{\partial}{\partial\bar{x}}\left(D_c\frac{\partial\bar{c}}{\partial\bar{x}}\right) = -\bar{c}\bar{h}, \quad \epsilon\frac{\partial\bar{h}}{\partial t} - \dot{s}\frac{\partial\bar{h}}{\partial\bar{x}} = -\bar{c}\bar{h}.$$

Before dealing with the exponentially small terms note that posing $\bar{c} \sim \bar{c}_0$ and $\bar{h} \sim \bar{h}_0$, yields

$$\frac{\partial}{\partial\bar{x}}\left(D_c\frac{\partial\bar{c}_0}{\partial\bar{x}}\right) = \bar{c}_0\bar{h}_0, \quad \dot{s}\frac{\partial\bar{h}_0}{\partial\bar{x}} = \bar{c}_0\bar{h}_0. \tag{A.4}$$

After matching to outer 1 and 2

$$a_0 = -\frac{\dot{s}h_i}{D_c}, \quad b_0 = -sa_0.$$

Thus in outer 1 we have

$$c_0 = \frac{H}{Hs-1}(s-x) \quad \text{with } \dot{s} = \frac{D_c}{h_i}\left(\frac{H}{Hs-1}\right). \tag{A.5}$$

Consider now the exponentially small terms. Matching to outer 2

$$\text{as } \bar{x} \to \infty \quad \mathrm{e}^{-\frac{\alpha_0}{\epsilon}} \to \mathrm{e}^{-\sqrt{\frac{h_i}{D_c}}\bar{x}} \quad \text{with } \bar{\alpha}_0 = -s\sqrt{\frac{h_i}{D_c}}.$$

Matching to outer 1

$$\text{as } \bar{x} \to -\infty \quad \mathrm{e}^{-\frac{\alpha_0}{\epsilon^2}} \to \mathrm{e}^{-\frac{h_i}{4D_c}\bar{x}^2} \quad \text{with } \bar{\alpha}_0 = \frac{h_i}{2D_c}\bar{x}^2 + \frac{sh_i}{2D_c}\left(s - \frac{2}{H}\right) - t.$$

Hence, collecting all the results we have the following ESTs:

For $0 < x < s(t)$,

$$h \sim A_h \text{exp}\left(-\frac{1}{\epsilon^2}\left(\frac{h_i}{2D_{c_0}}x^2 + \frac{sh_i}{2D_{c_0}}(s-x)\right)\right). \tag{A.6}$$

For $s(t) < x < 1$,

$$c \sim \epsilon^{1+n} A_c \text{exp}\left(-\frac{1}{\epsilon}\left(\sqrt{\frac{h_i}{D_{c_0}}}(x-s)\right)\right). \tag{A.7}$$

It remains to determine n in (A.7). In order to do this we need to analyse the behaviour of the inner region as $\bar{x} \to \infty$. From the leading order inner equations (A.4), we obtain

$$\frac{D_c}{2}\bar{c}_0^2 - \bar{h}_0 + h_i\left(1 + \ln\left(\frac{\bar{h}_0}{h_i}\right)\right) = 0. \tag{A.8}$$

As $\bar{x} \to \infty$, we perturb $\bar{h}_0$ around h_i such that $\bar{h}_0 \to h_i - h'$ where $h' \to 0$ and substituting this into (A.8) yields

$$h' = \frac{\sqrt{D_c h_i}}{\dot{s}}\bar{c}_0. \tag{A.9}$$

Now, (A.4) and (A.9) yield

$$\text{as } \bar{x} \to \infty \quad \bar{c}_0 \sim Ae^{-\sqrt{\frac{h_i}{D_c}}\bar{x}}.$$

Matching to outer 2 as $\bar{x} \to \infty$ yields $n = 0$. Hence, for $s(t) < x < 1$, (A.7) becomes

$$c \sim \epsilon A_c \text{exp}\left(-\frac{1}{\epsilon}\left(\sqrt{\frac{h_i}{D_{c_0}}}(x-s)\right)\right).$$

- **Case** $\lambda = O(1)$

We now have

$$\epsilon^2\left(\mu\frac{\partial c}{\partial t} - \frac{\partial}{\partial x}\left(D_c\frac{\partial c}{\partial x}\right)\right) = -ch, \quad \epsilon^2\left(\frac{\partial h}{\partial t} - \lambda\epsilon\frac{\partial}{\partial x}\left(D_h\frac{\partial h}{\partial x}\right)\right) = -ch,$$

with boundary conditions (2.8)-(2.9) and initial condition (2.10). We again obtain three separate regions

Outer 1 Posing the WKBJ expansions

$$c = \sum_{i=0}^{\infty}\epsilon^{i/2}c_{i/2} + \epsilon A_c \text{exp}\left(-\frac{1}{\epsilon^{\frac{3}{2}}}\left(\alpha_0(x,t) + \epsilon^{\frac{1}{2}}\alpha_{\frac{1}{2}}(x,t) + \epsilon\alpha_1(x,t)\right)\right),$$
$$h = A_h \text{exp}\left(-\frac{1}{\epsilon^{\frac{3}{2}}}\left(\alpha_0(x,t) + \epsilon^{\frac{1}{2}}\alpha_{\frac{1}{2}}(x,t) + \epsilon\alpha_1(x,t)\right)\right),$$

where

$$A_c = A_c(x,t;\epsilon) = A_c^0(x,t) + \epsilon^{\frac{1}{2}} A_c^{\frac{1}{2}}(x,t) + O(\epsilon),$$
$$A_h = A_h(x,t;\epsilon) = A_h^0(x,t) + \epsilon^{\frac{1}{2}} A_h^{\frac{1}{2}}(x,t) + O(\epsilon),$$

we obtain

$$\alpha_0 = \frac{2(a_0x+b_0)^{\frac{3}{2}}}{3a_0\sqrt{\lambda D_{h_0}}} + \bar{\alpha}_0(t),$$
$$\frac{\partial \alpha_0}{\partial t} + 2\lambda D_{h_0}\frac{\partial \alpha_0}{\partial x}\frac{\partial a_{\frac{1}{2}}}{\partial x} = c_{\frac{1}{2}}, \quad \frac{\partial \alpha_{\frac{1}{2}}}{\partial t} + 2\lambda D_{h_0}\frac{\partial \alpha_0}{\partial x}\frac{\partial \alpha_1}{\partial x} + \lambda D_{h_0}\left(\frac{\partial \alpha_{\frac{1}{2}}}{\partial x}\right)^2 = c_1,$$
$$2\lambda D_{h_0}\frac{\partial \alpha_0}{\partial x}\frac{\partial A_h^0}{\partial x} - \left(\frac{\partial \alpha_1}{\partial t} + 2\lambda D_{h_0}\frac{\partial \alpha_{\frac{1}{2}}}{\partial x}\frac{\partial \alpha_1}{\partial x} - \lambda D_{h_0}\frac{\partial^2 \alpha_0}{\partial x^2} - c_2\right)A_h^0 = 0,$$
$$A_c^0 = \lambda\frac{D_{h_0}}{D_{c_0}}A_h^0,$$

where $\bar{\alpha}_0$ will be determined via matching.

Outer 2 Posing the WKBJ expansions

$$c = \epsilon^{n+1}A_c\exp\left(-\frac{\alpha_0(x,t)}{\epsilon}\right), \quad h = h_i - \epsilon^n A_h\exp\left(-\frac{\alpha_0(x,t)}{\epsilon}\right),$$

where A_c, A_h are as in (A.1), (A.2) respectively, we obtain

$$\alpha_0 = \sqrt{\frac{h_i}{D_{c_0}}}x + \bar{\alpha}_0, \quad A_c^0 = A_c^0(t), \quad A_h^0 = \left(\frac{h_i}{\lambda\frac{D_{h_0}}{D_{c_0}}h_i - \frac{\mathrm{d}\bar{\alpha}_0}{\mathrm{d}t}}\right)A_c^0,$$

where $\bar{\alpha}_0$ will be determined via matching.

Inner This is as in the previous case where $\lambda = 0$ but with the modification of the diffusion term entering the leading order hydroxide equation. Nevertheless the scalings (A.3) apply as does the subsequent analysis culminating in (A.5).

Consider now the exponentially small terms and matching to outer 2

$$\text{as } \bar{x} \to \infty \quad \mathrm{e}^{-\frac{\alpha_0}{\epsilon}} \to \mathrm{e}^{-\sqrt{\frac{h_i}{D_c}}\bar{x}} \quad \text{with } \bar{\alpha}_0 = -s\sqrt{\frac{h_i}{D_c}}.$$

Matching to outer 1

$$\text{as } \bar{x} \to -\infty \quad \mathrm{e}^{-\frac{\alpha_0}{\epsilon^{\frac{3}{2}}}} \to \mathrm{e}^{\frac{2}{3}\sqrt{\frac{H}{\lambda D_h(1-Hs)}}\bar{x}^{\frac{3}{2}}} \quad \text{with } \bar{\alpha}_0(t) = 0.$$

Hence collecting all the results we have the following ESTs:

For $0 < x < s(t)$,

$$h \sim A_h \exp\left(-\frac{1}{\epsilon^{\frac{3}{2}}}\left(\frac{2}{3}\sqrt{\frac{H}{\lambda D_{h_0}(1-Hs)}}(s-x)^{\frac{3}{2}}\right)\right). \tag{A.10}$$

For $s(t) < x < 1$,

$$c \sim \epsilon^{1+n} A_c \exp\left(-\frac{1}{\epsilon}\left(\sqrt{\frac{h_i}{D_{c_0}}}(x-s)\right)\right). \tag{A.11}$$

Again it remains to determine n in (A.11) and so the behaviour of the inner region as $\bar{x} \to \infty$ has to be analysed. Here we use the following ansatz, $\bar{c}_0 \sim Ae^{a\bar{x}}$, motivated by the case $\lambda = 0$, to obtain after matching to outer 2 that $n = 0$. Hence, for $s(t) < x < 1$, (A.11) becomes

$$c \sim \epsilon A_c \exp\left(-\frac{1}{\epsilon}\left(\sqrt{\frac{h_i}{D_{c_0}}}(x-s)\right)\right).$$

- **Case $\lambda \to \infty$**

In the limit $\lambda \to \infty$, a different rescaling is needed. Consider $\delta^2 = \tilde{\lambda}\epsilon^2$ to obtain

$$\epsilon^2\left(\mu\frac{\partial c}{\partial t} - \frac{\partial}{\partial x}\left(D_c\frac{\partial c}{\partial x}\right)\right) = -ch, \quad \epsilon^2\left(\frac{\partial h}{\partial t} - \tilde{\lambda}\frac{\partial}{\partial x}\left(D_h\frac{\partial h}{\partial x}\right)\right) = -ch,$$

with boundary conditions (2.8)-(2.9) and initial condition (2.10). We again obtain three separate regions.

Outer 1 Posing the WKBJ expansions

$$c = \sum_{i=0}^{\infty}\epsilon^i c_i + \epsilon^n A_c \exp\left(-\frac{\alpha_0(x,t)}{\epsilon}\right), \quad h = \epsilon^n A_h \exp\left(-\frac{\alpha_0(x,t)}{\epsilon}\right),$$

where A_c, A_h are as in (A.1), (A.2) respectively, we obtain

$$\alpha_0 = \frac{2(a_0x+b_0)^{\frac{3}{4}}}{3a_0\sqrt{\tilde{\lambda}D_{h_0}}} + \bar{\alpha}_0(t),$$

$$2\sqrt{\tilde{\lambda}D_{h_0}c_0}\frac{\partial A_h^0}{\partial x} + \left(c_1 + \frac{a_0\sqrt{\tilde{\lambda}D_{h_0}}}{2\sqrt{c_0}} - \frac{\partial a_0}{\partial t}\right)A_h^0 = 0,$$

$$A_c^0 = \frac{D_{c_0}}{\tilde{\lambda}D_{h_0}}A_c^0.$$

Outer 2 Posing the WKBJ expansions

$$c = \epsilon^n A_c \exp\left(-\frac{\alpha_0(x,t)}{\epsilon}\right), \quad h = \sum_{i=0}^{\infty}\epsilon^i h_i + \epsilon^n A_h \exp\left(-\frac{\alpha_0(x,t)}{\epsilon}\right),$$

where A_c, A_h are as in (A.1), (A.2) respectively, we obtain

$$\frac{\partial \alpha_0}{\partial x} = \sqrt{\frac{h_0}{D_{c_0}}}, \quad 2\sqrt{h_0 D_{c_0}}\frac{\partial A_c^0}{\partial x} + \left(h_1 + \frac{\sqrt{D_{c_0}}}{2h_0}\frac{\partial h_0}{\partial x}\right) A_c^0 = 0, \quad A_h^0 = \frac{D_{c_0}}{\tilde{\lambda} D_{h_0}} A_c^0.$$

Inner The required inner scalings here are

$$x = s(t) + \epsilon^{\frac{2}{3}}\bar{x}, \quad c = \epsilon^{\frac{2}{3}}\bar{c}, \quad h = \epsilon^{\frac{2}{3}}\bar{h},$$

to obtain

$$\epsilon^{4/3}\mu\frac{\partial \bar{c}}{\partial t} - \epsilon^{2/3}\mu\dot{s}\frac{\partial \bar{c}}{\partial \bar{x}} - \frac{\partial}{\partial \bar{x}}\left(D_c\frac{\partial \bar{c}}{\partial \bar{x}}\right) = -\bar{c}\bar{h},$$
$$\epsilon^{4/3}\frac{\partial \bar{h}}{\partial t} - \epsilon^{2/3}\dot{s}\frac{\partial \bar{h}}{\partial \bar{x}} - \tilde{\lambda}\frac{\partial}{\partial \bar{x}}\left(D_h\frac{\partial \bar{h}}{\partial \bar{x}}\right) = -\bar{c}\bar{h}.$$

Posing $\bar{c} \sim \bar{c}_0$ and $\bar{h} \sim \bar{h}_0$, yields

$$\frac{\partial}{\partial \bar{x}}\left(D_c\frac{\partial \bar{c}_0}{\partial \bar{x}}\right) = \bar{c}_0\bar{h}_0, \quad \tilde{\lambda}\frac{\partial}{\partial \bar{x}}\left(D_h\frac{\partial \bar{h}_0}{\partial \bar{x}}\right) = \bar{c}_0\bar{h}_0.$$

Matching to outers 1 and 2 gives

$$a_0 = -\frac{\tilde{\lambda} D_{h_0}}{D_{c_0}}\frac{\partial h_0}{\partial x} \quad \text{and} \quad b_0 = -a_0 s.$$

Thus in outer 1 we have

$$c_0 = \frac{H}{Hs - 1}(s - x),$$

and in outer 2 we obtain the following non-standard Stefan problem

$$\begin{aligned}
&\text{in } s(t) < x < 1 && \frac{\partial h_0}{\partial t} - \frac{\partial}{\partial x}\left(D_{h_0}\frac{\partial h_0}{\partial x}\right) = 0,\\
&\text{on } x = s(t) && h_0 = 0, \quad \tilde{\lambda} D_{h_0}\frac{\partial h_0}{\partial x} = -\frac{D_{c_0} H}{1 - Hs},\\
&\text{on } x = 1 && D_{h_0}\frac{\partial h_0}{\partial x} = 0.
\end{aligned}$$

Considering the exponentially small terms we have that, for $0 < x < s(t)$

$$h \sim A_h \exp\left(-\frac{1}{\epsilon^{\frac{3}{2}}}\left(\frac{2}{3}\sqrt{\frac{H}{\lambda D_{h_0}(1 - Hs)}}(s - x)^{\frac{3}{2}}\right)\right).$$

Appendix B

Stage I Carbonation

B.1 Slowly varying diffusivities

Here we complete the analysis in the case $\delta = O(\epsilon)$ considered in subsection 2.3.3 for slowly varying diffusivities. The reaction zone remains at the surface until the hydroxide within it is consumed. As such $h = O(1)$ and for this inner region we consider the scalings

$$x = \epsilon^{\frac{2}{p+1}}\bar{x}, \quad c = \epsilon^{\frac{2}{p+1}}\bar{c}, \quad h = \bar{h}, \tag{B.1}$$

giving

$$\epsilon^{\frac{4}{p+1}}\mu\frac{\partial \bar{c}}{\partial t} - \frac{\partial}{\partial \bar{x}}\left(D_c\frac{\partial \bar{c}}{\partial \bar{x}}\right) = -\bar{c}^p\bar{h}^q,$$
$$\epsilon^{\frac{4}{p+1}}\mu\frac{\partial \bar{h}}{\partial t} - \frac{\partial}{\partial \bar{x}}\left(D_h\frac{\partial \bar{h}}{\partial \bar{x}}\right) = -\epsilon^{\frac{2}{p+1}}\bar{c}^p\bar{h}^q.$$

Posing

$$\bar{c} \sim \bar{c}_0 + \epsilon^{\frac{2}{p+1}}\bar{c}_1, \quad \bar{h} \sim \bar{h}_0 + \epsilon^{\frac{2}{p+1}}\bar{h}_1,$$

with

$$D_c(c,h;\epsilon) \sim D_c(c_0,h_0;0), \quad D_h(c,h;\epsilon) \sim D_h(c_0,h_0;0),$$

after an initial transient $t = O(\epsilon^{\frac{4}{p+1}})$, we obtain at leading order

$$\frac{\partial}{\partial \bar{x}}\left(D_c\frac{\partial \bar{c}_0}{\partial \bar{x}}\right) = \bar{c}_0^p\bar{h}_0^q, \quad \frac{\partial}{\partial \bar{x}}\left(D_h\frac{\partial \bar{h}_0}{\partial \bar{x}}\right) = 0, \tag{B.2}$$

subject to

$$\text{at } \bar{x} = 0 \quad D_c\frac{\partial \bar{c}_0}{\partial \bar{x}} = -H, \quad D_h\frac{\partial \bar{h}_0}{\partial \bar{x}} = 0,$$
$$\text{as } \bar{x} \to +\infty \quad \bar{c}_0 \to 0, \quad \bar{h}_0 \to h_0(0,t).$$

Consequently, taking D_c constant and $H = O(1)$,

$$\bar{h}_0 = h_0(0,t), \quad \bar{c}_0 = \begin{cases} \frac{H}{D_c\sigma_p(t)}\left(1+\frac{p-1}{2}\sigma_p(t)x\right)^{-\frac{2}{p-1}}, & p>1 \\ \frac{H}{D_c\sigma_1(t)}\exp(-\sigma_1(t)x), & p=1 \\ \left(\left(\frac{H}{D_c\tilde{\sigma}(t)}\right)^{\frac{1-p}{1+p}} - \frac{1-p}{2}\tilde{\sigma}(t)x\right)^{\frac{2}{1-p}}, & 0\le p<1, \end{cases}$$

where

$$\theta_p(t) = \left(\frac{2h_0(0,t)^q}{(1+p)D_c}\left(\frac{H}{D_c}\right)^{p-1}\right)^{\frac{1}{1+p}}, \quad \tilde{\theta}(t) = \left(\frac{2h_0(0,t)^q}{(1+p)D_c}\right)^{\frac{1}{2}},$$

and setting $p=1$ in $\theta_p(t)$ gives $\theta_1(t)$. At the next order for the hydroxide, we have

$$\frac{\partial}{\partial\bar{x}}\left(D_h\frac{\partial\bar{h}_1}{\partial\bar{x}}\right) = \bar{c}_0^p\bar{h}_0^q, \tag{B.3}$$

with

$$\text{at } \bar{x}=0 \quad D_h\frac{\partial\bar{h}_1}{\partial\bar{x}} = 0.$$

Combining (B.2) and (B.3) and using the boundary conditions at $\bar{x}=0$ gives

$$D_h\frac{\partial\bar{h}_1}{\partial\bar{x}} = D_c\frac{\partial\bar{c}_0}{\partial\bar{x}} + H. \tag{B.4}$$

The leading order outer 2 problem is thus the fixed domain problem

$$\text{in } 0<x<1,\, t>0 \quad \frac{\partial h_0}{\partial t} = \frac{\partial}{\partial x}\left(D_h\frac{\partial h_0}{\partial x}\right), \tag{B.5}$$

$$\text{on } x=0 \quad D_h\frac{\partial h_0}{\partial x} = H, \tag{B.6}$$

$$\text{on } x=1 \quad D_h\frac{\partial h_0}{\partial x} = 0, \tag{B.7}$$

$$\text{at } t=0 \quad h_0 = h_i \text{ for } 0\le x\le 1, \tag{B.8}$$

where condition (B.6) follows form the matching with the above two term inner solution and using (B.4). In the case when D_h and h_i are constants, consider the transformation

$$h_0(x,t) = \frac{H}{D_h}\left(\frac{x}{2}(2-x) + w(x,t)\right) - Ht.$$

Now a straight forward separation of variables using the Fourier method yields the solution for $w(x,t)$ and so we have the following explicit solution for $h_0(x,t)$

$$h_0(x,t) = h_i - Ht + \frac{H}{D_h}\left(\frac{x}{2}(2-x) + \sum_{n=0}^{\infty} f_n\exp(-D_h n^2\pi^2 t)\cos(n\pi x)\right), \tag{B.9}$$

where the Fourier coefficients are

$$f_0 = -\frac{1}{3}, \quad f_n = \frac{2}{n^2\pi^2} \text{ for } n \geq 1.$$

In the semi-infinite domain case we use Laplace transform to obtain

$$h_0(x,t) = h_i - \frac{2H}{\sqrt{\pi D_h}} \int_{\sqrt{\frac{x^2}{4D_h t}}}^{\infty} \left(\tau - \frac{x^2}{4D_h t}\right) \mathrm{e}^{-\tau^2} \mathrm{d}\tau. \tag{B.10}$$

We denote by $t = t_0$ the time at which the leading order hydroxide concentration falls to zero at the reaction zone i.e. $h_0(0,t) = 0$, the resulting concentration profile then being $H_i(x) = h_0(x,t_0)$. In the finite domain case, (B.9) gives a transcendental equation for t_0,

$$Ht_0 = h_i + \frac{H}{D_h} \sum_{n=0}^{\infty} f_n \exp(-D_h n^2 \pi^2 t_0), \tag{B.11}$$

with then

$$H_i(x) = h_i - Ht_0 + \frac{H}{D_h} \left(\frac{x}{2}(2-x) + \sum_{n=0}^{\infty} f_n \exp(-D_h n^2 \pi^2 t_0) \cos(n\pi x) \right).$$

B.2 Single rapidly varying diffusivity D_c

For the single rapidly varying CO_2 diffusivity considered in subsection 3.1.3, a stage I carbonation regime takes place analogous to the slowly varying case. The CO_2 diffusivity is now small in the reaction zone consequently the scalings (B.1) change to

$$x = \epsilon^{\frac{4}{p+1}} \bar{x}, \quad c = \epsilon^{\frac{4}{p+1}} \bar{c}, \quad h = \bar{h}, \quad D_c = \epsilon^2 \bar{D}_c,$$

and the expansion modified to

$$\bar{c} = \bar{c}_0 + \epsilon^{\frac{4}{p+1}} \bar{c}_1 + \ldots, \quad \bar{h} = \bar{h}_0 + \epsilon^{\frac{4}{p+1}} \bar{h}_1 + \ldots.$$

The rest of the analysis remains similar, with D_c replaced by $\bar{D}_c$ which we note for the specific form (3.1) is $\bar{D}_c = \frac{\nu_1}{h_0(0^+,t)^q}$. This pertains until $h_0(0^+,t)$ falls to $O(\epsilon^{\frac{2}{q}})$, the waiting time t_0 being the same in this case.

Appendix C

One Rapidly Varying Diffusion Coefficient - General Case

Here we perform the analogous calculations as done in chapter 3 but, instead of (3.1), we consider a more general form of the carbon dioxide diffusion coefficient

$$D_c = 1 - \exp\left(-\frac{\nu_1 \epsilon^2}{h^m}\right), \tag{C.1}$$

where ν_1, m_1 are positive constants and $D_c(c, 0; \epsilon)$=1. As such, it is no longer necessarily linked to the carbonation reaction and so h can take any power, m_1. The results obtained are similar to the ones in chapter 3, but now more care is needed on the scalings and matching, the most interesting case being the regime $\epsilon^2 < \delta < \epsilon$.

The case $\delta \leq \epsilon^2$

The scalings for the inner inner region are

$$x = s(t) + \epsilon^2 \bar{x}, \quad c = \bar{c}, \quad h = \bar{h}, \quad D_c = \epsilon^2 \bar{D}_c,$$

which give

$$\mu\epsilon^2 \frac{\partial \bar{c}}{\partial t} - \mu \dot{s} \frac{\partial \bar{c}}{\partial \bar{x}} - \frac{\partial}{\partial \bar{x}}\left(\bar{D}_c \frac{\partial \bar{c}}{\partial \bar{x}}\right) = -\bar{c}^p \bar{h}^q,$$
$$\epsilon^2 \frac{\partial \bar{h}}{\partial t} - \dot{s} \frac{\partial \bar{h}}{\partial \bar{x}} - \frac{\delta^2}{\epsilon^4} \frac{\partial}{\partial \bar{x}}\left(D_h \frac{\partial \bar{h}}{\partial \bar{x}}\right) = -\bar{c}^p \bar{h}^q.$$

Posing the expansions

$$\bar{c} = \bar{c}_0 + o(1), \quad \bar{h} = \bar{h}_0 + o(1),$$

we obtain at leading order

$$\mu\dot{s}\frac{\partial\bar{c}_0}{\partial\bar{x}}+\frac{\partial}{\partial\bar{x}}\left(\bar{D}_c\frac{\partial\bar{c}_0}{\partial\bar{x}}\right)=\bar{c}_0^p\bar{h}_0^q,$$
$$\dot{s}\frac{\partial\bar{h}_0}{\partial\bar{x}}+\frac{\delta^2}{\epsilon^4}\frac{\partial}{\partial\bar{x}}\left(D_h\frac{\partial\bar{h}_0}{\partial\bar{x}}\right)=\bar{c}_0^p\bar{h}_0^q,$$

together with the matching conditions

$$\text{as } \bar{x}\to-\infty \quad \bar{c}_0\to c_0(s^-,t), \quad \bar{D}_c\frac{\partial\bar{c}_0}{\partial\bar{x}}\to D_c\frac{\partial c_0(s^-,t)}{\partial x}, \quad \bar{h}_0\to 0, \tag{C.2}$$

$$\text{as } \bar{x}\to+\infty \quad \bar{c}_0\to 0, \quad \bar{h}_0\to h_0(s^+,t), \quad D_h\frac{\partial\bar{h}_0}{\partial\bar{x}}\to 0. \tag{C.3}$$

An additional region is required to facilitate the matching with outer 1 and explain (C.2) due to the change in the order of magnitude in the carbon dioxide diffusivity. We denote this region inner 1, the scalings for which are determined by the value of q. We consider first the case $1<q<m+1$ and we apply the scalings

$$x=s(t)+\epsilon^{2-\frac{2}{m}(q-1)}\bar{X}, \quad c=\bar{C}, \quad h=\epsilon^{\frac{2}{m}}\bar{H}, \tag{C.4}$$

so that

$$\epsilon^{\frac{4}{m}(m-q+1)}\frac{\partial\bar{C}}{\partial t}-\epsilon^{\frac{2}{m}(m-q+1)}\dot{s}\frac{\partial\bar{C}}{\partial\bar{X}}-\frac{\partial}{\partial\bar{X}}\left(D_c\frac{\partial\bar{C}}{\partial\bar{X}}\right)=-\epsilon^{\frac{2}{m}(m-q+2)}\bar{C}^p\bar{H}^q,$$
$$\epsilon^{\frac{2}{m}(m-q+1)}\frac{\partial\bar{H}}{\partial t}-\dot{s}\frac{\partial\bar{H}}{\partial\bar{X}}-\frac{\delta^2}{\epsilon^{\frac{2}{m}(2m-q+1)}}\frac{\partial}{\partial\bar{X}}\left(D_h\frac{\partial\bar{H}}{\partial\bar{X}}\right)=\bar{C}^p\bar{H}^q.$$

Note that in this case, the transition region is larger in size than the interior (reaction) layer and that the asymptotic structure for $q>m+1$ is quite different. Posing

$$\bar{C}\sim\bar{C}_0+\epsilon^{\frac{2}{m}(m-q+1)}\bar{C}_1, \quad \bar{H}\sim\bar{H}_0,$$

we obtain

$$\frac{\partial}{\partial\bar{X}}\left(D_c\frac{\partial\bar{C}_0}{\partial\bar{X}}\right)=0, \quad \dot{s}\frac{\partial\bar{H}_0}{\partial\bar{X}}=\bar{C}_0^p\bar{H}_0^q, \quad \mu\dot{s}\frac{\partial\bar{C}_0}{\partial\bar{X}}+\frac{\partial}{\partial\bar{X}}\left(D_c\frac{\partial\bar{C}_1}{\partial\bar{X}}\right)=0. \tag{C.5}$$

After matching to outer 1 and the inner inner we have, for $1<q<m+1$

$$\bar{C}_0=c_0(s^-,t)=\Phi_1, \quad D_c\frac{\partial\bar{C}_1}{\partial\bar{X}}=D_c\frac{\partial c_0(s^-,t)}{\partial x}, \tag{C.6a}$$

$$\bar{H}_0=\left(-\frac{q-1}{\dot{s}}c_0(s^-,t)^p\bar{X}\right)^{-\frac{1}{q-1}}. \tag{C.6b}$$

For $q=1$, the transition region is of the same size as the reaction layer and so the

spatial scaling (C.4) is modified to

$$x = s(t) + \epsilon^2(S(t) + \bar{X}),$$

where $1 < S(t) < 1/\epsilon^2$. Posing

$$\bar{C} \sim \bar{C}_0 + \epsilon^2 \bar{C}_1, \quad \bar{H} \sim \bar{H}_0,$$

we obtain (C.5) with the diffusion term entering the leading order hydroxide equation and matching yields (C.6a), but now with

$$\bar{H}_0 = \exp\left(\frac{\epsilon^4}{\delta^2}\frac{\dot{s}}{2D_h}\left(-1+\sqrt{1+\frac{\delta^2}{\epsilon^4}\frac{4D_h c_0(s^-,t)^p}{\dot{s}^2}}\right)\right)\bar{X}, \quad S(t) \sim \frac{2}{m}\frac{\dot{s}}{c_0(s^-,t)^p}\ln(\epsilon).$$

When $0 < q < 1$, the transition region is narrower than the inner inner. We introduce the scalings

$$x = s(t) + \epsilon^{2+\frac{1-q}{m}}\bar{X}, \quad c = \bar{C}, \quad h = \epsilon^{\frac{2}{m}}\bar{H},$$

and pose

$$\bar{C} \sim \bar{C}_0 + \epsilon^{2+\frac{1-q}{m}}\bar{C}_1, \quad \bar{H} \sim \bar{H}_0,$$

which lead to (C.5) with the equation for $\bar{H}_0$ now being

$$\frac{\delta^2}{\epsilon^4}\frac{\partial}{\partial \bar{X}}\left(D_h\frac{\partial \bar{H}_0}{\partial \bar{X}}\right) = \bar{C}_0^p \bar{H}_0^q.$$

Matching to outer 1 and the inner inner gives (C.6a) with $\bar{H}_0$ (taking D_h constant) given by

$$\bar{H}_0 = \begin{cases} \left(\frac{(1-q)^2 c_0(s^-,t)^p \epsilon^4}{2(1+q)D_h\delta^2}\bar{X}^2\right)^{\frac{1}{1-q}} & \text{for } \bar{X} > 0 \\ 0 & \text{for } \bar{X} < 0. \end{cases}$$

The inner inner region is now restricted to $\bar{x} > 0$ with the inner 1 matching conditions (C.6a) occurring as $\bar{x} \to 0^+$.

Summarising, for $\delta \leq \epsilon^2$, we obtain the same one-phase micro-macro problem as in the equivalent parameter regime in chapter 3.

The case $\epsilon^2 < \delta < \epsilon$

This case is more involved, where the reaction zone splits into four regions. In progressing from outer 2 to outer 1, we label the regions as inner 2, inner inner 2, inner inner 1, and finally inner 1. It is worth mentioning that for the special case $q = m$, inner inner 1 and inner inner 2 are equivalent and correspond to the inner inner region in section (3.1.2) .

The scalings for the inner 2 region are given by

$$x = s(t) + \left(\frac{\delta}{\epsilon}\right)^2 \hat{X}, \quad c = 0, \quad h = \hat{H}, \quad D_c = \epsilon^2 \hat{D}_c,$$

where c is actually exponentially small in ϵ if $p \geq 1$. The governing equation for the hydroxide at leading order in $\hat{X} > 0$ is

$$\dot{s}\frac{\partial \hat{H}_0}{\partial \hat{X}} + \frac{\partial}{\partial \hat{X}}\left(D_h \frac{\partial \hat{H}_0}{\partial \hat{X}}\right) = 0,$$

together with the outer 2 matching conditions

$$\text{as } \hat{X} \to +\infty \quad \hat{H}_0 \to h_0(s^+, t), \quad \frac{\partial \hat{H}_0}{\partial \hat{X}} \to 0.$$

Thus

$$D_h \frac{\partial \hat{H}_0}{\partial \hat{X}} = \dot{s}(h_0(s^+, t) - \hat{H}_0),$$

and for matching with inner inner 2, we have the behaviour

$$\text{as } \hat{X} \to 0^+ \quad \hat{H}_0 \to 0, \quad D_h \frac{\partial \hat{H}_0}{\partial \hat{X}} \to \dot{s} h_0(s^+, t).$$

In the case D_h a constant, we have the simple explicit solution

$$\hat{H}_0 = h_0(s^+, t)\left(1 - \exp\left(\frac{\dot{s}}{D_h}\hat{X}\right)\right).$$

For the inner inner 2 region, we adopt the scalings

$$x = s(t) + \bar{\epsilon}_2 \left(\frac{\delta}{\epsilon}\right)^2 \hat{x}, \quad c = \bar{\epsilon}_1 \hat{c}, \quad h = \bar{\epsilon}_2 \hat{h}, \quad D_c = \frac{\epsilon^2}{\bar{\epsilon}_2^m}\hat{D}_c, \tag{C.7}$$

where

$$\bar{\epsilon}_1 = \left(\frac{\epsilon^2}{\delta}\right)^{\frac{2(m-q)}{mp+p+q+1}} < 1, \qquad \bar{\epsilon}_2 = \left(\frac{\epsilon^2}{\delta}\right)^{\frac{2(p+1)}{mp+p+q+1}} < 1.$$

The governing equations are

$$\left(\frac{\delta}{\epsilon}\right)^2 \bar{\epsilon}_1 \bar{\epsilon}_2 \mu \frac{\partial \hat{c}}{\partial t} - \bar{\epsilon}_1 \mu \dot{s}\frac{\partial \hat{c}}{\partial \hat{x}} - \frac{\partial}{\partial \hat{x}}\left(\hat{D}_c \frac{\partial \hat{c}}{\partial \hat{x}}\right) = -\hat{c}^p \hat{h}^q,$$
$$\left(\frac{\delta}{\epsilon}\right)^2 \bar{\epsilon}_2^2 \frac{\partial \hat{h}}{\partial t} - \bar{\epsilon}_2 \dot{s}\frac{\partial \hat{h}}{\partial \hat{x}} - \frac{\partial}{\partial \hat{x}}\left(D_h \frac{\partial \hat{h}}{\partial \hat{x}}\right) = -\hat{c}^p \hat{h}^q.$$

At leading order we have, for $q \leq m$

$$\mu \dot{s} \frac{\partial \hat{c}_0}{\partial \hat{x}} \delta_{mq} + \frac{\partial}{\partial \hat{x}} \left(\hat{D}_c \frac{\partial \hat{c}_0}{\partial \hat{x}} \right) = \hat{c}_0^p \hat{h}_0^q, \quad \frac{\partial}{\partial \hat{x}} \left(D_h \frac{\partial \hat{h}_0}{\partial \hat{x}} \right) = \hat{c}_0^p \hat{h}_0^q, \tag{C.8}$$

together with the inner 2 matching conditions

$$\text{as } \hat{x} \to +\infty \quad \hat{c}_0 \to 0, \quad \hat{D}_c \frac{\partial \hat{c}_0}{\partial \hat{x}} \to 0, \quad D_h \frac{\partial \hat{h}_0}{\partial \hat{x}} \to D_h \frac{\partial \hat{H}_0(0^+, t)}{\partial \hat{X}}, \tag{C.9}$$

and the inner inner 1 matching behaviour

$$\text{as } \hat{x} \to 0^+ \quad \hat{D}_c \frac{\partial \hat{c}_0}{\partial \hat{x}} \to \bar{D}_c \frac{\partial \bar{c}_0}{\partial \bar{x}} \text{ if } q = m, \tag{C.10a}$$

$$\hat{D}_c \frac{\partial \hat{c}_0}{\partial \hat{x}} \to \bar{D}_c \frac{\partial \bar{c}_1}{\partial \bar{x}} \text{ if } q < m. \tag{C.10b}$$

For the inner inner 1 region, we adopt the scalings

$$x = s(t) + \left(\frac{\delta}{\epsilon} \right)^2 \epsilon_2^{\frac{m+2-q}{2}} \bar{x}, \quad c = \bar{c}, \quad h = \epsilon_2 \bar{h}, \quad D_c = \frac{\epsilon^2}{\epsilon_2^m} \bar{D}_c, \tag{C.11}$$

where

$$\epsilon_2 = \left(\frac{\epsilon^2}{\delta} \right)^{\frac{2}{m+1}} < 1.$$

The governing equations are now

$$\left(\frac{\delta}{\epsilon} \right)^2 \epsilon_2^{m+1-q} \mu \frac{\partial \bar{c}}{\partial t} - \epsilon_2^{\frac{m-q}{2}} \mu \dot{s} \frac{\partial \bar{c}}{\partial \bar{x}} - \frac{\partial}{\partial \bar{x}} \left(\bar{D}_c \frac{\partial \bar{c}}{\partial \bar{x}} \right) = -\bar{c}^p \bar{h}^q,$$

$$\left(\frac{\delta}{\epsilon} \right)^2 \epsilon_2^{m+2-q} \frac{\partial \bar{h}}{\partial t} - \epsilon^{\frac{m+2-q}{2}} \dot{s} \frac{\partial \bar{h}}{\partial \bar{x}} - \frac{\partial}{\partial \bar{x}} \left(D_h \frac{\partial \bar{h}}{\partial \bar{x}} \right) = -\bar{c}^p \bar{h}^q.$$

For $q < m$ we pose the expansions

$$\bar{c} \sim \bar{c}_0 + \epsilon_2^{\frac{m_1-q}{2}} \bar{c}_1, \quad \bar{h} \sim \bar{h}_0 + \epsilon_2^{\frac{m_1-q}{2}} \bar{h}_1.$$

At leading order for $q \leq m$, we have (C.8) together with the inner inner 2 matching conditions

$$\text{as } \bar{x} \to 0^- \quad D_h \frac{\partial \bar{h}_0}{\partial \bar{x}} \to D_h \frac{\partial \hat{h}_0}{\partial \hat{x}} \text{ if } q = m, \tag{C.12a}$$

$$D_h \frac{\partial \bar{h}_1}{\partial \bar{x}} \to D_h \frac{\partial \hat{h}_0}{\partial \hat{x}} \text{ if } q < m, \tag{C.12b}$$

and the inner 1 matching behaviour

$$\text{as } \bar{x} \to -\infty \quad \bar{c}_0 \to \bar{C}_0(0^-,t), \qquad \bar{D}_c \frac{\partial \bar{c}_0}{\partial \bar{x}} \to \bar{D}_c \frac{\partial \bar{C}_1(0^-,t)}{\partial \bar{X}} \text{ if } q = m, \tag{C.13a}$$

$$\bar{D}_c \frac{\partial \bar{c}_1}{\partial \bar{x}} \to \bar{D}_c \frac{\partial \bar{C}_1(0^-,t)}{\partial \bar{X}} \text{ if } q < m, \tag{C.13b}$$

$$\bar{h}_0 \to 0. \tag{C.13c}$$

To allow matching between the inner inner 1 and outer 1, an inner 1 region is required. The scalings are determined by the size of δ relative to a critical value $\delta_{CR} = \epsilon^{\frac{2m+1-q}{m}}$ and the value of q. We consider first the case $1 < q < m+1$, for which $\epsilon^2 < \delta_{CR} < \epsilon$. In this case, the transition region is larger in size than the inner inner 1 region and the asymptotic structure for $q > m+1$ will be quite different. For $\delta < \delta_{CR}$ the scalings (C.4) apply, as does the subsequent analysis culminating in (C.6). This also pertains when $\delta = \delta_{CR}$, with the modification of the diffusion term entering the leading order hydroxide equation. For $\delta > \delta_{CR}$, the scalings need adjusting to

$$x = s(t) + \left(\frac{\delta}{\epsilon}\right) \epsilon^{\frac{m+1-q}{m}} \bar{X}, \quad c = \bar{C}, \quad h = \epsilon^{\frac{2}{m}} \bar{H}, \tag{C.14}$$

which give

$$\left(\frac{\delta}{\epsilon}\right)^2 \epsilon^{\frac{2(m+1-q)}{m}} \mu \frac{\partial \bar{C}}{\partial t} - \left(\frac{\delta}{\epsilon}\right) \epsilon^{\frac{m+1-q}{m}} \mu \dot{s} \frac{\partial \bar{C}}{\partial \bar{X}} - \frac{\partial}{\partial \bar{X}} \left(D_c \frac{\partial \bar{C}}{\partial \bar{X}} \right) = - \left(\frac{\delta}{\epsilon}\right)^2 \epsilon^{\frac{2}{m}} \bar{C}^p \bar{H}^q, \tag{C.15}$$

$$\epsilon^{\frac{2(m+1-q)}{m}} \frac{\partial \bar{H}}{\partial t} - \left(\frac{\epsilon}{\delta}\right) \epsilon^{\frac{m+1-q}{m}} \dot{s} \frac{\partial \bar{H}}{\partial \bar{X}} - \frac{\partial}{\partial \bar{X}} \left(D_h \frac{\partial \bar{X}}{\partial \bar{X}} \right) = -\bar{C}^p \bar{H}^q. \tag{C.16}$$

Posing

$$\bar{C} \sim \bar{C}_0 + \left(\frac{\delta}{\epsilon}\right) \epsilon^{\frac{m+1-q}{m}} \bar{C}_1, \quad \bar{H} \sim \bar{H}_0, \tag{C.17}$$

we obtain

$$\frac{\partial}{\partial \bar{X}} \left(D_c \frac{\partial \bar{C}_0}{\partial \bar{X}} \right) = 0, \quad \mu \dot{s} \frac{\partial \bar{C}_0}{\partial \bar{X}} + \frac{\partial}{\partial \bar{X}} \left(D_c \frac{\partial \bar{C}_1}{\partial \bar{X}} \right) = 0, \quad \frac{\partial}{\partial \bar{X}} \left(D_h \frac{\partial \bar{H}_0}{\partial \bar{X}} \right) = \bar{C}_0^p \bar{H}_0^p. \tag{C.18}$$

After matching to outer 1 and inner inner 1, we obtain (C.6a) and taking D_h constant, for $q > 1$

$$\bar{H}_0 = \left(\frac{(q-1)^2 c_0(s^-,t)^p}{2(q+1) D_h} \bar{X}^2 \right)^{-\frac{1}{q-1}}. \tag{C.19}$$

For the range $q \leq 1$, we note that $\delta_{CR} \leq \epsilon^2$ and so it is the regime just discussed that occurs with slight modifications. For $q = 1$, the inner 1 region is the same size as the

inner inner 1 and so the spatial scaling in (C.14) is modified to

$$x = s(t) + \delta(S(t) + \bar{X}), \tag{C.20}$$

where $1 < S(t) < 1/\delta$. We again obtain (C.5) - (C.6a) but now, taking D_h constant

$$\bar{H}_0 = \exp(\sigma(t)\bar{X}) \quad \text{with} \;\; S(t) \sim \frac{2}{m(m+1)\sigma(t)} \ln\left(\left(\frac{\delta}{\epsilon}\right)^m \epsilon\right) \tag{C.21}$$

where

$$\sigma(t) = \sqrt{\frac{c_0(s^-,t)^p}{D_h}}.$$

When $q < 1$, the inner 1 region is narrower than inner inner 1. The scalings are as in (C.14) and again we have (C.6a) and (C.19), where the latter solution is now restricted to $\bar{X} > 0$ and continued by zero for $\bar{X} < 0$. The inner inner 1 region is now restricted to $\bar{x} > 0$ with the inner 1 matching conditions (C.6a) occurring as $\bar{x} \to 0^+$.

To finalise, the matching behaviour of inner 1 to outer 1 is

$$\text{as } \bar{X} \to -\infty \quad \bar{C}_0 \to c_0(s^-,t), \quad D_c \frac{\partial \bar{C}_1}{\partial \bar{X}} \to D_{c_0} \frac{\partial c_0(s^-,t)}{\partial x}.$$

Hence, for $\epsilon^2 < \delta < \epsilon$, we obtain the following one-phase micro-macro problem

$$\begin{aligned}
&\text{in } 0 < x < s(t),\, t > 0 && \mu \frac{\partial c_0}{\partial t} - \frac{\partial}{\partial x}\left(D_{c_0} \frac{\partial c_0}{\partial x}\right) = 0,\\
&\text{on } x = 0 && -D_c \frac{\partial c_0}{\partial x} = H(1 - c_0),\\
&\text{on } x = s(t) && c_0 = \Phi_1(\dot{s}), \quad -D_{c_0} \frac{\partial c_0}{\partial x} = \dot{s}(\mu c_0 \delta_{mq} + h_i(s)),\\
&\text{at } t = 0 && c_0 = c_i(x) \text{ for } 0 \le x \le s_0, \quad s = s_0,
\end{aligned}$$

with $h_0 = h_i(x)$ for $s(t) \le x \le 1$ and Φ_1 is determined by the solution of the inner inner problem

$$\begin{aligned}
\mu \dot{s} \frac{\partial \bar{c}_0}{\partial \bar{x}} \delta_{mq} + \frac{\partial}{\partial \bar{x}}\left(\bar{D}_c \frac{\partial \bar{c}_0}{\partial \bar{x}}\right) &= \bar{c}_0^p \bar{h}_0^q,\\
\bar{D}_c \frac{\partial \bar{c}_0}{\partial \bar{x}} - D_h \frac{\partial \bar{h}_0}{\partial \bar{x}} &= -\dot{s}(\mu \bar{c}_0 \delta_{mq} + h_i(s)),
\end{aligned}$$

with

$$\begin{aligned}
&\text{as } \bar{x} \to +\infty && \bar{c}_0 \to 0, \quad \bar{D}_c \frac{\partial \bar{c}_0}{\partial \bar{x}} \to 0 \quad D_h \frac{\partial \bar{h}_0}{\partial \bar{x}} \to \dot{s} h_i(s),\\
&\text{as } \bar{x} \to -\infty && \bar{c}_0 \to \Phi_1(\dot{s}), \quad \bar{h}_0 \to 0.
\end{aligned}$$

This is as in the equivalent parameter regime in chapter 3 but with some terms disappearing for $q < m$.

The case $\delta = \epsilon$

At the end of Stage I carbonation (where the reaction zone remains at the outer surface), stage II carbonation takes place in which the reaction zone moves into the concrete.

In this case, the reaction zone comprises three regions. We have an inner inner 1 region which allows the CO_2 concentration to fall to $o(1)$ and an inner inner 2 region that matches the order 1 flux of the hydroxide from the outer 2 region. Again an inner 1 region is needed to accommodate the fall in CO_2 diffusivity, allowing matching between the inner inner 1 and outer 1 regions. We only consider the parameter range $q \leq m$ and we note that, when $q = m$, the inner inner 1 and inner inner 2 regions coincide.

The details can be deduced from the previous case ($\epsilon^2 < \delta < \epsilon$) by setting $\delta = \epsilon$. Consequently, for the inner inner 2 region, the scalings (C.7) apply with $\bar{\epsilon}_1 = \epsilon^{\frac{2(m-q)}{mp+p+q+1}}$ and $\bar{\epsilon}_2 = \epsilon^{\frac{2(p+1)}{mp+p+q+1}}$ so that again we obtain (C.8) as the leading order equations. Since there is now no inner 2 region in this case, the matching conditions (C.9) now apply to outer 2, with $\hat{H}_0$ being replaced by h_0. Similarly, for the inner inner 1 region, the scalings (C.11) apply with $\epsilon_2 = \epsilon^{\frac{2}{m+1}}$ and we obtain (C.8) at leading order. The inner 1 matching conditions (C.13) remain the same as do the details for the inner 1 region as given by (C.14)-(C.21). Finally, the matching from inner inner 2 to inner inner 1 and vice versa as done in (C.10) and (C.12) respectively, also remains the same.

Bibliography

[1] M. Abramowitz and I. A. Stegun, *Handbook of mathematical functions with formulas, graphs, and mathematical tables*, vol. 55, Courier Dover Publications, 1964.

[2] D. Aregba-Driollet, F. Diele, and R. Natalini, *A mathematical model for the sulphur dioxide aggression to calcium carbonate stones: Numerical approximation and asymptotic analysis*, SIAM Journal on Applied Mathematics, 64 (2004), pp. 1636–1667.

[3] S. D. Bahador and J. H. Cahyadi, *Modelling of carbonation of PC and blended cement concrete*, The IES Journal Part A: Civil & Structural Engineering, 2 (2009), pp. 59–67.

[4] C. M. Bender and S. A. Orszag, *Advanced mathematical methods for scientists and engineers I: Asymptotic methods and perturbation theory*, vol. 1, Springer Verlag, 1999.

[5] S. A. Bernal, R. Mejía de Gutiérrez, A. L. Pedraza, J. L. Provis, E. D. Rodriguez, and S. Delvasto, *Effect of binder content on the performance of alkali-activated slag concretes*, Cement and Concrete Research, 41 (2011), pp. 1–8.

[6] M. Böhm, J. Kropp, and A. Muntean, *A two-reaction-zones moving-interface model for predicting Ca (OH) 2 carbonation in concrete*, Zentrum für Technomathematik, 2003.

[7] D. Bothe and D. Hilhorst, *A reaction–diffusion system with fast reversible reaction*, Journal of mathematical analysis and applications, 286 (2003), pp. 125–135.

[8] J. Caldwell and Y. Y. Kwan, *Numerical methods for one-dimensional Stefan problems*, Communications in numerical methods in engineering, 20 (2004), pp. 535–545.

[9] M. Castellote and C. Andrade, *Modelling the carbonation of cementitious matrixes by means of the unreacted-core model, UR-CORE*, Cement and concrete research, 38 (2008), pp. 1374–1384.

[10] J. Chadam and P. Ortoleva, *The stabilizing effect of surface tension on the development of the free boundary in a planar, one-dimensional, cauchy-stefan problem*, IMA Journal of Applied Mathematics, 30 (1983), pp. 57–66.

[11] C.-F. Chang and J.-W. Chen, *The experimental investigation of concrete carbonation depth*, Cement and Concrete Research, 36 (2006), pp. 1760–1767.

[12] X. Chen and F. Reitich, *Local existence and uniqueness of solutions of the stefan problem with surface tension and kinetic undercooling*, Journal of mathematical analysis and applications, 164 (1992), pp. 350–362.

[13] F. Clarelli, A. Fasano, and R. Natalini, *Mathematics and monuments conservation: free boundary models of marble sulphation*, SIAM Journal on Applied Mathematics, 69 (2008), pp. 149–168.

[14] COMSOL Multiphysics, *Reference Guide Version 4.2*, COMSOL Multiphysics, 2011.

[15] Construction Materials Consultants, Inc. Website: http://www.cmc-concrete.com/carbonation.htm.

[16] B. E. Deal and A. S. Grove, *General Relationship for the Thermal Oxidation of Silicon*, Journal of Applied Physics, 36 (1965), pp. 3770–3778.

[17] P. Degond, J.-G. Liu, and L. Mieussens, *Macroscopic fluid models with localized kinetic upscaling effects*, SIAM Multiscale Modeling & Simulation, 5 (2006), pp. 940–979.

[18] S. Doole, *A stefan-like problem with a kinetic condition and surface tension effects*, Mathematical and computer modelling, 23 (1996), pp. 55–67.

[19] C. M. Elliott and J. R. Ockendon, *Weak and variational methods for moving boundary problems*, vol. 59, Pitman London, 1982.

[20] J. D. Evans, *Control of Stress Fields in Silicon Device Fabrication*, PhD thesis, Oxford University, 1992.

[21] J. D. Evans and J. R. King, *Asymptotic results for the Stefan problem with kinetic undercooling*, The Quarterly Journal of Mechanics and Applied Mathematics, 53 (2000), pp. 449–473.

[22] ——, *On the Derivation of Heterogeneous Reaction Kinetics from a Homogeneous Reaction Model*, SIAM Journal of Applied Mathematics, 60 (2000), pp. 1977–1996.

[23] ——, *The Stefan problem with nonlinear kinetic undercooling*, The Quarterly Journal of Mechanics and Applied Mathematics, 56 (2003), pp. 139–161.

[24] A. Fasano, G. H. Meyer, and M. Primicerio, *On a problem in the polymer industry: Theoretical and numerical investigation of swelling*, SIAM Journal on Mathematical Analysis, 17 (1986), pp. 945–960.

[25] R. M. Furzeland, *A comparative study of numerical methods for moving boundary problems*, IMA Journal of Applied Mathematics, 26 (1980), pp. 411–429.

[26] P. S. Hagan, R. S. Polizzotti, and G. Luckman, *The effects of surface poisons on the oxidation of binary alloys*, SIAM Journal on Applied Mathematics, (1985), pp. 826–842.

[27] ——, *Internal oxidation of binary alloys*, SIAM Journal on Applied Mathematics, (1985), pp. 956–971.

[28] U. Hornung, *Homogenization and porous media*, vol. 6, Springer, 1997.

[29] M. H.-N. Hsieh, *Mathematical modelling of controlled drug release from polymer micro-spheres: incorporating the effects of swelling, diffusion and dissolution via moving boundary problems*, PhD thesis, Queensland University of Technology, 2012.

[30] J. R. King, *Mathematical Aspects of Semiconductor Process Modelling*, PhD thesis, Oxford University, 1986.

[31] ——, *The isolation oxidation of silicon*, SIAM Journal on Applied Mathematics, 49 (1989), pp. 264–280.

[32] J. Kropp, *Relations between transport characteristics and durability*, Performance criteria for concrete durability, RILEM Report, 12 (1995), pp. 97–137.

[33] A. A. Lacey and L. A. Herraiz, *Macroscopic models for melting derived from averaging microscopic Stefan problems I: Simple geometries with kinetic undercooling or surface tension*, European Journal of Applied Mathematics, 11 (2000), pp. 153–169.

[34] ——, *Macroscopic models for melting derived from averaging microscopic Stefan problems II: Effect of varying geometry and composition*, European Journal of Applied Mathematics, 13 (2002), pp. 261–282.

[35] M.-T. Liang and S.-M. Lin, *Mathematical modeling and applications for concrete carbonation*, Journal of Marine Science and Technology, 11 (2003), pp. 20–33.

[36] S. A. Meier, *A homogenisation-based two-scale model for reactive transport in media with evolving microstructure*, Comptes Rendus Mécanique, 336 (2008), pp. 623–628.

[37] S. A. Meier and A. Muntean, *A two-scale reaction–diffusion system with micro-cell reaction concentrated on a free boundary*, Comptes Rendus Mécanique, 336 (2008), pp. 481–486.

[38] S. A. Meier, M. A. Peter, A. Muntean, and M. Böhm, *Dynamics of the internal reaction layer arising during carbonation of concrete*, Chemical engineering science, 62 (2007), pp. 1125–1137.

[39] G. H. Meyer, *A numerical method for two-phase Stefan problems*, SIAM Journal on Numerical Analysis, 8 (1971), pp. 555–568.

[40] ——, *Initial value methods for boundary value problems: Theory and application of invariant imbedding*, Academic Press New York, 1973.

[41] ——, *One-dimensional parabolic free boundary problems*, SIAM Review, 19 (1977), pp. 17–34.

[42] I. Monteiro, F. A. Branco, J. d. Brito, and R. Neves, *Statistical analysis of the carbonation coefficient in open air concrete structures*, Construction and Building Materials, 29 (2012), pp. 263–269.

[43] A. Muntean, *On the interplay between fast reaction and slow diffusion in the concrete carbonation process: a matched-asymptotics approach*, Meccanica, 44 (2009), pp. 35–46.

[44] ——, *Well-posedness of a moving-boundary problem with two moving reaction strips*, Nonlinear Analysis: Real World Applications, 10 (2009), pp. 2541–2557.

[45] A. Muntean and M. Böhm, *A moving-boundary problem for concrete carbonation: global existence and uniqueness of weak solutions*, Journal of Mathematical Analysis and Applications, 350 (2009), pp. 234–251.

[46] A. Muntean, M. Böhm, and J. Kropp, *Moving carbonation fronts in concrete: a moving-sharp-interface approach*, Chemical Engineering Science, 66 (2011), pp. 538–547.

[47] P. Ortoleva, E. Merino, C. Moore, and J. Chadam, *Geochemical self-organization I; reaction-transport feedbacks and modeling approach*, American Journal of Science, 287 (1987), pp. 979–1007.

[48] F. Pacheco Torgal, S. Miraldo, J. Labrincha, and J. De Brito, *An overview on concrete carbonation in the context of eco-efficient construction: Evaluation, use of scms and/or rac*, Construction and Building Materials, 36 (2012), pp. 141–150.

[49] V. G. Papadakis, C. G. Vayenas, and M. N. Fardis, *A reaction engineering approach to the problem of concrete carbonation*, AIChE Journal, 35 (1989), pp. 1639–1650.

[50] V. G. Papadakis, C. G. Vayenas, and M. N. Fardis, *Experimental investigation and mathematical modeling of the concrete carbonation problem*, Chemical Engineering Science, 46 (1991), pp. 1333–1338.

[51] V. G. Papadakis, C. G. Vayenas, and M. N. Fardis, *Fundamental modeling and experimental investigation of concrete carbonation*, ACI Materials Journal, 88 (1991), pp. 363–373.

[52] D. Park, *Carbonation of concrete in relation to co¡ sub¿ 2¡/sub¿ permeability and degradation of coatings*, Construction and building materials, 22 (2008), pp. 2260–2268.

[53] M. A. Peter, *Homogenisation of a chemical degradation mechanism inducing an evolving microstructure*, Comptes Rendus Mécanique, 335 (2007), pp. 679–684.

[54] ——, *Coupled reaction–diffusion processes inducing an evolution of the microstructure: Analysis and homogenization*, Nonlinear Analysis: Theory, Methods & Applications, 70 (2009), pp. 806–821.

[55] G. W. Richardson and J. R. King, *Motion by curvature of a three-dimensional filament: similarity solutions*, Interfaces and Free Boundaries, 4 (2002), pp. 395–421.

[56] M. G. Richardson, *Fundamentals of durable reinforced concrete*, Taylor & Francis, 2004.

[57] X. Ruan and Z. Pan, *Mesoscopic simulation method of concrete carbonation process*, Structure and Infrastructure Engineering, 8 (2012), pp. 99–110.

[58] A. V. Saetta, B. A. Schrefler, and R. V. Vitaliani, *The carbonation of concrete and the mechanism of moisture, heat and carbon dioxide flow through porous materials*, Cement and Concrete Research, 23 (1993), pp. 761–772.

[59] ——, *2–D model for carbonation and moisture/heat flow in porous materials*, Cement and Concrete Research, 25 (1995), pp. 1703–1712.

[60] A. V. Saetta and R. V. Vitaliani, *Experimental investigation and numerical modeling of carbonation process in reinforced concrete structures: Part I: Theoretical formulation*, Cement and concrete research, 34 (2004), pp. 571–579.

[61] A. Steffens, D. Dinkler, and H. Ahrens, *Modeling carbonation for corrosion risk prediction of concrete structures*, Cement and Concrete Research, 32 (2002), pp. 935–941.

[62] S. Talukdar, N. Banthia, and J. Grace, *Carbonation in concrete infrastructure in the context of global climate change–part 1: Experimental results and model development*, Cement and Concrete Composites, 34 (2012), pp. 924–930.

[63] H. F. W. Taylor, *Cement chemistry*, Thomas Telford Services Ltd, 1997.

[64] M. Te Liang, W. Qu, and C.-H. Liang, *Mathematical modeling and prediction method of concrete carbonation and its applications*, Journal of Marine Science and Technology, 10 (2002), pp. 128–135.

[65] M. Thiery, G. Villain, P. Dangla, and G. Platret, *Investigation of the carbonation front shape on cementitious materials: effects of the chemical kinetics*, Cement and Concrete Research, 37 (2007), pp. 1047–1058.

[66] G. Villain, M. Thiery, and G. Platret, *Measurement methods of carbonation profiles in concrete: thermogravimetry, chemical analysis and gammadensimetry*, Cement and Concrete Research, 37 (2007), pp. 1182–1192.

[67] P. Wriggers and S. O. Moftah, *Mesoscale models for concrete: Homogenisation and damage behaviour*, Finite elements in analysis and design, 42 (2006), pp. 623–636.

[68] Q. Zhu, A. Peirce, and J. Chadam, *Initiation of shape instabilities of free boundaries in planar cauchy-stefan problems*, European J. Appl. Math, 4 (1993), pp. 419–436.